Universidad Autónoma de Madrid

Departamento de Física Teórica

Memoria de Tesis Doctoral

Journey through the ALPs

por

Jonathan-Gilbert Machado Rodríguez

presentada ante el Departamento de Física Teórica
de la Universidad Autónoma de Madrid
para la obtención del Título de Doctor en Ciencias

Tesis Doctoral dirigida por

Prof. Mª Belén Gavela Legazpi
Catedrática del Departamento de Física Teórica
de la Universidad Autónoma de Madrid
y
Prof. Jorge Fernández de Trocóniz Acha
Profesor titular del Departamento de Física Teórica
de la Universidad Autónoma de Madrid

Universidad Autónoma de Madrid

Instituto de Física Teórica UAM-CSIC

4 de Octubre de 2024, Madrid

Agradecimientos

El proceso que conlleva hacer un doctorado es complejo, tanto a nivel profesional, como vital. Todo gran proyecto personal es a la vez un espejo en el que vernos reflejados, junto con nuestras fortalezas, miedos, creencias y limitaciones. Me siento enormemente afortunado por todo lo que han supuesto para mí estos cuatro años, por todo lo que he aprendido de física de partículas, pero también de mí mismo. La persona que inició este viaje estaría orgullosa de la que hoy lo concluye. Gracias a todos los que habéis formado parte de este camino.

* * *

En primer lugar me gustaría agradecer a mis directores, Belén y Jorge, su labor durante estos cuatro años. A Belén, su pasión por la física, su exigencia, tan positiva para mi desarrollo, su orientación y haberme abierto camino en este campo tan maravilloso, teniendo siempre presente qué era lo mejor para mí. A Jorge, por haberme enseñado con paciencia desde el principio del doctorado hasta hoy, por las largas discusiones sobre física, y por su guía, rigor y meticulosidad.

También me gustaría agradecer a José Santiago, Luca Merlo, Ilaria Brivio, Ignazio Scimemi y Enrique Fernández por aceptar ser parte del tribunal de esta tesis.

A María Ramos, su pasión y esfuerzo a la hora de enseñarme todo lo que sé de teorías efectivas de campos. Por su amistad, por ser una gran colaboradora, un ejemplo a seguir como física, por las agotadoras discusiones, y por acompañarme en el proyecto que tanto he disfrutado y ha contribuído a forjar mi confianza como físico teórico de partículas. Atesoro con mucho cariño los recuerdos de nuestra estancia en California, compartidos con Carla y Guilherme.

Al resto de mis colaboradores, Jesús, Ilaria, Supratim, por haber recorrido conmigo una parte del camino, por haber compartido lo que sabíais, por haber creado un ambiente maravilloso para hacer ciencia, y, en definitiva, por haber contribuído a los proyectos que hoy constituyen esta tesis.

A mis compañeros de la oficina 313, Matilda, Gonzalo y Víctor, por las risas y la física compartidas. A Matilda, por su apoyo en la dificultad. A Gonzalo, por los *memes*, entrenos, burritos y grandes momentos. A Víctor, por compartir conmigo casi la totalidad de estos cuatro años de doctorado, las conferencias en París, Lisboa y Varsovia, por compartir este camino como hermano de doctorado y compañero de despacho. A Alexander, por compartir siempre su buen humor hasta en los días más grises. A Arturo, por compartir su pasión por la física y por la vida, las conferencias, y en especial por los *Rencontres de Moriond*. A Fer, por ser un gran compañero de despacho. A los doctorandos de primer año, por compartir muchas risas durante las comidas en este bonito y último año de doctorado. A Pablo Quílez, por los momentos compartidos en California, comiendo tacos y surfeando.

A Rubén, por haber sido un ejemplo de fortaleza mental y disciplina a lo largo de estos cuatro años.

A los profesores del IES La Laguna de Padul, que me han apoyado en mi recorrido académico. En especial a Manolo Álvarez, Socorro Gutierrez, Manuel Ruíz, Isabel María Sánchez, Fran, Mauri Ruíz, Elena Santofimia, Isidro García, María José Bohorquez, Juan Quero, María José Castillo... Gracias por vuestras enseñanzas, motivación y apoyo en una etapa vital tan importante.

A mis amigos de Padul y Granada. En especial a “los perros sin amo”, Bayo, Fabián, Fernando y José, por los veranos en Almuñecar, las briscas en el taller y las tardes de café en *la Eli*. A Juanma y Sánchez, por las pachangas de baloncesto y por nuestros reencuentros para ponernos al día. A Cipri, por su amistad desde los primeros años de instituto y por nuestro reencuentro en Lima. A Eli y Julio, por adentrarnos juntos en el fascinante mundo de la Física. Os sigo a todos con infinito cariño y orgullo desde la distancia.

A Carla, por su amor en los últimos años, y por recordarme cuando más lo he necesitado qué es lo esencial. Gracias a toda la familia Ramilo Fariña por su apoyo incondicional.

Por último, y en un lugar especial, a mi familia. A los que ya no están, mi abuela Carmen, mi abuelo Gilbert, mi tía Cele. Y a los que siempre han estado. A mis tíos, José y Mari Carmen. A mis primos, Miriam, Aure, José y Leo. A mi abuela Denise, por recordarme siempre lo orgullosa que está de mí. A mi hermana Marina, por su apoyo y por ser un ejemplo a seguir en la lucha que conlleva buscar su propio camino. A mis padres, José y Michèle, por su apoyo, ejemplo, confianza y por darme un hogar lleno de amor. Por ofrecerme siempre el espacio que he necesitado para crecer, buscar y desarrollarme con la tranquilidad de poder equivocarme sabiendo que siempre podría contar con ellos. Sin duda, todo lo que soy a día de hoy, mis valores, mis logros y, en definitiva, todo de cuanto me siento orgulloso, es gracias a vosotros.

* * *

“El impedimento a la acción avanza la acción.
Lo que se interpone en el camino se convierte en camino.”

— Marco Aurelio

Publications

This doctoral thesis is based on the following scientific publications.

Refereed journal articles

[1] **Nonresonant Searches for axion-like particles in vector boson scattering processes at the LHC**
J. Bonilla, I. Brivio, J. Machado-Rodríguez and J. F. de Trocóniz
*JHEP **06** (2022) 113* and *arXiv:2202.03450 [hep-ph]*

[2] **Running beyond ALPs: shift-breaking and CP-violating effects**
S. Das Bakshi, J. Machado-Rodríguez and M. Ramos
*JHEP **11** (2023) 133* and *arXiv: 2306.08036 [hep-ph]*

[3] **Limits on ALP-neutrino couplings from loop-level processes**
J. Bonilla, B. Gavela, J. Machado-Rodríguez,
*PRD **109** (2024) 055023* and *arXiv:2309.15910 [hep-ph]*

Proceedings

[4] **Nonresonant Searches for Axion-Like Particles at the LHC: Implications for Vector Boson Scattering**
J. Bonilla, I. Brivio, J. Machado-Rodríguez and J. F. de Trocóniz
*PoS **EPS-HEP2021** (2022) 692*

Abstract

The Standard Model (SM) of particle physics describes with exceptional accuracy almost everything we observe in the "visible" Universe. We know, however, that it is not the end of the story. There are major experimental phenomena which cannot be satisfactorily explained within the SM. Namely, dark matter (DM), dark energy, neutrino masses and the matter-antimatter asymmetry. These, together with the currently open theoretical questions concerning several of its free parameters —the hierarchy problem, the flavor puzzle and the strong-CP problem—, hint at some underlying unknown structure beyond the SM (BSM).

This thesis is devoted to the phenomenology of axion-like particles (ALPs), hypothetical pseudo-Goldstone bosons (pGB) which are the telltale of hidden spontaneously broken global symmetries. The fact that (p)GBs have already been observed in Nature, in mesons and the longitudinal components of the electroweak gauge bosons, and the ubiquity of ALPs in a plethora of BSM extensions with a rich phenomenology across energies suggest that ALPs are ideal candidates to extend the SM particle content. We use the power of the model-independent effective field theory (EFT) framework throughout this thesis. The results presented here fall into two domains.

On the one hand, this thesis explores the phenomenology of ALPs in high-energy collider searches. Specifically, we propose a powerful novel search window that takes advantage of the derivative nature of ALP interactions, to probe its couplings to the EW gauge bosons independently of the coupling to gluons: vector boson scattering processes at the LHC mediated by a very off-shell or *nonresonant* ALP.

On the other hand, the high-energy and high precision era of experimental particle physics requires theoretical predictions to include radiative corrections. In this thesis, we study the one-loop impact of ALP-neutrino effective interactions on the ALP couplings to the EW gauge boson. Using these results, we impose novel constraints on the ALP-neutrino parameter space recasting bounds from collider data. Moreover, if a new scalar signal is detected at experiments, a compelling question to answer is whether this new particle is an ALP or not. Here we also present the full renormalization group equations (RGEs) of the SMEFT extended with a real scalar singlet up to dimension-five with one-loop accuracy, including CP-violating and shift-breaking interactions, and keeping track of mixing effects in the scalar sector. These results provide a useful tool for future phenomenological analyses targeting new physics signals in the scalar sector, allowing to pinpoint the differences between a generic scalar and a true ALP. The full set of RGEs of the singlet EFT are implemented in a new `Mathematica` package.

Resumen

El Modelo Estándar (ME) de la física de partículas describe con una precisión excepcional casi todo lo que observamos en el Universo “visible”. Sin embargo, sabemos que tiene que haber algo más. Hay fenómenos experimentales importantes que no pueden explicarse satisfactoriamente dentro del ME. A saber, la materia oscura, la energía oscura, las masas de los neutrinos y la asimetría materia-antimateria. Estos, junto con las preguntas teóricas relativas a varios de los parámetros libres del ME que siguen sin tener respuesta —el problema de jerarquía, el puzle del sabor y el problema de CP fuerte–, sugieren alguna estructura subyacente desconocida más allá del ME.

Esta tesis se centra en la fenomenología de las partículas tipo axión (o *ALPs* por sus siglas en inglés), pseudo-bosones de Goldstone (pBG) hipotéticos indicativos de simetrías globales ocultas rotas espontáneamente. Que (p)BG ya hayan sido observados en la naturaleza, en los mesones y las componentes longitudinales de los bosones *gauge* electrodébiles, y la ubicuidad de los ALPs en cuantiosas extensiones más allá del ME con una rica fenomenología, sugiere que los ALPs son candidatos ideales para extender el ME. En esta tesis trabajamos en el marco de las teoría efectivas de campos (TEC), que permite hacer estudios fenomenológicos de forma general sin especificar un modelo de ALPs concreto. Los resultados presentados aquí se pueden diferenciar en dos líneas.

Por un lado, esta tesis explora la fenomenología de los ALPs en búsquedas en colisionadores de alta energía. Proponemos una nueva ventana de búsqueda que aprovecha la naturaleza derivativa de las interacciones de los ALPs para probar sus acoplos a los bosones *gauge* electrodébiles independientemente del acoplo a gluones: procesos de *scattering* de bosones vectoriales en el LHC mediados por un ALP *no resonante*, es decir, mucho más ligero que la energía de los pares de bosones *gauge* involucrados en el proceso.

Por otro lado, la era de alta energía y alta precisión de la física experimental de partículas requiere que las predicciones teóricas incluyan correcciones radiativas. En esta tesis, estudiamos el impacto a un *loop* de las interacciones efectivas ALP-neutrino en los acoplos de los ALPs a los bosones electrodébiles. Utilizando estos resultados, imponemos nuevas restricciones en el espacio de parámetros ALP-neutrino reinterpretando límites derivados de los datos de colisionadores. Además, si se detecta una nueva señal escalar en los experimentos, una pregunta importante es si esta nueva partícula es un ALP o no. Presentamos también el conjunto completo de ecuaciones del grupo de renormalización (EGR) de la TEC del ME extendido con un singlete escalar real hasta dimensión cinco y con precisión a un *loop*, incluyendo interacciones que violan la simetría CP y la simetría *shift*, y teniendo en cuenta los efectos de mezcla en el sector escalar. Estos resultados son una herramienta útil para futuros análisis fenomenológicos que busquen señales de nueva física en el sector escalar, permitiendo distinguir entre una particula escalar genérica y un verdadero ALP, y se han implementado en un nuevo paquete de `Mathematica`.

Contents

Motivation and goals

The Standard Model of particle physics (SM) brings together quantum mechanics and special relativity, describing nature on the most fundamental level as an interplay of field excitations governed by three —out of the four— fundamental forces: the strong, weak and electromagnetic interactions. The SM can explain almost everything we observe in the "visible" Universe and has proved an unprecedented accuracy in its predictions of many of the experimental results obtained within the particle physics community.

Notwithstanding its success, we know that it is not the end of the story, since there are several open problems both at the experimental and theoretical level. Experiments point towards the need of physics beyond the SM (BSM), since four major experimental observations cannot be satisfactorily explained:

- **Dark matter:** Cosmological observations indicate that only 5% of the energy density of the universe corresponds to visible matter —described by the SM—, while 26% is attributed to an elusive new type of matter, *cold dark matter* (DM). The nature and composition of DM remains a mistery since its existence has only been inferred through its gravitational effects on visible matter.

- **Dark energy:** The remaining 69% of this energy density is responsible for the observed accelerated expansion of the universe and is known as *dark energy*. Dark energy is described within general relativity in terms of a cosmological constant term in Einsteins's equations. However, attempts to explain this in terms of the vaccuum energy of the SM fields have failed to match satisfactorily cosmological observations.

- **Neutrino masses:** SM neutrinos are massless particles. However, the measurement of their oscillations at experiments requires, at least, two massive neutrinos. Both the mechanism behind the non-vanishing small neutrinos masses and their nature —Dirac or Majorana— remain unknown and point to new physics.

- **Matter-antimatter asymmetry:** The universe is mostly made of matter while only a small amount corresponds to antimatter. Although the SM predicts certain amount of asymmetry between the matter and antimatter abundances, it has been proven that the amount of CP-violation in the SM cannot explain the observed amount of asymmetry. Furthermore, the Higgs mass is too heavy for this purpose.

Additionaly, an increasing number of experimental discrepancies between experimental observations and the SM predictions hint to the existence of new physics. These anomalies span over a broad energy range and include, for example, the anomalous magnetic moment of the muon, measurements of neutrino appearance and disappearance and others[1]. Nevertheless, their statistical significance is still insufficient to confirm them as evidences of new physics. The data of the third Run of the Large Hadron collider (LHC), as well as other ongoing and future precision experiments, are crucial for the future clarification/confirmation of these anomalies.

On the other hand, despite its elegance and beauty, there are other less elegant aspects of the theory that seem to hint at some underlying structure beyond the SM. There are 19 free parameters within the SM —26, if neutrino masses and lepton flavor mixing are included—, which cannot be predicted from first principles. Furthermore, some of them —the Higgs mass and $\overline{\theta}$ parameter— must be fine tuned to really specific values without any sort of theoretical justification. The major theoretical issues in the SM are:

- **Electroweak hierarchy problem:** This problem presumes the existence of other energy scales. The mass of the Higgs boson is unexpectedly light since it is not protected from radiative corrections by any sort of symmetry. In order to accomodate the SM Higgs mass to observations, its bare mass must be fine tuned to partially cancel one-loop quadratic sensitivity to hypothetical higher energy scales.

- **Flavor puzzle:** There are three generations of fermions in the SM with identical quantum numbers but different masses. While quark and charged leptons present a large hierarchy in mass, spanning over five and three orders of magnitude, respectively, neutrinos masses are many orders of magnitude away. Furthermore, mixing is small in the quark sector while large in the leptonic one. Although technically no fine-tuning is required, this problem suggests the existence of an underlying structure beyond the SM.

- **Strong-CP problem:** Since CP is not a fundamental symmetry of the SM, the so called $\overline{\theta}$-term, which characterizes the QCD vacuum and parametrizes the only source of CP-violation in Quantum chromodynamics (QCD), is a priori allowed. However, experimental attempts have failed so far to measure the neutron electric dipole moment requiring $\overline{\theta}$ to be fine tuned to an extremely small value $\overline{\theta} \lesssim 10^{-10}$. Although still consistent with the SM, there is no explanation for this apparent restoration of CP symmetry in QCD.

- **Gravity** is the fourth fundamental interaction and it is not included in the SM. It governs the dynamics of the universe at large distances and is described at the classical level by Eintein's theory of general relativity. However, the quantization of gravity has not yet been achieved, aside from the string hipothesis.

The topic of my research is partially inspired and motivated by the strong-CP problem. Among the several models which have been proposed to address it, one of the most elegant and simple is the so called *QCD axion*, based on the Peccei-Quinn (PQ) mechanism. Axion models are built around a new global abelian symmetry, the PQ symmetry, which is exact at the classical level but broken by anomalous quantum effects. Due to its pGB nature, axion interactions with the SM particles are of two kinds: shift-invariant —when the derivative of the axion couples to an axial fermionic current—, and anomalous. My research deals more in general with pGBs which are the telltale signs of hidden global symmetries. A generic neutral pseudoscalar pGB of a new spontaneously broken global symmetry is typically called an *axion-like particle* (ALP). Due to its pGB nature, their is a separation in energy between the ALP mass

[1]See Ref. [5] for an extended up-to-date review.

and the “new physics scale”. This allows ALP interactions to be parametrized by means of an effective field theory (EFT) consistent with the SM gauge symmetry. The ALP EFT offers a model-independent approach, where the ALP mass as well as the new physics scale and the anomalous and derivative couplings are free parameters. Thus, the motivation for ALP searches extends way beyond QCD axions and the strong-CP problem. However, although ALPs *a priori* do not intend to solve the strong-CP problem —as the relation between their mass and scale does not need to be that of the QCD axion—, it is not excluded that heavy or very light ALPs can address that problem.

In fact, (p)GBs —originated from a spontaneous breaking of an (almost) exact symmetry of the theory— have already been observed in nature and predicted by the SM. For instance, the longitudinal modes of the Z and $W^{\pm}$ gauge bosons correspond to the would-be Goldstone bosons that arise after the electroweak symmetry breaking, “eaten” by the EW gauge bosons in order to acquire a mass. Similarly, SM mesons originate at lower energies as composite pGBs after the breaking of the chiral symmetry of QCD. If there is an underlying UV BSM theory of particle physics with pGBs, we might be able to find them at the energies that are being probed at current experiments.

ALPs are predicted in a plethora of BSM extensions. Some paradigmatic scenarios include: *(i)* the *Majoron*, which is the pGB born of the spontaneous breaking of the lepton number symmetry in models that attempt to explain the small neutrino masses; *(ii) axiflavons*, in dynamical flavor theories which attempt to solve both the strong-CP problem and the flavor puzzle; *(iii)* the *relaxion*, in theories that adress the strong-CP and hierarchy problems; *(iv) familons*, arising from the breaking of global family symmetries; *(v)* string theory; *(vi)* theories involving extra dimensions; or *(vii)* scenarios where the Higgs boson is a pGB, such as composite-Higgs models. Axions and ALPs are also compelling dark matter (DM) candidates, which enhances their interest.

The main goal of this thesis is to deepen the understanding of ALP phenomenology, in order to enable the discovery of ALP signals at experiments. My contributions have pushed the state-of-the-art knowledge in two directions:

- **ALPs at colliders.** In this thesis I propose a new search window for ALPs at colliders: nonresonant ALPs in vector boson scattering proccesses at the LHC. Furthermore, the impact of ALP-electroweak couplings and their collider probes on the ALP-neutrino parameter space is presented for the first time.

- **ALP effective field theory.** The precision era of experimental particle physics requires of theoretical predictions that go beyond the renormalizable level and include running effects. In this thesis I present the full renormalization group equations (RGEs) of the SMEFT extended with a real scalar singlet up to dimension-five with one-loop accuracy, including CP-violating and shift-breaking interactions, and taking into account mixing effects in the scalar sector. We compare our results with the ALP EFT. These results are implemented in a new `Mathematica` package that allows to solve the RGEs for a given UV scenario.

This thesis is divided in two main parts. The first part extends from Chapter 1 to 3 and presents a review of the SM, the strong-CP problem and ALPs. The second part extends from Chapter 4 to 6 and contains the original contribution of this thesis.

Motivación y objetivos

El Modelo Estándar de la física de partículas (ME) reúne la mecánica cuántica y la relatividad especial, describiendo la naturaleza al nivel más fundamental como una interacción de excitaciones de campo gobernadas por tres de las cuatro fuerzas fundamentales: las interacciones fuerte, débil y electromagnética. El ME puede explicar casi todo lo que observamos en el Universo “visible” y ha demostrado una precisión sin precedentes en sus predicciones de muchos de los resultados experimentales obtenidos dentro de la comunidad de la física de partículas.

A pesar de su éxito, sabemos que no tiene que haber algo más, ya que existen varios problemas abiertos tanto a nivel experimental como teórico. Los experimentos apuntan hacia la necesidad de una física más allá del ME, ya que cuatro observaciones experimentales importantes no pueden ser explicadas satisfactoriamente:

- **Materia oscura:** Las observaciones cosmológicas indican que sólo el 5% de la densidad de energía del universo corresponde a la materia visible —descrita por el ME—, mientras que el 26% se atribuye a un nuevo tipo de materia esquiva, la *materia oscura fría* (MO). La naturaleza y composición de la MO sigue siendo un misterio, ya que su existencia sólo se ha inferido a través de sus efectos gravitacionales sobre la materia visible.

- **Energía oscura:** El 69% restante de esta densidad de energía es responsable de la expansión acelerada del universo que observamos y se conoce como *energía oscura*. La energía oscura se describe dentro de la relatividad general en términos de un término de constante cosmológica en las ecuaciones de Einstein. Sin embargo, los intentos de explicar esto en términos de la energía del vacío de los campos del ME no han logrado coincidir satisfactoriamente con las observaciones cosmológicas.

- **Masas de los neutrinos:** Los neutrinos del ME son partículas sin masa. Sin embargo, la medición de sus oscilaciones en los experimentos requiere de, al menos, dos neutrinos masivos. Tanto el mecanismo detrás de las masas tan pequeñas y no nulas de los neutrinos como su naturaleza —Dirac o Majorana— siguen siendo desconocidos y apuntan a nueva física.

- **Asimetría materia-antimateria:** El universo está compuesto mayoritariamente de materia mientras que sólo una pequeña cantidad corresponde a la antimateria. Aunque el ME predice cierta cantidad de asimetría entre las abundancias de materia y antimateria, se ha demostrado que la cantidad de violación de CP en el ME no puede explicar la cantidad observada de asimetría. Además, la masa del Higgs es demasiado pesada para este propósito.

Además, un número creciente de discrepancias experimentales entre las observaciones y las predicciones del ME apuntan a la existencia de nueva física. Estas anomalías abarcan un amplio rango de energías e incluyen, por ejemplo, el momento magnético anómalo del muón, mediciones de aparición y desaparición de neutrinos y otros[2]. No obstante, su significancia estadística aún es insuficiente para confirmarlas como evidencias de nueva física. Los datos del *Run 3* del Gran Colisionador de Hadrones (o *LHC* por sus siglas en inglés), así como otros experimentos de precisión —en curso y futuros—, son cruciales para la futura clarificación/confirmación de estas anomalías.

Por otro lado, a pesar de su elegancia y belleza, hay otros aspectos menos elegantes de la teoría que parecen apuntar a alguna estructura subyacente más allá del ME. Hay 19 parámetros libres dentro del ME —26, si se incluyen las masas de los neutrinos y la mezcla de sabores de los leptones—, que no pueden predecirse desde primeros principios. Además, algunos de ellos —la masa del Higgs y el parámetro $\overline{\theta}$— deben ser ajustados a valores muy específicos sin ninguna justificación teórica. Los principales problemas teóricos en el ME son:

- **Problema de la jerarquía electrodébil:** Este problema supone la existencia de otras escalas de energía. La masa del bosón de Higgs es inesperadamente ligera ya que no está protegida de correcciones radiativas por ningún tipo de simetría. Para acomodar la masa del Higgs del ME a las observaciones, su masa desnuda debe ajustarse finamente para cancelar parcialmente la sensibilidad cuadrática a una hipotética escala de energía más alta.

- **El puzle del sabor:** Hay tres generaciones de fermiones en el ME con números cuánticos idénticos pero masas diferentes. Mientras que los quarks y los leptones cargados presentan una gran jerarquía en masa, abarcando más de cinco y tres órdenes de magnitud, respectivamente, las masas de los neutrinos están muchos órdenes de magnitud por debajo. Además, la mezcla es pequeña en el sector de los quarks mientras que es grande en el leptónico. Aunque técnicamente no se requiere de un ajuste fino, este problema sugiere la existencia de una estructura subyacente más allá del ME.

- **Problema del CP fuerte:** Dado que CP no es una simetría fundamental del ME, el llamado término $\overline{\theta}$, que caracteriza el vacío de las interacciones fuertes y parametriza la única fuente de violación de CP en cromodinámica cuántica (*QCD por sus siglas en inglés*), está permitido *a priori*. Sin embargo, los intentos experimentales han fallado hasta ahora en medir el momento dipolar eléctrico del neutrón, requiriendo que $\overline{\theta}$ sea ajustado a un valor extremadamente pequeño $\overline{\theta} \lesssim 10^{-10}$. Aunque aún es consistente con el ME, no hay explicación para esta aparente restauración de la simetría CP en QCD.

- **Gravedad:** es la cuarta interacción fundamental y no está incluida en el ME. Gobierna la dinámica del universo a grandes distancias y se describe a nivel clásico por la teoría de la relatividad general de Einstein. Sin embargo, la cuantización de la gravedad aún no se ha logrado, más allá de la hipótesis de cuerdas.

El tema de mi investigación está parcialmente inspirado y motivado por el problema de CP fuerte. Entre los varios modelos que se han propuesto para abordarlo, uno de los más elegantes y simples es el llamado *axión de QCD*, basado en el mecanismo de Peccei-Quinn (PQ). Los modelos de axiones se construyen alrededor de una nueva simetría abeliana global, la simetría PQ, que es exacta a nivel clásico pero que está rota

[2]Ver Ref. [5] para una revisión extensa y actualizada.

por efectos cuánticos anómalos. Debido a su naturaleza pBG, las interacciones de los axiones con las partículas del ME son de dos tipos: invariante bajo desplazamientos o *shifts* del campo del axión —es decir, cuando la derivada del axión se acopla a una corriente fermiónica axial— y anómalas. Mi investigación trata más en general con pBG, que evidencian la existencia de simetrías globales ocultas. Un pBG neutro genérico de una nueva simetría global rota espontáneamente se llama típicamente una *partícula tipo axión* (o *ALP* por sus siglas en inglés). Debido a su naturaleza pBG, hay una separación en energía entre la masa de la ALP y la "escala de nueva física". Esto permite que las interacciones del ALP se puedan parametrizar por medio de una teoría de efectiva de campos (TEC) consistente con la simetría *gauge* del ME. La TEC del ALP ofrece un enfoque independiente del modelo, donde la masa del ALP así como la escala de nueva física y los acoplos anómalos y derivativos son parámetros libres. Así, la motivación para la búsqueda de ALPs va más allá de los axiones de QCD y el problema de CP fuerte. Sin embargo, aunque las ALPs *a priori* no intentan resolver el problema de CP fuerte —ya que la relación entre su masa y escala no necesita ser la del axión de QCD—, no se excluye que ALPs pesados o muy ligeros puedan abordar este problema.

De hecho, los (p)BG —originados de una ruptura espontánea de una simetría (casi) exacta de la teoría— ya se han observado en la naturaleza y predicho por el ME. Por ejemplo, los modos longitudinales de los bosones *gauge* Z y $W^{\pm}$ corresponden a los que serían bosones de Goldstone que surgen después de la ruptura de la simetría electrodébil, y que son "absorbidos" por los bosones *gauge* electrodébiles para adquirir una masa no nula. De manera similar, los mesones del ME se originan a energías más bajas como pBG compuestos después de la ruptura de la simetría quiral de QCD. Si hay una teoría en el "ultravioleta" (UV) subyacente más allá del ME de la física de partículas con pBG, podríamos ser capaces de encontrarlos a las energías que están siendo empleadas en los experimentos actuales. Las ALPs aparecen como predicciones de una gran variedad de extensiones más allá del ME. Algunos escenarios paradigmáticos incluyen: *(i)* el *Majoron*, que es el pBG nacido de la ruptura espontánea de la simetría de número leptónico en modelos que intentan explicar las pequeñas masas de los neutrinos; *(ii) axiflavons*, en teorías de sabor dinámico que intentan resolver tanto el problema de CP fuerte como el puzle del sabor; *(iii)* el *relaxion*, en teorías que abordan los problemas de CP fuerte y de jerarquía; *(iv) familons*, que surgen de la ruptura de simetrías globales de familia; *(v)* teoría de cuerdas; *(vi)* teorías que involucran dimensiones extra; o *(vii)* escenarios donde el bosón de Higgs es un pBG, como los modelos de Higgs compuesto. Los axiones y las ALPs también son candidatos a explicar la composición de la materia oscura, lo que aumenta su interés.

El objetivo principal de esta tesis es profundizar en la comprensión de la fenomenología de las ALPs, para permitir el descubrimiento de señales de ALP en los experimentos. Mis contribuciones han avanzado el conocimiento actual en dos direcciones:

- **ALPs en colisionadores.** En esta tesis propongo una nueva ventana de búsqueda para ALPs en colisionadores: ALPs no resonantes en procesos de *scattering* de bosones vectoriales en el LHC (*VBS* por sus siglas en inglés). Además, se presenta por primera vez el impacto de los acoplos electrodébiles del ALP y sus límites experimentales derivados de datos de colisionadores en el espacio de parámetros ALP-neutrino.

- **Teoría efectiva de campos del ALP.** La era de precisión de la física de partículas experimental requiere de predicciones teóricas que vayan más allá del nivel renormalizable e incluyan efectos de *running*. En esta tesis presento las ecuaciones completas del grupo de renormalización (EGR) de la TEC del ME —o *SMEFT* por sus siglas en inglés— extendido con un singlete escalar real hasta dimensión cinco y a una precisión de un *loop*, incluyendo interacciones que violan CP y la simetría *shift*, y teniendo en cuenta los efectos de mezcla en el sector escalar. Comparamos nuestros resultados con la TEC del ALP. Estos resultados se implementan en un nuevo paquete de `Mathematica` que permite resolver los EGR para un escenario UV dado.

Esta tesis está dividida en dos partes principales. La primera parte se extiende desde el Capítulo 1 hasta el 3 y presenta una revisión del ME, el problema de CP fuerte y los ALPs. La segunda parte se extiende desde el Capítulo 4 hasta el 6 y contiene la contribución original de esta tesis.

Part I

Foundations

Chapter 1

The Standard Model of Particle Physics

The SM is built as a quantum field theory (QFT) consistent with the principles of locality, causality and Lorentz symmetry, inherited from special relativity. Two ingredients hold the secrets to describe our universe: gauge symmetries and fields. Gauge symmetries determine the nature and properties of the distinct fundamental interactions, while particles arise as excitations of the fundamental fields, which correspond to different representations of the Lorentz symmetry group: scalars (*spin*-0), fermions (*spin*-$\frac{1}{2}$) and gauge bosons (*spin*-1).

All the SM predictive power can be boiled down to an astonishingly beautiful and compact Lagrangian

$$\mathscr{L}_{\text{SM}} = \mathscr{L}_{\text{gauge}} + \mathscr{L}_{\text{Dirac}} + \mathscr{L}_{\text{Yukawa}} + \mathscr{L}_{\text{Higgs}} + \mathscr{L}_{\theta} \,, \tag{1.0.1}$$

where

$$\begin{aligned}
\mathscr{L}_{\text{gauge}} &= -\frac{1}{4} G^{\alpha}_{\mu\nu} G^{\mu\nu,\alpha} - \frac{1}{4} W^{i}_{\mu\nu} W^{\mu\nu,i} - \frac{1}{4} B_{\mu\nu} B^{\mu\nu} \,, \\
\mathscr{L}_{\text{Dirac}} &= i\overline{Q}_L \not{D} Q_L + i\overline{U}_R \not{D} U_R + i\overline{D}_R \not{D} D_R + i\overline{L}_L \not{D} L_L + i\overline{E}_R \not{D} E_R \,, \\
\mathscr{L}_{\text{Yukawa}} &= -\overline{Q}_L \mathbf{Y}_u \tilde{\Phi} U_R - \overline{Q}_L \mathbf{Y}_d \Phi D_R - \overline{L}_L \mathbf{Y}_e \Phi E_R + \text{h.c.} \,, \\
\mathscr{L}_{\text{Higgs}} &= (D_\mu \Phi)^\dagger D^\mu \Phi + \mu^2 \Phi^\dagger \Phi - \lambda \left(\Phi^\dagger \Phi\right)^2 \,, \\
\mathscr{L}_{\theta} &= \theta \frac{\alpha_S}{8\pi} G^{\alpha}_{\mu\nu} \widetilde{G}^{\mu\nu,\alpha} \,.
\end{aligned} \tag{1.0.2}$$

In the following sections I will review the fundamental aspects of the SM, the role and properties of each of the fields involved in its Lagrangian, as well as the state of the art experimental measurements of its parameters.

1.1 The gauge sector

Gauge symmetries in the Standard Model are tightly connected to the three fundamental interactions in nature (other than gravity): the strong nuclear force, the weak nuclear force and electromagnetism. Each of these forces is related to a particular Lie group, and the product of all of them leads to the SM gauge group:

$$G_{\text{SM}} = SU(3)_C \times SU(2)_L \times U(1)_Y \,. \tag{1.1.1}$$

Here $SU(3)_C$ is the *color* group and is associated to strong interactions or *quantum chromodynamics* (QCD). $SU(2)_W$ is associated to weak interactions and $U(1)_Y$, to the hypercharge force, and the product of the two $SU(2)_L \times U(1)_Y$ is refered as the *electroweak* (EW) sector. The electromagnetic force is connected to a $U(1)_{EM}$ group, which lies "hidden" in the electroweak group

$$U(1)_{EM} \subset SU(2)_L \times U(1)_Y \,. \tag{1.1.2}$$

Each fundamental interaction is mediated by as many gauge bosons as infinitesimal generators the corresponding gauge group has. Which means that in the SM, 8 massless gluons $G_\mu^{\alpha=1,\dots,8}$ mediate strong interactions, and four gauge bosons $W_\mu^{i=1,2,3}$ and B_μ mediate the electroweak interactions.

$$\begin{aligned} SU(3)_C: &\qquad G_\mu^\alpha\,, \quad \alpha = 1,\dots,8 \\ SU(2)_L: &\qquad W_\mu^i\,, \quad i = 1,2,3 \\ U(1)_Y: &\qquad B_\mu\,. \end{aligned} \tag{1.1.3}$$

The kinetic terms of these gauge fields contribute to the SM Lagrangian as

$$\mathcal{L}_{\text{gauge}} = -\frac{1}{4} G_{\mu\nu}^\alpha G^{\mu\nu,\alpha} - \frac{1}{4} W_{\mu\nu}^i W^{\mu\nu,i} - \frac{1}{4} B_{\mu\nu} B^{\mu\nu}\,, \tag{1.1.4}$$

where $G_{\mu\nu}^\alpha$, $W_{\mu\nu}^i$ and $B_{\mu\nu}$ are the gauge field strength tensors

$$\begin{aligned} G_{\mu\nu}^\alpha &= \partial_\mu G_\nu^\alpha - \partial_\nu G_\mu^\alpha + g_S f_{\alpha\beta\gamma} G_\mu^\beta G_\nu^\gamma\,, \\ W_{\mu\nu}^i &= \partial_\mu W_\nu^i - \partial_\nu W_\mu^i + g \varepsilon_{ijk} W_\mu^j W_\nu^k\,, \\ B_{\mu\nu} &= \partial_\mu B_\nu - \partial_\nu B_\mu\,, \end{aligned} \tag{1.1.5}$$

$f_{\alpha\beta\gamma}$ and ε_{ijk} are the structure constants associated to the non-abelian Lie groups, $SU(3)$ and $SU(2)$, respectively, and g_S and g are the strong and weak coupling constants.

Eq. (1.1.4) describes the propagation and self-interactions of 12 massless gauge bosons. However, this picture is not complete, since experimental evidence indicate that only 9 physical gauge bosons (8 gluons and 1 photon) are massless, whereas other 3, the EW gauge bosons $W^\pm$ and Z, are massive. Moreover, adding an explicit mass term to Eq. (1.1.4) would violate gauge invariance, and therefore, a dynamical mechanism is needed to provide a mass to the physical gauge bosons. Namely, the Brout-Englert-Higgs (BEH) mechanism [6–8], more commonly known as "Higgs" mechanism.

1.2 The scalar sector

The Higgs mechanism adresses this problem by introducing a complex scalar doublet, Φ charged under $SU(2)_L$. The beauty of this mechanism lies in the fact that while the most general renormalizable Lagrangian involving the Higgs doublet,

$$\mathcal{L}_{\text{Higgs}} = (D_\mu \Phi)^\dagger D^\mu \Phi + \mu^2 \Phi^\dagger \Phi - \lambda \left(\Phi^\dagger \Phi\right)^2\,, \tag{1.2.1}$$

preserves the EW gauge symmetry $SU(2)_L \times U(1)_Y$, the vacuum of the theory v, i.e. the vacuum expectation value or *vev* of the scalar field,

$$\langle \Phi^\dagger \Phi \rangle \equiv \frac{v^2}{2} \equiv \frac{\mu^2}{2\lambda}\,, \tag{1.2.2}$$

does not exhibit this symmetry for μ^2, $\lambda > 0$. This is refered to as EW "spontaneous" symmetry breaking, which manifests at the Lagrangian level once we choose a specific *vev* satisfying Eq. (1.2.2), leaving a residual electromagnetic gauge symmetry $U(1)_{EM}$:

$$\langle \Phi \rangle = \frac{1}{\sqrt{2}} \begin{pmatrix} 0 \\ v \end{pmatrix} , \qquad SU(2)_L \times U(1)_Y \xrightarrow{\text{SSB}} U(1)_{EM} \,. \tag{1.2.3}$$

The Goldstone theorem [9, 10] states that whenever a continuous symmetry of the Lagrangian is spontaneously broken, spin-0 massless particles arise known as *Goldstone bosons*, with one of them per each broken generator. If the broken symmetry is gauge, these massless d.o.f. do not explicitly appear in the Lagrangian but get "eaten" by the originally massless gauge bosons in order to acquire a mass. Let us take a closer look to the Higgs the covariant derivative –required by gauge invariance–

$$D_\mu \Phi = \left(\partial_\mu + ig\frac{\sigma^i}{2} W^i_\mu + i\frac{g'}{2} B_\mu \right) \Phi \,, \tag{1.2.4}$$

where g' is the hypercharge $U(1)_Y$ coupling constant and σ^a are the Pauli matrices, plays a key role to provide gauge bosons with a physical mass in a gauge invariante way. After EW symmetry breaking, one out of the original four degrees of freedom (d.o.f.) of the Higgs doublet remains explicitly as the physical Higgs field h which corresponds to the excitations of a scalar field around the minimum of the potential

$$\Phi = \begin{pmatrix} \phi^+ \\ \phi^0 \end{pmatrix} \xrightarrow{\text{SSB}} \frac{1}{\sqrt{2}} \begin{pmatrix} 0 \\ v + h \end{pmatrix} . \tag{1.2.5}$$

This mechanism, therefore, predicts the existence of the Higgs boson, discovered in 2012 at CERN [11, 12]. The other three "missing" degrees of freedom correspond to the goldstone bosons of the spontaneously broken symmetry, which have been "eaten" by the EW gauge bosons:

$$(D_\mu \Phi)^\dagger D^\mu \Phi \xrightarrow{\text{SSB}} \frac{1}{2}\partial_\mu h \partial^\mu h + \frac{(v+h)^2}{4} g^2 W^+_\mu W^{-\mu} + \frac{(v+h)^2}{8} \left(g^2 + g'^2 \right) Z_\mu Z^\mu \,. \tag{1.2.6}$$

The physical gauge bosons, $W^\pm_\mu$, Z_μ and A_μ, originate from the mixing of the massless W^i_μ and B_μ gauge fields after the EW symmetry breaking:

$$\begin{aligned} W^\pm_\mu &\equiv \frac{1}{\sqrt{2}} \left(W^2_\mu \mp i W^2_\mu \right) , \\ Z_\mu &\equiv \cos\theta_W W^3_\mu - \sin\theta_W B_\mu \,, \\ A_\mu &\equiv \sin\theta_W W^3_\mu + \cos\theta_W B_\mu \,, \end{aligned} \tag{1.2.7}$$

where θ_W is the so-called weak mixing angle, defined at tree level as

$$\tan\theta_W \equiv \frac{g}{g'} \,, \tag{1.2.8}$$

and whose value is determined experimentally with extraordinary precision [13]: $\sin^2\theta_W = 0.22339(10)$.

The $W^\pm_\mu$ and Z_μ fields correspond to the massive physical gauge bosons, while the photon field A_μ remains massless. This is a consequence of the residual electromagnetic gauge symmetry $U(1)_{EM}$ that survives the EW spontaneous symmetry breaking:

$$SU(2)_L \times U(1)_Y \xrightarrow{\text{SSB}} U(1)_{EM} \qquad e \equiv g \sin\theta_W = g' \cos\theta_W \,, \tag{1.2.9}$$

where e is the electromagnetic coupling constant. From Eq. (1.2.6), we obtain the masses for the physical gauge bosons:

$$M_W = \frac{vg}{2}\,, \qquad M_Z = \frac{v\left(g^2+g'^2\right)^{1/2}}{2}\,, \tag{1.2.10}$$

whose most recent world average values are [13]

$$M_W = 80.377 \pm 0.012 \text{ GeV}\,, \qquad M_Z = 91.1876 \pm 0.0021 \text{ GeV}\,. \tag{1.2.11}$$

As for the Higgs self-interactions, after EW symmetry breaking we obtain

$$\mathscr{L}_{\text{Higgs}} \subset \mu^2\Phi^\dagger\Phi - \lambda\left(\Phi^\dagger\Phi\right)^2 \xrightarrow{\text{SSB}} -\frac{m_h^2}{2}h^2 - \frac{\lambda_{h^3}}{3!}h^3 - \frac{\lambda_{h^4}}{4!}h^4\,, \tag{1.2.12}$$

where $m_h = \sqrt{2}\mu$ is the Higgs mass, and λ_{h^3} and λ_{h^4} are the triple and quartic gauge couplings, respectively:

$$\lambda_{h^3} = 3\frac{m_h^2}{v}\,, \qquad \lambda_{h^4} = 3\frac{m_h^2}{v^2}\,, \tag{1.2.13}$$

which satisfy at tree level the relation $\lambda_{h^3} = v\lambda_{h^4}$. The world average experimental values for the Higgs mass and *vev* [13] are

$$m_h = 125.25 \pm 0.17 \text{ GeV}\,, \qquad v = 246.2196402393(15) \text{ GeV}\,. \tag{1.2.14}$$

1.3 The fermion sector

While gauge fields are a consequence of the fundamental symmetries of the SM and the Higgs field answers the need for a dynamical mechanism to provide mass in a gauge invariant way, the fermion fields are not derived from any first principle in the theory but through observations.

They constitute the building blocks of matter and are categorized into quarks and leptons, which can be classified according to their EW gauge charge. There are 3 quark fields: one left-handed (LH) $SU(2)_L$ doublet –Q_L–, and two right-handed (RH) singlets –U_R and D_R; and 2 lepton fields, a LH doublet –L_L– and one RH singlet E_R. Observations show that each of these fermion fields appears in 3 families, generations or *flavors* with identical quantum numbers but different masses and mixings, and can be written in a compact way as:

$$\begin{aligned} Q_L &= \begin{pmatrix} U_L \\ D_L \end{pmatrix} = \left\{\begin{pmatrix} u_L \\ d_L \end{pmatrix}, \begin{pmatrix} c_L \\ s_L \end{pmatrix}, \begin{pmatrix} t_L \\ b_L \end{pmatrix}\right\}, & U_R &= \{u_R, c_R, t_R\}\,, \\ & & D_R &= \{d_R, s_R, b_R\}\,, \\ L_L &= \begin{pmatrix} \nu_L \\ E_L \end{pmatrix} = \left\{\begin{pmatrix} \nu_L^e \\ e_L \end{pmatrix}, \begin{pmatrix} \nu_L^\mu \\ \mu_L \end{pmatrix}, \begin{pmatrix} \nu_L^\tau \\ \tau_L \end{pmatrix}\right\}, & E_R &= \{e_R, \mu_R, \tau_R\}\,. \end{aligned} \tag{1.3.1}$$

Notice that there is no RH counterpart for neutrinos in the SM, at least disregarding neutrino masses. Only LH neutrinos and RH anti-neutrinos have been “observed” at experiments, and therefore a LH Weyl fermion $\nu_L^{e,\mu,\tau}$ suffices.

The transformation properties of the fundamental fermions are determined exclusively by observation of particle interactions and gauge anomaly cancellation (necessary

	$SU(3)_C$	$SU(2)_L$	$U(1)_Y$
G_μ	**8**	**1**	0
W_μ	**1**	**3**	0
B_μ	**1**	**1**	-1
Φ	**1**	**2**	1/2
Q_L	**3**	**2**	1/6
U_R	**3**	**1**	2/3
D_R	**3**	**1**	-1/3
L_L	**1**	**2**	-1/2
E_R	**1**	**1**	-1

	T_3	Y	Q
U_L	1/2	1/6	2/3
D_L	-1/2	1/6	-1/3
U_R	0	2/3	2/3
D_L	0	-1/3	-1/3
ν_L	1/2	-1/2	0
E_L	-1/2	-1/2	-1
E_R	0	-1	-1

Table 1.1: Transformation properties of the SM fundamental fields under its gauge group $G_{\rm SM} = SU(3)_C \times SU(2)_L \times U(1)_Y$.

to ensure the quantum consistency of the SM gauge symmetry). Experimental evidence shows that EW interactions do not preserve parity and consequently, LH and RH fermions transform differently under $SU(2)_L$, i.e. EW interactions are chiral. In the SM, LH fermions transform as doublets under $SU(2)_L$ while RH fermions are singlets. Similarly, LH and RH fermion field transform differently under $U(1)_Y$, as shown by their hypercharges in Tab. 1.1. After EW symmetry breaking, the EM charge Q of the fermion fields is obtained from their third component of weak isospin $T_3 \equiv \frac{\sigma_3}{2}$ and their weak hypercharge Y:

$$Q = T_3 + Y\,, \tag{1.3.2}$$

which turns out to be identical for LH and RH fermions, i.e., electromagnetism is a vectorial interaction and therefore preserves parity. The same happens for QCD, where quarks "live" in the fundamental representation of $SU(3)_C$ while leptons are singlets, this is, they do not carry color charge.

The kinetic and interaction terms of the SM fermion are contained in

$$\mathscr{L}_{\rm Dirac} = i\overline{Q}_L \not{D} Q_L + i\overline{U}_R \not{D} U_R + i\overline{D}_R \not{D} D_R + i\overline{L}_L \not{D} L_L + i\overline{E}_R \not{D} E_R\,, \tag{1.3.3}$$

where $\not{D} \equiv D_\mu \gamma^\mu$ is the fermionic covariant derivative –required to preserve gauge symmetry in the fermion sector– and γ^μ are the Dirac matrices:

$$\begin{aligned}
D_\mu Q_L &= \left(\partial_\mu + i g_S \frac{\lambda^\alpha}{2} G^\alpha_\mu + i g \frac{\sigma^i}{2} W^i_\mu + i \frac{g'}{6} B_\mu\right) Q_L\,,\\
D_\mu U_R &= \left(\partial_\mu + i g_S \frac{\lambda^\alpha}{2} G^\alpha_\mu + i \frac{2g'}{3} B_\mu\right) U_R\,,\\
D_\mu D_R &= \left(\partial_\mu + i g_S \frac{\lambda^\alpha}{2} G^\alpha_\mu - i \frac{g'}{3} B_\mu\right) U_R\,,\\
D_\mu L_L &= \left(\partial_\mu + i g \frac{\sigma^i}{2} W^i_\mu - i \frac{g'}{2} B_\mu\right) L_L\,,\\
D_\mu E_R &= \left(\partial_\mu - i g' B_\mu\right) E_R\,,
\end{aligned} \tag{1.3.4}$$

where λ^α denote the Gell-Mann matrices. Notice that the theory is defined from its gauge symmetries and matter content, while the number of gauge bosons, their self-interactions and their interactions with all the fermions in the theory are predicted from the gauge principle once a gauge group is chosen.

Eq.(1.3.3) describes the propagation and interactions of massless fermions, and in fact gauge invariance leaves no room for fermion mass terms. These, however, are encoded in a gauge invariant way in their interactions with the Higgs doublet

$$\mathscr{L}_{\text{Yukawa}} = -\overline{Q}_L \mathbf{Y}_u \tilde{\Phi} U_R - \overline{Q}_L \mathbf{Y}_d \Phi D_R - \overline{L}_L \mathbf{Y}_e \Phi E_R + \text{h.c.}\,, \tag{1.3.5}$$

where $\mathbf{Y}_{u,d,e}$ are, in all generality, 3×3 non-diagonal complex matrices in flavor space and $\tilde{\Phi} \equiv i\sigma^2\Phi^*$. Once the Higgs develops a non-vanishing (*vev*), leading to EW symmetry breaking (Eq. (1.2.5)), the SM fermions acquire a mass:

$$\begin{aligned}\mathscr{L}_{\text{Yukawa}} \xrightarrow{\text{SSB}} & -\overline{U}_L \mathbf{M}_u U_R - \overline{D}_L \mathbf{M}_d D_R - \overline{E}_L \mathbf{M}_e E_R \\ & - h\overline{U}_L \frac{\mathbf{Y}_u}{\sqrt{2}} U_R - h\overline{D}_L \frac{\mathbf{Y}_D}{\sqrt{2}} D_R - h\overline{E}_L \frac{\mathbf{Y}_e}{\sqrt{2}} E_R + \text{h.c.}\,,\end{aligned} \tag{1.3.6}$$

where

$$\mathbf{M}_f \equiv \frac{\mathbf{Y}_f v}{\sqrt{2}} \tag{1.3.7}$$

are the Dirac mass matrices of the fermions. As a consequence of this mechanism, the interactions between the SM fermions and the physical Higgs h are now proportional to the fermion masses.

Similarly, after EW symmetry breaking, the covariant derivatives in Eq. (1.3.4) for LH and RH fermions become

$$\begin{aligned}D_\mu f_L &\xrightarrow{\text{SSB}} \left[\partial_\mu + i\frac{g}{\sqrt{2}}\left(\sigma_+ W_\mu^+ + \sigma_- W_\mu^-\right) + i\frac{g}{\cos\theta_W}\left(T_3 - Q\sin^2\theta_W\right) Z_\mu + ieQA_\mu\right] f_L\,, \\ D_\mu f_R &\xrightarrow{\text{SSB}} \left[\partial_\mu - i\frac{g}{\cos\theta_W} Q\sin^2\theta_W Z_\mu + ieQA_\mu\right] f_R\,,\end{aligned}$$

where $\sigma_\pm \equiv \frac{\sigma_1 \pm i\sigma_2}{\sqrt{2}}$.

The fermion mass matrices can be made diagonal and real via fermion field redefinitions

$$\begin{aligned} U_L &\to \mathbf{V}_L^u U_L & D_L &\to \mathbf{V}_L^d D_L & E_L &\to \mathbf{V}_L^e E_L\,, \\ U_R &\to \mathbf{V}_R^u U_R & D_R &\to \mathbf{V}_R^d D_R & E_R &\to \mathbf{V}_R^e E_R\,, \end{aligned} \tag{1.3.8}$$

where $\mathbf{V}_{L,R}^f$ are unitary matrices $\mathbf{V}_{L,R}^{f\dagger}\mathbf{V}_{L,R}^f = \mathbb{1}$. These act as bilinear transformations on the mass matrices:

$$\begin{aligned}\mathbf{M}_u^{\text{diag}} &= \mathbf{V}_L^{u\dagger}\mathbf{M}_u\mathbf{V}_R^u = \text{diag}\left(m_u,\, m_c,\, m_t\right)\,, \\ \mathbf{M}_d^{\text{diag}} &= \mathbf{V}_L^{d\dagger}\mathbf{M}_d\mathbf{V}_R^d = \text{diag}\left(m_d,\, m_s,\, m_b\right)\,, \\ \mathbf{M}_e^{\text{diag}} &= \mathbf{V}_L^{e\dagger}\mathbf{M}_e\mathbf{V}_R^e = \text{diag}\left(m_e,\, m_\mu,\, m_\tau\right)\,,\end{aligned} \tag{1.3.9}$$

where m_f are the physical fermion masses, whose most recent experimental world average values according to the Particle Data Group collaboration [13] read

$$\begin{aligned} m_u &= 2.16^{+0.49}_{-0.26}\ \text{MeV}\,, & m_d &= 4.67^{+0.48}_{-0.17}\ \text{MeV}\,, & m_e &= 510.99895000(15)\ \text{keV}\,, \\ m_c &= 1.27 \pm 0.02\ \text{MeV}\,, & m_s &= 93.4^{+8.6}_{-3.4}\ \text{MeV}\,, & m_\mu &= 105.6583755(23)\ \text{MeV}\,, \\ m_t &= 172.69 \pm 0.30\ \text{GeV}\,, & m_b &= 4.18^{+0.03}_{-0.02}\ \text{GeV}\,, & m_\tau &= 1776.86 \pm 0.12\ \text{MeV}\,. \end{aligned} \tag{1.3.10}$$

These fermion field redefinitions however are not a symmetry of the theory. For instance, while fermion interactions with neutral gauge bosons, G_μ, Z_μ and A_μ remain unchanged, those with the $W_\mu^\pm$ do not, leading to flavor-changing charged current interactions in the quark sector[1]

$$\mathscr{L}_{\text{Dirac}} \supset -\frac{g}{\sqrt{2}}\left(\overline{U}_L\gamma^\mu W_\mu^+ \mathbf{V}_{\text{CKM}} D_L + \text{h.c.}\right) , \tag{1.3.11}$$

where $\mathbf{V}_{\text{CKM}} \equiv \mathbf{V}_L^{u\dagger}\mathbf{V}_L^d$ is the Cabibbo-Kobayashi-Maskawa (CKM) matrix [14, 15]

$$\mathbf{V}_{\text{CKM}} = \begin{pmatrix} V_{\text{ud}} & V_{\text{us}} & V_{\text{ub}} \\ V_{\text{cd}} & V_{\text{cs}} & V_{\text{cb}} \\ V_{\text{td}} & V_{\text{ts}} & V_{\text{tb}} \end{pmatrix} , \tag{1.3.12}$$

which describes the mixing in flavor between LH up- and down-type quarks. This matrix is physical and measureable, and its unitarity –predicted within the SM– has actually been tested experimentally with astonishing agreement so far.

1.3.1 Quark sector

Let us now identify the physical degrees of freedom in the quark sector. The Yukawa couplings $\mathbf{Y}_u$ and $\mathbf{Y}_d$ are general complex matrices, defined by $2n_g^2$ real parameters (where n_g is the number of fermion generations). There is a global flavor symmetry $\mathcal{G}_f^{\text{quark}}$ in the quark sector explicitly broken by the Yukawas, leaving a residual $U(1)_B$ baryon number symmetry:

$$\mathcal{G}_f^{\text{quark}} \equiv U(3)_Q \times U(3)_D \times U(3)_D \longrightarrow U(1)_B \, , \tag{1.3.13}$$

where $U(3)_Q \times U(3)_D \times U(3)_D$ are unitary rotations in flavor space of the Q_L, U_R and D_R quark fields, respectively[2]. These rotations, excluding the residual $U(1)_B$ symmetry, can be used to reabsorb unphysical parameters in the Yukawas, which means that within the quark sector there are

$$\text{d.o.f}\,(\mathbf{Y}_u) + \text{d.o.f}\,(\mathbf{Y}_d) - \text{d.o.f}\left(U(n_g)^3\right) + \text{d.o.f}\,(U(1)_B) = 2n_g^2 + 2n_g^2 - 3n_g^2 + 1 = n_g^2 + 1 \tag{1.3.14}$$

degrees of freedom, which for $n_g = 3$ correspond the 6 quark masses and to the 4 physical parameters of the CKM matrix.

With this in mind the CKM can be parametrized in terms of three mixing angles, θ_{12}, θ_{13} and θ_{23}, and a CP-violating phase δ:

$$\mathbf{V}_{\text{CKM}} = \begin{pmatrix} 1 & 0 & 0 \\ 0 & c_{23} & s_{23} \\ 0 & -s_{23} & c_{23} \end{pmatrix} \begin{pmatrix} c_{13} & 0 & s_{13}e^{-i\delta} \\ 0 & 1 & 0 \\ -s_{13} & 0 & c_{13} \end{pmatrix} \begin{pmatrix} c_{12} & s_{12} & 0 \\ -s_{12} & c_{12} & 0 \\ 0 & 0 & 1 \end{pmatrix} \tag{1.3.15}$$

$$= \begin{pmatrix} c_{12}c_{13} & s_{12}c_{13} & s_{13}e^{-i\delta} \\ -s_{12}c_{23} - c_{12}s_{13}s_{23}e^{i\delta} & c_{12}c_{23} - s_{12}s_{13}s_{23}e^{i\delta} & s_{23}c_{13} \\ s_{12}s_{23} - c_{12}s_{13}c_{23}e^{i\delta} & -c_{12}s_{23} - s_{12}s_{13}c_{23}e^{i\delta} & c_{23}c_{13} \end{pmatrix} , \tag{1.3.16}$$

[1]The lepton sector is not affected by flavor mixing because neutrinos are massless, within the SM.

[2]Actually, a particular combination $U(1)_A$ of these rotations is anomalous, i.e. it is a symmetry at the classical level but not at the quantum level. This is known as the axial anomaly, and when taken into account it leads to an additional physical d.o.f. in eq. (1.3.18), related to the θ_{QCD} parameter. This will be further discussed in Chap. 2.

where $c_{ij} \equiv \cos\theta_{ij}$ and $s_{ij} \equiv \sin\theta_{ij}$, and $\theta_{ij} \in [0, \pi/2]$. These is the most recent global fit result by the Particle Data Group collaboration [13] for the modulus of CKM components

$$|\mathbf{V}_{\mathrm{CKM}}| = \begin{pmatrix} 0.97435 \pm 0.00016 & 0.22500 \pm 0.00067 & 0.00369 \pm 0.00011 \\ 0.22486 \pm 0.00067 & 0.97349 \pm 0.00016 & 0.04182^{+0.00085}_{-0.00074} \\ 0.00857^{+0.00018}_{-0.00020} & 0.04110^{+0.00083}_{-0.00072} & 0.999118^{+0.000031}_{0.000036} \end{pmatrix} \tag{1.3.17}$$

and its complex phase $\delta = 1.144 \pm 0.02$.

1.3.2 Lepton sector

If we now consider the lepton sector disregarding neutrino masses, we observe a global flavor symmetry $\mathcal{G}_f^{\mathrm{lepton}}$ only broken by the Yukawa coupling $\mathbf{Y}_e$, which only preserves the three lepton family lepton number symmetries:

$$\mathcal{G}_f^{\mathrm{quark}} \equiv U(3)_Q \times U(3)_D \times U(3)_D \longrightarrow U(1)_e \times U(1)_\mu \times U(1)_\tau \,. \tag{1.3.18}$$

In this scenario, there are

$$\mathrm{d.o.f}\,(\mathbf{Y}_e) - \mathrm{d.o.f}\left(U(n_g)^2\right) + \mathrm{d.o.f}\left(U(1)^3\right) = 2n_g^2 - 2n_g^2 + 3 = 3 \tag{1.3.19}$$

degrees of freedom, corresponding to the 3 charged lepton masses.

Although astonishingly successful, we know that the SM cannot have the last word. As discussed in the previous section, no flavor mixing is predicted in the lepton sector. Nevertheless, we have solid experimental evidence of "neutrino oscillations", one of the strongest proofs of physics beyond the SM (BSM). These require at least two massive neutrinos and mixing in the lepton sector. This is described in terms of a mixing matrix –equivalent to the CKM in the quark sector– known as the Pontercorvo-Maki-Nakagawa-Sakata (PMNS) matrix $\mathbf{U}_{\mathrm{PMNS}}$ [16, 17],

$$\mathscr{L}_{\mathrm{Dirac}}^{\mathrm{BSM}} \supset -\frac{g}{\sqrt{2}}\left(\overline{\nu}_L \gamma^\mu W_\mu^+ \mathbf{U}_{\mathrm{PMNS}} E_L + \mathrm{h.c.}\right)\,, \tag{1.3.20}$$

with three independent mixing angles and one CP-violating complex phase. The most recent global fit using data from the NuFit collaboration has set the following 3σ limits for the modulus of the PMNS matrix elements [18]

$$|\mathbf{U}_{\mathrm{PMNS}}| = \begin{pmatrix} 0.801 \to 0.845 & 0.513 \to 0.579 & 0.143 \to 0.155 \\ 0.234 \to 0.500 & 0.471 \to 0.689 & 0.637 \to 0.776 \\ 0.271 \to 0.525 & 0.477 \to 0.694 & 0.613 \to 0.756 \end{pmatrix}, \tag{1.3.21}$$

and measured the PMNS CP-violating phase to be $\delta = 195^{+51}_{-24}$ and $\delta = 286^{+27}_{-32}$ for normal ordering (NO) and inverted ordering (IO), respectively. Normal ordering corresponds to the scenario in which the neutrino mass eigenstates $\{\nu_1,\ \nu_2,\ \nu_3\}$ are mainly composed of the EW eigenstates $\{\nu_e,\ \nu_\mu,\ \nu_\tau\}$, respectively, with ascending order in masses, this is $m_1 < m_2 < m_3$. Inverted ordering describes the alternative scenario in which $m_3 < m_1 < m_2$. Similarly, the best fit values for the mass squared differences $\delta m_{ij} \equiv m_{\nu_i}^2 - m_{\nu_j}^2$ between the three generations [18] are

$$\delta m_{21}^2 = (7.42^{+0.21}_{-0.20} \times 10^{-5}\ \mathrm{eV})\,, \quad \delta m_{3\ell}^2 = \left\{ \begin{array}{c} +(2.517^{+0.026}_{-0.028}) \times 10^{-3}\ \mathrm{eV}^2\ \mathrm{NO} \\ -(2.498^{+0.028}_{-0.028}) \times 10^{-3}\ \mathrm{eV}^2\ \mathrm{IO} \end{array} \right., \tag{1.3.22}$$

where $\delta_{3\ell}^2 \equiv \delta_{31}^2 > 0$ for NO, and $\delta_{3\ell}^2 \equiv \delta_{32}^2 < 0$ for IO.

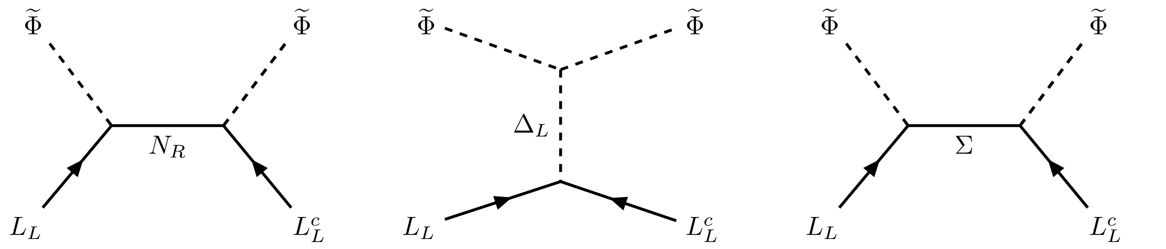

Figure 1.1: The three basic seesaw models: type-I, mediated by a fermionic singlet N_R, type-II mediated by a scalar $SU(2)_L$ triplet Δ_L, and type-III, mediated by a fermionic $SU(2)_L$ triplet Σ.

The origin of neutrino masses, however, remains uncertain. One of the simplest options is introducing three RH neutrinos N_R^i, singlets under the SM gauge group, also known as *sterile* neutrinos, which allow for a Dirac mass term:

$$\mathscr{L}_\nu \supset -\overline{L}_L \mathbf{Y}_\nu \tilde{\Phi} N_R + \text{h.c.}\,. \tag{1.3.23}$$

where $\mathbf{Y}_\nu$ is the complex 3×3 Yukawa matrix. If neutrinos are Dirac fermions, then $(\mathbf{Y}_\nu)^{ii} \lesssim 10^{-12}$, with $i = 1, 2, 3$. However, neutrinos can also be Majorana particles, i.e. fermions which are their own antiparticles, since gauge invariance allows Majorana mass terms. In the effective field theory (EFT) approach, these arise from the (only) dimension $d = 5$ operator, i.e. the Weinberg operator [19]:

$$\mathscr{L}_{d=5} = \frac{\overline{L}_L^c \tilde{\Phi}^* \tilde{\Phi}^\dagger L_L}{\Lambda}\,, \tag{1.3.24}$$

where Λ is the new physics scale. After EWSB, a Majorana mass term for the LH neutrinos is originated from the Weinberg operator, proportional to v^2/Λ, which provides an explanation for the smallness of neutrino masses under the assumption that $\Lambda \gg v$. This is known as the *seesaw mechanism* [20].

Since EFTs are a model independent approach, the Weinberg operator can be generated at lower energies from distinct UV scenarios, once heavy d.o.f. are integrated out. For instance, when a Majorana mass term for the sterile neutrinos N_R^i is included in Eq. (1.3.23), we have the type-I *seesaw* [20–23]:

$$\mathscr{L}_\nu = -\overline{L}_L \mathbf{Y}_\nu \tilde{\Phi} N_R - \frac{1}{2} \overline{N}_R^c \mathbf{M}_N^M N_R + \text{h.c.}\,, \tag{1.3.25}$$

where $N_R^c \equiv C\overline{N}_R^T$, with the charge conjugation matrix $C \equiv i\gamma_2\gamma_1$ and $\mathbf{M}_N^M$ is the symmetric 3×3 Majorana mass matrix. After EWSB, masses are generated

$$\mathscr{L}_\nu \xrightarrow{\text{SSB}} -\overline{\nu}_L \mathbf{M}_\nu^D N_R - \frac{1}{2} \overline{N}_R^c \mathbf{M}_N^M N_R - h\overline{\nu} - h\overline{\nu}_L \frac{\mathbf{Y}_\nu}{\sqrt{2}} N_R \text{h.c.}\,, \tag{1.3.26}$$

where $\mathbf{M}_\nu^D \equiv \mathbf{Y}_\nu v/\sqrt{2}$ is the Dirac neutrino mass. This can be expressed in terms of a neutrino mass matrix

$$-\frac{1}{2} \begin{pmatrix} \overline{\nu}_L & \overline{N}_R^c \end{pmatrix} \begin{pmatrix} 0 & \mathbf{M}_\nu^D \\ (\mathbf{M}_\nu^D)^T & \mathbf{M}_N^M \end{pmatrix} \begin{pmatrix} \nu_L \\ N_R \end{pmatrix}\,. \tag{1.3.27}$$

After block diagonalization, we obtain

$$\mathbf{M}_\nu \approx -(\mathbf{M}_\nu^D)^T (\mathbf{M}_N^M)^{-1} \mathbf{M}_\nu^D\,, \qquad\qquad \mathbf{M}_N \approx \mathbf{M}_N^M\,, \tag{1.3.28}$$

where the LH neutrino mass is suppressed by the RH Majorana mass $\mathbf{M}_N^M$, which is a free parameter of the theory and can be arbitrarily large since it is not protected by any symmetry. Similarly, as depicted in Fig. 1.1, the type-II [24–28] and type-III *seesaws* [29–35] lead to the Weinberg operator after integrating out the exotic scalar and fermion $SU(2)_L$ triplets, respectively.

We will disregard neutrino masses in the actual computations of this thesis, unless otherwise stated, as they have negligible impact.

1.4 SM equations of motion

In this section we present the SM equations of motion (EOM) for the fermion and Higgs fields, which will be relevant for our discussion in Sec. 3.1. For chiral fermions, the EOM are the following:

$$i\not{D}Q_L = \Phi \mathbf{Y}_d D_R + \tilde{\Phi}\mathbf{Y}_u U_R\,, \qquad i\not{D}U_R = \tilde{\Phi}^\dagger \mathbf{Y}_u^\dagger Q_L\,, \qquad i\not{D}D_R = \Phi^\dagger \mathbf{Y}_d^\dagger Q_L\,, \tag{1.4.1}$$

$$i\not{D}L_L = \Phi \mathbf{Y}_e E_R\,, \qquad i\not{D}E_R = \Phi^\dagger \mathbf{Y}_e^\dagger L_L\,, \tag{1.4.2}$$

where the sum over flavor indices is implicit. Similarly, for the Higgs field we have

$$\Box\Phi_i = -\left[\overline{D}_R \mathbf{Y}_d^\dagger (Q_L)_i + (\overline{Q}_L i\sigma^2)_i \mathbf{Y}_u U_R + \overline{E}_R \mathbf{Y}_e^\dagger (L_L)_i\right] + \frac{m_h^2}{2}\Phi_i - 2\lambda(\Phi^\dagger\Phi)\Phi_i\,, \tag{1.4.3}$$

where i denotes the $SU(2)_L$ index.

At the classical level, the use of fermion EOM is equivalent to chiral rotations of fermion fields. However, when considering loop effects, contributions from the SM anomalous global currents must be taken into account [36]:

$$\partial_\mu\left(\overline{Q}_L^f\gamma^\mu Q_L^f\right) \supset \frac{g'^2}{96\pi^2}B_{\mu\nu}\widetilde{B}^{\mu\nu} + \frac{3g^2}{32\pi^2}W^i_{\mu\nu}\widetilde{W}^{i\mu\nu} + \frac{g_S^2}{16\pi^2}G^\alpha_{\mu\nu}\widetilde{G}^{\alpha\mu\nu}\,, \tag{1.4.4}$$

$$\partial_\mu\left(\overline{U}_R^f\gamma^\mu U_R^f\right) \supset -\frac{g'^2}{12\pi^2}B_{\mu\nu}\widetilde{B}^{\mu\nu} - \frac{g_S^2}{32\pi^2}G^\alpha_{\mu\nu}\widetilde{G}^{\alpha\mu\nu}\,, \tag{1.4.5}$$

$$\partial_\mu\left(\overline{D}_R^f\gamma^\mu D_R^f\right) \supset -\frac{g'^2}{48\pi^2}B_{\mu\nu}\widetilde{B}^{\mu\nu} - \frac{g_S^2}{32\pi^2}G^\alpha_{\mu\nu}\widetilde{G}^{\alpha\mu\nu}\,, \tag{1.4.6}$$

$$\partial_\mu\left(\overline{L}_L^f\gamma^\mu L_L^f\right) \supset \frac{g'^2}{32\pi^2}B_{\mu\nu}\widetilde{B}^{\mu\nu} + \frac{g^2}{32\pi^2}W^i_{\mu\nu}\widetilde{W}^{i\mu\nu}\,, \tag{1.4.7}$$

$$\partial_\mu\left(\overline{E}_R^f\gamma^\mu E_R^f\right) \supset -\frac{g'^2}{16\pi^2}B_{\mu\nu}\widetilde{B}^{\mu\nu}\,, \tag{1.4.8}$$

where we are not summing over the flavor index f.

Chapter 2

The Strong-CP Problem and the Axion Solution

2.1 Instantons and the QCD vacuum

After EWSB, the QCD Lagrangian, $\mathscr{L}_{\rm QCD}$ reads

$$\mathscr{L}_{\rm QCD} = -\frac{1}{4}G^{\alpha}_{\mu\nu}G^{\mu\nu,\alpha} + \theta\frac{\alpha_S}{8\pi}G^{\alpha}_{\mu\nu}\widetilde{G}^{\mu\nu,\alpha} + \overline{Q}(i\not{D} - \mathbf{M}_Q)Q + \text{h.c.}\,, \tag{2.1.1}$$

where $Q = Q_R + Q_L$ for $Q = U,\, D$, and $M_{u,d}$ are the complex mass matrices defined in eq. (1.3.7). This Lagrangian contains all the possible sources of CP violation in the SM: the quark mass matrices[1] and the θ-parameter.

If we now define the Chern-Simons current

$$K^{\mu} \equiv 2\varepsilon^{\mu\nu\rho\sigma}G^{\alpha}_{\nu}\left(\partial_{\rho}G^{\alpha}_{\rho} + \frac{g_S}{3}f_{\alpha\beta\gamma}G^{\beta}_{\rho}G^{\gamma}_{\sigma}\right) = \varepsilon^{\mu\nu\rho\sigma}G^{\alpha}_{\nu}\left(G^{\alpha}_{\rho\sigma} - \frac{g_S}{3}f_{\alpha\beta\gamma}G^{\beta}_{\rho}G^{\gamma}_{\sigma}\right)\,, \tag{2.1.2}$$

it becomes clear that the $G^{\alpha}_{\mu\nu}\widetilde{G}^{\mu\nu,\alpha}$ is equivalent to its total derivative[2]

$$\partial_{\mu}K^{\mu} = \partial_{\mu}\left[\varepsilon^{\mu\nu\rho\sigma}G^{\alpha}_{\nu}\left(G^{\alpha}_{\rho\sigma} - \frac{g_S}{3}f_{\alpha\beta\gamma}G^{\beta}_{\rho}G^{\gamma}_{\sigma}\right)\right] = G^{\alpha}_{\mu\nu}\widetilde{G}^{\mu\nu,\alpha}\,, \tag{2.1.3}$$

suggesting that the θ-term can be integrated out from the action $S = \int d^4x\mathscr{L}$, as it is a boundary term.

However this is only true if the gluon fields G^{α}_{μ} decay sufficiently fast with distance — in the limit $r \to \infty$ — as $G^{\alpha}_{\mu} \sim \frac{1}{r^{1+\epsilon}}$, with $\epsilon > 0$, which does not hold for QCD. There are gauge-field configurations in the QCD vacuum that do not satisfy this condition, leading to finite boundary terms, and therefore contributing to the action. These configurations generate a non-trivial QCD vacuum structure and are called *instantons* [37–39]. Instantons are classical finite-action solutions of the gluon equation of motion (EOM) in Euclidian spacetime, which is obtained when replacing the Minkowski time t by $\tau \equiv it$, which turns the metric Euclidian $(+,+,+,+)$. The contribution of the Yang-Mills $\mathscr{L}_{\rm gauge}$ QCD term to the Euclidean action S_E reads

$$S_E \supset -\frac{1}{2}\int d^4x \mathrm{Tr}\left[G_{\mu\nu}G^{\mu\nu}\right]\,, \tag{2.1.4}$$

[1] After diagonalization into the physical mass matrix, its CP-violation is boiled down to the complex phase δ of the CKM.

[2] This is known as Bardeen's identity.

where $G_{\mu\nu} \equiv G^{\alpha}_{\mu\nu}\lambda^{\alpha}/2$, from which the usual gauge field EOM is derived

$$D_\mu G^{\mu\nu} = 0\,. \tag{2.1.5}$$

For a given a field $G_\mu = G^{\alpha}_{\mu}\lambda^{\alpha}/2$, its gauge transformed field $G^{(\Omega)}_\mu$ reads

$$G^{(\Omega)}_\mu = \Omega(x) G_\mu \Omega^{-1}(x) + \frac{i}{g_S}\Omega(x)\partial_\mu \Omega^{-1}(x)\,, \tag{2.1.6}$$

where $\Omega(x)$ is a map from space into elements of the QCD gauge group:

$$\Omega(x) = e^{i\omega^\alpha \frac{\lambda^\alpha}{2}}\,. \tag{2.1.7}$$

The trivial solution to Eq. (2.1.5) is $G_{\mu\nu} = 0$ which corresponds to the so called *pure gauge configurations*, i.e., the null gluon field $G_\mu = 0$ and any of its gauge transformations:

$$G^{(\Omega)}_\mu = \frac{i}{g_S}\Omega(x)\partial_\mu \Omega^{-1}(x)\,. \tag{2.1.8}$$

However, we are interested in the non-trivial solutions. For the action in Eq. (2.1.4) to be finite when integrating in the Euclidean R^4 space, its integrand must decrease faster than

$$G_{\mu\nu}G^{\mu\nu} \sim 1/r^{4+\epsilon} \implies G_{\mu\nu} \sim 1/r^{2+\epsilon}\,, \tag{2.1.9}$$

for large distances $r \to \infty$ and $\epsilon > 0$, where r is the radial coordinate in a S^3 sphere. We might conclude from this that gluon fields need to go as $G_\mu \sim 1/r^{1+\epsilon}$ at large distances, but this is not complete, as we must take into account any of the gauge transformations of such expression:

$$G^{(\Omega)}_\mu \sim \mathcal{O}\left(\frac{1}{r^{1+\epsilon}}\right) + \frac{i}{g_S}\Omega(x)\partial_\mu \Omega^{-1}(x)\,, \tag{2.1.10}$$

which tend to *pure gauge configurations* at infinity. Consequently, these solutions are determined by the element of the QCD gauge group $\Omega(x)$ evaluated at $r \to \infty$, i.e., by functions of the 3-sphere at infinity —S^3_∞— to the gauge group: $\Omega(x) : S^3_\infty \to SU(3)_C$.

Not all of these field configurations can be gauge transformed into the trivial one $G_\mu = 0$. The different $\Omega(x)$ maps, at infinity, fall into disjoint *homotopy* classes, i.e., not all of them can be connected via a continuous transformation. It can be shown that for any non-abelian $SU(N)$ gauge group these different classes are characterized by an integer called *Pontryagin index* or *winding number* [37–39],

$$\nu(\Omega) \equiv \frac{1}{24\pi^2}\int_{S^3_\infty} dS_\mu \varepsilon^{\mu\nu\rho\sigma}\mathrm{Tr}\left(\Omega\partial_\nu\Omega^{-1}\Omega\partial_\rho\Omega^{-1}\Omega\partial_\sigma\Omega^{-1}\right)\,, \tag{2.1.11}$$

which is a topological quantity depending only on the boundary conditions —at infinity— of the field configurations. The maps in a same class are homotopic to the so called *standard map*:

$$\Omega^{(\nu)}(x) = \left(\frac{\tau + i\sigma^i x^i}{r}\right)^\nu\,, \tag{2.1.12}$$

from which it becomes clear that trivial solutions, homotopic to $G_\mu = 0$, correspond to the class with $\nu = 0$.

Therefore, only $\nu \neq 0$ configurations will give finite contributions to the action S_E. Starting from Eq.(2.1.3), the integral of the θ-term can be expressed as the surface integral at infinity of the Chern-Simons current via the Gauss theorem:

$$\int d^4x G^{\alpha}_{\mu\nu}\widetilde{G}^{\mu\nu,\alpha} = \int d^4x \partial_\mu K^\mu \,, \tag{2.1.13}$$

$$= \int_{S^3_\infty} dS_\mu K^\mu \,, \tag{2.1.14}$$

$$= \int_{S^3_\infty} \varepsilon^{\mu\nu\rho\sigma} G^{\alpha}_{\nu} \left(G^{\alpha}_{\rho\sigma} - \frac{g_S}{3} f_{\alpha\beta\gamma} G^{\beta}_{\rho} G^{\gamma}_{\sigma} \right) , \tag{2.1.15}$$

where dS_μ is the surface differential on the surface of a 3-sphere with infinite radius S^3_∞. For a non-trivial field configuration (2.1.10), only the *pure gauge* term survives at $r \to \infty$:

$$\int d^4x G^{\alpha}_{\mu\nu}\widetilde{G}^{\mu\nu,\alpha} = -\frac{g_S}{3} \int_{S^3_\infty} dS_\mu \varepsilon^{\mu\nu\rho\sigma} f_{\alpha\beta\gamma} \left[\mathcal{O}\left(\frac{1}{r^{3+\epsilon}}\right) + G^{\alpha}_{\nu} G^{\beta}_{\rho} G^{\gamma}_{\sigma} \right] , \tag{2.1.16}$$

$$= i\frac{4}{3} g_S \int_{S^3_\infty} dS_\mu \varepsilon^{\mu\nu\rho\sigma} \mathrm{Tr}\left[G_\nu G_\rho G_\sigma\right] , \tag{2.1.17}$$

$$= \frac{4}{3g_S^2} \int_{S^3_\infty} dS_\mu \varepsilon^{\mu\nu\rho\sigma} \mathrm{Tr}\left(\Omega\partial_\nu\Omega^{-1}\Omega\partial_\rho\Omega^{-1}\Omega\partial_\sigma\Omega^{-1}\right) . \tag{2.1.18}$$

Therefore, applying Eq. (2.1.11), it follows that the winding number arises from the anomalous θ-term,

$$\nu = \frac{\alpha_S}{8\pi} \int G^{\alpha}_{\mu\nu}\widetilde{G}^{\mu\nu,\alpha} \,, \tag{2.1.19}$$

which gives a non-zero contribution to the action $S_E \supset \theta\nu$, proportional to the winding number.

To sum up, although the θ-term is a total derivative, we have found non-trivial field configurations called *instantons*, which lead to a non-vanishing contribution to the action. This turns out to be proportional to a topological charge, the *winding number*, justifying the need for CP-violating anomalous gluon interactions in the SM Lagrangian.

2.2 Missing meson problem

The QCD Lagrangian after EWSB reads:

$$\mathscr{L} = -\frac{1}{4} G^{\alpha}_{\mu\nu} G^{\mu\nu,\alpha} + \theta\frac{\alpha_S}{8\pi} G^{\alpha}_{\mu\nu}\widetilde{G}^{\mu\nu,\alpha} + i\overline{q}_L \not{D} q_L + i\overline{q}_R \not{D} q_R - \left(\overline{q}_L \mathbf{M}_q q_R + \text{h.c.}\right) , \tag{2.2.1}$$

where $q^{i=1,\ldots,6}_{L,R}$ are the LH and RH quarks and $\mathbf{M}_q$ is the corresponding (real) diagonal mass matrix.

Let us consider now the scenario with only two light quark flavors, for simplicity. Our theory includes gluons G_μ and the two lightest quarks $q_{L,R} = (u_{L,R},\, d_{L,R})^T$, with mass given by

$$\mathbf{M}_q = \begin{pmatrix} m_u & 0 \\ 0 & m_d \end{pmatrix} . \tag{2.2.2}$$

This theory has a $SU(3)_C$ gauge group and a global symmetry $SU(2)_V \times SU(2)_A \times U(1)_B \times U(1)_A$, also known as *chiral symmetry*, which is only broken by the light quark

	$SU(3)_C$	$SU(2)_V$	$SU(2)_A$	$U(1)_B$	$U(1)_A$
G_μ	$\mathbf{8}$	$\mathbf{1}$	$\mathbf{1}$	0	0
q_L	$\mathbf{3}$	$\mathbf{2}$	$\overline{\mathbf{2}}$	1	-1
q_R	$\mathbf{3}$	$\mathbf{2}$	$\mathbf{2}$	1	1
$\mathbf{M}_q$	$\mathbf{1}$	$\mathbf{2}\times\overline{\mathbf{2}}$	$\overline{\mathbf{2}}\times\overline{\mathbf{2}}$	0	2

Table 2.1: Transformation properties of the 2-flavor scheme QCD.

masses $m_{u,\,d} \ll \Lambda_{\rm QCD}$. These can be neglected to a good approximation. The quark phase transformations read

$$U(1)_B \times SU(2)_V : \qquad q \to e^{i\left(\alpha_B + \alpha_V^i \sigma^i\right)} q\,, \tag{2.2.3}$$

$$U(1)_A \times SU(2)_A : \qquad q \to e^{i\gamma_5\left(\alpha_A^0 + \alpha_A^i \sigma^i\right)} q\,, \tag{2.2.4}$$

consistently with the transformation properties of gluons and quarks as well as the spurion mass described in Tab. 2.1. The Noether currents of these global symmetries correspond to the (vectorial $R+L$) baryon number and isospin currents

$$j_B^\mu = \overline{q}\gamma^\mu q\,, \qquad j_V^{\mu,i} = \overline{q}\gamma^\mu \frac{\sigma^i}{2} q\,, \tag{2.2.5}$$

and the axial $(R-L)$ currents

$$j_A^\mu = \overline{q}\gamma^\mu \gamma_5 q\,, \qquad j_A^{\mu,i} = \overline{q}\gamma^\mu \gamma_5 \frac{\sigma^i}{2} q\,. \tag{2.2.6}$$

Nonetheless, after QCD confinement at low energies, the theory becomes strongly coupled, and the global symmetry is spontaneously broken by the quark condensate $\langle \overline{q}q\rangle \neq 0$:

$$SU(2)_V \times SU(2)_A \times U(1)_B \times U(1)_A \longrightarrow SU(2)_V \times U(1)_B\,. \tag{2.2.7}$$

Therefore, according to the Goldstone theorem [9, 10], we should expect at low energies 4 massless Goldstone bosons: 3 pions $\pi^\pm$, π^0 corresponding to the broken generators of $SU(2)_A$, and the η' that arises from the breaking of $U(1)_A$. Since the spontaneously broken symmetry is not exact but approximate (due to the quark masses), the Goldstone bosons acquire small masses and are usually called *pseudo-Goldstone bosons* (pGBs). These can be computed promoting the axial transformation parameters, α_A^0 and α_A^i, to pGBs fields, Π^0 and Π^i, respectively:

$$\alpha_A^0 \to \frac{\Pi^0(x^\mu)}{2f_\pi}\,, \qquad \alpha_A^i \to \frac{\Pi^i(x^\mu)}{2f_\pi}\,, \tag{2.2.8}$$

where f_π is an energy scale related to $\Lambda_{\rm QCD}$, which are introduced into our theory via

$$q \to e^{i\gamma_5\left(\frac{\Pi^0 + \Pi^i\sigma^i}{2f_\pi}\right)} q\,. \tag{2.2.9}$$

After this field redefinition, the quark mass term originates a potential for the pGBs, once we replace the quark pair $\overline{q}q$ by its condensate $\langle\overline{q}q\rangle$:

$$\begin{aligned} \mathscr{L} \supset -\overline{q}_L \mathbf{M}_q q_R + \text{h.c.} \to &-(m_u + m_d)\langle\overline{q}q\rangle + \frac{\langle\overline{q}q\rangle}{2f_\pi^2}(m_u+m_d)\pi^+\pi^- \\ &+ \frac{\langle\overline{q}q\rangle}{2f_\pi^2}\begin{pmatrix}\pi^0 & \eta'\end{pmatrix}\begin{pmatrix} m_u & 0 \\ 0 & m_d\end{pmatrix}\begin{pmatrix}\pi^0 \\ \eta'\end{pmatrix}\,, \end{aligned} \tag{2.2.10}$$

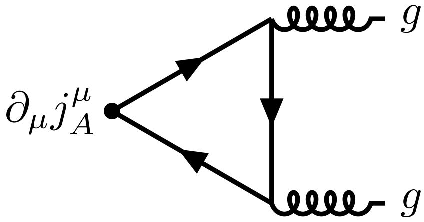

Figure 2.1: One-loop diagram contributing to the ABJ anomaly of the axial current $j^\mu_A = \overline{q}\gamma^\mu\gamma_5 q$.

where

$$\pi^+ \equiv \frac{\Pi^1 + \Pi^2}{\sqrt{2}}\,, \qquad \pi^- \equiv \frac{\Pi^1 - \Pi^2}{i\sqrt{2}}\,, \qquad \pi^0 \equiv \frac{\Pi^0 + \Pi^3}{\sqrt{2}}\,, \qquad \eta' \equiv \frac{\Pi^0 - \Pi^3}{\sqrt{2}}\,, \tag{2.2.11}$$

correspond to the mass eigenstates mesons, whose masses satisfy

$$2m^2_{\pi^+} = m^2_{\pi^0} + m^2_{\eta'}\,. \tag{2.2.12}$$

Experimental masses, however, $m_{\pi^+} \approx m_{\pi^0} \approx 140$ MeV and $m_{\eta'} \approx 960$ MeV, do not obey this sum rule.

The theory predicts a neutral meson η' with mass similar to that of the pions, which is not found in nature. This is known as the Weinberg's $U(1)_A$ missing meson problem [40]. Its solution was found by 't Hooft [38, 41, 42], who realized that $U(1)_A$ is actually not a good symmetry of the theory, not even in the massless quark limit. In other words, it is broken at the quantum level by the Adler-Bell-Jackiw (ABJ) or *axial* anomaly [43, 44], which contributes through the triangle diagram in Fig. 2.1 to the divergence of the $U(1)_A$ current:

$$\partial_\mu j^\mu_A = -2m_u\overline{u}i\gamma_5 u - 2m_d\overline{d}i\gamma_5 d + 4\frac{\alpha_S}{8\pi}G^\alpha_{\mu\nu}\widetilde{G}^{\mu\nu,\alpha}\,, \tag{2.2.13}$$

where the factor in front of the anomalous contribution is a consequence of the two-flavor scenario considered here.

If follows that we should expect only 3 pGBs arising from the spontaneous symmetry breaking of $SU(2)_V \times SU(2)_A \times U(1)_B$, while η' cannot be considered as such, as the breaking scale of the $U(1)_A$ symmetry is $\Lambda \sim \Lambda_{QCD}$, explaining why its mass is of the order of the rest of the QCD bound states [45, 46]:

$$m_{\pi^0} = \frac{\langle\overline{q}q\rangle}{2f^2_\pi}(m_u + m_d)\,, \qquad\qquad m_{\eta'} \approx 4\Lambda + \mathcal{O}\left(\langle\overline{q}q\rangle m_q\right)\,. \tag{2.2.14}$$

2.3 The strong-CP problem

To improve our understanding of the ABJ anomaly and its connection to the θ-term, let us consider an axial field rotation with phase $\frac{\beta_i}{2} \ll 1$ and the corresponding mass matrix redefinition:

$$q^i \longrightarrow e^{i\frac{\beta_i}{2}\gamma_5}q^i\,, \qquad\qquad \mathbf{M}_q \to e^{i\frac{\beta_i}{2}\gamma_5}\mathbf{M}_q e^{-i\frac{\beta_i}{2}\gamma_5} \tag{2.3.1}$$

The Noether current associated to this transformation is the axial current $j^\mu_A = \overline{q}\gamma^\mu\gamma_5 q$. At the classical level, $U(1)_A$ is broken by the quark masses, however there is an additional contribution arising from the *anomalous* θ-term:

$$\delta\mathscr{L} = \sum_i^{n_q} \beta_i \partial_\mu j_A^{\mu,i} = \sum_i^{n_q} \beta_i \left(-i m_i \overline{q}^i \gamma_5 q^i + \frac{\alpha_S}{8\pi} G^\alpha_{\mu\nu} \widetilde{G}^{\mu\nu,\alpha} \right) ,$$
$$= -\sum_i^{n_q} \beta_i i m_i \overline{q}^i \gamma_5 q^i + \arg\det\left(\mathbf{M}_q\right) \frac{\alpha_S}{8\pi} G^\alpha_{\mu\nu} \widetilde{G}^{\mu\nu,\alpha} , \tag{2.3.2}$$

where n_q is the number of quark flavors in our theory and m_i are the physical quark masses. This can be obtained via the so-called Fujikawa method[3] [47], or by computing the triangle diagram in Fig. 2.1.

From Eqs. (2.2.1) and (2.3.2), it becomes clear that the only quantity that remains invariant under these axial field redefinitions is

$$\overline{\theta} \equiv \theta + \arg\det\left(\mathbf{M}_q\right) , \tag{2.3.3}$$

which corresponds to the only physical CP-violating phase in the strong sector, the so called $\overline{\theta}$ *parameter*.

The $\overline{\theta}$-term,

$$\mathscr{L}_\theta = \overline{\theta} \frac{\alpha_S}{8\pi} G^\alpha_{\mu\nu} \widetilde{G}^{\mu\nu,\alpha} , \tag{2.3.4}$$

together with the complex phase δ in the CKM constitutes the only sources of CP violation in the SM. For instance, $G^\alpha_{\mu\nu}\widetilde{G}^{\mu\nu,\alpha}$ can be expressed in the classical limit in terms of *chromoelectric* and *chromomagnetic* fields, $\vec{E}_{QCD}$ and $\vec{B}_{QCD}$:

$$G^\alpha_{\mu\nu}\widetilde{G}^{\mu\nu,\alpha} \sim -4\vec{E}_{QCD} \cdot \vec{B}_{QCD} , \tag{2.3.5}$$

which is odd under parity P and time-reversal T transformations. From the CPT theorem [48], which states that the combined action of the charge conjugation C transformation, P and T, is a fundamental symmetry of nature, we conclude that the $\overline{\theta}$-term is indeed odd under CP.

A non-zero $\overline{\theta}$ parameter would lead to additional contributions to hadron masses, couplings and would even affect the rate of synthesis of heavy elements in the early universe. Due to its CP-odd nature, CP violating observables are sensitive to $\overline{\theta}$, being the neutron electric dipole moment (nEDM) the most sensitive probe. The leading order contribution to d_n within the SM EW sector, occurs at the three-loop level [49–51], and is expected to be of order [52, 53]:

$$d_n^{\mathrm{EW}} \sim 10^{-31}\ \mathrm{e} \cdot \mathrm{cm} . \tag{2.3.6}$$

So far, experimental attempts to measure the nEDM d_n have set stringent upper bounds. The current world average bound according to the Particle Data Group (2022) [13] is

$$d_n^{\mathrm{exp}} < 1.8 \times 10^{-26}\ \mathrm{e} \cdot \mathrm{cm} , \tag{2.3.7}$$

with 90% C.L. This, consistently with current estimations of the $\overline{\theta}$ contributions to d_n [54–60],

$$d_n^{\overline{\theta}} \sim (0.8 - 2) \times 10^{-15}\, \overline{\theta}\ \mathrm{e} \cdot \mathrm{cm} , \tag{2.3.8}$$

[3] This is the method to compute the transformation of the integral measure under this fermion redefinition.

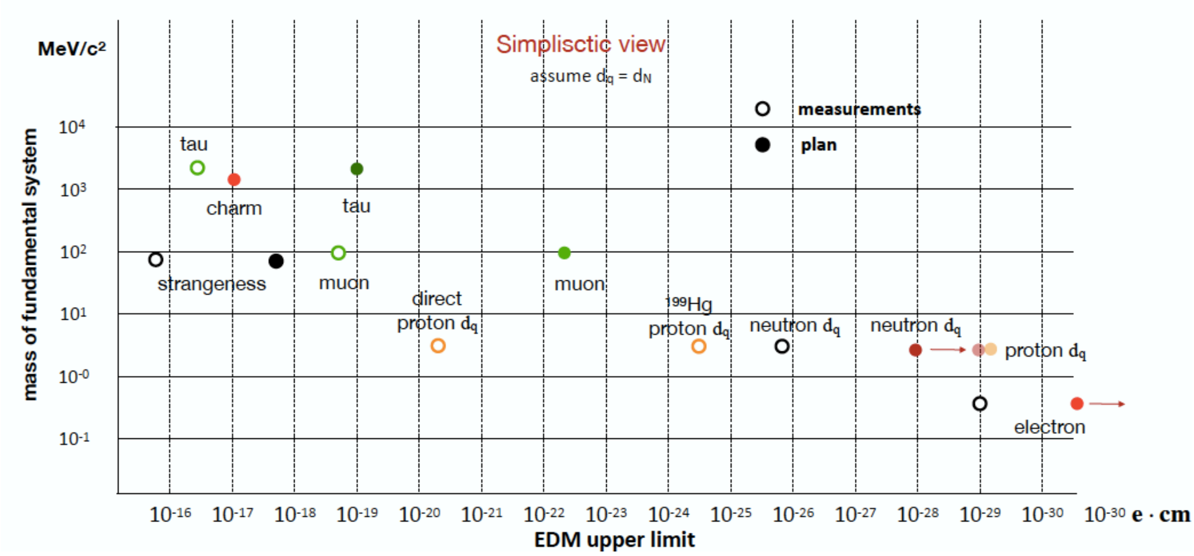

Figure 2.2: Summary of current EDM bounds (empty circles) as well as short and mid-term planned sensitivities (full circles) for protons and neutrons, strange and charm quarks, electrons, muons and taus [61].

translates into an upper limit on the amount of CP violation in the strong sector of the SM:

$$\bar{\theta} \lesssim 10^{-10} \, . \tag{2.3.9}$$

Given that $\bar{\theta}$ is expected to take an arbitrary $\mathcal{O}(1)$ value between 0 and 2π, there is no explanation within the SM for this extreme $\mathcal{O}(10^{-10})$ suppression. This unexplained adjustment is known as the *strong-CP problem*, which is in fact a puzzle rather than a problem.

Future nEDM prospects (see Fig. 2.2) are expected to improve current limits by 3 orders of magnitude whereas there are several proposals to measure the EDM of the proton using storage rings aiming at sensitivities of order 10^{-29} e·cm [61]. In the following decades experiments will be able to probe the SM electroweak contribution to the nEDM, which will shed light on one of the of the most intriguing open problems in the SM.

In the next sections, I will review the most popular attempts to explain the *strong-CP problem*.

2.4 Solutions to the strong-CP problem

The two main approaches to solve the strong-CP problem are dynamical relaxation and symmetry. The most elegant and popular solution is the Peccei-Quinn mechanism (see Sec. 2.4.4), which is of the former kind. However, there are alternative solutions based on the assumption that Parity or CP are fundamental symmetries of nature, as in such cases the $\bar{\theta}$-term must be zero.

2.4.1 Massless u quark

The simplest solution to the strong-CP problem is having a massless u quark, which would render unphysical the $\bar{\theta}$-parameter. In the previous section we discussed its connection to the ABJ anomaly. From Eq. (2.3.2), it becomes clear that an axial rotation on the hypothetically massless u quark with phase $-\overline{\theta}/2$

$$u \longrightarrow e^{-i\frac{\overline{\theta}_i}{2}\gamma_5} u\,, \tag{2.4.1}$$

allows us to rotate away the $\overline{\theta}$.

However, the possibility of having a massless quark within the SM has been ruled out by current lattice results [62–64].

Alternatively, one could think of beyond the SM (BSM) scenarios with additional exotic massless quarks. There have been attempts to enlarge the strong sector with new quarks and additional confining gauge groups, where the new physics scale Λ_{BSM} is much larger than Λ_{QCD}, which makes new exotic "hadrons" too heavy to be observed at experiments [65–68].

2.4.2 Parity-based solutions

Parity-based solutions [69–74] usually extend the SM gauge group with $SU(2)_R$, and introduce a RH Higgs doublet Φ_R as well as RH neutrinos to make the EW sector parity invariant:

$$P : SU(2)_L \leftrightarrow SU(2)_R : \qquad Q_L \leftrightarrow Q_R^\dagger\,, \qquad L_L \leftrightarrow L_R^\dagger\,, \qquad \Phi_L \leftrightarrow \Phi_R^\dagger\,, \tag{2.4.2}$$

where Φ_L refers to the usual SM Higgs doublet, $Q_R = (u_R,\, d_R)^T$ and $L_R = (\nu_R,\, e_R)^T$.

If parity P were a good symmetry of nature, the neutron EDM would then be zero, as the θ-term —both P and CP odd— is now forbidden. Therefore a non-zero $\overline{\theta}$ can only be generated from complex phases in the quark mass terms $\overline{\theta} = \arg\det(\mathbf{M}_q)$. Fermion masses arise from interactions of the form

$$\mathscr{L} \supset \frac{\mathbf{y}_u Q_L \Phi_L Q_R \Phi_R}{\Lambda_u} + \frac{\mathbf{y}_d Q_L \Phi_L^\dagger Q_R \Phi_R^\dagger}{\Lambda_d} + \text{h.c.}\,, \tag{2.4.3}$$

where the SM Yukawa couplings $\mathbf{Y}_{u,d}$ are now hermitian matrices —so that parity is preserved— and can be obtained after the RH Higgs acquires its *vev* v_R

$$\mathbf{Y}_{u,d} = \frac{\mathbf{y}_{u,d} v_R}{\Lambda_{u,d}}\,. \tag{2.4.4}$$

The hermiticity of the Yukawa couplings ensures that $\arg\det(\mathbf{M}_q) = 0$, and therefore that $\overline{\theta} = 0$ at tree level.

Parity can be soflty broken if the RH Higgs mass is larger than that of its LH partner. This would explain the observed parity violation in the weak sector while preserving the interesting properties of parity-based solutions. Although these provide a simple mechanism to adress the strong-CP problem, the fact that tree-level phases —such as δ in the CKM— are allowed can lead to 1-loop contributions to θ that need to be addressed.

2.4.3 Nelson-Barr mechanism

One possible symmetry-based solution to the strong-CP problem is setting CP as a fundamental symmetry of nature, via the so called Nelson-Barr mechanism [75, 76]. In these scenarios both the CP-violating phase δ in the CKM and $\overline{\theta}$ vanish in the UV. The observed CP violation in the weak sector is generated through an additional scalar singlet that spontaneously breaks CP acquiring a complex *vev*. However, these models must be carefully built so that the breaking induces $\mathcal{O}(1)$ CKM complex phase while preserving a vanishing $\overline{\theta}$ at tree level.

One of the simplest realizations of this mechanism is the Bento-Branco-Parada (BBP) model [77, 78], which introduces an exotic down-type vector-like quark $q = (q_R, q_L)^T$ as well as new neutral complex scalar fields η_i with $i = 1, ..., n_\eta$. The down sector terms read

$$\mathscr{L} \supset -\mu_q \overline{q}_L q_R - \eta \mathbf{A} \overline{D}_R q_L - \overline{Q}_L \mathbf{Y}_d \Phi D_R \,, \tag{2.4.5}$$

where $\mathbf{A}$ is a $n_\eta \times 3$ real matrix, and μ_q and $\mathbf{Y}_d$ are real. As we go down in energy the exotic scalars will acquire a *vev* $\langle \eta_i \rangle$ breaking CP invariance and eventually EWSB will take place, inducing the following 4×4 quark mass matrix:

$$\mathbf{M} = \begin{pmatrix} \mu_q & \langle \eta \rangle \cdot \mathbf{A} \\ 0 & \mathbf{M}_d \end{pmatrix} \,, \tag{2.4.6}$$

where $\mathbf{M}_d$ is the down quark Dirac mass as defined in Eq. (1.3.7).

As the only complex phases in Eq. (2.4.6) are contained in $\langle \eta \rangle$, it follows automatically that $\arg\det(\mathbf{M}) = 0$ —ensuring $\overline{\theta} = 0$ at tree level— while the generated CKM phase is non-zero and large as long as $\mu_q \lesssim (\langle \eta \rangle \cdot \mathbf{A})_f$ with $f = 1, 2, 3$.

Nevertheless, CP-based solutions tend to be very “fragile”, as the *vevs* of the different exotic scalars need to be tuned in order to reproduce a large CKM phase, causing a new hierarchy problem. Furthermore, the Lagrangian in Eq. (2.4.5) is not completely general, as allowed couplings such as $\eta \overline{q}_L q_R$ and $\Phi \overline{Q}_L q_R$ must be forbidden to prevent $\overline{\theta}$ to appear at tree level.

2.4.4 Peccei-Quinn mechanism

The Peccei-Quinn (PQ) mechanism [79, 80] is an elegant and yet simple solution to the strong-CP problem. The cornerstone of this approach is a new global abelian symmetry, the Peccei-Quinn symmetry $U(1)_{\rm PQ}$, which is exact at the classical level but is affected by the ABJ anomaly

$$\partial_\mu j^\mu_{\rm PQ} = \frac{\alpha_S}{8\pi} G^\alpha_{\mu\nu} \widetilde{G}^{\mu\nu,\alpha} \,, \tag{2.4.7}$$

breaking the symmetry at the quantum level. Furthermore, the —anomalous— PQ symmetry is spontaneously broken at a scale f_a, originating a new light pseudo-Goldstone boson: the *QCD axion*[4], with a low energy effective coupling to gluons given by

$$\mathscr{L}_a \supset \frac{a}{f_a} \frac{\alpha_S}{8\pi} G^\alpha_{\mu\nu} \widetilde{G}^{\mu\nu,\alpha} \,. \tag{2.4.8}$$

where $\mathscr{L}_a$ refers to those terms in the Lagrangian that depend on the axion field.

Thus, a transformation of the fields charged under $U(1)_{\rm PQ}$ or, equivalently, a redefinition of the axion

$$a \to a - \overline{\theta} f_a \,, \tag{2.4.9}$$

[4]This was pointed out by Weinberg [81] and Wilczek [82] after the original proposal of Peccei and Quinn.

allows to rotate the $\overline{\theta}$ parameter away. Furthermore, the axion suffers a potential due to non-perturbative QCD effects which has a minimum at

$$\overline{\theta}_{\text{eff}} \equiv \overline{\theta} + \langle \frac{a}{f_a} \rangle = 0 \,. \tag{2.4.10}$$

Therefore, the PQ mechanism not only renders $\overline{\theta}$ unphysical via an axion field redefinition, but it dinaymically settles it to a CP-preserving minimum, i.e., $\overline{\theta}_{\text{eff}} = 0$, solving the strong-CP problem.

QCD axion mass

One of the most robust predictions of "QCD axion" models is the dependence of the axion mass on f_a. The axion mass originates from $aG\widetilde{G}$ after QCD confinement, when instanton field configurations generate a non-perturbative potential.

Below the QCD confinement scale, the axion and the η' meson mix due to their coupling to $G\tilde{G}$. While the mass eigenstate corresponding to the physical η' acquires a mass $\sim \Lambda_{\text{QCD}}$, the physical QCD axion remains much lighter. The explicit expressions for the pseudoscalar masses can be obtained from chiral perturbation theory —which describes the interactions of mesons below the QCD confinement scale—, following Refs. [83–86].

Considering the psedoscalar degrees of freedom of the chiral theory at leading order in the chiral expansion we have:

$$\begin{aligned} \mathscr{L}^{\chi\text{PT}} \supset 2v_\chi^3 \bigg[& m_u \cos\left(\frac{\tilde{\pi}_0}{f_\pi} + \frac{\tilde{\eta}}{\sqrt{3}f_\pi} + \frac{\sqrt{2}\tilde{\eta}'}{\sqrt{3}f_\eta}\right) + m_d \cos\left(\frac{\tilde{\pi}_0}{f_\pi} - \frac{\tilde{\eta}}{\sqrt{3}f_\pi} - \frac{\sqrt{2}\tilde{\eta}'}{\sqrt{3}f_\eta}\right) \\ & + m_s \cos\left(-\frac{2\tilde{\eta}}{\sqrt{3}f_\pi} + \frac{\sqrt{2}\tilde{\eta}'}{\sqrt{3}f_\eta}\right)\bigg] + K \cos\left(\frac{\sqrt{6}\tilde{\eta}'}{f_\eta} + \frac{\tilde{a}}{f_a}\right) , \end{aligned} \tag{2.4.11}$$

where $\{\tilde{\pi}_0, \tilde{\eta}, \tilde{\eta}', \tilde{a}\}$ are the neutral pion, η, η' and axion fields before mixing, respectively[5], the term $K\cos(...)$ is the instanton-induced potential, which can be computed by the dilute gas approximation [87], and $v_\chi^3 \equiv \langle \overline{q}q \rangle$ is the QCD chiral condensate. Here, f_π and f_η correspond to the pion and η decay constants while K denotes the QCD anomaly contribution to the $\tilde{\eta}'$ and $\tilde{a}$ fields, which arises from the instanton configurations.

The 4×4 pseudoscalar mass matrix is obtained by expanding the Lagrangian in Eq. (2.4.11):

$$\mathbf{M^2} = \begin{pmatrix} \frac{2v_\chi^3}{f_\pi^2}(m_u + m_d) & \frac{2v_\chi^3}{\sqrt{3}f_\pi^2}(m_u - m_d) & \frac{4v_\chi^3}{\sqrt{6}f_\pi f_\eta}(m_u - m_d) & 0 \\ \frac{2v_\chi^3}{\sqrt{3}f_\pi^2}(m_u - m_d) & \frac{2v_\chi^3}{3f_\pi^2}(m_u + m_d + 4m_s) & \frac{4v_\chi^3}{3\sqrt{2}f_\pi f_\eta}(m_u + m_d - 2m_s) & 0 \\ \frac{4v_\chi^3}{\sqrt{6}f_\pi f_\eta}(m_u - m_d) & \frac{4v_\chi^3}{3\sqrt{2}f_\pi f_\eta}(m_u + m_d - 2m_s) & \frac{6K}{f_\eta^2} + \frac{4v_\chi^3}{3f_\eta^2}(m_u + m_d + m_s) & \frac{\sqrt{6}K}{f_\eta f_a} \\ 0 & 0 & \frac{\sqrt{6}K}{f_\eta f_a} & \frac{K}{f_a^2} \end{pmatrix} , \tag{2.4.12}$$

which after diagonalization lead to the the mass of the physical QCD axion a:

$$m_a^2 = \frac{1}{f_a^2} \frac{K}{1 + \frac{K}{2v_\chi^3}\text{Tr}(\mathbf{M}_Q^{-1})} , \tag{2.4.13}$$

[5] Corrections from heavier pseudoscalar degrees of freedom are disregarded here.

with $\mathbf{M}_Q = \mathrm{diag}(m_u, m_d, m_s)$. In the limit $m_{u,d} \ll f_\pi, f_\eta, K, v_\chi \ll f_a$, this results in

$$m_a^2 \approx \frac{m_\pi^2 f_\pi^2}{f_a^2} \frac{m_u m_d}{(m_u + m_d)^2} \,. \tag{2.4.14}$$

which is a robust prediction of typical QCD axion models where QCD instantons are the only source of breaking of the PQ symmetry[6]. Here, the physical QCD axion corresponds to

$$a \approx \tilde{a} + \theta_{a\pi}\tilde{\pi}_0 + \theta_{a\eta}\tilde{\eta} + \theta_{a\eta 0}\tilde{\eta}' \,, \tag{2.4.15}$$

where

$$\theta_{a\pi} \approx -\frac{f_\pi}{2f_a}\frac{m_d - m_u}{m_u + m_d} \,, \qquad \theta_{a\eta} \approx -\frac{f_\pi}{2\sqrt{3}f_a} \,, \qquad \theta_{a\eta'} \approx -\frac{-f_\eta}{\sqrt{6}f_a} \,, \tag{2.4.16}$$

denote to the pseudoscalar mixing angles.

QCD axion coupling to photons

Axion interactions below the EWSB scale can be parametrized as

$$\mathscr{L}_a \supset \frac{\partial_\mu a}{2f_{\mathrm{PQ}}} \sum_\psi c_\psi \bar{\psi}\gamma^\mu\gamma^5\psi + N\frac{\alpha_S}{8\pi}\frac{a}{f_{\mathrm{PQ}}} G^\alpha_{\mu\nu}\widetilde{G}^{\mu\nu,\alpha} + E\frac{\alpha_{EM}}{8\pi}\frac{a}{f_{\mathrm{PQ}}} F_{\mu\nu}\widetilde{F}^{\mu\nu} \,, \tag{2.4.17}$$

where the sum runs over $\psi = \{u, c, t, d, s, b, e, \mu, \tau\}$, c_ψ denotes the couplings to fermions, and N and E are the model-dependent anomalous couplings to gluons and photons, respectively. The "axion energy scale", f_a, is typically defined as

$$f_a \equiv \frac{f_{\mathrm{PQ}}}{N} \,, \tag{2.4.18}$$

such that the axion coupling to gluons remains model-independent while the axion-photon coupling depends on the ratio E/N:

$$\mathscr{L}_a \supset \frac{\alpha_S}{8\pi}\frac{a}{f_a} G^\alpha_{\mu\nu}\widetilde{G}^{\mu\nu,\alpha} + \frac{E}{N}\frac{\alpha_{EM}}{8\pi}\frac{a}{f_a} F_{\mu\nu}\widetilde{F}^{\mu\nu} \,. \tag{2.4.19}$$

Below the QCD confinement scale, we must take into account the implications of the axion-meson mixing. For instance, an effective contribution to the axion-photon coupling is added to that in Eq. (2.4.19), leading to

$$\mathscr{L}_a \supset -\frac{1}{4} g_{a\gamma\gamma} a F_{\mu\nu}\widetilde{F}^{\mu\nu} \,, \tag{2.4.20}$$

with

$$g_{a\gamma\gamma} \equiv g^0_{a\gamma\gamma} + \theta_{a\pi}g_{\pi\gamma\gamma} + \theta_{a\eta}g_{\eta\gamma\gamma} + \theta_{a\eta'}g_{\eta'\gamma\gamma} \,, \tag{2.4.21}$$

where the first term denotes the $\sim E/N$ term in Eq. (2.4.19), while the others correspond to the photon couplings of the pseudoscalar mesons. After replacing the mixing angles in Eq. (2.4.16), we finally obtain the physical axion-photon coupling

$$g_{a\gamma\gamma} = -\frac{\alpha_{EM}}{2\pi f_a}\left(\frac{E}{N} - \frac{2}{3}\frac{m_u + 4m_d}{m_u + m_d}\right) \,, \tag{2.4.22}$$

[6] If corrections from the strange quark mass are included, the expression reads:

$$m_a^2 \approx \frac{m_\pi^2 f_\pi^2}{f_a^2} \frac{4 m_u m_d m_s}{(m_u + m_d)(4m_u m_s + 4m_d m_s + 13 m_u m_d)} \,.$$

at leading order of the chiral expansion. A more accurate expression can be derived if NLO corrections in chiral perturbation theory are taken into account [88]:

$$g_{a\gamma\gamma} = -\frac{\alpha_{EM}}{2\pi f_a}\left(\frac{E}{N} - 1.92(4)\right) . \tag{2.4.23}$$

As a final remark, tipically for QCD axions, the physical coupling to photons receives two contributions: a model-dependent $\sim E/N$ contribution —already present in the UV Lagrangian—, and a model-independent contribution arising from axion-meson mixing, which is common to all QCD axion models. Similar computations can be performed to derive model-independent components of axion couplings to leptons, nucleons or EW gauge bosons [89, 90].

2.5 QCD axion models

In the last decades a plethora of axion models have been proposed: The original Peccei-Quinn-Weinberg-Wilczek (PQWW) axion [79, 80] —ruled out by rare meson decay experiments soon after its proposal—, the "mainstream" axion models known as *canonical QCD axions* or *invisible* axions [91–94], the Kim-Choi composite axion [65, 66], as well as more recent attempts to build an axion heavier or lighter than the invisible one [95–97]. In other words, the enlarged ALP parameter space can account for the strong-CP problem in these models. Furthermore, the interest on axions extends beyond the strong-CP problem, since in an important sub-eV range of masses, axions are among the main candidates to explain dark matter. In this section I will review the most relevant and paradigmatic axion models proposed in the last decades.

2.5.1 The Peccei-Quinn-Weinberg-Wilczek axion

In order to implement the PQ mechanism we need a classically exact abelian symmetry in our theory, only broken by the ABJ anomaly, and this cannot be achieved with the SM particle content. Peccei and Quinn proposed in 1977 [79, 80] a two Higgs doublet model (2HDM) extension, where the two Higgs fields $\Phi_u = (\mathbf{1}, \mathbf{2}, 1/2)$ and $\Phi_d = (\mathbf{1}, \mathbf{2}, 1/2)$ live in the same representation under the SM gauge group as the standard Higgs.

Yukawa interactions can be written as follows:

$$\mathscr{L}_{\text{Yukawa}} = -\overline{Q}_L \mathbf{Y}_u \tilde{\Phi}_u U_R - \overline{Q}_L \mathbf{Y}_d \Phi_d D_R - \overline{L}_L \mathbf{Y}_e \Phi_{u,d} E_R + \text{h.c.} , \tag{2.5.1}$$

where leptons can either couple to Φ_d (type II 2HDM [98, 99]) or to Φ_u (flipped 2HDM [100]). On the other hand, the Higgs sector is now described by a two-dimensional scalar potential $V(\Phi_u, \Phi_d)$, which induces both PQ and EW symmetry breaking after the two Higgs doublets gain non-vanishing *vevs* v_u and v_d:

$$\Phi_u \to \frac{1}{\sqrt{2}} e^{i\eta_u/v_u} \begin{pmatrix} \Phi_u^+ \\ v_u + \phi_u^0 \end{pmatrix} , \qquad \Phi_d \to \frac{1}{\sqrt{2}} e^{i\eta_d/v_d} \begin{pmatrix} \Phi_d^+ \\ v_d + \phi_d^0 \end{pmatrix} , \tag{2.5.2}$$

where the EW scale is given by $v \equiv \sqrt{v_u^2 + v_d^2}$.

Other than the standard baryon number $U(1)_B$, lepton number $U(1)_L$ and hypercharge $U(1)_Y$ symmetries, we now have a new abelian $U(1)_{\rm PQ}$ symmetry:

$$\begin{aligned} U(1)_{\rm PQ}: \quad & Q_L \to e^{-i\chi_Q\alpha} Q_L\,, && U_R \to e^{-i\chi_u\alpha} U_R\,, && D_R \to e^{-i\chi_d\alpha} D_R\,, \\ & L_L \to e^{-i\chi_L\alpha} L_L\,, && E_R \to e^{-i\chi_e\alpha} E_R\,, \\ & \Phi_u \to e^{-i\left(\chi_u-\chi_Q\right)\alpha}\Phi_u\,, && \Phi_d \to e^{-i\left(\chi_Q-\chi_d\right)\alpha}\Phi_d\,, \end{aligned} \tag{2.5.3}$$

where χ_f with $f = Q, u, d, L, e$ are the PQ charges of the corresponding SM fermions and α is a generic transformation parameter. Depending on which realization of the 2HDM we are considering, χ_e must satisfy one of the following relation in order to preserve (classically) the PQ symmetry:

$$\text{Type II 2HDM:} \qquad \chi_e = \chi_L - \chi_Q + \chi_d\,, \tag{2.5.4}$$

$$\text{Flipped 2HDM:} \qquad \chi_e = \chi_L + \chi_Q - \chi_u\,. \tag{2.5.5}$$

Notice however that the definition of the PQ transformation is not unique at this point, since there are four independent parameters $\{\chi_Q, \chi_u, \chi_d, \chi_L\}$. A common choice, since the axion coupling to fermions depend on the axial combination of the PQ charges $(\chi_{\psi_R} - \chi_{\psi_L})$, is setting the LH PQ charges to 0 via lepton and baryon number transformations: $\chi_Q = \chi_L = 0$. This will leave the physical couplings of the axions —both to fermions and gauge bosons— unaffected.

An additional condition can be imposed on the two remaining PQ charges $\{\chi_u, \chi_d\}$ if we take into account that η_u and η_d contain the physical d.o.f. corresponding to the *PQWW axion* —pGB of $U(1)_{\rm PQ}$ [81, 82]— and the would-be GB of $U(1)_Y$, later "eaten" by the longitudinal mode of the physical Z boson upon acquisition of its mass. Under these symmetries, the η's transform via shifts:

$$\begin{aligned} U(1)_{\rm PQ}: \quad & \eta_u \to \eta_u - \alpha v_u \chi_u\,, && \eta_d \to \eta_d + \alpha v_d \chi_d\,, \\ U(1)_{\rm Y}: \quad & \eta_u \to \eta_u - \frac{\alpha}{2} v_u\,, && \eta_d \to \eta_d - \frac{\alpha}{2} v_d\,, \end{aligned} \tag{2.5.6}$$

with α the transformation parameter. Thus, we want the combinations of η_u and η_d corresponding to the axion a and the would-be GB G_Z to remain invariant under $U(1)_Y$ and $U(1)_{\rm PQ}$, respectively. Defining

$$a = \frac{v_d\eta_u - v_u\eta_d}{v}\,, \qquad G_Z = \frac{v_u\eta_u + v_d\eta_d}{v}\,, \tag{2.5.7}$$

if follows that

$$\begin{aligned} U(1)_{\rm PQ}: \quad & a \to a - \alpha f_{\rm PQ}\,, && G_Z \to G_Z\,, \\ U(1)_{\rm Y}: \quad & a \to a\,, && G_Z \to G_Z - \frac{\alpha}{2} v\,, \end{aligned} \tag{2.5.8}$$

if we impose the condition $\chi_u/\chi_d = v_d^2/v_u^2 \equiv x^2$, where

$$f_{\rm PQ} \equiv \frac{v_u v_d}{v}\left(\chi_u + \chi_d\right) \tag{2.5.9}$$

is the so-called Peccei-Quinn scale. A conventional choice to fix the remaining free parameter χ_u is

$$\chi_u = x\,, \qquad \chi_d = \frac{1}{x}\,, \tag{2.5.10}$$

which equals the PQ energy scale to the EW scale[7] $f_{\rm PQ} = v$. Thus, for the PQWW axion, m_a is expected to be of order $\mathcal{O}(100)$ keV, which is incompatible with observations [91].

Alternative axion models where f_a is order $\sim 10^9 - 10^{12}$ GeV, originate a much lighter axion mass $m_a \sim 10^{-5} - 10^{-2}$ eV, with couplings to SM particles that elude experimental bounds. Among the most paradigmatic models we find the so-called *invisible* axions, which will be reviewed in the next section.

PQWW axion couplings

After EWSB, fermion masses and interactions with the axion are induced from the Yukawa terms:

$$\begin{aligned}\mathscr{L}_{\rm Yukawa} \overset{\rm EWSB}{\supset} & -\sum_\psi m_\psi \bar{\psi}_L e^{-ia\left(\chi_{\psi_R}-\chi_{\psi_L}\right)/f_{\rm PQ}}\psi_R + \text{ h.c.} \\ &= -\sum_\psi m_\psi\bar{\psi}\psi + \frac{\partial_\mu a}{2f_{\rm PQ}}\sum_\psi c_\psi \bar{\psi}\gamma^\mu\gamma^5\psi + N\frac{\alpha_S}{8\pi}\frac{a}{f_{\rm PQ}}G^\alpha_{\mu\nu}\widetilde{G}^{\mu\nu,\alpha} + E\frac{\alpha_{EM}}{8\pi}\frac{a}{f_{\rm PQ}}F_{\mu\nu}\widetilde{F}^{\mu\nu}\,,\end{aligned} \tag{2.5.11}$$

where the sum runs over $\psi = \{u, c, t, d, s, b, e, \mu, \tau\}$ and $c_\psi \equiv (\chi_{\psi_R} - \chi_{\psi_L})$. The three interaction terms have been obtained after Taylor expanding up to order $\mathrm{O}\left(1/f_a\right)$ and applying the fermion EOM taking into account the effect of the ABJ triangle anomaly.

The anomalous couplings N and E can be computed from the PQ and EM charges —$\chi_{\psi_{L,R}}$ and q_ψ, respectively— and the QCD representation indices $T(R_\psi)$ of the fermions[8] running in the triangle loop (Fig. 2.1):

$$N \equiv 2\sum_\psi c_\psi T(R_\psi)\,, \qquad\qquad E \equiv 2\sum_\psi c_\psi q_\psi^2\,. \tag{2.5.12}$$

For our choice of PQ charges $\chi_Q = \chi_L = 0$ and $\chi_u = \chi_d^{-1} = x$ we have

$$N = n_g\left(x + \frac{1}{x}\right)\,, \qquad E = \ n_g\left(x + \frac{1}{x}\right) \times \begin{cases} 8/3\,, & \text{Type II 2HDM} \\ 2/3\,, & \text{Flipped 2HDM}\end{cases}\,, \tag{2.5.13}$$

where n_g is the number of fermion generations.

2.5.2 Invisible axion models

Although the original PQWW axion is already ruled out experimentally —due to the strong constraints which come with an axion scale $f_a \sim v$—, alternative models achieve much larger f_a scales by enlarging the exotic matter content. In this case, consistently with Eq. 2.4.14, the axion becomes very light, with strongly suppressed couplings that evade experimental bounds. These are known as *invisible* axion models. In most cases, a new singlet scalar is added such that the PQ is broken by its *vev* much above the EW scale. Among the most paradigmatic models following this strategy we find the DFSZ [93, 94] and KSVZ [91, 92] axions, which will be reviewd here.

[7] For different PQ charge assignments $f_{\rm PQ}$ remains of order $\sim v$.

[8] Given a representation R_ψ of a non abelian group with generators T_α, its *Dynkin index* $T(R_\psi)$ is defined as $\mathrm{Tr}\left(T^\alpha T^\beta\right) = T(R_\psi)\delta_{\alpha\beta}$.

DFSZ axion

In addition to the second Higgs doublet required by the original PQWW axion, the model proposed by Zhitnitsky [93] and Dine, Fischler and Srednicki [94] —the DFSZ axion— enlarges the particle content with a new complex scalar S, singlet under the SM gauge group and charged under $U(1)_{\rm PQ}$. The scalar potential in the original DFSZ model reads:

$$V\left(\Phi_u,\Phi_d,S\right)=\frac{\lambda_S}{2}|S|^4+\delta_1\left(\Phi_u^\dagger\Phi_u\right)|S|^2+\delta_2\left(\Phi_d^\dagger\Phi_d\right)|S|^2+\delta_3\left(\Phi_u^\dagger\Phi_d\right)S^2+\delta_3\left(\Phi_d^\dagger\Phi_u\right)S^{*2}\,, \tag{2.5.14}$$

where λ_S and $\delta_{1,2,3}$ are dimensionless parameters. Consistently with the PQ charge assignment in Eq. (2.5.3) and the choice $\chi_Q = 0$ the exotic scalar must transform under $U(1)_{\rm PQ}$ as

$$U(1)_{\rm PQ}: S \to e^{-i\chi_S} S\,, \tag{2.5.15}$$

with $\chi_S \equiv (\chi_u + \chi_d)/2$.

The potential in (2.5.14) induces a non-zero vacuum expectation value for S, spontaneously breaking the PQ symmetry:

$$S=\frac{1}{\sqrt{2}}(v_S+\rho_S)e^{i\eta_S/v_S}\,, \tag{2.5.16}$$

where

$$\langle S\rangle=\frac{v_S}{\sqrt{2}}\gg v=\sqrt{v_d^2+v_u^2}\,. \tag{2.5.17}$$

The DFSZ axion a results from the combination of the new pseudoscalar field η_S and the CP-odd components of the Higgs doublets in Eq. (2.5.2), imposing that a is only shifted under $U(1)_{\rm PQ}$, while it remains invariant under the orthogonal transformations:

$$a=\frac{1}{f_{\rm PQ}}\left(-\chi_u v_u\eta_u+\chi_d v_d\eta_d+\chi_S v_S\eta_S\right)\xrightarrow{v_S\gg v}\eta_S\,, \tag{2.5.18}$$

where

$$f_{\rm PQ}=\sqrt{\chi_u^2v_u^2+\chi_d^2v_d^2+\chi_S^2v_S^2}\xrightarrow{v_S\gg v}\chi_S v_S\,. \tag{2.5.19}$$

Thus, if the singlet gets a *vev* at a scale much higher than the EW scale ($v_S \gg v$), then the PQ energy scale is of that same order $f_{\rm PQ}\sim v_S$ while the DFSZ axion can be identified with its axial component: $a\approx\eta_S$.

Finally, the DFSZ axion couplings to SM particles correspond to those in the PQWW model, now suppressed by a the larger PQ scale, which is equivalent to rescaling the PQWW couplings by a factor $\sim v/v_S$. Since v_S is a free parameter of the DFSZ model, the axion couplings can be arbitrarily suppressed to elude experimental constraints. Furthermore, the properties derived in the previous section, such as the relation between m_a and f_a in Eq. (2.4.14), hold. Consequently, the DFSZ axion is expected to be a factor $\sim v/v_S$ lighter than the original axion.

KSVZ axion

The model proposed by Kim [91] and Shifman, Vainshtein and Zakharov [92] simply enlarges the SM matter content with a vectorial QCD-colored fermion ψ and a complex scalar singlet S, which plays a similar to that in the DFSZ model. The terms that extend the SM Lagrangian in the KSVZ model read

$$\mathscr{L}_{\text{KSVZ}} = i\overline{\psi}\not{D}\psi + \partial_\mu S^* \partial^\mu S - \left(y_\psi S \overline{\psi}_L \psi_R + \text{h.c.}\right) + \mu_S^2 |S|^2 - \lambda_S |S|^4 - \lambda_{\Phi S} \left(\Phi^\dagger \Phi\right) |S|^2 \,, \tag{2.5.20}$$

where y_ψ is a Yukawa-like coupling for the exotic fermion and μ_S, λ_S and $\lambda_{\Phi S}$ are free parameters of the scalar potential.

This Lagrangian presents two $U(1)$ symmetries: an exact vectorial rotation of the exotic quark ψ and an axial symmetry under which both ψ and S transform, which corresponds to the PQ symmetry. Without loss of generality, we choose the PQ charges: $\chi_{\psi_R} = -\chi_{\psi_L} = 1/2$ and $\chi_S = -1$, so that

$$U(1)_{\text{PQ}}: \qquad \psi \to e^{-i\gamma_5 \beta/2} \psi \,, \qquad S \to e^{i\beta} S \,. \tag{2.5.21}$$

Notice that this symmetry is QCD-anomalous since ψ is charged under $SU(3)_C$, which allows the strong-CP problem to be solved.

On the other hand, the minimum of the scalar potential induces a non-zero *vev* $\langle S \rangle = v_S/\sqrt{2}$ for the scalar singlet, which spontaneously breaks the PQ symmetry. As usual, the axion can be identified with the axial component in the following parametrizaiton of S:

$$S = \frac{1}{\sqrt{2}}(v_S + \rho_S) e^{i a_S / v_S} \,, \tag{2.5.22}$$

where the PQ scale corresponds in this scenario to $f_{\text{PQ}} = v_S$. Both the radial component of S and the exotic fermion gain large masses, $m_{\rho_S} \sim f_{\text{PQ}}$ and $m_\psi = y_\psi f_{\text{PQ}}/\sqrt{2}$ respectively, decoupling from the low-energy theory.

Unlike the PQWW and DFSZ QCD axions, the KSVZ axion does not couple at tree-level to SM fermions. The usual "model independent" anomalous couplings to gluons and photons can be obtained from Eq. (2.5.12), replacing the PQ charges defined in Eq. (2.5.21), which lead to:

$$N_{\text{KSVZ}} = 1 \,, \qquad E_{\text{KSVZ}} = 6\, q_\psi^2 \,, \tag{2.5.23}$$

where q_ψ denotes the EM charge of the exotic fermion. The low-energy relations for the axion mass and photon coupling in Eqs. (2.4.14) and (2.4.23) remain unchanged.

Composite axions

It is also possible to follow a completely different approach in order to build an invisible axion model. This is the case of the, sometimes overlooked, Kim-Choi composite axion [65, 66]. Inheriting the main ideas from the massless quark solution, these models introduce new exotic massless quarks, rendering $\overline{\theta}$ unphysical, which can now be rotated away. In order to "hide" such quarks at low-energies, these must be charged under a new non-abelian gauge group $SU(N)_a$, also known as *axicolor* interaction, which becomes confining at a scale $\Lambda_a \gg \Lambda_{\text{QCD}}$. Consequently, new exotic hadrons arise, among which we find the axion, which is now a light exotic pseudoscalar meson.

A complete review can be found in the original proposal by Kim [65], as well as in Ref. [65, 88].

2.5.3 Heavier and lighter axion models

While invisible axion models predict a very light pGB with extremely feeble couplings to SM particles, more recent models —known as *heavy axion* models [67, 68, 101–115]— explore scenarios with new sources of PQ breaking. These extend the strong interactions sector of the SM, leading at low-energy to additional terms to the axion pontential which contribute to the make the axion mass heavier. For instance, if a new strong-interacting group is introduced, with confining scale $\Lambda' \gg \Lambda_{QCD}$, the axion mass will receive a contribution from the new confining source:

$$m_a^2 f_a^2 \approx m_\pi^2 f_\pi^2 \frac{m_u m_d}{(m_u + m_d)^2} + \Lambda'^4 \,, \tag{2.5.24}$$

Extra CP-violating interactions, similar to the θ-term, might be allowed after enlarging the strong interactions sector. Some proposals address these issues imposing new discrete symmetries which force the SM and exotic θ parameters to be equal, so that they can be rotated away by a common PQ transformation [102, 104, 108, 109]. Other works follow an alternative approach in which QCD is originated from the spontaneous breaking of a larger "strong" group. Instantons at the scale of such spontaneous breaking constitute new sources of PQ violation which raise the axion mass [68, 110].

Following a completely different approach, in Ref. [97] it is shown that a heavier true QCD axion —i.e., a heavier axion solving the strong-CP problem,— is possible, with QCD being the only source of PQ breaking. They consider the case in which the QCD axion field is not the only (exotic) singlet scalar but it mixes with others, which leads to precise sum rules linking the masses of the axion eigenstates.

On the other hand, there are alternative proposals in which the axion is much ligther than the canonical QCD axion, like the one in Refs. [95, 96], where N mirror and degenerate worlds linked by the axion field are considered.

Chapter 3

Axion-like Particles

In the previous chapter we have reviewed the strong-CP problem, the Peccei-Quinn mechanism as well as the most paradigmatic QCD axion models. In these SM extensions, the axion typically arises as the neutral pGB of the spontaneous breaking of a global $U(1)$ symmetry: the PQ symmetry. Due to its pGB nature, the axion shares a lot of properties with generic neutral pseudoscalar pGBs of any hidden spontaneously broken global symmetry, which are then referred as *axion-like particles*. As argued in the motivation, the reasons to study and explore the phenomenology of ALPs extend way beyond axions and the strong-CP problem.

ALPs are predicted in a plethora of BSM extensions. Some paradigmatic scenarios include:

(i) The *Majoron*, which is the pGB arising from the spontaneous breaking of the $U(1)_L$ lepton number symmetry in models that attempt to explain the small neutrino masses [116–118].

(ii) *Axiflavons*, in dynamical flavor theories which attempt to solve both the strong-CP problem and the flavor puzzle [119–121].

(iii) The *relaxion*, in theories that adress the strong-CP and hierarchy problems [122].

(iv) *Familons*, pGBs arising from the breaking of global family symmetries [119, 123, 124].

(v) String theory, where we find ALPs in the form of Kaluza-Klein zero modes —known as *closed string* axions [125–127]— as well as pGBs arising from the breaking of accidental $U(1)$ symmetries [128–131].

(vi) Theories involving extra dimensions.

(vii) Scenarios where the Higgs boson itself is a pGB, such as Composite-Higgs models [132].

In this Chapter I will review the theory and experimental status of ALPs. In Sec. 3.1 I will present the ALP EFT, a fundamental tool to explore the phenomenology of ALPs at experiments, while Sec. 3.2 will be devoted to discuss current experimental limits on the ALP parameter space.

3.1 ALP linear EFT

3.1.1 ALP EFT above the EWSB scale

The ALP effective field theory can be traced back to the work by Georgi, Kaplan and Randall in Ref. [84] —where the most general dimension-five effective Lagrangian for the axion was proposed—, followed by the work by Choi, Kang and Kim [83]. The rich phenomenology of ALPs together with their ubiquity in BSM extensions has motivated an increasing number of theoretical [2, 36, 133–135] and phenomenological advancements [1, 133, 136–149], and brought them into the spotlight of current and future experimental searches across a wide range of energies and using diversified techniques [150, 151].

ALPs —denoted by a— are broadly defined as neutral pseudoscalar singlets, pGBs of any hidden spontaneously broken global symmetry, only restored at energies much above the EW scale. They are studied most conveniently in the EFT framework, since ALPs —as pGBs— are much lighter than the energy scale f_a of the BSM sector they originate from. At next-to-leading order (NLO) in the linear expansion on the ALP characteristic scale f_a, the mass-dimension five Lagrangian can be written as [36]

$$\mathscr{L} = \mathscr{L}_{\rm SM} + \mathscr{L}_{ALP}\,, \tag{3.1.1}$$

where $\mathscr{L}_{ALP}$ encodes the ALP sector:

$$\mathscr{L}_{ALP} = \frac{1}{2}\partial_\mu a \partial^\mu a - \frac{m_a^2}{2}a^2 + \mathscr{L}_{ALP}^{X\widetilde{X}} + \mathscr{L}_{ALP}^{\Psi}\,, \tag{3.1.2}$$

and $m_a \ll f_a$ is the ALP mass [1]. Consistently with the effective axion Lagrangian in Ref. [84], ALP interactions are either invariant under shifts $a(x) \to a(x) + c$,

$$\mathscr{L}_{ALP}^{\Psi} = \frac{\partial_\mu a}{f_a}\left(\overline{Q}_L\gamma^\mu \hat{\mathbf{c}}_Q Q_L + \overline{U}_R\gamma^\mu \hat{\mathbf{c}}_u U_R + \overline{D}_R\gamma^\mu \hat{\mathbf{c}}_d D_R + \overline{L}_L\gamma^\mu \hat{\mathbf{c}}_L L_L + \overline{E}_R\gamma^\mu \hat{\mathbf{c}}_e E_R\right)\,, \tag{3.1.3}$$

consistently with their pGB nature, or anomalous, i.e. induced by the chiral anomaly,

$$\mathscr{L}_{ALP}^{X\widetilde{X}} = -c_{\widetilde{G}}\frac{a}{f_a}G^\alpha_{\mu\nu}\widetilde{G}^{\mu\nu,\alpha} - c_{\widetilde{W}}\frac{a}{f_a}W^i_{\mu\nu}\widetilde{W}^{\mu\nu,i} - c_{\widetilde{B}}\frac{a}{f_a}B_{\mu\nu}\widetilde{B}^{\mu\nu}\,. \tag{3.1.4}$$

Here, $\{Q_L, U_R, D_R, L_L, E_R\}$ are the chiral fermion fields with flavor indices —defined in Eq. (1.3.1)—, $\hat{\mathbf{c}}_\Psi$ are $n_g \times n_g$ hermitian matrices in flavor space and $c_{\widetilde{G}}$, $c_{\widetilde{W}}$ and $c_{\widetilde{B}}$ are real Wilson coefficients [2]. Notice that ALP interactions are consistent with the SM gauge group, whereas CP is preserved if couplings to fermions are real, $\hat{\mathbf{c}}_\Psi = \hat{\mathbf{c}}_\Psi^T$.

Finally, although the ALP operator basis in Eqs. (3.1.2)–(3.1.4) is complete, there are redundant parameters which can be removed making use of baryon and lepton number conservation, integration by parts and the SM EOM (see Sec. 1.4):

$$\frac{\partial_\mu a}{f_a}j^\mu_B = \frac{\partial_\mu a}{f_a}\left(\frac{\overline{U}\gamma^\mu U + \overline{D}\gamma^\mu D}{3}\right) = -\frac{n_g}{32\pi^2}\frac{a}{f_a}\left(g^2 W^i_{\mu\nu}\widetilde{W}^{\mu\nu,i} - g'^2 B_{\mu\nu}\widetilde{B}^{\mu\nu}\right)\,, \tag{3.1.5}$$

$$\frac{\partial_\mu a}{f_a}j^\mu_{L_f} = \frac{\partial_\mu a}{f_a}\left(\overline{E}^f\gamma^\mu E^f\right) = -\frac{1}{32\pi^2}\frac{a}{f_a}\left(g^2 W^i_{\mu\nu}\widetilde{W}^{\mu\nu,i} - g'^2 B_{\mu\nu}\widetilde{B}^{\mu\nu}\right)\,, \tag{3.1.6}$$

[1] Notice that the ALP mass is a free parameter of the EFT and is therefore not affected by the characteristic dependence on f_a predicted in QCD axion models (see Eq. (2.4.14)), as discussed in Sec. 2.5.1 [67, 68, 81, 82, 95, 96, 101–115, 152]).

[2] Alternative definitions can be found in the literature with an additional prefactor $\frac{\alpha_X}{4\pi}$.

where $j^\mu_{B,L}$ are the baryon and lepton number currents, respectively, $f = 1,2,3$ denotes the flavor index, and $\Psi \equiv \begin{pmatrix}\Psi_L & \Psi_R\end{pmatrix}^T$ for $\Psi = U, D, E$. Thus, among $\{\hat{\mathbf{c}}_Q, \hat{\mathbf{c}}_u, \hat{\mathbf{c}}_d, \hat{\mathbf{c}}_L, \hat{\mathbf{c}}_E\}$, 4 parameters can be removed: either 4 fermion diagonal components —1 in the quark sector and 3 in the leptonic sector—, or 3 fermion diagonal elements plus one of the two gauge couplings.

Chirality-flipping operators and shift-symmetry breaking

ALP-fermion interactions are sometimes parametrized in terms of the chirality-flipping (c.f.) operators:

$$\mathscr{L}^{\Psi(\text{c.f.})}_{ALP} \supset i\frac{a}{f_a}\left(\overline{Q}_L\widetilde{\mathbf{Y}}_u\tilde{\Phi}U_R + \overline{Q}_L\widetilde{\mathbf{Y}}_d\Phi D_R + \overline{L}_L\widetilde{\mathbf{Y}}_e\Phi E_R\right) + \text{h.c.}\,, \tag{3.1.7}$$

where $\widetilde{\mathbf{Y}}_f$ —with $f = u, d, e$— are generic $n_g \times n_g$ complex matrices. Obviously, $\mathscr{L}^{\Psi(\text{c.f.})}_{ALP}$ cannot be equivalent to the ALP Lagrangian above —$\mathscr{L}^{\Psi}_{ALP}$—, as the generic $\widetilde{\mathbf{Y}}_f$ matrices have many more parameters, $6n_g^2 = 54$, than the $\hat{\mathbf{c}}_\Psi$ hermitian matrices, $5n_g^2 - (n_g + 1) = 41$. Indeed, chirality-flipping operators do not neccesarily preserve *a priori* shift-symmetry. If we integrate by parts derivative interactions in Eq. (3.1.3) and make use of the SM EOM in Eq. (1.4.1) supplemented with contributions from the anomalous currents in Eq. (1.4.4), we find that

$$\begin{aligned}
\frac{\partial_\mu a}{f_a}\left(\overline{Q}_L\gamma^\mu\hat{\mathbf{c}}_Q Q_L\right) &= \left[i\frac{a}{f_a}\left(\overline{Q}_L\hat{\mathbf{c}}_Q\mathbf{Y}_u\tilde{\Phi}U_R + \overline{Q}_L\hat{\mathbf{c}}_Q\mathbf{Y}_d\Phi D_R\right) + \text{h.c.}\right] \\
&\quad - \frac{\text{Tr}(\hat{\mathbf{c}}_Q)}{32\pi^2}\frac{a}{f_a}\left(\frac{g'^2}{3}B\widetilde{B} + 3g^2W\widetilde{W} + 2g_S^2G\widetilde{G}\right)\,, \\
\frac{\partial_\mu a}{f_a}\left(\overline{U}_R\gamma^\mu\hat{\mathbf{c}}_u U_R\right) &= -\left[i\frac{a}{f_a}\overline{Q}_L\mathbf{Y}_u\hat{\mathbf{c}}_u\tilde{\Phi}U_R + \text{h.c.}\right] + \frac{\text{Tr}(\hat{\mathbf{c}}_u)}{32\pi^2}\frac{a}{f_a}\left(\frac{8g'^2}{3}B\widetilde{B} + g_S^2G\widetilde{G}\right)\,, \\
\frac{\partial_\mu a}{f_a}\left(\overline{D}_R\gamma^\mu\hat{\mathbf{c}}_d D_R\right) &= -\left[i\frac{a}{f_a}\overline{Q}_L\mathbf{Y}_d\hat{\mathbf{c}}_d\Phi D_R + \text{h.c.}\right] + \frac{\text{Tr}(\hat{\mathbf{c}}_d)}{32\pi^2}\frac{a}{f_a}\left(\frac{2g'^2}{3}B\widetilde{B} + g_S^2G\widetilde{G}\right)\,, \\
\frac{\partial_\mu a}{f_a}\left(\overline{L}_L\gamma^\mu\hat{\mathbf{c}}_L L_L\right) &= \left[i\frac{a}{f_a}\overline{L}_L\hat{\mathbf{c}}_L\mathbf{Y}_e\Phi E_R + \text{h.c.}\right] - \frac{\text{Tr}(\hat{\mathbf{c}}_L)}{32\pi^2}\frac{a}{f_a}\left(g'^2B\widetilde{B} + g^2W\widetilde{W}\right)\,, \\
\frac{\partial_\mu a}{f_a}\left(\overline{E}_R\gamma^\mu\hat{\mathbf{c}}_e E_R\right) &= -\left[i\frac{a}{f_a}\overline{L}_L\mathbf{Y}_e\hat{\mathbf{c}}_e\Phi E_R + \text{h.c.}\right] + \text{Tr}(\hat{\mathbf{c}}_e)\frac{g'^2}{16\pi^2}\frac{a}{f_a}B\widetilde{B}\,,
\end{aligned} \tag{3.1.8}$$

where $B\widetilde{B} \equiv B_{\mu\nu}\widetilde{B}^{\mu\nu}$, $W\widetilde{W} \equiv W^i_{\mu\nu}\widetilde{W}^{\mu\nu,i}$ and $G\widetilde{G} \equiv G^\alpha_{\mu\nu}\widetilde{G}^{\mu\nu,\alpha}$. It is straightforward from these equalities to derive the conditions to preserve shift-symmetry in the chirality-flipping basis:

$$\widetilde{\mathbf{Y}}_u = \left(\hat{\mathbf{c}}_Q\mathbf{Y}_u - \mathbf{Y}_u\hat{\mathbf{c}}_u\right)\,, \quad \widetilde{\mathbf{Y}}_d = \left(\hat{\mathbf{c}}_Q\mathbf{Y}_d - \mathbf{Y}_d\hat{\mathbf{c}}_d\right)\,, \quad \widetilde{\mathbf{Y}}_e = \left(\hat{\mathbf{c}}_L\mathbf{Y}_e - \mathbf{Y}_e\hat{\mathbf{c}}_e\right)\,, \tag{3.1.9}$$

although it is not possible in general to map the couplings back to the chirality-preserving in Eq. (3.1.3), unless specific assumptions, such as Minimal flavor Violation, are made [36, 134, 135].

However, the chirality-flipping basis can still be used to study ALPs/shift-symmetric scenarios without having to refer implicitly to the chirality-preserving couplings $\hat{\mathbf{c}}_\Psi$ [36, 134, 135]. A useful complete set of flavor invariants associated to the shift symmetry of a generic scalar singlet is constructed in Ref. [153]:

$$I_f^{(1)} = \mathrm{Im}\left[\mathrm{Tr}\left(\widetilde{\mathbf{Y}}_f \mathbf{Y}_f^\dagger\right)\right], \quad I_f^{(2)} = \mathrm{Im}\left[\mathrm{Tr}\left(\mathbf{X}_f \widetilde{\mathbf{Y}}_f \mathbf{Y}_f^\dagger\right)\right], \quad I_f^{(3)} = \mathrm{Im}\left[\mathrm{Tr}\left(\mathbf{X}_f^2 \widetilde{\mathbf{Y}}_f \mathbf{Y}_f^\dagger\right)\right],$$
$$I_{ud}^{(1)} = \mathrm{Im}\left[\mathrm{Tr}\left(\mathbf{X}_d \widetilde{\mathbf{Y}}_u \mathbf{Y}_u^\dagger + \mathbf{X}_u \widetilde{\mathbf{Y}}_d \mathbf{Y}_d^\dagger\right)\right],$$
$$I_{ud,u}^{(2)} = \mathrm{Im}\left[\mathrm{Tr}\left(\mathbf{X}_u^2 \widetilde{\mathbf{Y}}_d \mathbf{Y}_d^\dagger + \{\mathbf{X}_u, \mathbf{X}_d\} \widetilde{\mathbf{Y}}_u \mathbf{Y}_u^\dagger\right)\right],$$
$$I_{ud,d}^{(2)} = \mathrm{Im}\left[\mathrm{Tr}\left(\mathbf{X}_d^2 \widetilde{\mathbf{Y}}_u \mathbf{Y}_u^\dagger + \{\mathbf{X}_d, \mathbf{X}_u\} \widetilde{\mathbf{Y}}_d \mathbf{Y}_d^\dagger\right)\right],$$
$$I_{ud}^{(3)} = \mathrm{Im}\left[\mathrm{Tr}\left(\mathbf{X}_d \mathbf{X}_u \mathbf{X}_d \widetilde{\mathbf{Y}}_u \mathbf{Y}_u^\dagger + \mathbf{X}_u \mathbf{X}_d \mathbf{X}_u \widetilde{\mathbf{Y}}_d \mathbf{Y}_d^\dagger\right)\right], \tag{3.1.10}$$
$$I_{ud}^{(4)} = \mathrm{Re}\left\{\mathrm{Tr}\left[\left[\mathbf{X}_u, \mathbf{X}_d\right]^2 \left(\left[\mathbf{X}_u, \widetilde{\mathbf{Y}}_d \mathbf{Y}_d^\dagger\right] - \left[\mathbf{X}_d, \widetilde{\mathbf{Y}}_u \mathbf{Y}_u^\dagger\right]\right)\right]\right\},$$

where $\mathbf{X}_f \equiv \mathbf{Y}_f \mathbf{Y}_f^\dagger$ with $f = u, d, e$. When the 14 invariants vanish, shift symmetry is preserved.

Purely bosonic basis

In some cases it might be convenient to focus only on the *purely bosonic* interactions of an ALP. The most general bosonic EFT at NLO in the linear expansion on f_a contains the three anomalous couplings plus an additional derivative ALP-Higgs interaction:

$$\mathscr{L}_{ALP}^{\text{boson}} = -c_{\widetilde{G}} \frac{a}{f_a} G_{\mu\nu}^\alpha \widetilde{G}^{\mu\nu,\alpha} - c_{\widetilde{W}} \frac{a}{f_a} W_{\mu\nu}^i \widetilde{W}^{\mu\nu,i} - c_{\widetilde{B}} \frac{a}{f_a} B_{\mu\nu} \widetilde{B}^{\mu\nu} + c_{a\Phi} \frac{\partial^\mu a}{f_a} \left(\Phi^\dagger i \overleftrightarrow{D}_\mu \Phi\right), \tag{3.1.11}$$

where $c_{a\Phi}$ is a real and constant coupling and $\Phi^\dagger \overleftrightarrow{D}_\mu \Phi \equiv \Phi^\dagger (D_\mu \Phi) - \left(D_\mu \Phi^\dagger\right)\Phi$.

After EWSB, the ALP-Higgs operator induces mixing between the ALP and the would-be GB associated to the longitudinal mode of the Z boson. Such mixing can be removed performing a Higgs field redefinition in terms of the ALP field $\Phi \to \Phi e^{ic_{a\Phi} a/f_a}$ [36, 84, 133, 154], which is tantamount to the application of the Higgs EOM. This leads to

$$c_{a\Phi} \frac{\partial_\mu a}{f_a} \left(\Phi^\dagger i \overleftrightarrow{D}_\mu \Phi\right) \longrightarrow i c_{a\Phi} \frac{a}{f_a} \left(\overline{Q}_L \mathbf{Y}_u \widetilde{\Phi} U_R - \overline{Q}_L \mathbf{Y}_d \Phi D_R - \overline{L}_L \mathbf{Y}_e \Phi E_R\right) + \text{h.c.}\,. \tag{3.1.12}$$

From Eq. (3.1.9), it becomes clear that these can be expressed in terms of flavor-universal chirality-preserving couplings $\hat{\mathbf{c}}_f = \hat{c}_f \mathbb{1}$,

$$c_{a\Phi} \frac{\partial_\mu a}{f_a} \left(\Phi^\dagger i \overleftrightarrow{D}_\mu \Phi\right) \longrightarrow \frac{\partial_\mu a}{f_a} \Big(\hat{c}_Q \overline{Q}_L \gamma^\mu Q_L + \hat{c}_u \overline{U}_R \gamma^\mu U_R + \hat{c}_d \overline{D}_R \gamma^\mu D_R$$
$$+ \hat{c}_L \overline{L}_L \gamma^\mu L_L + \hat{c}_e \overline{E}_R \gamma^\mu E_R\Big), \tag{3.1.13}$$

as long as the following conditions are satisfied:

$$\hat{c}_u - \hat{c}_Q = -c_{a\Phi}, \qquad \hat{c}_d - \hat{c}_Q = c_{a\Phi}, \qquad \hat{c}_e - \hat{c}_L = c_{a\Phi}. \tag{3.1.14}$$

In addition, in order to ensure that the fermion current in Eq. (3.1.12) is anomaly free, as corresponds to a bosonic operator, we need to impose

$$3\hat{c}_Q + \hat{c}_L = 0\,. \tag{3.1.15}$$

as we will see in the following subsection.

Basis reduction

In order to reduce the operator basis in Eqs. (3.1.2)–(3.1.4), or to find the relation between chirality-preserving and chirality-flipping operators we made use of integration by parts together with the SM EOM in Eq. (1.4.1). When considering loop effects, these need to supplemented with contributions from the anomalous global currents in Eq. (1.4.4).

An alternative approach is using ALP-dependent field redefinitions. Although the Lagrangian is affected by field redefinitions, physical observables remain unchaged, consistently with the EFT *equivalenece theorem* [155, 156]. However, EOM only provide correct equivalence relations at order $\mathcal{O}(1/f_a)$, while relations derived from field redefinitions hold at all orders in the $1/f_a$ expansion.

A general field redefinition can be parametrized as follows:

$$\Psi \to \exp\left(i\mathbf{x}_\Psi \frac{a}{f_a}\right)\Psi\,, \qquad \Phi \to \exp\left(ix_\Phi \frac{a}{f_a}\right)\Phi\,, \tag{3.1.16}$$

where $\Psi = \{Q_L, U_R, D_R, L_L, E_R\}$, $\mathbf{x}_\Psi$ are hermitian matrices in flavor space and x_Φ is a real parameter. Once applied to the Lagrangian in Eq. (3.1.1), and after expanding up to order $\mathcal{O}(1/f_a)$, we obtain a shift in the Lagrangian in terms of the rotation parameters[3] [36]:

$$\begin{aligned}
\Delta\mathscr{L} =& \frac{a}{f_a}\Big[i\overline{Q}_L\left(\mathbf{x}_Q\mathbf{Y}_u - \mathbf{Y}_u\mathbf{x}_u + x_\Phi\mathbf{Y}_u\right)\widetilde{\Phi}U_R + i\overline{Q}_L\left(\mathbf{x}_Q\mathbf{Y}_d - \mathbf{Y}_d\mathbf{x}_d - x_\Phi\mathbf{Y}_d\right)\Phi D_R \\
&+ i\overline{L}_L\left(\mathbf{x}_L\mathbf{Y}_e - \mathbf{Y}_e\mathbf{x}_e - x_\Phi\mathbf{Y}_e\right)\Phi E_R + \text{h.c.}\Big] \\
&- \frac{g'^2}{32\pi^2}\frac{a}{f_a}B_{\mu\nu}\widetilde{B}^{\mu\nu}\,\text{Tr}\left(\frac{1}{3}\mathbf{x}_Q - \frac{8}{3}\mathbf{x}_u - \frac{2}{3}\mathbf{x}_d + \mathbf{x}_L - 2\mathbf{x}_e\right) \\
&- \frac{g^2}{32\pi^2}\frac{a}{f_a}W^i_{\mu\nu}\widetilde{W}^{\mu\nu,i}\,\text{Tr}\left(3\mathbf{x}_Q + \mathbf{x}_L\right) - \frac{g_S^2}{32\pi^2}\frac{a}{f_a}G^\alpha_{\mu\nu}\widetilde{G}^{\mu\nu,\alpha}\,\text{Tr}\left(2\mathbf{x}_Q - \mathbf{x}_u - \mathbf{x}_d\right) \\
&- x_\Phi\frac{\partial^\mu a}{f_a}\left(\Phi^\dagger i\overleftrightarrow{D}_\mu\Phi\right) - \frac{\partial_\mu a}{f_a}\sum_\Psi\left(\overline{\Psi}\gamma^\mu\mathbf{x}_\Psi\Psi\right)\,.
\end{aligned} \tag{3.1.17}$$

For instance, the relations between chirality-preserving and chirality-flipping fermionic operators in Eq. (3.1.9) can be obtained choosing $\mathbf{x}_\Psi = \hat{\mathbf{c}}_\Phi$, while the choice

$$\mathbf{x}_u = -\mathbf{x}_d = -\mathbf{x}_e = c_{a\Phi}\mathbb{1}\,, \qquad \mathbf{x}_Q = \mathbf{x}_L = 0 \qquad x_\Phi = c_{a\Phi}\,, \tag{3.1.18}$$

leads to Eq. (3.1.13).

3.1.2 ALP EFT below the EWSB scale

ALP couplings to gauge bosons

After EWSB, the ALP couples to the physical gauge bosons: photons, W's and Z's and gluons. These interactions are typically expressed as follows

$$\begin{aligned}
\mathscr{L}^{X\widetilde{X}}_{ALP} \supset& -\frac{1}{4}g_{a\gamma\gamma}aF_{\mu\nu}\widetilde{F}^{\mu\nu} - \frac{1}{4}g_{a\gamma Z}aF_{\mu\nu}\widetilde{Z}^{\mu\nu} - \frac{1}{4}g_{aZZ}aZ_{\mu\nu}\widetilde{Z}^{\mu\nu} \\
&- \frac{1}{2}g_{aWW}aW^+_{\mu\nu}\widetilde{W}^{\mu\nu,-} - \frac{1}{4}g_{agg}aG^\alpha_{\mu\nu}\widetilde{G}^{\mu\nu,\alpha}\,,
\end{aligned} \tag{3.1.19}$$

[3] Bear in mind that, up to order $\mathcal{O}(1/f_a)$, only the SM Lagrangian contributes to such shift.

where $Z_{\mu\nu}$ and $W^{\pm}_{\mu\nu}$ are the field strengths of the Z and the $W^{\pm}$ bosons. The physical couplings $\{g_{a\gamma\gamma}, g_{a\gamma Z}, g_{aZZ}, g_{aWW}, g_{agg}\}$ are in turn related to the three high-energy anomalous couplings $\{c_{\widetilde{W}}, c_{\widetilde{B}}, c_{\widetilde{G}}\}$ as a consequence of gauge invariance in the ALP EFT:

$$
\begin{aligned}
g_{a\gamma\gamma} &= \frac{4}{f_a}\left(c_w^2 c_{\widetilde{B}} + s_w^2 c_{\widetilde{W}}\right), & g_{a\gamma Z} &= \frac{8}{f_a} c_w s_w \left(c_{\widetilde{W}} - c_{\widetilde{B}}\right), \\
g_{aZZ} &= \frac{4}{f_a}\left(s_w^2 c_{\widetilde{B}} + c_w^2 c_{\widetilde{W}}\right), & g_{aWW} &= \frac{4}{f_a} c_{\widetilde{W}}, \\
& & g_{agg} &= \frac{4}{f_a} c_{\widetilde{G}},
\end{aligned}
\tag{3.1.20}
$$

where $c_w(s_w)$ is the cosine (sine) of the weak mixing angle. Notice that the four ALP-EW interactions depend only on two couplings, $c_{\widetilde{W}}$ and $c_{\widetilde{B}}$, which can be used to recast bounds from a subset of the four EW physical couplings to the others.

ALP couplings to fermions

Fermion rotations in Eq. (1.3.9), required to diagonalize the fermion mass matrices after EWSB, must also be applied to the ALP-fermion operators. Since up and down sectors undergo different rotations, the ALP now couples differently to LH up and down quarks below the EWSB scale:

$$
\begin{aligned}
\mathscr{L}^{\Psi}_{ALP} = &\frac{\partial_\mu a}{f_a}\Big(\overline{U}_L\gamma^\mu \mathbf{c}_U U_L + \overline{D}_L\gamma^\mu \mathbf{c}_D D_L + \overline{U}_R\gamma^\mu \mathbf{c}_u U_R + \overline{D}_R\gamma^\mu \mathbf{c}_d D_R \\
&+ \overline{L}_L\gamma^\mu \mathbf{c}_L L_L + \overline{E}_R\gamma^\mu \mathbf{c}_e E_R\Big), \\
= &\frac{\partial_\mu a}{f_a}\Big[\overline{U}\gamma^\mu\left(\mathbf{c}_U P_L + \mathbf{c}_u P_R\right)U + \overline{D}\gamma^\mu\left(\mathbf{c}_D P_L + \mathbf{c}_d P_R\right)D \\
&+ \overline{E}\gamma^\mu\left(\mathbf{c}_L P_L + \mathbf{c}_e P_R\right)E + \overline{\nu}_L\gamma^\mu\left(\mathbf{c}_L P_L\right)\nu_L\Big],
\end{aligned}
\tag{3.1.21}
$$

where $P_{L,R}$ denotes the LH and RH projectors, respectively, and the phenomenological ALP-fermion couplings $\mathbf{c}_\Psi$ read

$$
\begin{aligned}
\mathbf{c}_U &\equiv \mathbf{V}^{u\dagger}_L \hat{\mathbf{c}}_Q \mathbf{V}^u_L, & \mathbf{c}_D &\equiv \mathbf{V}^{d\dagger}_L \hat{\mathbf{c}}_Q \mathbf{V}^d_L, & \mathbf{c}_L &\equiv \mathbf{V}^{e\dagger}_L \hat{\mathbf{c}}_L \mathbf{V}^e_L, \\
\mathbf{c}_u &\equiv \mathbf{V}^{u\dagger}_R \hat{\mathbf{c}}_u \mathbf{V}^u_R, & \mathbf{c}_d &\equiv \mathbf{V}^{d\dagger}_R \hat{\mathbf{c}}_d \mathbf{V}^d_R, & \mathbf{c}_e &\equiv \mathbf{V}^{e\dagger}_R \hat{\mathbf{c}}_e \mathbf{V}^e_R.
\end{aligned}
\tag{3.1.22}
$$

On the other hand, Eq. (3.1.21) can be expressed as explained above, in terms of chirality-flipping operators, after integration by parts and application of the SM EOM:

$$
\mathscr{L}^{\Psi}_{ALP} = -i\frac{a}{f_a}\sum_{\Psi}\sum_{k,l}\left[\left(m_{\Psi^k} - m_{\Psi^l}\right)\left(\widetilde{\mathbf{Y}}^S_\Psi\right)_{kl}\Psi^k\Psi^l + \left(m_{\Psi^k} + m_{\Psi^l}\right)\left(\widetilde{\mathbf{Y}}^P_\Psi\right)_{kl}\Psi^k\gamma^5\Psi^l\right],
\tag{3.1.23}
$$

where k and l are flavor indices, $\Psi = U, D, E$ and m_{Ψ^k} labels the mass of its k-th flavor component. The $n_g \times n_g$ matrices, $\widetilde{\mathbf{Y}}^S$ and $\widetilde{\mathbf{Y}}^P$, denote the ALP couplings to the scalar and pseudoscalar fermion currents, respectively, and are defined as

$$
\widetilde{\mathbf{Y}}^{S,P}_U \equiv \frac{1}{2}\left(\mathbf{c}_u \pm \mathbf{c}_U\right), \qquad \widetilde{\mathbf{Y}}^{S,P}_D \equiv \frac{1}{2}\left(\mathbf{c}_d \pm \mathbf{c}_D\right), \qquad \widetilde{\mathbf{Y}}^{S,P}_E \equiv \frac{1}{2}\left(\mathbf{c}_e \pm \mathbf{c}_L\right).
\tag{3.1.24}
$$

It is noteworthy that only pseudoscalar couplings contribute to flavor-diagonal interactions in Eq. (3.1.23). Furthermore, tree-level ALP-fermion interactions are proportional to the fermion masses, which is not *a priori* expected from the chirality-preserving

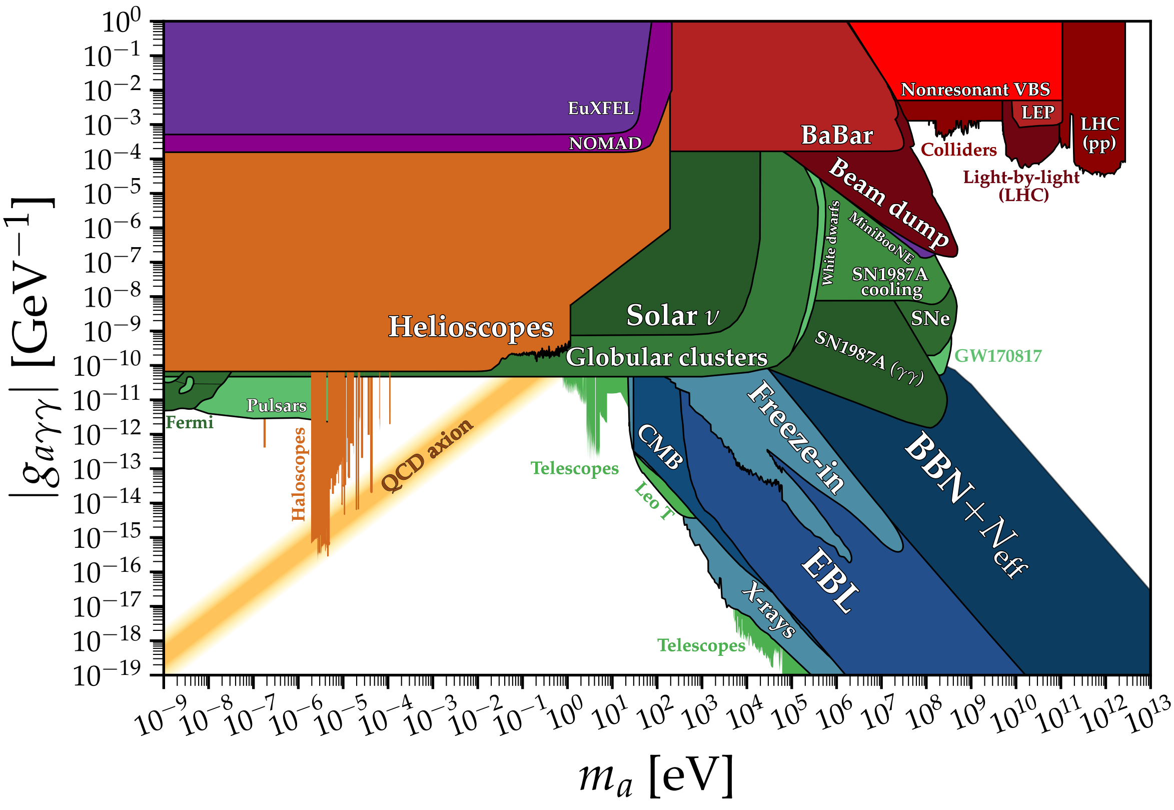

Figure 3.1: Current bounds on ALP coupling to photons $g_{a\gamma\gamma}$ as a function of the axion mass m_a. Figure adapted from Ref. [157].

basis in Eq. (3.1.21). Thus, ALP couplings to light fermions are expected to be mass-suppressed and therefore subdominant with respect to couplings to heavier fermions. The caveat is that in passing from the derivative basis to the chirality-flipping one, anomalous terms appear, not suppressed by fermion masses, a fact that we will profit from in Chap. 5.

3.2 Experimental constraints on the ALP parameter space

We present the most recent experimental bounds on ALP couplings to SM particles in the ALP EFT framework. We include plots for the coupling to photons, illustrating the excluded regions in the $\{m_a, g_{a\gamma\gamma}\}$ parameter space, and for the coupling to top quarks, which is particularly relevant for ALP searches at colliders. We also discuss the numerical limits for couplings to the other gauge bosons, electrons and nucleons. Additional plots for ALP coupling to gauge bosons and ALP couplings to charged leptons and neutrinos can be found in Chap. 4 and 6, respectively.

3.2.1 ALP coupling to EW gauge bosons

As discussed in Sec. 3.1.2, the ALP couplings to EW gauge bosons $\{g_{a\gamma\gamma}, g_{a\gamma Z}, g_{aZZ}, g_{aWW}\}$ depend on the two EW anomalous couplings $\{c_{\widetilde{W}}, c_{\widetilde{B}}\}$ in Eq. (3.1.11), as a consequence of gauge invariance in the ALP EFT. Although classical searches used to focus on the ALP coupling to photons, which is significantly constrained by a plethora of experimental searches across a wide range of masses, such as astrophysical observations, haloscopes or diphoton production at the LHC, more recently interest has extended to the ALP couplings to the massive EW gauge bosons, which are, in turn, harder to access.

At present, these couplings can only be probed indirectly, via loop effects in low-energy procceses [36, 90, 139, 140, 144, 149, 158–162], or directly at colliders. For instance, at the LHC, depending on the ALP mass and decay width, ALP-EW interactions can be probed via the associated production of a gauge boson —γ, Z or $W^\pm$— and an ALP, where the ALP can either escape detection [133, 137] or decay resonantly [141, 163, 164]; or in nonresonant processes, where the ALP enters as a very off-shell mediator [146], which are further discussed in Sec. 3.3.

ALP coupling to photons

The ALP coupling to photons $g_{a\gamma\gamma}$ —through $c_{\widetilde{W}}$ and $c_{\widetilde{B}}$— is a free parameter of the ALP EFT, and therefore independent of the ALP mass. In turn, the QCD axion coupling to photons (see Eq. (2.4.23)) does depend on the axion mass, via the m_a dependence on f_a in Eq. (2.4.14).

Current experimental constraints on $\{m_a, g_{a\gamma\gamma}\}$ are represented in Fig. 3.1. Since the QCD axion mass receives two contributions, a model-dependent $\sim E/N$ term, and a model-independent term, QCD axion models are characterized by a “dilute” band in this parameter space, depicted in yellow in Fig. 3.1.

Bounds in orange correspond mainly to searches based on the ALP-photon conversion in the presence of an external magnetic field, also known as *Primakoff effect* [165, 166]. These include: helioscope searches for solar axions, such as CAST [167, 168]; haloscopes, aiming to detect axions and ALP candidates to DM either via resonant cavities, such as ADMX [169–172], ADMX SLIC [173], CAPP [174–179], RBF [180], HAYSTAC [181–183], QUAX [184–186] and ORGAN [187, 188], or using strong toroidal magnetic fields like ABRACADABRA [189, 190] and SHAFT [191]; “light shining through a wall” experiments, like CROWS [192], ALPS-I [193] or OSQAR [194]; and others.

Stellar bounds are shown in green. We include constraints derived from: searches for spectral irregularities due to ALP-photon oscillations with the Fermi telescope [195]; ALP production in pulsar magnetospheres [196], in metastable hypermassive neutron stars [197] (GW170817), and its effects on stellar evolution at globular clusters [198, 199]; helioseismology and solar neutrino observations [200]; supernovae (SNe) [201], and in particular, those derived from the possible contribution of ALPs to the cooling [201] and explosion energy [202] of SN1987A; the gas temperature of the *Leo T* galaxy [203]; and telescopes searches targeting photon-pair production from the decay of DM ALPs, such as JWST [204], WINERED [205], MUSE [206], VIMOS [207], HST [208, 209], XMM-Newton [210], NuSTAR [211–213] and INTEGRAL [214].

Bounds from cosmological observables —which typically assume that DM is mainly made of ALPs who participate in the cosmological evolution of the universe— are depicted in blue. We include limits derived from searches targeting distortions on the CMB [215, 216]; from the contribution of ALP decays into the X-ray background as well as the extragalactic background light (EBL) spectrum [217]; constraints derived from the impact of ALPs on the abundance of light elements produced during Big Bang Nucleosynthesis, taking into account additional effects on N_{eff} [218]; and bounds from the contribution of an irreducible freeze-in to the relic density of axions [219].

Bounds in red correspond to high-energy collider searches. We find: constraints from beam-dump experiments [220–224]; light-by-light scattering in Pb-Pb nuclei collisions at CMS [225] and ATLAS [226]; proton-proton (pp) collisions at the LHC [227]; new physics searches in $e^+e^- \to 2\gamma$, 3γ at LEP [138]; searches targeting charged lepton flavor fiolation of mesons at BaBar [222]; among others [138, 227–230]. We also include the bound derived from our study of vector boson scattering procceses mediated by a very off-shell —or *nonresonant*— ALP at the LHC [1], which will be discussed in detail in Chap. 4.

Finally, in different shades of purple, we find constraints from neutrino experiments, such as NOMAD [231] and MiniBooNE [232], as well as bounds obtained at the European X-ray Free Electron Laser facility (EuXFEL) [233].

ALP coupling to γZ

The most constraining bounds on $g_{a\gamma Z}$ are derived from searches targeting Z-boson observables at LEP. In particular, for ALPs lighter than the Z boson, the non-observation of exotic $Z \to \gamma +$ invisible decays allows to set stringent constraints [90, 141]

$$|g_{a\gamma Z}| \lesssim 6 \times 10^{-5}\ \mathrm{GeV}^{-1}\,, \qquad \text{for } m_a \lesssim 400\ \mathrm{MeV}\,; \tag{3.2.1}$$

whereas if the assumption of a stable ALP is relaxed, we find a more conservative bound from the measurement of the total Z-decay width [133, 141]:

$$|g_{a\gamma Z}| \lesssim 2 \times 10^{-3}\ \mathrm{GeV}^{-1}\,, \qquad \text{for } m_a \lesssim M_Z\,. \tag{3.2.2}$$

For higher ALP masses, the $\{m_a, g_{a\gamma Z}\}$ parameter space is dominated by LHC searches, such as the nonresonant ALP-mediated VBS bounds obtained in our work in Ref. [1] (see Chap. 4):

$$|g_{a\gamma Z}| \lesssim 5 \times 10^{-3}\ \mathrm{GeV}^{-1}\,, \qquad \text{for } m_a \lesssim 100\ \mathrm{GeV}\,, \tag{3.2.3}$$

derived from a reinterpretation of four CMS VBS analyses [234–237]; or limits from resonant triboson searches [141]:

$$|g_{a\gamma Z}| \lesssim 5 \times 10^{-2}\ \mathrm{GeV}^{-1}\,, \qquad \text{for } 100\ \mathrm{GeV} \lesssim m_a \lesssim 500\ \mathrm{GeV}\,. \tag{3.2.4}$$

ALP coupling to ZZ

The ALP coupling to the Z boson, g_{aZZ}, is harder to access experimentally since it cannot be probed via Z-boson decays. The most stringent constraints stem from LHC searches for exotic mono-Z channels

$$|g_{aZZ}| \lesssim 8 \times 10^{-4}\ \mathrm{GeV}^{-1}\,, \qquad \text{for } m_a \lesssim 400\ \mathrm{MeV}\,, \tag{3.2.5}$$

and from nonresonant ALP-mediated VBS searches at CMS [1]:

$$|g_{aZZ}| \lesssim 3 \times 10^{-3}\ \mathrm{GeV}^{-1}\,, \qquad \text{for } m_a \lesssim 100\ \mathrm{GeV}\,. \tag{3.2.6}$$

ALP coupling to WW

For sub-GeV ALP masses, g_{aWW} is constrained via its loop contribution to rare meson decays [149]:

$$|g_{aWW}|\lesssim 3\times 10^{-6}\ \mathrm{GeV}^{-1}\,, \qquad\qquad \text{for } m_a \lesssim 400\ \mathrm{MeV}\,. \tag{3.2.7}$$

For larger masses, we find again out limits from nonresonant VBS processes [1]

$$|g_{aWW}|\lesssim 3\times 10^{-3}\ \mathrm{GeV}^{-1}\,, \qquad\qquad \text{for } m_a \lesssim 100\ \mathrm{GeV}\,, \tag{3.2.8}$$

and constraints from resonant triboson searches at CMS [238]:

$$|g_{aWW}|\lesssim 2\times 10^{-2}\ \mathrm{GeV}^{-1}\,, \qquad \text{for } 200\ \mathrm{GeV} \lesssim m_a \lesssim 600\ \mathrm{GeV}\,. \tag{3.2.9}$$

3.2.2 ALP coupling to gluons

ALP interactions with gluons $aG\widetilde{G}$ depend on one parameter in Eq. (3.1.19), $g_{agg} \propto c_{\widetilde{G}}$, which is a free parameter of the ALP EFT, and therefore independent of the ALP mass. On the other hand, a non-zero coupling to gluons is required in QCD axion models in order to solve the Strong CP problem. In particular, *photophobic* QCD axion models, i.e. models where $E/N \approx 1.92$, so that the coupling to photons in Eq. (2.4.23) is approximately zero, the constraints in Fig. 3.1 might be eluded. In such scenarios, the alternative parameter space is that of the axion coupling to gluons $\{m_a, g_{agg}\}$.

For masses $m_a \lesssim 100$ MeV, the most constraining bounds [149] are derived from experimental tests of the branching ratio for the rare kaon decay to missing energy, $K^+ \to \pi^+ +$invisible [239]. While in the SM, this is dominated by the decay to neutrinos, $K^+ \to \pi^+\overline{\nu}\nu$, if there is a light ALP, stable at collider distances, the process $K^+ \to \pi^+ a$, where a escapes the NA62 detector [239], will contribute as well, which allows to set an upper limit on g_{agg}:

$$|g_{agg}|\lesssim 3\times 10^{-6}\ \mathrm{GeV}^{-1}\,, \qquad\qquad \text{for } m_a \lesssim 100\ \mathrm{MeV}\,. \tag{3.2.10}$$

The ALP coupling to gluons can also be tested at colliders. For instance: in mono-jet searches [240, 241] at the LHC, where ALP production in association with a gluon allows to set limits on g_{agg} [137]:

$$|g_{agg}|\lesssim 6\times 10^{-5}\ \mathrm{GeV}^{-1}\,, \qquad\qquad \text{for } m_a \lesssim 1\ \mathrm{GeV}\,; \tag{3.2.11}$$

and in dijet production in association with an ALP [242]:

$$|g_{agg}|\lesssim 1.8\times 10^{-6}\ \mathrm{GeV}^{-1}\,, \qquad\qquad \text{for } m_a \lesssim 1\ \mathrm{MeV}\,. \tag{3.2.12}$$

3.2.3 ALP coupling to tops

Since ALP coupling to fermions are proportional to the fermion mass, there is a strong motivation to target the ALP couplings to the top quark at colliders. We review here the strongest experimental limits on the $\{m_a, c_{tt}\}$ parameter space, where c_{tt} is defined as[4]

$$\mathscr{L}_{ALP} \supset \frac{c_{tt}}{f_a}\partial_\mu a\left(\bar{t}\gamma^\mu\gamma^5 t\right)\,. \tag{3.2.13}$$

[4]As discussed in Sec. 3.1.2, only ALP couplings to pseudoscalar fermionic currents contribute to flavor-diagonal interactions.

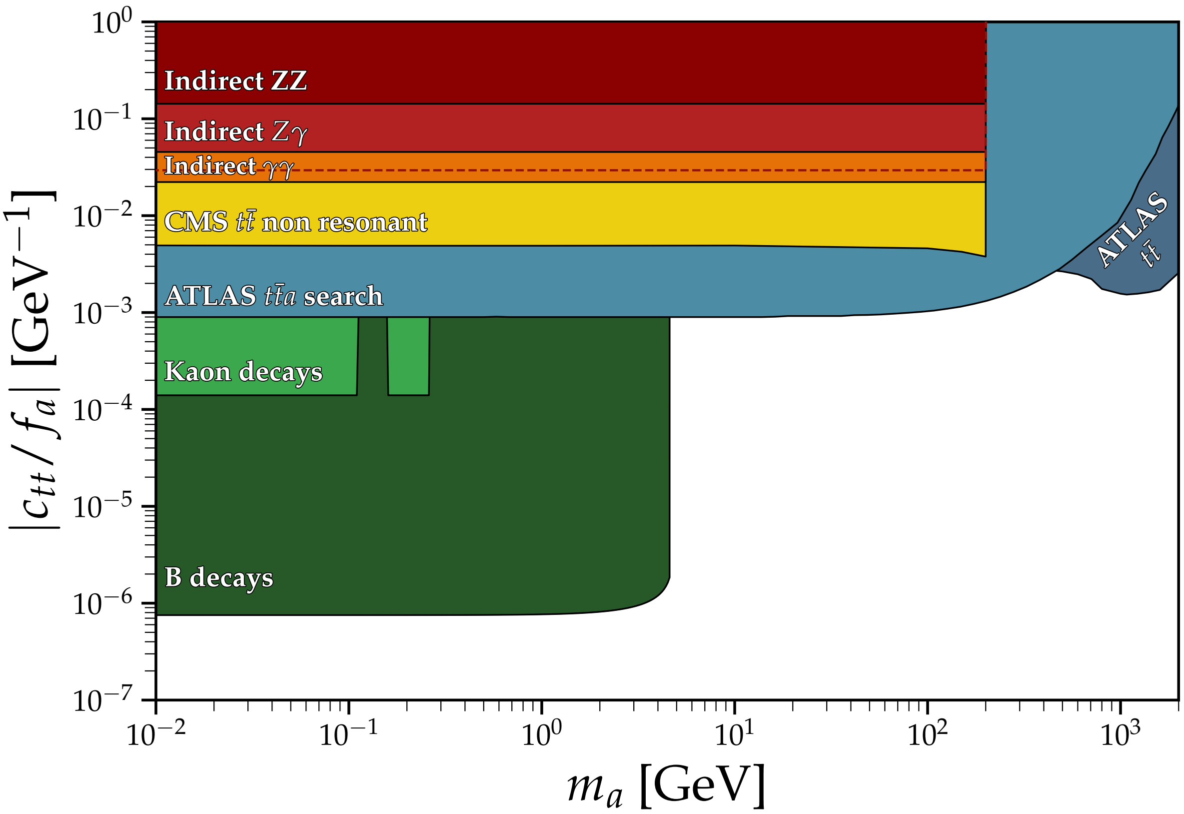

Figure 3.2: Current bounds on ALP coupling to top quarks c_{tt} as a function of the axion mass m_a. Figure adapted from Refs. [157, 243].

The limits in the top left corner of Fig. 3.2 have been recasted in Ref. [243] from the one-loop impact of the ALP coupling to top quarks on the couplings to gauge bosons. Regions in dark and light red, orange and yellow correspond to the nonresonant ALP-mediated bounds on $g_{agg} \cdot g_{aVV'}$ —where $g_{aVV'}$ denotes the ALP-EW couplings— in Ref. [146], while the dashed red line corresponds to that of the most recent nonresonant limit on g_{aZZ} in Ref. [244].

In blue we show bounds obtained from the reinterpretation of two ATLAS analyses [243]: direct constraints from the associated production of an ALP and a top pair $pp \to t\bar{t} + a$ [245]; and ALP-mediated $t\bar{t}$ production [246, 247].

Finally, bounds in green [243] are obtained from Kaon and B-meson decays to invisibles, $K \to \pi +$ invisible [239] and $B \to K +$ invisible [248].

3.2.4 ALP coupling to electrons

In Chap. 5 we review in detail constraints on pseudoscalar ALP couplings to charged leptons and neutrinos, illustrated in Figs. 2, 3 and 4. We provide here a concise overview of the strongest experimental limits on the ALP coupling to electrons c_{ee},

$$\mathscr{L}_{ALP} \supset \frac{c_{ee}}{f_a} \partial_\mu a \left(\bar{e} \gamma^\mu \gamma^5 e \right) , \tag{3.2.14}$$

since they are relevant in a wide range of masses and experiments, from astrophysical observations to colliders.

For sub-GeV ALP masses, the $\{m_a, c_{ee}\}$ parameter space is dominated by astrophysical and cosmological bounds. In particular, we find constraints derived from the luminosity evolution of low-energy supernovae as well as SN1987A [197, 201, 202], which are recasted from those in Fig. 3.1, via the loop-induced ALP-photon coupling due to ALP-electron interactions [249],

$$|c_{ee}/f_a| \lesssim 10^{-8}\ \text{GeV}^{-1}\,, \qquad \text{for } 1\ \text{MeV} \lesssim m_a \lesssim 200\ \text{MeV}\,. \tag{3.2.15}$$

Others bounds populate the parameter space for smaller masses, such as those derived from the contribution of an irreducible freeze-in to the relic density of axions [219], from the DM experiments XENON1T [250–252] and XENONnT [253], and from the measurement of the brightness of red giants in the globular cluster ω Centauri [254].

On the other hand, for larger masses we find constraints from rare B meson decays [149]

$$|c_{ee}/f_a| \lesssim 10^{-2}\ \text{GeV}^{-1}\,, \qquad \text{for } 200\ \text{MeV} \lesssim m_a \lesssim 3\ \text{GeV}\,, \tag{3.2.16}$$

and from collider searches such as light-by-light scattering procceses in Pb-Pb collisions [225, 255], diphoton production at the LHC [256] and resonant triboson searches [141, 238]

$$\begin{aligned} |c_{ee}/f_a| &\lesssim 10^{-1}\ \text{GeV}^{-1}\,, \qquad &&\text{for } 3\ \text{GeV} \lesssim m_a \lesssim 100\ \text{GeV}\,,\\ |c_{ee}/f_a| &\lesssim 1\ \text{GeV}^{-1}\,, &&\text{for } 100\ \text{GeV} \lesssim m_a \lesssim 1\ \text{TeV}\,. \end{aligned} \tag{3.2.17}$$

3.2.5 ALP coupling to nucleons

In order to describe ALP interactions with mesons and nucleons below the QCD confinement scale, it is appropriate to match the Lagrangian in Eq. (3.1.19) to a chiral effective theory [84, 89, 140, 148, 257–259]. In particular, ALP coupling to nucleons can be expressed in terms of the following operator:

$$\mathscr{L}_a \supset \frac{C_{aN}}{2f_a}\partial_\mu a \left(\overline{\Psi}_N \gamma^\mu \gamma^5 \Psi_N\right)\,, \tag{3.2.18}$$

where C_{aN} is a real coupling and $N = \{p, n\}$ denotes the nucleon —proton or neutron, respectively— with field Ψ_N.

The strongest constraints on ALP couplings to neutrons are derived from isolated neutron star cooling due to ALP emission [260], while those on couplings to protons come from the non-observation of extra events inside the Kamiokande-II [261, 262] neutrino detector at the time of SN1987a [263]:

$$\begin{aligned} |C_{an}/f_a| &\lesssim 1.4\times 10^{-9}\ \text{GeV}^{-1}\,, \qquad &&\text{for } m_a \lesssim 16\ \text{meV}\,,\\ |C_{ap}/f_a| &\lesssim 8.9\times 10^{-10}\ \text{GeV}^{-1}\,, &&\text{for } m_a \lesssim 100\ \text{MeV}\,. \end{aligned} \tag{3.2.19}$$

3.3 Nonresonant ALP searches

Nonresonant ALP searches were originally proposed in Ref. [146] in the context of ALP-mediated gluon-initiated $2 \to 2$ processes with EW bosons, gluons and $t\bar{t}$ final states. Since the ALP is too light to be produced resonantly, the signals and limits of such processes do not depend on the ALP mass and decay width up to the resonant threshold. In this sense, nonresonant searches are more model-independent than resonant analyses,

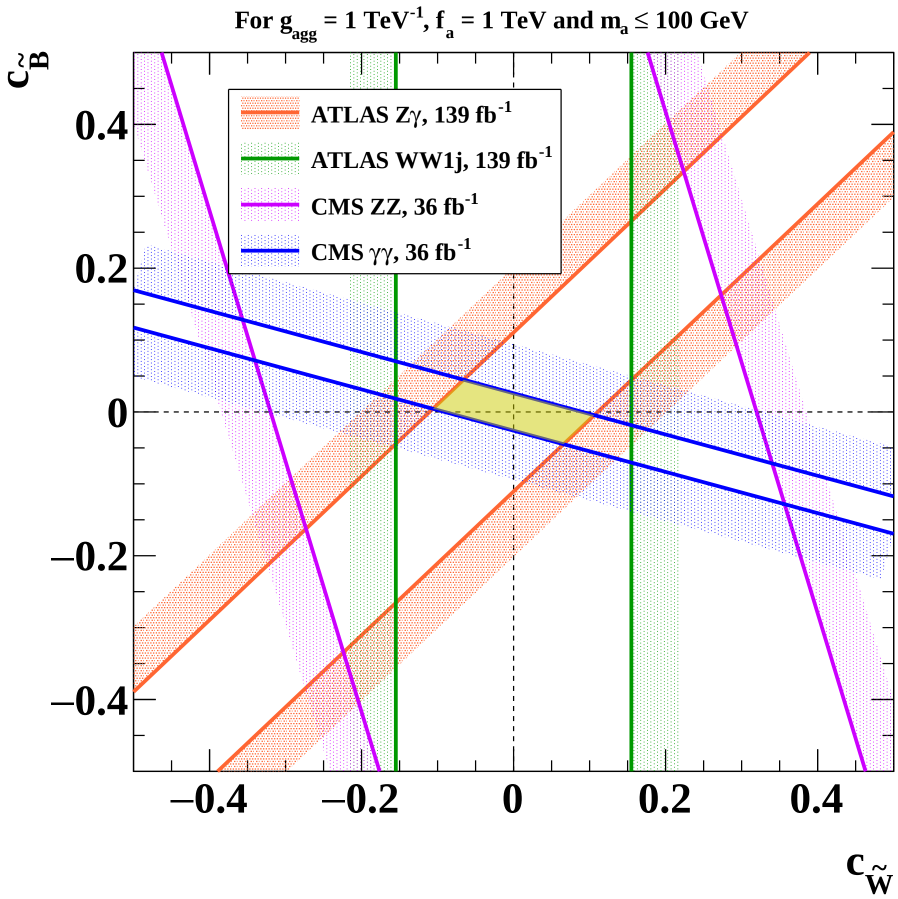

Figure 3.3: 95% CL constraints on the ALP-EW parameter space $\left(c_{\widetilde{W}}, c_{\widetilde{B}}\right)$ from Ref. [154] (ZZ and $\gamma\gamma$) and from Ref. [266] ($Z\gamma$ and WW), for $g_{agg} = 1$ TeV^{-1}. Figure extracted from Ref. [266].

for which the dependence on other ALP couplings may appear through the partial decay widths.

The key observation is that, these novel searches take advantage of the derivative nature of ALP interactions, which enhances the cross sections for center-of-mass energies $\hat{s} \gg m_a^2$ with respect to usual SM-mediated channels. For instance, the cross section for the ALP-mediated gluon-initiated diboson production $gg \to a^* \to V_1 V_2$ scales as

$$\sigma \propto g_{agg}^2 g_{aV_1V_2}^2 \frac{\hat{s}}{f_a^4} \sim \frac{\hat{s}}{f_a^4}\,, \tag{3.3.1}$$

where $\sqrt{\hat{s}} = m_{V_1V_2}$ is the invariant diboson mass, while the usual SM s-channel process scales as $\sim 1/\hat{s}$.

The power of this novel type of search is illustrated by deriving new limits on the product of the ALP-coupling to the EW gauge bosons and the ALP coupling to gluons from gluon-initiated diboson production scattering processes, using public data from LHC Run 2 CMS searches [264, 265] (see Fig. 3.3). These results [146] led to a dedicated ALP search at CMS, targeting ZZ and Zh gluon-initiated diboson production [244].

In Chap. 4, we discuss this novel technique in the context of ALP-mediated VBS processes at the LHC, where we obtain new bounds on ALP couplings to EW gauge bosons independently of the coupling to gluons. Nonresonant ALP constraints on the

ALP-EW couplings (see Fig. 6 in Chap. 4) either probe previously unexplored regions of the ALP parameter space or overlap with other limits, with the advantage of being model-independent.

Finally, it is noteworthy that the dark and light red, orange and yellow bounds on the ALP-top coupling in Fig. 3.2 [243] were also derived from nonresonant ALP constraints [146, 244, 246].

Part II

ALP Phenomenology

Chapter 4

Nonresonant Searches for Axion-Like Particles in Vector Boson Scattering Processes at the LHC

This chapter contains the publication in Ref. [1]. In this work a new experimental search window for ALPs at colliders is proposed: nonresonant ALP-mediated vector boson scattering (VBS).

Nonresonant ALP searches were originally proposed in the context of ALP-mediated diboson production [146]. The point is that, in the same way that, e.g., off-shell photons or Z bosons at LEP were key to explore new parameter space, ALPs can also be exchanged off-shell contrary to previous assumptions in the literature. These novel searches take advantage of the derivative nature of ALP interactions, which originate a harder scaling with energy than usual SM-mediated channels. Since the ALP is too light to be produced resonantly, the signals of such processes are independent of the ALP mass and decay width up to ALP masses $m_a \lesssim 100$ GeV. In addition, VBS processes provide access to the ALP couplings to the EW gauge bosons independently of the coupling to gluons —i.e., nonresonant ALP-mediated VBS signals depend only on the two ALP-EW parameters ($c_{\widetilde{W}}/f_a$, $c_{\widetilde{B}}/f_a$)—, while the derivative character of ALP interactions is expected to originate a deviation in the tail of the diboson invariant and transverse mass distributions.

Five CMS VBS analyses with lepton and photon final states are reinterpreted here. These searches target the EW production of ZZ, $Z\gamma$, $W^\pm\gamma$, $W^\pm Z$ and same-sign $W^\pm W^\pm$ pairs with large diboson invariant mass in association with two forward jets in VBS processes [234–237]. We simulate the ALP signal and its interference with the SM EW contribution, which can be parametrized polynomically in terms of the ALP-EW effective couplings. Since no excess is found, current limits, using CMS Run 2 data, are obtained on the UV effective couplings

$$c_{\widetilde{W}}/f_a < 0.75 \text{ TeV}^{-1}\,, \qquad\qquad c_{\widetilde{B}}/f_a < 1.59 \text{ TeV}^{-1}\,,$$

and consequently —via gauge invariance— on the phenomenological couplings to the EW gauge bosons, $g_{a\gamma\gamma}$, $g_{a\gamma Z}$, g_{aZZ} and g_{aWW}, for masses $m_a \lesssim 100$ GeV. Similarly, we obtain projected limits for Run 3,

$$c_{\widetilde{W}}/f_a < 0.71 \text{ TeV}^{-1}\,, \qquad\qquad c_{\widetilde{B}}/f_a < 1.12 \text{ TeV}^{-1}\,,$$

and the High-Luminosity LHC (HL-LHC),

$$c_{\widetilde{W}}/f_a < 0.55 \text{ TeV}^{-1}\,, \qquad\qquad c_{\widetilde{B}}/f_a < 0.79 \text{ TeV}^{-1}\,.$$

The constraints inferred on the ALP-EW couplings are independent of the ALP mass and decay width up to masses $m_a \lesssim 100$ GeV, and —unlike previous resonant searches [146, 244, 266]— of the coupling to gluons. The bounds obtained in this work are either very competitive with other limits or probe previously unexplored regions of the ALP parameter space, demonstrating the power of future dedicated nonresonant searches at ATLAS and CMS.

This chapter is structured as follows. In Sec. 3 of the present chapter, ALP-mediated VBS processes are reviewed. We discuss their characteristic observables and the relevant regions so as to distinguish the ALP signal from the SM background, the contributing topologies, and the functional dependence of the pure ALP signal and its interference with the SM in the ALP parameter space. We also comment on the validity of the ALP EFT approach for our proposal. The details concerning the simulation and analysis of the ALP signal are discussed in Sec. 4. Selection cuts, data and backgrounds are taken from the original CMS analyses. Results are presented in Sec. 5 and are obtained from a maximum likelihood fit of signal and background to the invariant and transverse diboson masses. The log-likelihood is constructed based on a Poisson distribution. Systematic uncertainties of the ALP signal are taken to be fully correlated across all channels and bins, with a a total size of 20% obtained adding in quadrature the contributions from different sources of uncertainty. Finally, we compare our results to existing experimental bounds in Sec. 6. We have used MadGraph5_aMC@NLO 2.8.2 [267] in combination with the `ALP_linear` UFO model in Ref. [133, 268] for the simulation of the ALP signal and its interference with the SM EW channel, as well as Pythia 8 [269] for the simulation of parton showering, hadronization and decays, and Delphes 3 [270] for the CMS detector simulation. The latter is calibrated comparing the expected yields in the SM EW channel obtained by the CMS simulation with ours, which results in a scale factor that is later applied to the ALP signal.

Published for SISSA by Springer

Received: *February 28, 2022*
Revised: *May 3, 2022*
Accepted: *May 17, 2022*
Published: *June 20, 2022*

Nonresonant searches for axion-like particles in vector boson scattering processes at the LHC

J. Bonilla,[a,b] I. Brivio,[c] J. Machado-Rodríguez[a,b] and J.F. de Trocóniz[a]

[a] *Departamento de Física Teórica, Universidad Autónoma de Madrid, Cantoblanco, E-28049, Madrid, Spain*
[b] *Instituto de Física Teórica IFT-UAM/CSIC, Cantoblanco, E-28049, Madrid, Spain*
[c] *Institut für Theoretische Physik, Universität Heidelberg, Philosophenweg 16, D-69120 Heidelberg, Germany*

E-mail: jesus.bonilla@uam.es, brivio@thphys.uni-heidelberg.de, jonathan.machado@uam.es, jorge.troconiz@uam.es

Abstract: We propose a new search for Axion-Like Particles (ALPs), targeting Vector Boson Scattering (VBS) processes at the LHC. We consider nonresonant ALP-mediated VBS, where the ALP participates as an off-shell mediator. This process occurs whenever the ALP is too light to be produced resonantly, and it takes advantage of the derivative nature of ALP interactions with the electroweak Standard Model bosons. We study the production of ZZ, $Z\gamma$, $W^{\pm}\gamma$, $W^{\pm}Z$ and $W^{\pm}W^{\pm}$ pairs with large diboson invariant masses in association with two jets. Working in a gauge-invariant framework, upper limits on ALP couplings to electroweak bosons are obtained from a reinterpretation of Run 2 public CMS VBS analyses. The constraints inferred on ALP couplings to ZZ, $Z\gamma$ and $W^{\pm}W^{\pm}$ pairs are very competitive for ALP masses up to 100 GeV. They have the advantage of being independent of the ALP coupling to gluons and of the ALP decay width. Simple projections for LHC Run 3 and HL-LHC are also calculated, demonstrating the power of future dedicated analyses at ATLAS and CMS.

Keywords: Axions and ALPs, Electroweak Precision Physics, Specific BSM Phenomenology

ArXiv ePrint: 2202.03450

https://doi.org/10.1007/JHEP06(2022)113

JHEP06(2022)113

Contents

JHEP06(2022)113

1 Introduction

Axion-Like Particles (ALPs) constitute a particularly attractive class of hypothetical particles, that are predicted in a variety of Standard Model (SM) extensions, ranging from invisible axion models [1–8] to string theory [9]. They are defined as the pseudo-Goldstone bosons of a generic, spontaneously broken global symmetry, that is restored only at energy scales much higher compared to the electroweak (EW) one. Besides the Peccei-Quinn symmetry, typical examples are the lepton number [10–12] or flavor symmetries [13–15]. Being pseudo-Goldstone bosons, ALPs are pseudo-scalar particles, singlets under the SM gauge groups, and naturally much lighter than the beyond-SM (BSM) sector they originate from. As a consequence, they are most conveniently studied in an Effective Field Theory (EFT) framework, constructed as an expansion in inverse powers of the ALP characteristic scale f_a.

At the leading order, the ALP EFT only includes very few parameters (up to flavor indices). Nevertheless, the ranges allowed *a priori* for both the ALP mass m_a and scale f_a are extremely vast, spanning several orders of magnitude. As a result, the phenomenology of ALPs is one of the richest in particle and astroparticle physics. This peculiarity, together with their ubiquity in BSM models, has recently brought this class of particles into the spotlight, stimulating enormous theoretical and experimental advancements. A plethora of experiments searching for ALPs in different regimes and exploiting very diversified techniques are either already taking data or scheduled to do so in the next decade, see e.g. [16, 17] for recent reports.

Most of these experiments are sensitive to ALPs coupling to photons, electrons or gluons. ALP interactions with the massive gauge bosons, on the other hand, are harder to access: at present, they can only be probed indirectly via loop corrections to low-energy processes [18–28] or directly at colliders. At the LHC, depending on the ALP mass and decay width, ALP-gauge interactions can be probed in V+ALP associated production processes, with $V = \gamma, Z, W^{\pm}$ and the ALP either escaping detection [29, 30] or decaying resonantly [31–33], in resonant ALP decays into diboson pairs [31], or in nonresonant processes where the ALP enters as an off-shell mediator. The latter were first studied in the context of inclusive diboson production at the LHC, where the ALP appears in s-channel, being produced via gluon fusion [34]. These channels are sensitive to the product of the ALP coupling to gluons with the relevant coupling to dibosons and probe previously unexplored areas of the ALP parameter space. Moreover, the nonresonant cross sections and kinematical distributions are found to be independent of the ALP mass from arbitrarily light masses up to masses of the order of 100 GeV [34]. The experimental strategy is to look for deviations with respect to SM expectations in the tails of the bosons transverse momenta or diboson mass distributions. ALP coupling limits derived from reinterpretations of CMS and ATLAS Run 2 measurements were presented in refs. [34, 35], while the CMS Collaboration has recently published a dedicated search for nonresonant ALP-mediated ZZ production in semileptonic final states at the LHC [36].

In this paper we study for the first time nonresonant ALP signals in EW Vector Boson Scattering (VBS) processes at the LHC (see [37] for a review). We focus on channels containing massive EW bosons: ALP EW VBS processes with the ALP going to a photon pair were studied in ref. [38] for the LHC, in ref. [39] for CLIC and in ref. [40] for the EIC. Figure 1 depicts the leading order Feynman diagrams for ALP-mediated EW production of $q_1 q_2 \to q_1' q_2' V_1 V_2$. The two jets in the final state, q_1' and q_2', are required to have a large invariant mass and to be well separated in rapidity. These processes are particularly convenient for a number of reasons: first, they allow us to access the couplings of the ALP to EW bosons independently of the coupling to gluons. At the same time, the richness of VBS in terms of different final states helps constraining the parameter space from multiple complementary directions.

Searching for signals beyond the SM in VBS final states is a major goal for the ATLAS and CMS experiments and both collaborations have recently reported Run 2 measurements of these processes [41–56]. These analyses allow us to perform a first comparison of the ALP VBS predictions to the data, a calibration of the available simulation tools and a calculation of educated predictions for higher LHC luminosities. Moreover, nonresonant searches are generally expected to become more and more competitive during the upcoming LHC runs. They will benefit, on the one hand, from the large increase in the accumulated statistics and, on the other, from the technological developments currently driven by studies of the Standard Model EFT (SMEFT) formalism, that are encouraging a global, comprehensive approach to new physics searches. Interestingly, while SMEFT analyses rely on the assumption of new particles being too heavy to be produced on-shell, nonresonant

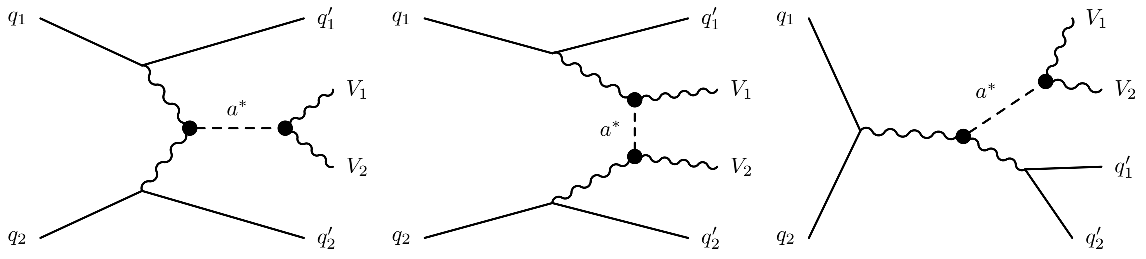

Figure 1. Feynman diagrams for ALP contributions to a generic process $q_1 q_2 \to q_1' q_2' V_1 V_2$. Fermion lines represent both quarks and antiquarks. In the last diagram, the final state quarks can be emitted from any of the outgoing bosons.

ALP searches target the opposite limit, i.e. where the ALP is *too light* to decay resonantly. In this way, they provide access to parameter space regions complementary to those probed in other LHC searches. In particular, compared to resonant or large-missing-momentum processes, they require only very minimal assumptions on the ALP decay width.

The manuscript is organized as follows: the theoretical framework adopted is defined in section 2. In section 3 we discuss the general characteristics of nonresonant ALP EW VBS production. The details of the ALP VBS simulation and analysis are explained in section 4. We first extract current constraints on ALP-gauge interactions from measurements of differential VBS observables published by the CMS Collaboration, and subsequently estimate projected limits for the LHC Run 3 and for the High Luminosity (HL-LHC) phase. The results are presented in section 5. In section 6 we compare them to other existing constraints. In section 7 we conclude.

2 The ALP effective Lagrangian

We define the ALP a as a pseudo-scalar state whose interactions are either manifestly invariant under shifts $a(x) \to a(x) + c$ (as befits its Goldstone origin) or generated via the chiral anomaly. Adopting an EFT approach, all ALP interactions are weighted down by inverse powers of the characteristic scale $f_a \gg m_a$, that is unknown and naturally close to the mass scale of the heavy sector the ALP originates from. We implicitly assume $f_a \gg v \simeq 246\,\text{GeV}$ and require all ALP interactions to be invariant under the full SM gauge group. We neglect CP violating terms and ALP-fermion interactions. The latter only give highly suppressed contributions at tree-level, as their physical impact is always proportional to the mass of the fermion itself and only light fermions appear in LO VBS diagrams.

The SM is then extended by the Lagrangian [57, 58]

$$\mathscr{L}_{\text{ALP}} = \frac{1}{4}\partial_\mu a \partial^\mu a - \frac{m_a^2}{2}a^2 - c_{\widetilde{B}}\frac{a}{f_a}B_{\mu\nu}\tilde{B}^{\mu\nu} - c_{\widetilde{W}}\frac{a}{f_a}W^i_{\mu\nu}\tilde{W}^{i\mu\nu} - c_{\widetilde{G}}\frac{a}{f_a}G^A_{\mu\nu}\tilde{G}^{A\mu\nu}\,, \qquad (2.1)$$

that contains a complete and non-redundant set of dimension-5 bosonic operators.[1] Here B_μ, W^i_μ, G^A_μ denote the bosons associated to the U(1), SU(2) and SU(3) gauge symmetries

[1]One more bosonic dimension 5 operator could be written down, namely $O_{a\Phi} = \partial^\mu a(\Phi^\dagger i\overleftrightarrow{D}_\mu\Phi)$, where Φ the Higgs doublet. However, this operator can be fully traded for ALP-fermion terms via the Higgs equations of motion [57]. Therefore, its impact on VBS processes is negligible.

of the SM, respectively. The associated coupling constants will be denoted by g', g, g_s. Unless otherwise specified, we will use i, j, k and A, B, C to denote isospin and color indices. Covariant derivatives are defined with a minus sign convention, such that $W^i_{\mu\nu} = \partial_\mu W^i_\nu - \partial_\nu W^i_\mu + g\epsilon^{ijk} W^j_\mu W^k_\nu$ and analogously for gluons. Dual field strengths are defined as $\tilde{X}_{\mu\nu} = \frac{1}{2}\varepsilon_{\mu\nu\rho\sigma} X^{\rho\sigma}$.

In the analysis presented below, we only consider EW ALP contributions to the VBS processes, while we neglect those containing ALP-gluon interactions, which is tantamount to setting $c_{\widetilde{G}} = 0$. This is a very good approximation for the $W^\pm\gamma$, $W^\pm Z$ and same-sign $W^\pm W^\pm$ channels where the ALP QCD contribution is absent at tree level. For the ZZ and $Z\gamma$ channels, an ALP QCD contribution is present in principle. However, the ALP QCD component is reduced by requiring consistency with the limits obtained in [34–36], the rejection of the VBS selection cuts and the large diboson invariant masses involved. In particular, for values of the EW couplings $\gtrsim 1\,\mathrm{TeV}^{-1}$, the theoretical prediction is dominated by the pure EW ALP signal, with a smaller contribution from the pure QCD ALP signal. Here, both the EW and QCD ALP signal components are positive and their interference is subdominant. This rules out the possibility of cancellations between the ALP EW and QCD components, and implies that the final bounds for $c_{\widetilde{W}}/f_a$ and $c_{\widetilde{B}}/f_a$ for $c_{\widetilde{G}} = 0$ are conservative.

It is then safe to restrict the parameter space to the four ALP couplings to the electroweak gauge bosons. In unitary gauge, they are usually parameterized as

$$\mathscr{L}_{\mathrm{ALP,EW}} = -\frac{g_{a\gamma\gamma}}{4} a F^{\mu\nu}\tilde{F}_{\mu\nu} - \frac{g_{a\gamma Z}}{4} a Z^{\mu\nu}\tilde{F}_{\mu\nu} - \frac{g_{aZZ}}{4} a Z^{\mu\nu}\tilde{Z}_{\mu\nu} - \frac{g_{aWW}}{2} a W^{+\mu\nu}\tilde{W}^-_{\mu\nu}, \tag{2.2}$$

with $F_{\mu\nu}, Z_{\mu\nu}, W^\pm_{\mu\nu}$ are the field strengths of the photon, Z and $W^\pm$ bosons respectively,

$$g_{a\gamma\gamma} = \frac{4}{f_a}(s^2_\theta c_{\widetilde{W}} + c^2_\theta c_{\widetilde{B}}), \qquad g_{a\gamma Z} = \frac{4}{f_a} s_{2\theta}(c_{\widetilde{W}} - c_{\widetilde{B}}), \tag{2.3}$$

$$g_{aZZ} = \frac{4}{f_a}(c^2_\theta c_{\widetilde{W}} + s^2_\theta c_{\widetilde{B}}), \qquad g_{aWW} = \frac{4}{f_a} c_{\widetilde{W}}, \tag{2.4}$$

and s_θ, c_θ the sine and cosine of the weak mixing angle. For later convenience, we also define

$$g_{agg} = \frac{4}{f_a} c_{\widetilde{G}}. \tag{2.5}$$

3 General characteristics of ALP-mediated EW VBS production

We consider the production of ZZ, $Z\gamma$, $W^\pm\gamma$, $W^\pm Z$ and same-sign $W^\pm W^\pm$ pairs in association with two forward jets. These five VBS channels are those for which differential measurements of the diboson invariant mass (or transverse mass) have been reported by the CMS Collaboration, using data collected at the LHC Run 2. At parton level we treat them, for simplicity, as $2 \to 4$ scatterings, with either photons or weak bosons in the final state. As described in section 4, the weak bosons are decayed to leptons at a later stage.

ALPs give EW contributions to these processes via the diagram topologies shown in figure 1. All of them necessarily present two insertions of ALP operators, leading to

JHEP06(2022)113

Process	$c_{\widetilde{B}}^2$	$c_{\widetilde{W}}^2$	$c_{\widetilde{B}} c_{\widetilde{W}}$	$c_{\widetilde{B}}^4$	$c_{\widetilde{W}}^4$	$c_{\widetilde{B}}^2 c_{\widetilde{W}}^2$	$c_{\widetilde{B}}^3 c_{\widetilde{W}}$	$c_{\widetilde{B}} c_{\widetilde{W}}^3$
$pp \to jjZZ$	✓	✓	✓	✓	✓	✓	✓	✓
$pp \to jjZ\gamma$	✓	✓	✓	✓	✓	✓	✓	✓
$pp \to jjW^\pm\gamma$		✓	✓		✓	✓		✓
$pp \to jjW^\pm Z$		✓	✓		✓	✓		✓
$pp \to jjW^\pm W^\pm$		✓			✓			

Table 1. List of VBS processes considered in this work. For each, we indicate which terms in the polynomial dependence on $c_{\widetilde{W}}$, $c_{\widetilde{B}}$ (eq. (3.1)) are present in the parameterization of the ALP signal.

JHEP06(2022)113

amplitudes that scale as f_a^{-2}, and cross sections of order f_a^{-4}. A generic VBS cross section, including both SM and EW ALP contributions, has the structure

$$\begin{aligned} \sigma_{\rm ALP} &= \sigma_{\rm SM} + \frac{1}{f_a^2}\,\sigma_{\rm interf.} + \frac{1}{f_a^4}\,\sigma_{\rm signal}\,, \\ \sigma_{\rm interf.} &= c_{\widetilde{B}}^2\,\sigma_{B2} + c_{\widetilde{W}}^2\,\sigma_{W2} + c_{\widetilde{B}} c_{\widetilde{W}}\,\sigma_{BW}\,, \\ \sigma_{\rm signal} &= c_{\widetilde{B}}^4\,\sigma_{B4} + c_{\widetilde{W}}^4\,\sigma_{W4} + c_{\widetilde{B}}^2 c_{\widetilde{W}}^2\,\sigma_{B2W2} + c_{\widetilde{B}}^3 c_{\widetilde{W}}\,\sigma_{B3W} + c_{\widetilde{B}} c_{\widetilde{W}}^3\,\sigma_{BW3}\,, \end{aligned} \tag{3.1}$$

where all the σ_i quantities can be evaluated numerically from the simulations. This structure holds after selection cuts. Not all processes receive contributions from all terms in this polynomial expansion: the dependence is summarized in table 1. The pattern observed can be easily explained: all processes with a W boson in final state require an insertion of $g_{aWW} \sim c_{\widetilde{W}}/f_a$. Pure $c_{\widetilde{B}}$ contributions are then absent, which means that these channels cannot constrain the ALP parameter space along the $c_{\widetilde{B}}$ axis. Same-sign $W^\pm W^\pm$ production represents an extreme case where $c_{\widetilde{B}}$ does not enter at all. Explicit expressions of $\sigma_{\rm interf.}$, $\sigma_{\rm signal}$ are given in appendix A for the integrated cross-section of each channel, calculated after the selection cuts, see section 4.

Among the diagrams shown in figure 1, the first, where the ALP is exchanged in s-channel, only contributes to VBS with ZZ and $Z\gamma$ final states.[2] The second, with the ALP in t-channel, is relevant for all VBS processes, and it is the only one contributing to $W^\pm\gamma$, $W^\pm Z$ and $W^\pm W^\pm$. Finally, the third topology is triboson-like: although these diagrams were included for consistency in our calculation, we have verified that their contribution is efficiently suppressed with a cut on the dijet invariant mass $M_{q_1' q_2'} > 120\,\text{GeV}$.

We take the ALP to be too light for any of the V_1V_2 pairs to be produced resonantly. As a consequence, the ALP is always off-shell and its propagator acts as a suppression of the scattering amplitudes. However, this effect is overcompensated by the momentum enhancement induced by the ALP interaction vertices. The net result is that the ALP-mediated cross section falls more slowly with the diboson invariant mass of the boson pair $M_{V_1V_2}$ than the SM backgrounds. Figure 2 shows a parton-level comparison of the dijet invariant mass $M_{q_1' q_2'}$, jet pseudo-rapidity separation $\Delta\eta_{q_1' q_2'}$ and diboson invariant mass

[2]The s-channel diagram contributes also to VBS with opposite-sign WW or diphoton final states. However, these channels are not considered here.

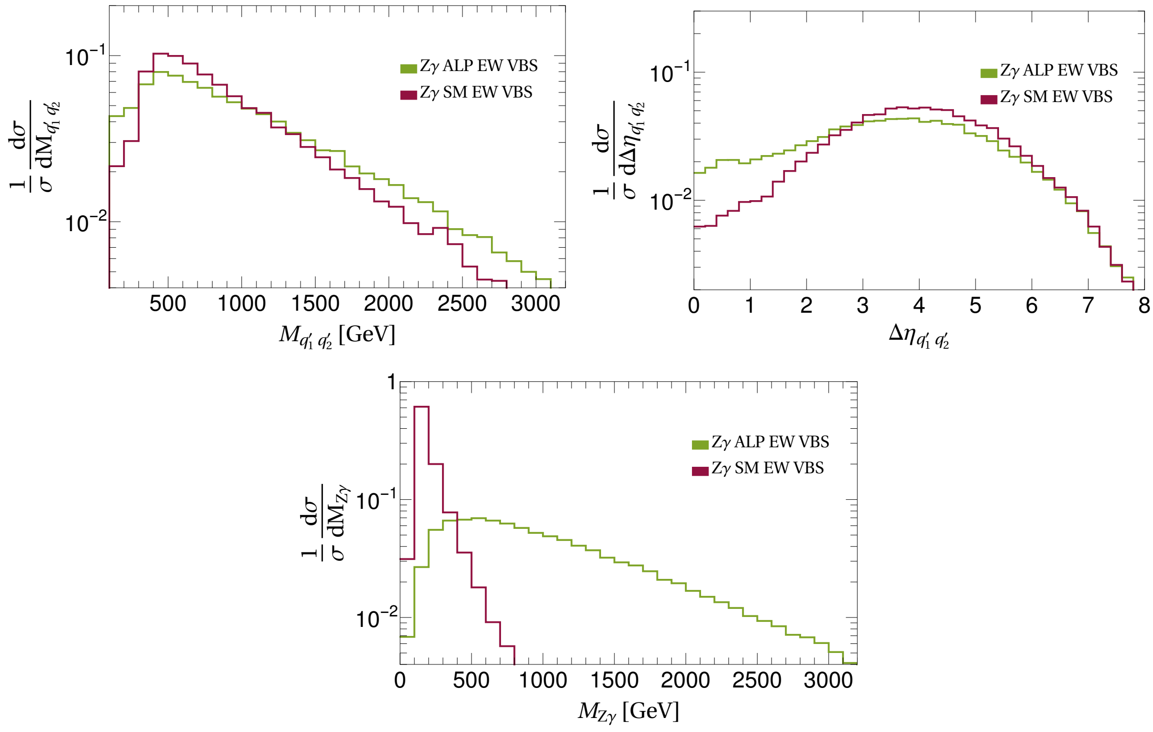

Figure 2. Normalized parton level distributions of the dijet invariant mass $M_{q_1' q_2'}$, jet pseudo-rapidity separation $\Delta\eta_{q_1' q_2'}$ and diboson invariant mass $M_{Z\gamma}$ for ALP EW VBS (green) and SM EW VBS (red) $Z\gamma$ production. The ALP curves include the pure signal and ALP-SM interference contributions, computed for $m_a = 1\,\mathrm{MeV}$ and $c_{\widetilde{W}}/f_a = c_{\widetilde{B}}/f_a = 1\,\mathrm{TeV}^{-1}$.

$M_{Z\gamma}$ distributions for ALP EW VBS and SM EW VBS $Z\gamma$ production. The ALP curves include the pure signal and ALP-SM interference contributions, computed for $m_a = 1\,\mathrm{MeV}$ and $c_{\widetilde{W}}/f_a = c_{\widetilde{B}}/f_a = 1\,\mathrm{TeV}^{-1}$. The dijet distributions are qualitatively similar, and dijet selection criteria designed to measure the SM EW VBS component should work efficiently for the ALP case as well. On the other hand, the very different tails of the diboson invariant mass distributions allow discrimination of the two processes for $M_{Z\gamma} \gtrsim 500\,\mathrm{GeV}$. This general behavior holds for all ALP EW VBS final states, independently of the presence or absence of s-channel ALP Feynman diagrams.

3.1 Comments on the EFT power counting

Before discussing the details of the numerical analysis, a few comments on the validity of the EFT approach are in order. In particular, concerns might be raised about the fact that an ALP signal of $\mathcal{O}(f_a^{-4})$ is extracted from a Lagrangian defined at $\mathcal{O}(f_a^{-1})$. First of all, it should be noted that, because two insertions of ALP operators are always required in order to generate corrections to SM processes, the dimension-5 Lagrangian does provide complete VBS predictions up to $\mathcal{O}(f_a^{-2})$. However, it is indeed possible for $d \geq 6$ ALP operators to induce further contributions at $\mathcal{O}(f_a^{-3}, f_a^{-4})$ that are neglected in this work. Specifically, at tree-level, these missing terms can be exclusively corrections to $\sigma_{\text{interf.}}$ from ALP diagrams

JHEP06(2022)113

containing $d = 6$ or $d = 7$ operator insertions, while the expression for σ_{signal} is already complete to $\mathcal{O}(f_a^{-4})$. Note, in addition, that the parameterization in eq. (3.1) is complete to quartic order in the parameter space $(c_{\widetilde{B}}/f_a, c_{\widetilde{W}}/f_a)$, i.e. it accounts for *all* contributions up to $\mathcal{O}(f_a^{-4})$ generated by the $d = 5$ Lagrangian.[3] These considerations, together with the fact that the analysis presented in the next sections is numerically dominated by σ_{signal} (see e.g. table 6), suggest that the final results of this work would not change significantly if the missing $\mathcal{O}(f_a^{-4})$ terms were restored.[4]

For these reasons, we deem the Lagrangian in eq. (2.1) adequate for the scope of this work and we believe that the resulting constraints on $(c_{\widetilde{B}}/f_a, c_{\widetilde{W}}/f_a)$ are quite solid. We stress that these conclusions are based on considerations made *a posteriori*, having evaluated the sensitivity of LHC and HL-LHC VBS searches to $d = 5$ ALP couplings. They do not necessarily apply to processes different from VBS or in scenarios with very different sensitivity. A systematic and more quantitative assessment of the impact of higher-order ALP operators is left for future work. Note that this would require, among other things, the definition of a complete and non-redundant ALP operator basis beyond dimension-5, which has not been constructed to date.

4 ALP-mediated EW VBS simulation and analysis

In order to understand the potential of the LHC experiments, we perform a reinterpretation of the analyses recently published by the CMS Collaboration studying the production of ZZ [51], $Z\gamma$ [54], $W^\pm\gamma$ [52], $W^\pm Z$ [50] and same-sign $W^\pm W^\pm$ [50] bosons in association with two jets. All channels use leptonic (electron and muon) decays of the W and Z bosons in the final state.

The nonresonant ALP-mediated EW VBS diboson signal is simulated with the software MadGraph5_aMC@NLO 2.8.2 [59]. Employing the `ALP_linear` UFO model from [30, 60], we generate $q_1 q_2 \to V_1 V_2 q_1' q_2'$ events at leading order in the ALP and EW couplings and at zeroth order in the QCD coupling, using a 4-flavor-scheme. The parton distribution functions (PDFs) of the colliding protons are given by the NNPDF 3.0 PDF set [61] for all simulated samples. Kinematical cuts requiring

$$\begin{aligned} &p_T(q'_{1,2}) > 20\,\text{GeV}\,, \quad \eta(q'_{1,2}) < 6\,, \qquad \Delta R(q'_1 q'_2) > 0.1\,, \quad M_{q'_1 q'_2} > 120\,\text{GeV}\,, \\ &\quad p_T(\gamma) > 10\,\text{GeV}\,, \qquad \eta(\gamma) < 2.5\,, \quad \Delta R(\gamma q'_{1,2}) > 0.4\,, \end{aligned} \tag{4.1}$$

are imposed at generation level for all VBS processes, except for the ZZ channel where the $M_{q'_1 q'_2}$ cut is removed. The angular separation is defined as $\Delta R = \sqrt{\Delta\eta^2 + \Delta\phi^2}$, with η the parton's pseudorapidity and ϕ its azimuthal angle. The ALP EW VBS signals are generated fixing $m_a = 1\,\text{MeV}$, $f_a = 1\,\text{TeV}$ and $\Gamma_a = 0$. The specific values of the ALP

[3]This is at variance e.g. with the SMEFT case, where the square of the $d = 6$ amplitude does not contain all $\mathcal{O}(c_6^2/\Lambda^4)$ contributions, because certain $d = 6$ operators can induce extra higher-order corrections, e.g. via redefinitions of SM fields or parameters, or via double insertions in a given diagram.

[4]The results could change significantly only if $d \geq 6$ ALP operators introduced very large kinematic enhancements to $\sigma_{\text{interf.}}$, sufficient to make it competitive with σ_{signal} within the region of sensitivity. Very preliminary considerations about the possible structure of such operators suggest that this is unlikely.

mass and decay width do not have significant consequences in the nonresonant regime, see section 5.3. We generate separated samples for pure ALP-mediated production and the interference between the ALP and the SM EW VBS production. As discussed in section 3, the ALP EW VBS cross sections have a polynomial dependence on the parameters $c_{\widetilde{W}}$ and $c_{\widetilde{B}}$, whose coefficients need to be determined individually. This requires to evaluate the ALP-SM interference at a minimum of three linearly independent points in the $(c_{\widetilde{W}}, c_{\widetilde{B}})$ plane, and the pure ALP signal at a minimum of five points. This is achieved by exploiting the interaction orders syntax in MadGraph5_aMC@NLO, used both in independent event generations and with the MadGraph5 reweighting tool [62]. For cross-checking purposes, we consider a redundant set of points, namely

$$\begin{aligned} &p_0 = (1,1), &&p_1 = (0,2), &&p_2 = (1,0), \\ &p_3 = (1,-1), &&p_4 = (1,-0.305), &&p_5 = (1,-3.279)\,, \end{aligned} \tag{4.2}$$

where p_0 lies on the $c_{\widetilde{B}} = c_{\widetilde{W}}$ line, where $g_{a\gamma Z} = 0$; p_4 is on the photophobic $c_{\widetilde{B}} = -t_\theta^2 c_{\widetilde{W}}$ line, where $g_{a\gamma\gamma} = 0$; and p_5 is on the $c_{\widetilde{B}} = -c_{\widetilde{W}}/t_\theta^2$ line, where $g_{aZZ} = 0$. Here t_θ is the tangent of the Weinberg angle. We use five of these points to determine the polynomials and verify that the results extrapolated to the sixth point match those from direct simulation. This operation has been repeated on all possible subsets to verify the robustness of the predictions. The resulting polynomial expressions for the total cross sections, obtained after the full simulation and analysis procedure, are reported in appendix A. These can be employed to estimate the overall normalizations of the ALP signal for all distributions used in the final fits to the data. The production cross sections at $\sqrt{s} = 13\,\text{TeV}$ for benchmark points p_0 and p_4 are summarized in table 2. They have additionally a 11% systematic uncertainty related to the renormalization and factorization scales and a 4% systematic uncertainty related to the PDFs.

SM EW VBS diboson background events are generated with MadGraph5 at leading order in the EW couplings and zeroth order in the QCD coupling. This is an irreducible source of background for the analysis. Cross sections at $\sqrt{s} = 13\,\text{TeV}$ are presented in table 2.

For all the simulated samples in the analysis, parton showering, hadronization and decays are described by interfacing the event generators with PYTHIA 8 [63]. Massive EW bosons V_1 and V_2 are forced to decay leptonically (electrons and muons). No additional pileup pp interactions were added. All samples were processed through a simulation of the CMS detector and reconstruction of the experimental objects using DELPHES 3 [64], including FastJet [65] for the clustering of anti-k_T jets with a distance parameter of 0.4 (AK4 jets). The CMS DELPHES card was modified to improve the lepton isolation requirements and to reduce the lepton detection transverse momentum threshold to 5 GeV.

For the detector-level analysis, we apply the set of requirements designed to constrain anomalous quartic gauge couplings in the CMS publications. The most important cuts are those imposed on the dijet system, and on the photon transverse momentum if relevant, indicated in table 3. Differences between our generation and simulation procedure and the ones used by the CMS experiment are taken into account by comparing the predicted numbers of events after selection cuts for the SM EW VBS processes. In this context, the expected sources of discrepancy are calibration, efficiency or resolution effects in the

Process	$\sigma_{\rm SM}$ [fb]	Point	$\sigma_{\rm interf.}$ [fb]	$\sigma_{\rm signal}$ [fb]
$pp \to jjZZ$	98 ± 1	p_0	-13.5 ± 0.1	42.4 ± 0.2
		p_4	-9.3 ± 0.1	18.5 ± 0.1
$pp \to jjZ\gamma$	393 ± 1	p_0	0.3 ± 0.1	11.1 ± 0.1
		p_4	-9.1 ± 0.1	20.9 ± 0.1
$pp \to jjW^\pm\gamma$	994 ± 3	p_0	4.3 ± 0.1	28.7 ± 0.1
		p_4	1.7 ± 0.1	5.4 ± 0.1
$pp \to jjW^\pm Z$	386 ± 1	p_0	1.7 ± 0.1	18.4 ± 0.1
		p_4	0.1 ± 0.1	23.9 ± 0.1
$pp \to jjW^\pm W^\pm$	256 ± 1	p_0, p_4	-4.0 ± 0.1	16.0 ± 0.1

Table 2. EW VBS SM background and ALP signal partonic cross sections for $\sqrt{s} = 13\,\text{TeV}$, before decaying the vector bosons and applying only the selection cuts in eq. (4.1). The ALP signal cross sections are presented for two benchmark points p_0 and p_4 defined in eq. (4.2). For same-sign $W^\pm W^\pm$, both points give the same results. The reported errors are the statistical errors of the MadGraph5_aMC@NLO calculation.

Channel	Obs.	Lum. [fb^{-1}]	Selection Criteria	ρ
ZZ	M_{ZZ}	137	$M_{jj} > 100\,\text{GeV}$	0.8 ± 0.1
$Z\gamma$	$M_{Z\gamma}$	137	$M_{jj} > 500\,\text{GeV}$, $\Delta\eta_{jj} > 2.5$, $p_T^\gamma > 120\,\text{GeV}$	1.4 ± 0.2
$W^\pm\gamma$	$M_{W\gamma}$	35.9	$M_{jj} > 800\,\text{GeV}$, $\Delta\eta_{jj} > 2.5$, $p_T^\gamma > 100\,\text{GeV}$	3.1 ± 0.5
$W^\pm Z$	M_{WZ}^T	137	$M_{jj} > 500\,\text{GeV}$, $\Delta\eta_{jj} > 2.5$	1.5 ± 0.4
$W^\pm W^\pm$	M_{WW}^T	137	$M_{jj} > 500\,\text{GeV}$, $\Delta\eta_{jj} > 2.5$	1.3 ± 0.2

Table 3. Summary of the CMS VBS analyses: the diboson mass observable, the integrated luminosity, the most important selection criteria and the normalization scale factor ρ.

reconstruction of the experimental observables. We observe that all these affect primarily the normalization and therefore we define a scale factor ρ as the ratio of the number of expected events delivered by our generation and simulation procedure and the number of CMS expected events. We have verified that, after applying this rescaling, our simulation reproduces correctly the relevant kinematic distributions by CMS within the uncertainties. The same scale factors are then applied to the predictions for pure ALP-mediated EW VBS and ALP-SM interference simulated samples. For each channel, we assign an uncertainty to ρ, that stems from the uncertainty on the expected event yield for SM EW VBS production, reported in the CMS publications. A systematic uncertainty of 16% on the simulated ALP event yields is assigned, fully correlated across all channels. This is estimated as the average relative error on the scale factors ρ. A summary of the CMS VBS analyses is presented in table 3: the diboson mass observable, the integrated luminosity, the selection criteria and the normalization scale factor ρ.

JHEP06(2022)113

As anticipated in section 3, the discrimination between signal and background is based on the diboson mass distributions shown in appendix A. These include the fully reconstructed diboson invariant masses M_{ZZ} and $M_{Z\gamma}$; the diboson invariant mass $M_{W^\pm\gamma}$, where the longitudinal momentum of the neutrino is constrained by the condition $M_{\ell\nu} = m_W$ [52]; and the diboson transverse masses $M^T_{W^\pm W^\pm}$ and $M^T_{W^\pm Z}$, defined as

$$M^T_{V_1V_2} = \left[\left(\sum_i E_i\right)^2 - \left(\sum_i p_{z,i}\right)^2\right]^{1/2}, \tag{4.3}$$

where the index i runs over all the leptons in the final state, and assuming that the neutrinos longitudinal momenta are zero [50].

In order to provide a handle on possible issues concerning the validity of the ALP EFT expansion [66] and to estimate the impact of the highest-energy bins, we introduce an upper cut on $M_{V_1V_2}$, that is applied on the signal simulation only. We consider two benchmark selections: $M_{V_1V_2} < 2\,\text{TeV}$ and $M_{V_1V_2} < 4\,\text{TeV}$. These cuts are satisfied, respectively, by 85% and > 99% of the events in the ALP generated samples and mainly impact the signal predictions in the last bin of each distribution, as shown in figures 7–11.

The log-likelihood is constructed based on a Poisson distribution. For each VBS channel, it has the form:

$$\log L(c_{\widetilde{B}}, c_{\widetilde{W}}) = \sum_k \left[-\left(B_k + S_k(c_{\widetilde{B}}, c_{\widetilde{W}})\right) + D_k \log\left(B_k + S_k(c_{\widetilde{B}}, c_{\widetilde{W}})\right)\right] \tag{4.4}$$

where the index k runs over the bins of the relevant distribution. The number of events for the data (D_k) and for the SM background predictions (B_k) are taken from the CMS experimental publications. The expected number of signal events (S_k) accounts for both the pure ALP EW VBS signal and the ALP-SM interference contributions, that are parameterised as fourth- and second-degree polynomials in ($c_{\widetilde{W}}/f_a$, $c_{\widetilde{B}}/f_a$) respectively, as explained in section 3. The combined log-likelihood is simply constructed as the sum of $\log L$ for the individual channels.

Systematic uncertainties affecting the SM background distributions are considered fully correlated among bins of a distribution, but uncorrelated among different VBS channels. They are described by one nuisance parameter for each VBS channel, that multiplies both background and ALP signal yields, and is taken to be Gaussian-distributed. The systematic uncertainty on the signal prediction is implemented analogously and applied to S_k only. It is taken to be fully correlated across all channels and bins and we assign it a total size of 20%, obtained adding in quadrature the 16% uncertainty on the signal normalization, the 11% uncertainty on the renormalization and factorization scales choice and the 4% error related to the PDFs.

5 Results

5.1 Results from LHC Run 2 measurements

Table 4 shows the branching fractions and selection efficiencies for each VBS channel. The latter are relative to the simulated events in which the bosons are decayed to electrons and muons. The products of efficiencies and branching fractions range from 0.2% to 0.9%.

Analysis	ZZ	$Z\gamma$	$W^{\pm}\gamma$	$W^{\pm}Z$	$W^{\pm}W^{\pm}$
Branching fraction	0.45%	6.7%	22%	1.5%	4.8%
Efficiency	35.7%	14.0%	1.6%	11.3%	17.0%

Table 4. Summary of branching fractions and selection efficiencies for each VBS channel. The efficiencies are relative to the simulated events in which the W and Z bosons decay to electrons or muons.

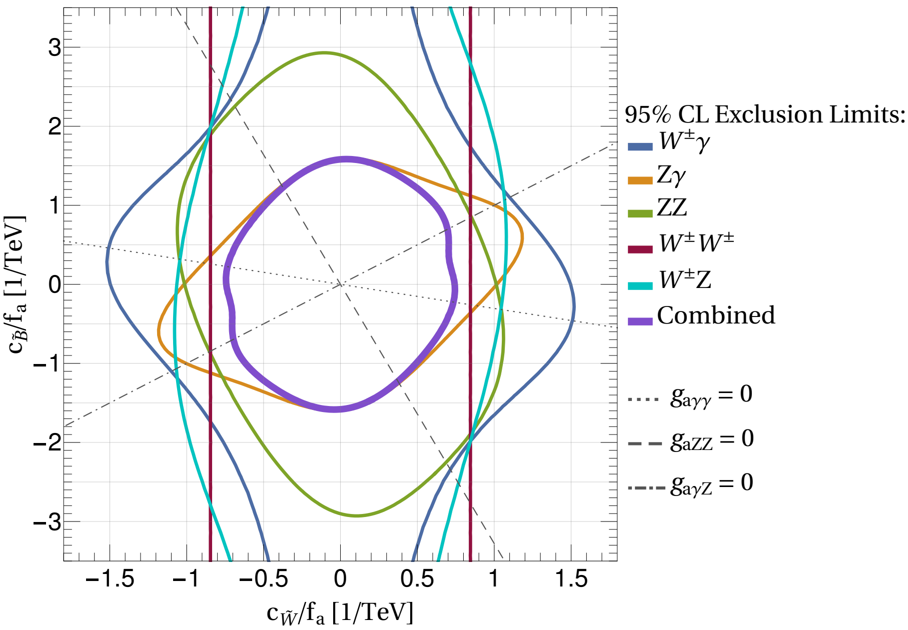

Figure 3. Observed 95% CL exclusion limits in the $(c_{\widetilde{W}}/f_a,\ c_{\widetilde{B}}/f_a)$ plane using the data of the Run 2 CMS publications and signal events with $M_{V_1V_2} < 4\,\text{TeV}$. The limits have been calculated individually for the five different experimental channels considered and for their combination. The thin dotted, dashed and dot-dashed lines indicate the directions of vanishing couplings to neutral gauge bosons.

Results are extracted from a maximum likelihood fit of signal and background to the diboson invariant mass (ZZ, $Z\gamma$ and $W^{\pm}\gamma$) or transverse mass ($W^{\pm}Z$ and $W^{\pm}W^{\pm}$) distributions, individually and simultaneously in all the experimental channels used in the analysis. The likelihood is defined as described in the previous section and the background-only hypothesis is tested against the combined background and signal hypothesis.

No significant excess was observed by CMS with respect to the SM expectations. ALP couplings $c_{\widetilde{W}}/f_a$ and $c_{\widetilde{B}}/f_a$ are considered excluded at 95% confidence level (CL) when the negative log likelihood (NLL) $(-\log L)$ of the combined signal and background hypothesis exceeds 3.84/2 units the NLL of the background-only hypothesis.

Figure 3 shows the observed 95% CL exclusion limits in the $(c_{\widetilde{W}}/f_a, c_{\widetilde{B}}/f_a)$ plane using the data of the Run 2 CMS publications and signal events with $M_{V_1V_2} < 4\,\text{TeV}$. The limits have been calculated individually for the five different experimental channels considered and for their combination. Table 5 reports the upper bounds obtained projecting the combined

JHEP06(2022)113

Coupling	Run 2 Observed (Expected)		$300\,\mathrm{fb}^{-1}$		$3000\,\mathrm{fb}^{-1}$	
$[\mathrm{TeV}^{-1}]$	$M_{V_1V_2} < 4\,\mathrm{TeV}$	$< 2\,\mathrm{TeV}$	$< 4\,\mathrm{TeV}$	$< 2\,\mathrm{TeV}$	$< 4\,\mathrm{TeV}$	$< 2\,\mathrm{TeV}$
$\lvert c_{\widetilde{W}}/f_a \rvert$	0.75 (0.83)	0.86 (0.94)	0.71	0.80	0.55	0.62
$\lvert c_{\widetilde{B}}/f_a \rvert$	1.59 (1.35)	1.73 (1.47)	1.12	1.23	0.79	0.87
$\lvert g_{a\gamma\gamma} \rvert$	4.99 (4.24)	5.45 (4.63)	3.50	3.84	2.43	2.68
$\lvert g_{a\gamma Z} \rvert$	5.54 (4.74)	6.15 (5.25)	3.98	4.42	2.94	3.30
$\lvert g_{aZZ} \rvert$	2.84 (3.02)	3.19 (3.38)	2.53	2.81	1.94	2.16
$\lvert g_{aWW} \rvert$	2.98 (3.33)	3.43 (3.74)	2.84	3.18	2.21	2.49

Table 5. 95% CL upper limits on the absolute value of the Wilson coefficients $c_{\widetilde{W}}/f_a$ and $c_{\widetilde{B}}/f_a$ and projected onto the ALP couplings to physical bosons, eq. (2.2). The various columns report current bounds extracted from CMS Run 2 measurements and projected sensitivities for $\sqrt{s} = 14\,\mathrm{TeV}$ and LHC higher luminosities, for signal events with $M_{V_1V_2}$ below 4 TeV or 2 TeV.

95% CL allowed region onto different directions in the $(c_{\widetilde{W}}/f_a, c_{\widetilde{B}}/f_a)$ plane, namely the two axes and the combinations corresponding to the ALP couplings to physical bosons defined in eq. (2.2), which are orthogonal to the dotted, dashed and dot-dashed lines in figure 3. Table 5 also presents the 95% CL limits obtained with the more conservative cut $M_{V_1V_2} < 2\,\mathrm{TeV}$, which are about 10–15% weaker than the ones in figure 3. The modest impact of this additional cut indicates that the ALP VBS cross section does not grow indefinitely with energy (see also figure 2). Instead, only a small number of signal events populate the very high $M_{V_1V_2}$ region.

In most of the parameter space, the limits are dominated by the $Z\gamma$ measurement, that is the most stringent along the $c_{\widetilde{B}}$ direction. The only other measurement capable of bounding this parameter is ZZ, which however pays the price of the small $\mathrm{Br}(Z \to \ell\ell)$ and the current loose selection cuts on the dijet system. The sensitivity of the $W^{\pm}\gamma$ channel is reduced by the smaller integrated luminosity of the published CMS analysis. A measurement of the $\gamma\gamma$ VBS final state at large diphoton invariant masses, that has not been performed by ATLAS or CMS to date, would bring additional sensitivity to $c_{\widetilde{B}}$, with a great potential for improving the current bounds [38].

5.2 Prospects for LHC Run 3 and HL-LHC

In this section we investigate the sensitivity of the nonresonant ALP VBS searches at the LHC Run 3 and HL-LHC. For simplicity, we apply the same selection criteria as the CMS Run 2 analyses, and rescale the integrated luminosities to $300\,\mathrm{fb}^{-1}$ and $3000\,\mathrm{fb}^{-1}$, respectively. An additional scaling factor κ is applied to account for an increase in the proton collision center-of-mass energy from 13 to 14 TeV. In our approximation, κ is taken to be constant over all distribution bins and identical for all VBS channels. Using MadGraph5_aMC@NLO and the cuts in eq. (4.1), we obtain κ-factors of 1.14, 1.26 and 1.20 for the SM background, the ALP EW VBS signal and their interference, respectively.

Figure 4 shows the projected 95% CL upper limits in the $(c_{\widetilde{W}}/f_a, c_{\widetilde{B}}/f_a)$ plane for $\sqrt{s} = 14\,\mathrm{TeV}$, $M_{V_1V_2} < 4\,\mathrm{TeV}$ and integrated luminosities $300\,\mathrm{fb}^{-1}$ and $3000\,\mathrm{fb}^{-1}$. For

JHEP06(2022)113

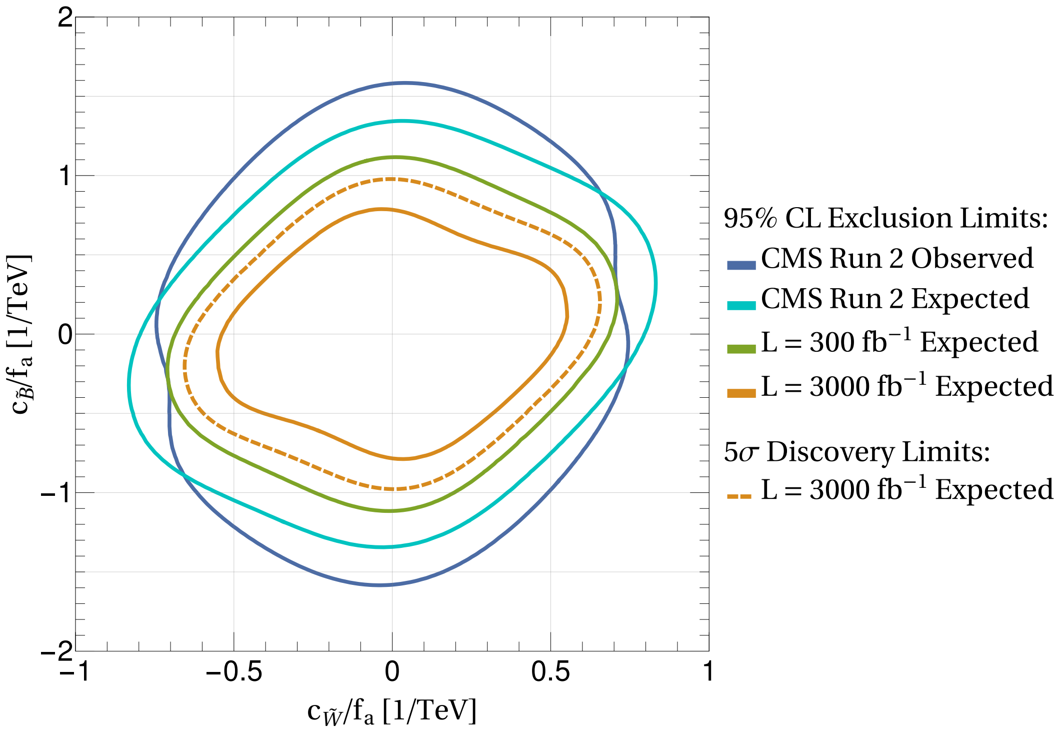

Figure 4. Projected 95% CL upper limits on the couplings $(c_{\widetilde{W}}/f_a, c_{\widetilde{B}}/f_a)$ for $\sqrt{s} = 14\,\text{TeV}$, $M_{V_1V_2} < 4\,\text{TeV}$ and integrated luminosities of 300 (green) and 3000 fb^{-1} (orange), obtained combining all VBS channels. The blue and light blue lines show, for comparison, the observed and expected limits with Run 2 luminosities. The dashed orange line marks the 5σ-discovery limit for the HL-LHC.

comparison, the observed and expected Run 2 limits have been included as well. The interplay between the individual channels is not shown in figure 4 as it remains qualitatively unchanged compared to figure 3. As expected, the largest individual improvement is found for the $W^\pm\gamma$ channel. However, the combined limits are still dominated by the $Z\gamma$ channel and with a significant contribution of $W^\pm W^\pm$ for the highest values of $c_{\widetilde{W}}/f_a$. We find that the bounds on $c_{\widetilde{B}}$ can improve by roughly a factor 2 at the HL-LHC compared to current constraints, while those on $c_{\widetilde{W}}$ by a factor ~ 1.4.

Figure 4 also shows, for reference, the curve corresponding to the expected discovery limit for $\sqrt{s} = 14\,\text{TeV}$, $M_{V_1V_2} < 4\,\text{TeV}$ and an integrated luminosity of 3000 fb^{-1}, defined as the set of $(c_{\widetilde{W}}/f_a, c_{\widetilde{B}}/f_a)$ values for which the SM point is excluded by 5 standard deviations, assuming that the measurement matches the predicted ALP EW VBS signal. The fact that it is fully contained inside the projected exclusion limits for current and Run 3 luminosities indicates that null results at previous LHC Runs will not exclude a priori the possibility of a discovery at the HL-LHC.

5.3 Dependence on the ALP mass and decay width

Our results were derived assuming that the ALP gives only off-shell contributions to all VBS processes considered. Specifically, in the simulations we fixed the ALP mass and decay width to $m_a = 1\,\text{MeV}, \Gamma_a = 0$, which satisfy $\sqrt{|p_a^2|} \gg m_a, \Gamma_a$, being p_a the momentum flowing

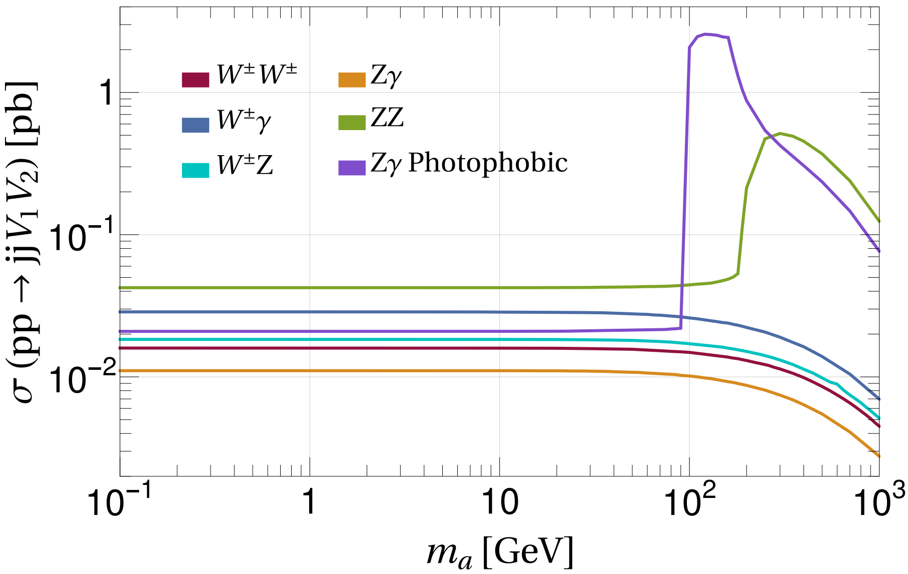

Figure 5. Total cross sections at $\sqrt{s} = 13\,\text{TeV}$ for the ALP contributions to the different VBS channels as a function of the ALP mass. All lines are evaluated at $c_{\widetilde{W}}/f_a = c_{\widetilde{B}}/f_a = 1\,\text{TeV}^{-1}$, that corresponds to the benchmark point p_0 in eq. (4.2). The exception is the "$Z\gamma$ photophobic" case, that is evaluated at p_4 instead. At each point in the plot, the ALP decay width was re-computed as a function of $m_a, c_{\widetilde{W}}$ and $c_{\widetilde{B}}$.

through the ALP propagator. As long as this kinematic condition is verified, the bounds are essentially independent of the specific m_a and Γ_a assumed. This is an important difference with respect to resonant searches, that only apply for limited mass and width windows.

Figure 5 provides a basic check of the validity of the off-shell approximation, showing the cross section for the ALP signal at $\sqrt{s} = 13\,\text{TeV}$ with the cuts in eq. (4.1), as a function of m_a for fixed values of $c_{\widetilde{W}}$, $c_{\widetilde{B}}$ and f_a. The width Γ_a was implicitly computed at every point as a function of m_a and of the ALP couplings, and it scales as $\Gamma_a \propto m_a^3 (c_i/f_a)^2$. The lines in figure 5 extend indefinitely to the left, confirming that the simulations apply to arbitrarily small m_a. In the direction of larger m_a the cross sections for $W^\pm Z, W^\pm\gamma, W^\pm W^\pm$ start falling once the t-channel propagator becomes kinematically dominated by the ALP mass. For the $Z\gamma$ and ZZ channels, the resonant behavior is visible for $(c_{\widetilde{W}}, c_{\widetilde{B}})$ benchmark points that allow the ALP exchange in s-channel. As $g_{a\gamma Z} = 0$ is enforced at p_0, we evaluate the $Z\gamma$ channel also at the "photophobic" point p_4 in order to test the resonant case.

Based on these indications, our results can be safely taken to hold up to $m_a \lesssim 100\,\text{GeV}$. At this mass, the ZZ and $W^\pm V$ cross sections have deviated by about 10% from their asymptotic values for $m_a \to 0$. At the same time, the $Z\gamma$ resonance is present but not visible in the CMS measurement, that requires $M_{Z\gamma} > 160\,\text{GeV}$ [54].

6 Comparison to existing bounds

Figure 6 shows the observed bounds obtained in this work as a function of the EW g_{aVV} couplings defined in eq. (2.2), and of m_a, compared to previously derived bounds. The

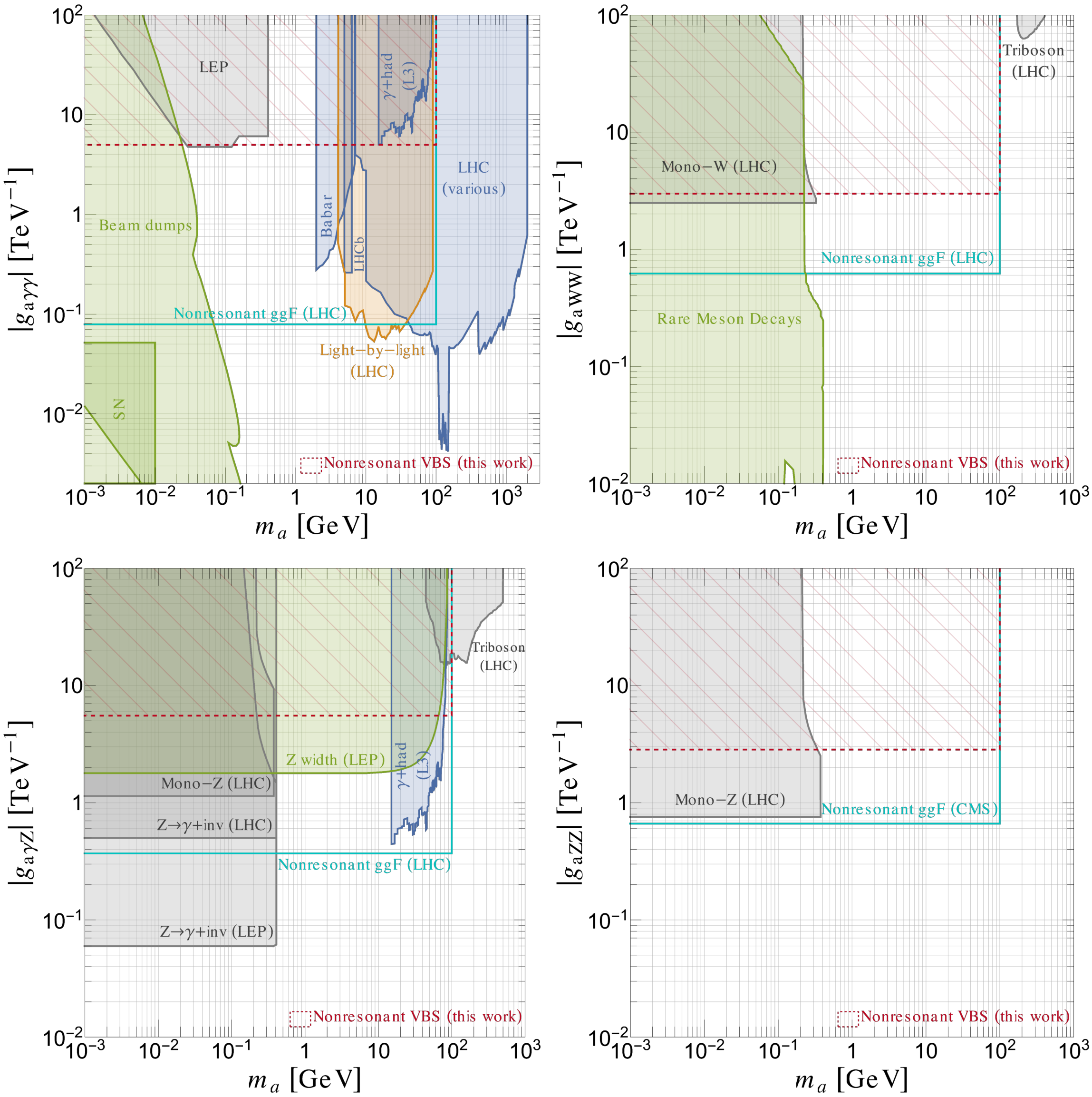

Figure 6. Summary of current constraints on ALP couplings to EW gauge bosons defined in eq. (2.2), as a function of the ALP mass m_a. Limits derived in this work are labeled "Nonresonant VBS" and shown in **red**. Previous constraints are shown with a color coding that indicates different underlying theory assumptions. **Orange** indicates a $\text{Br}(a \to \gamma\gamma) = 1$ assumption, **dark blue** indicates an assumed gluon dominance $g_{agg} \gg g_{aV_1V_2}$, while bounds in **light blue** scale with $1/g_{agg}$ and are given for $g_{agg} = 1\,\text{TeV}^{-1}$. **Grey** indicates more complex assumptions on the ALP EW couplings. Genuine bounds, that hold without further assumptions, are in **green**. See the main text for more details.

JHEP06(2022)113

numerical results of our study are also reported in table 5 for observed, expected and projected limits.

Most of the constraints shown in the figure are taken from the compilation in ref. [20] and updated to include more recent results. For ALP masses in the MeV-GeV window and within the range shown, the ALP coupling to photons is constrained by beam-dump experiments [67–70], by new physics searches in $e^+e^- \to 2\gamma, 3\gamma$ at LEP [29, 71] and by explosion energy arguments in supernovae [72, 73] (labeled "SN"). At higher ALP masses, all constraints on $g_{a\gamma\gamma}$ are due to searches at colliders, where the ALP decays resonantly either to hadrons or to photon pairs. In the first case, the relevant processes are $\Upsilon \to \gamma + \text{hadrons}$ at BaBar [74] and $e^+e^- \to \gamma + \text{hadrons}$ at L3 [75], that also constrains $g_{a\gamma Z}$. In the second case, the leading bounds stem from photon pair production at the LHC, both in proton-proton collisions [76, 77] (labeled "LHC" for those from ATLAS and CMS measurements and "LHCb" for those from LHCb searches [78]) and in light-by-light scattering $\gamma\gamma \to a \to \gamma\gamma$ measured in Pb-Pb collisions [79, 80] (labeled "Light-by-light (LHC)"). Most constraints on the couplings of the ALP to massive gauge bosons assume a stable ALP and cover the sub-GeV mass region. In this case, limits are inferred from mono-W and mono-Z [30] at the LHC and, for $g_{a\gamma Z}$, from the non-observation of exotic $Z \to \gamma + \text{invisible}$ decays at LEP [31] and at the LHC [81] (labeled "$Z \to \gamma + \text{inv.}$ (LHC)"). If the assumption of a stable ALP is relaxed, the latter constraint can be replaced by the more conservative bound due to the measurement of the total Z decay width at LEP, that extends up to $m_a \lesssim m_Z$ [30, 31]. In the region where the ALP can decay to hadrons, the same process leads to $Z \to \gamma + \text{hadrons}$ [75]. The ALP coupling to W bosons is the only one contributing to rare meson decays at 1-loop, which allow to set very stringent limits for light ALPs [18, 82]. For ALP masses above 100 GeV, the dominant bounds stem from resonant triboson searches [31]. Finally, nonresonant searches in diboson production via gluon fusion at the LHC (labeled "Nonresonant ggF") allow to constrain all four ALP interactions. Each nonresonant bound is extracted from a single process $gg \to a^* \to V_1 V_2$: the constraint on $g_{a\gamma\gamma}$ was derived in ref. [34], those on $g_{aWW}, g_{a\gamma Z}$ in ref. [35], and the constraint on g_{aZZ} in ref. [36].

An important aspect to consider is that, in general, any given measurement can depend on several ALP couplings. In order to represent the corresponding bound in the 2D (m_a, g_{aVV}) plane, it is then necessary to define a projection rationale or introduce theoretical assumptions, which can vary significantly from constraint to constraint. These differences should be taken into account for a proper comparison. In figure 6, the bounds derived in this work (red dashed) are those corresponding to the 95% C.L. limits in table 5. As they are derived from the allowed region in the $(c_{\widetilde{W}}/f_a, c_{\widetilde{B}}/f_a)$ plane, they automatically take into account gauge invariance relations. Because of the arguments laid down in section 2, they also have limited sensitivity to the coupling to gluons. The remaining bounds are derived with alternative strategies, that we highlight with color coding in figure 6. Bounds that apply without extra assumptions, are reported in green. The bounds drawn in light blue, that include nonresonant $gg \to a^* \to V_1 V_2$ processes, scale with $1/g_{agg}$ and for $c_{\widetilde{G}} \to 0$ are lifted completely. In the figure, they are normalized to $g_{agg} = 1\,\text{TeV}^{-1}$. Bounds drawn in dark blue assume gluon-dominance, i.e. $g_{agg} \gg g_{aV_1V_2}$, and in this limit they are largely independent of $c_{\widetilde{G}}$, see ref. [20]. Among these, bounds on $g_{a\gamma\gamma}$ labeled as "LHC" additionally assume negligible branching fractions to fermions and heavy EW bosons in the mass region where they are kinematically allowed. The limit from light-by-light scattering, shown in orange, assumes $\mathrm{Br}(a \to \gamma\gamma) = 1$, which corresponds to vanishing couplings to gluons and light fermions. Bounds that make more elaborate assumptions about the ALP parameter space or assumptions on the EW sector itself are shown in grey. Among these, triboson constraints on g_{aWW} and $g_{a\gamma Z}$ assume a photophobic ALP scenario [31]. All searches for a stable ALP (mono-W, mono-Z, $Z \to \gamma + \mathrm{inv.}$) implicitly assume a small enough ALP decay width, which, in the relevant mass range, translates into assumptions on the coupling to photons, electrons and muons. The LEP constraints assume negligible branching fractions to leptons. Note also that this bound is truncated to $m_a \leq 3m_\pi \simeq 0.5\,\mathrm{GeV}$ because, beyond this threshold, hadronic ALP decay channels are kinematically open. This would introduce a further dependence on $c_{\widetilde{G}}$ whose modeling would require a dedicated analysis [20]. Constraints derived with assumptions that explicitly violate the gauge invariance relations, e.g. by explicitly requiring only one non-zero EW coupling, are omitted.

Overall, we find that the main value of nonresonant searches in VBS is that they probe the ALP interactions with EW bosons directly (at tree level) and independently of the coupling to gluons. In particular, nonresonant VBS constraints are stronger than those from nonresonant diboson production whenever g_{agg} is smaller than a certain threshold, that roughly ranges between $0.01\,\mathrm{TeV}^{-1}$ and $0.2\,\mathrm{TeV}^{-1}$ depending on the EW coupling of interest. For cases where the ALP-gluon coupling is very suppressed, such as Majorons,[5] VBS bounds are the most stringent in the 0.5–100 GeV mass region for g_{aWW}, g_{aZZ}, and in the 0.5–4 GeV region for $g_{a\gamma\gamma}$. In the case of $g_{a\gamma Z}$, the current best bounds for $m_a < m_Z$ come from the total Z width measurement at LEP.

7 Conclusions

We have investigated the possibility of constraining EW ALP interactions via the measurement of EW VBS processes at the LHC, where the ALP can induce nonresonant signals if it is too light to be produced resonantly. We have studied the production of ZZ, $Z\gamma$, $W^\pm\gamma$, $W^\pm Z$ and same-sign $W^\pm W^\pm$ pairs with large diboson invariant masses in association with two jets. New upper limits on ALP couplings to EW bosons have been derived from a reinterpretation of Run 2 public CMS VBS analyses. Among the channels considered, the most constraining ones are currently $Z\gamma$ and $W^\pm W^\pm$.

The limits have been calculated both in the plane of the gauge-invariant ALP EW couplings $(c_{\widetilde{W}}/f_a, c_{\widetilde{B}}/f_a)$ and projected onto the 4 mass-eigenstate couplings defined in eq. (2.2), to facilitate the comparison with other results. The constraints inferred on ALP couplings to ZZ, $W^\pm W^\pm$ and $Z\gamma$ pairs are very competitive with other LHC and LEP limits for ALP masses up to 100 GeV. They probe previously unexplored regions of the parameter space and have the advantage of being independent of the ALP coupling to

[5] A priori, the ALP-gluon interaction is not protected by any symmetry. Therefore, technically, it cannot be assumed to be exactly vanishing, even starting from a $c_{\widetilde{G}} = 0$ condition. In the Majoron case it is generated at 2-loops [83] and therefore remains very suppressed.

gluons and of the ALP decay width. This is important in view of a global analysis of ALP couplings, where VBS can help disentangling EW from gluon interactions. All the constraints extracted in this work can be further improved in the future, for instance, by adopting a finer binning for the kinematic distributions, or by incorporating into the fit measurements by the ATLAS Collaboration or measurements of other VBS channels (e.g. opposite-sign $W^{\pm}W^{\pm}$ or semileptonic ZV).

Simple projections for integrated luminosities up to $3000\,\mathrm{fb}^{-1}$ have been calculated, demonstrating the power of future dedicated analyses. Searches for nonresonant new physics signals in VBS production at the LHC Run 3 and HL-LHC performed by the ATLAS and CMS Collaborations will be able to probe the existence of ALPs for relevant values of their couplings to EW bosons.

Acknowledgments

We are grateful to G. Alonso and P. Quilez for providing code and information for the comparisons presented in section 6, to E. Vitagliano for guidance on the update of supernova constraints and to B. Gavela and V. Sanz for their continuous support. We also acknowledge the contributions of J.M. No to the initial phase of this work. J.B. and I.B. thank B. Heinemann, S. Heim, S. Bruggisser and P. Govoni for several illuminating discussions. The authors acknowledge the support of the CA16108 VBSCan COST Action. The work of J.B. was supported by the Spanish MICIU through the National Program FPU (grant number FPU18/03047). The work of J.M.R. was supported by the Spanish MICIU through the National Program FPI-Severo Ochoa (grant number PRE2019-089233). J.B. and J.M.R. acknowledge partial financial support by the Spanish MINECO through the Centro de excelencia Severo Ochoa Program under grant SEV-2016-0597, by the Spanish "Agencia Estatal de Investigacíon" (AEI) and the EU "Fondo Europeo de Desarrollo Regional" (FEDER) through the project PID2019-108892RB-I00/AEI/10.13039/501100011033. J.F.T. acknowledges support from the AEI and the EU FEDER through the project PID2020-116262RB-C43.

A Expected ALP EW VBS diboson mass distributions

Table 6 reports the expected ALP EW VBS pure signal and interference cross sections at $\sqrt{s} = 13\,\mathrm{TeV}$ as a function of the Wilson coefficients $c_{\widetilde{W}}$ and $c_{\widetilde{B}}$ for $f_a = 1\,\mathrm{TeV}$, after selection cuts and $M_{V_1V_2} < 4\,\mathrm{TeV}$.

The diboson invariant mass or transverse mass distributions after selection cuts for the five VBS channels studied are shown in figures 7–11. The data points and the total SM background (orange line) are taken from the CMS publications. The dashed and solid green lines represent the total ALP EW VBS signal contributions for $c_{\widetilde{B}}/f_a = c_{\widetilde{W}}/f_a = 1\,\mathrm{TeV}^{-1}$ with a cut of $M_{V_1V_2} < 2\,\mathrm{TeV}$ and $4\,\mathrm{TeV}$, respectively. As discussed in section 4, the total systematic uncertainty on the signal normalization is 20% (green band). The background systematics errors are taken bin-by-bin from the CMS publications (orange band).

Process	ALP EW VBS Cross Section [fb]
$pp \to jjZZ$	$\sigma_{\text{interf.}} = \left(0.04\, c_{\widetilde{B}}^2 - 0.55\, c_{\widetilde{B}}\, c_{\widetilde{W}} - 1.80\, c_{\widetilde{W}}^2\right) \cdot 10^{-2}$ $\sigma_{\text{signal}} = \left(0.05\, c_{\widetilde{B}}^4 + 0.15\, c_{\widetilde{B}}^3\, c_{\widetilde{W}} + 1.55\, c_{\widetilde{B}}^2\, c_{\widetilde{W}}^2 + 1.66\, c_{\widetilde{B}}\, c_{\widetilde{W}}^3 + 3.39\, c_{\widetilde{W}}^4\right) \cdot 10^{-2}$
$pp \to jjZ\gamma$	$\sigma_{\text{interf.}} = \left(0.01\, c_{\widetilde{B}}^2 + 6.60\, c_{\widetilde{B}}\, c_{\widetilde{W}} - 6.56\, c_{\widetilde{W}}^2\right) \cdot 10^{-2}$ $\sigma_{\text{signal}} = \left(0.19\, c_{\widetilde{B}}^4 - 0.29\, c_{\widetilde{B}}^3\, c_{\widetilde{W}} + 2.04\, c_{\widetilde{B}}^2\, c_{\widetilde{W}}^2 - 2.07\, c_{\widetilde{B}}\, c_{\widetilde{W}}^3 + 1.23\, c_{\widetilde{W}}^4\right) \cdot 10^{-1}$
$pp \to jjW^\pm\gamma$	$\sigma_{\text{interf.}} = c_{\widetilde{W}}\, \left(-1.38\, c_{\widetilde{B}} + 0.29\, c_{\widetilde{W}}\right) \cdot 10^{-3}$ $\sigma_{\text{signal}} = c_{\widetilde{W}}^2\, \left(5.20\, c_{\widetilde{B}}^2 + 2.12\, c_{\widetilde{B}}\, c_{\widetilde{W}} + 2.81\, c_{\widetilde{W}}^2\right) \cdot 10^{-2}$
$pp \to jjW^\pm Z$	$\sigma_{\text{interf.}} = c_{\widetilde{W}}\, \left(1.15\, c_{\widetilde{B}} - 0.55\, c_{\widetilde{W}}\right) \cdot 10^{-3}$ $\sigma_{\text{signal}} = c_{\widetilde{W}}^2\, \left(0.90\, c_{\widetilde{B}}^2 - 1.00\, c_{\widetilde{B}}\, c_{\widetilde{W}} + 3.17\, c_{\widetilde{W}}^2\right) \cdot 10^{-2}$
$pp \to jjW^\pm W^\pm$	$\sigma_{\text{interf.}} = -0.0405\, c_{\widetilde{W}}^2$ $\sigma_{\text{signal}} = 0.135\, c_{\widetilde{W}}^4$

Table 6. Expected ALP EW VBS interference and pure signal cross sections at $\sqrt{s} = 13\,\text{TeV}$ as a function of the Wilson coefficients $c_{\widetilde{W}}$ and $c_{\widetilde{B}}$ for $f_a = 1\,\text{TeV}$ after selection cuts and requiring $M_{V_1V_2} < 4\,\text{TeV}$. These expressions can be used to estimate the overall normalizations of the ALP signal for all distributions used in the final fits to the data.

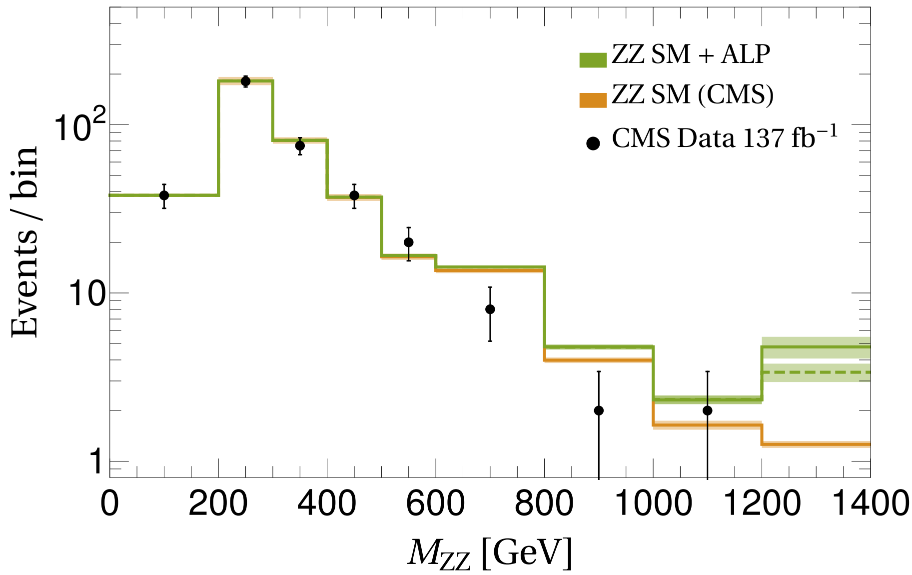

Figure 7. M_{ZZ} distribution for the $pp \to jjZZ \to jj\ell^+\ell^-\ell^+\ell^-$ channel. The data points and the total SM background (orange) are taken from the measurement in ref. [51]. The last bin contains the overflow events. The dashed and solid green lines show the total ALP EW VBS signal for $c_{\widetilde{B}}/f_a = c_{\widetilde{W}}/f_a = 1\,\text{TeV}^{-1}$ with a cut of $M_{ZZ} < 2\,\text{TeV}$ and 4 TeV, respectively.

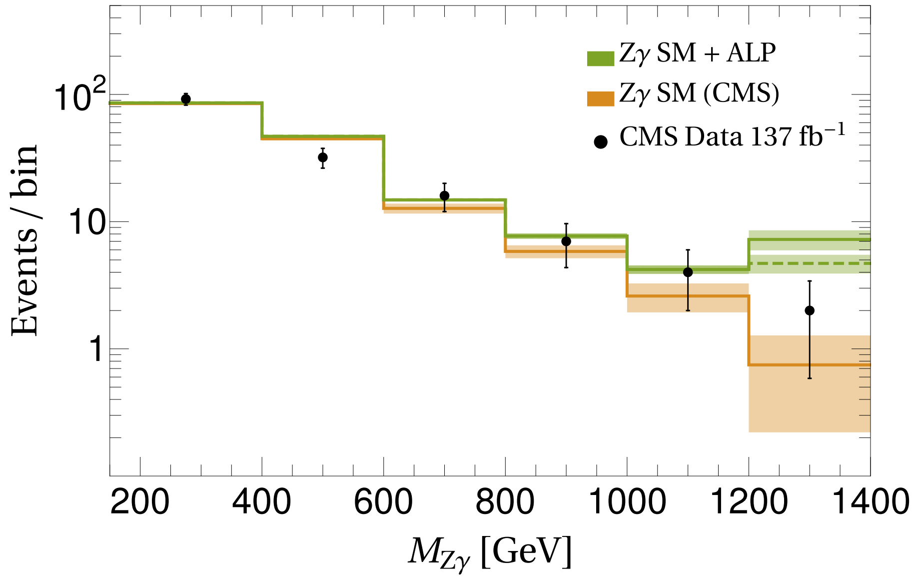

Figure 8. $M_{Z\gamma}$ distribution for the $pp \to jjZ\gamma \to jj\ell^+\ell^-\gamma$ channel. The data points and the total SM background (orange) are taken from the measurement in ref. [54]. The last bin contains the overflow events. The dashed and solid green lines show the total ALP EW VBS signal for $c_{\widetilde{B}}/f_a = c_{\widetilde{W}}/f_a = 1\,\text{TeV}^{-1}$ with a cut of $M_{Z\gamma} < 2\,\text{TeV}$ and $4\,\text{TeV}$, respectively.

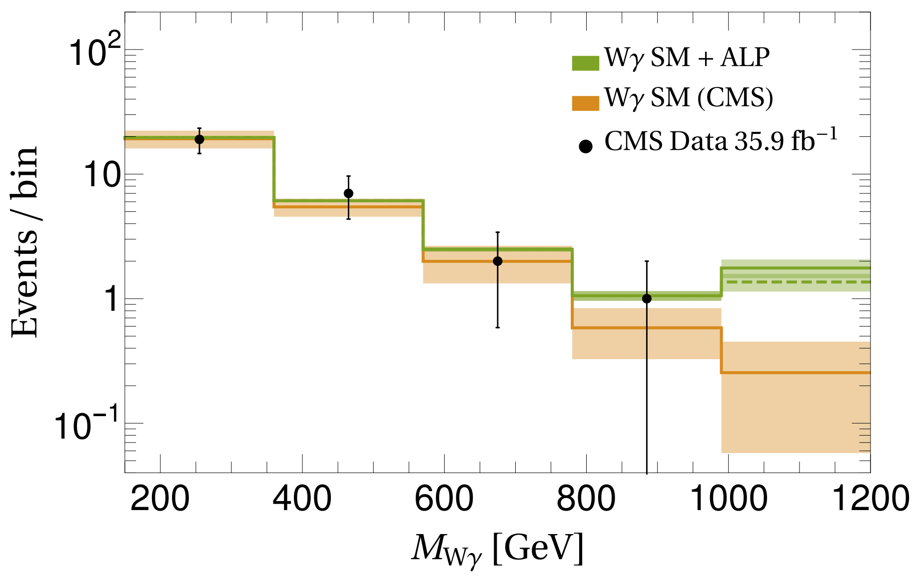

Figure 9. $M_{W\gamma}$ distribution for the $pp \to jjW^{\pm}\gamma \to jj\gamma\ell^{\pm}\nu$ channel.The data points and the total SM background (orange) are taken from the measurement in ref. [52]. The last bin contains the overflow events. The dashed and solid green lines show the total ALP EW VBS signal for $c_{\widetilde{B}}/f_a = c_{\widetilde{W}}/f_a = 1\,\text{TeV}^{-1}$ with a cut of $M_{W\gamma} < 2\,\text{TeV}$ and $4\,\text{TeV}$, respectively.

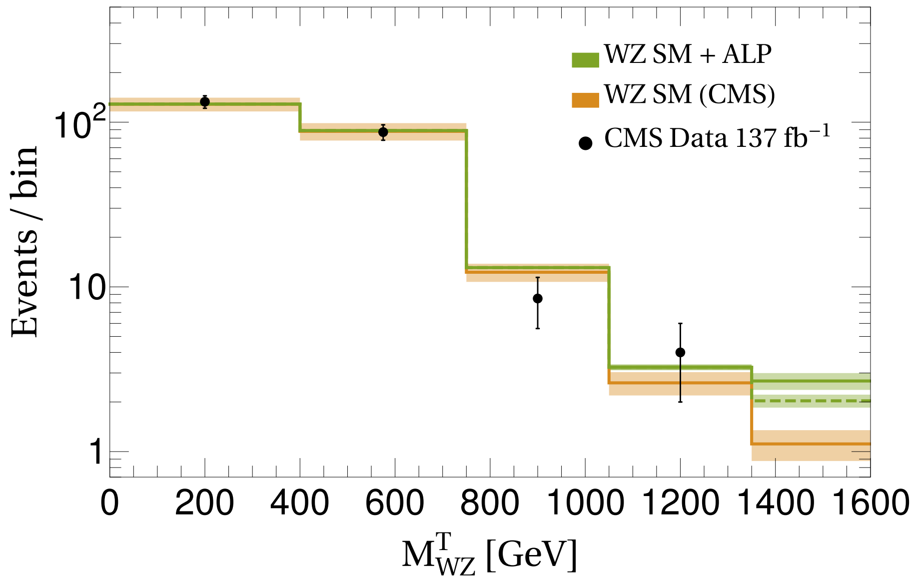

Figure 10. M^T_{WZ} distribution for the $pp \to jjW^\pm Z \to jj\ell^+\ell^-\ell'^\pm\nu$ channel.The data points and the total SM background (orange) are taken from the measurement in ref. [50]. The last bin contains the overflow events. The dashed and solid green lines show the total ALP EW VBS signal for $c_{\widetilde{B}}/f_a = c_{\widetilde{W}}/f_a = 1\,\text{TeV}^{-1}$ with a cut of $M_{WZ} < 2\,\text{TeV}$ and $4\,\text{TeV}$, respectively.

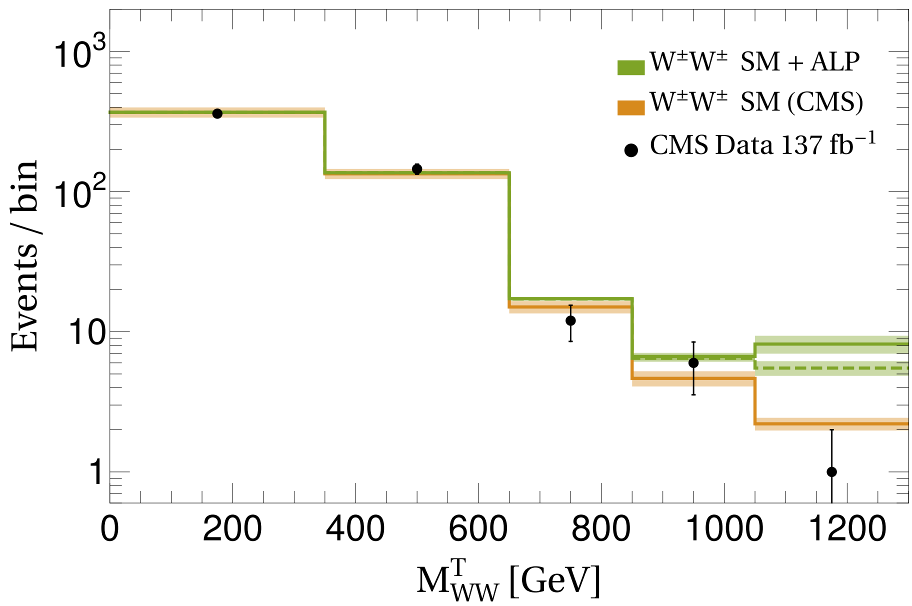

Figure 11. M^T_{WW} distribution for the $pp \to jjW^\pm W^\pm \to jj\ell^\pm\ell^\pm\nu\nu$ channel. The data points and the total SM background (orange) are taken from the measurement in ref. [50]. The last bin contains the overflow events. The dashed and solid green lines show the total ALP EW VBS signal for $c_{\widetilde{B}}/f_a = c_{\widetilde{W}}/f_a = 1\,\text{TeV}^{-1}$ with a cut of $M_{WW} < 2\,\text{TeV}$ and $4\,\text{TeV}$, respectively.

JHEP06(2022)113

References

[1] R.D. Peccei and H.R. Quinn, *CP Conservation in the Presence of Instantons*, *Phys. Rev. Lett.* **38** (1977) 1440 [INSPIRE].

[2] R.D. Peccei and H.R. Quinn, *Constraints Imposed by CP Conservation in the Presence of Instantons*, *Phys. Rev. D* **16** (1977) 1791 [INSPIRE].

[3] S. Weinberg, *A New Light Boson?*, *Phys. Rev. Lett.* **40** (1978) 223 [INSPIRE].

[4] F. Wilczek, *Problem of Strong P and T Invariance in the Presence of Instantons*, *Phys. Rev. Lett.* **40** (1978) 279 [INSPIRE].

[5] J.E. Kim, *Weak Interaction Singlet and Strong CP Invariance*, *Phys. Rev. Lett.* **43** (1979) 103 [INSPIRE].

[6] M.A. Shifman, A.I. Vainshtein and V.I. Zakharov, *Can Confinement Ensure Natural CP Invariance of Strong Interactions?*, *Nucl. Phys. B* **166** (1980) 493 [INSPIRE].

[7] M. Dine, W. Fischler and M. Srednicki, *A Simple Solution to the Strong CP Problem with a Harmless Axion*, *Phys. Lett. B* **104** (1981) 199 [INSPIRE].

[8] A.R. Zhitnitsky, *On Possible Suppression of the Axion Hadron Interactions* (in Russian), *Sov. J. Nucl. Phys.* **31** (1980) 260 [INSPIRE].

[9] M. Cicoli, *Axion-like Particles from String Compactifications*, in *9th Patras Workshop on Axions, WIMPs and WISPs*, pp. 235–242 (2013) [DOI] [arXiv:1309.6988] [INSPIRE].

[10] G.B. Gelmini and M. Roncadelli, *Left-Handed Neutrino Mass Scale and Spontaneously Broken Lepton Number*, *Phys. Lett. B* **99** (1981) 411 [INSPIRE].

[11] P. Langacker, R.D. Peccei and T. Yanagida, *Invisible Axions and Light Neutrinos: Are They Connected?*, *Mod. Phys. Lett. A* **1** (1986) 541 [INSPIRE].

[12] G. Ballesteros, J. Redondo, A. Ringwald and C. Tamarit, *Standard Model-axion-seesaw-Higgs portal inflation. Five problems of particle physics and cosmology solved in one stroke*, *JCAP* **08** (2017) 001 [arXiv:1610.01639] [INSPIRE].

[13] F. Wilczek, *Axions and Family Symmetry Breaking*, *Phys. Rev. Lett.* **49** (1982) 1549 [INSPIRE].

[14] Y. Ema, K. Hamaguchi, T. Moroi and K. Nakayama, *Flaxion: a minimal extension to solve puzzles in the standard model*, *JHEP* **01** (2017) 096 [arXiv:1612.05492] [INSPIRE].

[15] L. Calibbi, F. Goertz, D. Redigolo, R. Ziegler and J. Zupan, *Minimal axion model from flavor*, *Phys. Rev. D* **95** (2017) 095009 [arXiv:1612.08040] [INSPIRE].

[16] J. Beacham et al., *Physics Beyond Colliders at CERN: Beyond the Standard Model Working Group Report*, *J. Phys. G* **47** (2020) 010501 [arXiv:1901.09966] [INSPIRE].

[17] P. Agrawal et al., *Feebly-interacting particles: FIPs 2020 workshop report*, *Eur. Phys. J. C* **81** (2021) 1015 [arXiv:2102.12143] [INSPIRE].

[18] E. Izaguirre, T. Lin and B. Shuve, *Searching for Axionlike Particles in Flavor-Changing Neutral Current Processes*, *Phys. Rev. Lett.* **118** (2017) 111802 [arXiv:1611.09355] [INSPIRE].

[19] M. Bauer, M. Neubert and A. Thamm, *Collider Probes of Axion-Like Particles*, JHEP **12** (2017) 044 [arXiv:1708.00443] [INSPIRE].

[20] G. Alonso-Álvarez, M.B. Gavela and P. Quilez, *Axion couplings to electroweak gauge bosons*, Eur. Phys. J. C **79** (2019) 223 [arXiv:1811.05466] [INSPIRE].

[21] M.B. Gavela, R. Houtz, P. Quilez, R. Del Rey and O. Sumensari, *Flavor constraints on electroweak ALP couplings*, Eur. Phys. J. C **79** (2019) 369 [arXiv:1901.02031] [INSPIRE].

[22] J. Ebadi, S. Khatibi and M. Mohammadi Najafabadi, *New probes for axionlike particles at hadron colliders*, Phys. Rev. D **100** (2019) 015016 [arXiv:1901.03061] [INSPIRE].

[23] F. Ertas and F. Kahlhoefer, *On the interplay between astrophysical and laboratory probes of MeV-scale axion-like particles*, JHEP **07** (2020) 050 [arXiv:2004.01193] [INSPIRE].

[24] S. Gori, G. Perez and K. Tobioka, *KOTO vs. NA62 Dark Scalar Searches*, JHEP **08** (2020) 110 [arXiv:2005.05170] [INSPIRE].

[25] K.J. Kelly, S. Kumar and Z. Liu, *Heavy axion opportunities at the DUNE near detector*, Phys. Rev. D **103** (2021) 095002 [arXiv:2011.05995] [INSPIRE].

[26] A.M. Galda, M. Neubert and S. Renner, *ALP — SMEFT interference*, JHEP **06** (2021) 135 [arXiv:2105.01078] [INSPIRE].

[27] J. Bonilla, I. Brivio, M.B. Gavela and V. Sanz, *One-loop corrections to ALP couplings*, JHEP **11** (2021) 168 [arXiv:2107.11392] [INSPIRE].

[28] M. Bauer, M. Neubert, S. Renner, M. Schnubel and A. Thamm, *Flavor probes of axion-like particles*, arXiv:2110.10698 [INSPIRE].

[29] K. Mimasu and V. Sanz, *ALPs at Colliders*, JHEP **06** (2015) 173 [arXiv:1409.4792] [INSPIRE].

[30] I. Brivio et al., *ALPs Effective Field Theory and Collider Signatures*, Eur. Phys. J. C **77** (2017) 572 [arXiv:1701.05379] [INSPIRE].

[31] N. Craig, A. Hook and S. Kasko, *The Photophobic ALP*, JHEP **09** (2018) 028 [arXiv:1805.06538] [INSPIRE].

[32] D. Wang, L. Wu, J.M. Yang and M. Zhang, *Photon-jet events as a probe of axionlike particles at the LHC*, Phys. Rev. D **104** (2021) 095016 [arXiv:2102.01532] [INSPIRE].

[33] J. Ren, D. Wang, L. Wu, J.M. Yang and M. Zhang, *Detecting an axion-like particle with machine learning at the LHC*, JHEP **11** (2021) 138 [arXiv:2106.07018] [INSPIRE].

[34] M.B. Gavela, J.M. No, V. Sanz and J.F. de Trocóniz, *Nonresonant Searches for Axionlike Particles at the LHC*, Phys. Rev. Lett. **124** (2020) 051802 [arXiv:1905.12953] [INSPIRE].

[35] S. Carra et al., *Constraining off-shell production of axionlike particles with $Z\gamma$ and WW differential cross-section measurements*, Phys. Rev. D **104** (2021) 092005 [arXiv:2106.10085] [INSPIRE].

[36] CMS collaboration, *Search for heavy resonances decaying to ZZ or ZW and axion-like particles mediating nonresonant ZZ or ZH production at $\sqrt{s} = 13$ TeV*, JHEP **04** (2022) 087 [arXiv:2111.13669] [INSPIRE].

[37] R. Covarelli, M. Pellen and M. Zaro, *Vector-Boson scattering at the LHC: Unraveling the electroweak sector*, Int. J. Mod. Phys. A **36** (2021) 2130009 [arXiv:2102.10991] [INSPIRE].

[38] A. Flórez et al., *Probing axionlike particles with $\gamma\gamma$ final states from vector boson fusion processes at the LHC*, *Phys. Rev. D* **103** (2021) 095001 [arXiv:2101.11119] [INSPIRE].

[39] C.-X. Yue, H.-Y. Zhang and H. Wang, *Production of axion-like particles via vector boson fusion at future electron-positron colliders*, *Eur. Phys. J. C* **82** (2022) 88 [arXiv:2112.11604] [INSPIRE].

[40] Y. Liu and B. Yan, *Searching for the axion-like particle at the EIC*, arXiv:2112.02477 [INSPIRE].

[41] CMS collaboration, *Observation of electroweak production of same-sign W boson pairs in the two jet and two same-sign lepton final state in proton-proton collisions at $\sqrt{s} = 13$ TeV*, *Phys. Rev. Lett.* **120** (2018) 081801 [arXiv:1709.05822] [INSPIRE].

[42] ATLAS collaboration, *Observation of electroweak $W^{\pm}Z$ boson pair production in association with two jets in pp collisions at $\sqrt{s} = 13$ TeV with the ATLAS detector*, *Phys. Lett. B* **793** (2019) 469 [arXiv:1812.09740] [INSPIRE].

[43] CMS collaboration, *Measurement of electroweak WZ boson production and search for new physics in WZ + two jets events in pp collisions at $\sqrt{s} = 13$ TeV*, *Phys. Lett. B* **795** (2019) 281 [arXiv:1901.04060] [INSPIRE].

[44] CMS collaboration, *Search for anomalous electroweak production of vector boson pairs in association with two jets in proton-proton collisions at 13 TeV*, *Phys. Lett. B* **798** (2019) 134985 [arXiv:1905.07445] [INSPIRE].

[45] ATLAS collaboration, *Search for the electroweak diboson production in association with a high-mass dijet system in semileptonic final states in pp collisions at $\sqrt{s} = 13$ TeV with the ATLAS detector*, *Phys. Rev. D* **100** (2019) 032007 [arXiv:1905.07714] [INSPIRE].

[46] ATLAS collaboration, *Observation of electroweak production of a same-sign W boson pair in association with two jets in pp collisions at $\sqrt{s} = 13$ TeV with the ATLAS detector*, *Phys. Rev. Lett.* **123** (2019) 161801 [arXiv:1906.03203] [INSPIRE].

[47] ATLAS collaboration, *Evidence for electroweak production of two jets in association with a $Z\gamma$ pair in pp collisions at $\sqrt{s} = 13$ TeV with the ATLAS detector*, *Phys. Lett. B* **803** (2020) 135341 [arXiv:1910.09503] [INSPIRE].

[48] CMS collaboration, *Measurement of the cross section for electroweak production of a Z boson, a photon and two jets in proton-proton collisions at $\sqrt{s} = 13$ TeV and constraints on anomalous quartic couplings*, *JHEP* **06** (2020) 076 [arXiv:2002.09902] [INSPIRE].

[49] ATLAS collaboration, *Observation of electroweak production of two jets and a Z-boson pair with the ATLAS detector at the LHC*, arXiv:2004.10612 [INSPIRE].

[50] CMS collaboration, *Measurements of production cross sections of WZ and same-sign WW boson pairs in association with two jets in proton-proton collisions at $\sqrt{s} = 13$ TeV*, *Phys. Lett. B* **809** (2020) 135710 [arXiv:2005.01173] [INSPIRE].

[51] CMS collaboration, *Evidence for electroweak production of four charged leptons and two jets in proton-proton collisions at $\sqrt{s} = 13$ TeV*, *Phys. Lett. B* **812** (2021) 135992 [arXiv:2008.07013] [INSPIRE].

[52] CMS collaboration, *Observation of electroweak production of $W\gamma$ with two jets in proton-proton collisions at $\sqrt{s} = 13$ TeV*, *Phys. Lett. B* **811** (2020) 135988 [arXiv:2008.10521] [INSPIRE].

[53] CMS collaboration, *Measurements of production cross sections of polarized same-sign W boson pairs in association with two jets in proton-proton collisions at $\sqrt{s} = 13$ TeV*, Phys. Lett. B **812** (2021) 136018 [arXiv:2009.09429] [INSPIRE].

[54] CMS collaboration, *Measurement of the electroweak production of $Z\gamma$ and two jets in proton-proton collisions at $\sqrt{s} = 13$ TeV and constraints on anomalous quartic gauge couplings*, Phys. Rev. D **104** (2021) 072001 [arXiv:2106.11082] [INSPIRE].

[55] CMS collaboration, *Evidence for WW/WZ vector boson scattering in the decay channel $\ell\nu qq$ produced in association with two jets in proton-proton collisions at $\sqrt{s} = 13$ TeV*, arXiv:2112.05259 [INSPIRE].

[56] CMS collaboration, *First observation of the electroweak production of a leptonically decaying W^+W^- pair in association with two jets in $\sqrt{s} = 13$ TeV pp collisions*, CMS-PAS-SMP-21-001 (2021).

[57] H. Georgi, D.B. Kaplan and L. Randall, *Manifesting the Invisible Axion at Low-energies*, Phys. Lett. B **169** (1986) 73 [INSPIRE].

[58] K. Choi, K. Kang and J.E. Kim, *Effects of η' in Low-energy Axion Physics*, Phys. Lett. B **181** (1986) 145 [INSPIRE].

[59] J. Alwall et al., *The automated computation of tree-level and next-to-leading order differential cross sections, and their matching to parton shower simulations*, JHEP **07** (2014) 079 [arXiv:1405.0301] [INSPIRE].

[60] http://feynrules.irmp.ucl.ac.be/wiki/ALPsEFT.

[61] NNPDF collaboration, *Parton distributions for the LHC Run II*, JHEP **04** (2015) 040 [arXiv:1410.8849] [INSPIRE].

[62] P. Artoisenet, V. Lemaitre, F. Maltoni and O. Mattelaer, *Automation of the matrix element reweighting method*, JHEP **12** (2010) 068 [arXiv:1007.3300] [INSPIRE].

[63] T. Sjöstrand et al., *An introduction to PYTHIA 8.2*, Comput. Phys. Commun. **191** (2015) 159 [arXiv:1410.3012] [INSPIRE].

[64] DELPHES 3 collaboration, *DELPHES 3, A modular framework for fast simulation of a generic collider experiment*, JHEP **02** (2014) 057 [arXiv:1307.6346] [INSPIRE].

[65] M. Cacciari, G.P. Salam and G. Soyez, *FastJet User Manual*, Eur. Phys. J. C **72** (2012) 1896 [arXiv:1111.6097] [INSPIRE].

[66] I. Brivio, O.J.P. Éboli and M.C. Gonzalez-Garcia, *Unitarity constraints on ALP interactions*, Phys. Rev. D **104** (2021) 035027 [arXiv:2106.05977] [INSPIRE].

[67] B. Döbrich, J. Jaeckel, F. Kahlhoefer, A. Ringwald and K. Schmidt-Hoberg, *ALPtraum: ALP production in proton beam dump experiments*, JHEP **02** (2016) 018 [arXiv:1512.03069] [INSPIRE].

[68] J.D. Bjorken et al., *Search for Neutral Metastable Penetrating Particles Produced in the SLAC Beam Dump*, Phys. Rev. D **38** (1988) 3375 [INSPIRE].

[69] E.M. Riordan et al., *A Search for Short Lived Axions in an Electron Beam Dump Experiment*, Phys. Rev. Lett. **59** (1987) 755 [INSPIRE].

[70] J. Blümlein and J. Brunner, *New Exclusion Limits on Dark Gauge Forces from Proton Bremsstrahlung in Beam-Dump Data*, Phys. Lett. B **731** (2014) 320 [arXiv:1311.3870] [INSPIRE].

JHEP06(2022)113

[71] J. Jaeckel and M. Spannowsky, *Probing MeV to 90 GeV axion-like particles with LEP and LHC*, Phys. Lett. B **753** (2016) 482 [arXiv:1509.00476] [INSPIRE].

[72] A. Caputo, G. Raffelt and E. Vitagliano, *Muonic boson limits: Supernova redux*, Phys. Rev. D **105** (2022) 035022 [arXiv:2109.03244] [INSPIRE].

[73] A. Caputo, H.-T. Janka, G. Raffelt and E. Vitagliano, *Low-Energy Supernovae Severely Constrain Radiative Particle Decays*, Phys. Rev. Lett. **128** (2022) 221103 [arXiv:2201.09890] [INSPIRE].

[74] BaBar collaboration, *Search for hadronic decays of a light Higgs boson in the radiative decay* $\Upsilon \to \gamma A^0$, Phys. Rev. Lett. **107** (2011) 221803 [arXiv:1108.3549] [INSPIRE].

[75] L3 collaboration, *Isolated hard photon emission in hadronic Z0 decays*, Phys. Lett. B **292** (1992) 472 [INSPIRE].

[76] J. Jaeckel, M. Jankowiak and M. Spannowsky, *LHC probes the hidden sector*, Phys. Dark Univ. **2** (2013) 111 [arXiv:1212.3620] [INSPIRE].

[77] A. Mariotti, D. Redigolo, F. Sala and K. Tobioka, *New LHC bound on low-mass diphoton resonances*, Phys. Lett. B **783** (2018) 13 [arXiv:1710.01743] [INSPIRE].

[78] X. Cid Vidal, A. Mariotti, D. Redigolo, F. Sala and K. Tobioka, *New Axion Searches at Flavor Factories*, JHEP **01** (2019) 113 [*Erratum ibid.* **06** (2020) 141] [arXiv:1810.09452] [INSPIRE].

[79] CMS collaboration, *Evidence for light-by-light scattering and searches for axion-like particles in ultraperipheral PbPb collisions at* $\sqrt{s_{\rm NN}} = 5.02$ *TeV*, Phys. Lett. B **797** (2019) 134826 [arXiv:1810.04602] [INSPIRE].

[80] ATLAS collaboration, *Measurement of light-by-light scattering and search for axion-like particles with* $2.2\,nb^{-1}$ *of Pb+Pb data with the ATLAS detector*, JHEP **03** (2021) 243 [*Erratum ibid.* **11** (2021) 050] [arXiv:2008.05355] [INSPIRE].

[81] ATLAS collaboration, *Search for dark matter in association with an energetic photon in pp collisions at* $\sqrt{s} = 13$ *TeV with the ATLAS detector*, JHEP **02** (2021) 226 [arXiv:2011.05259] [INSPIRE].

[82] BNL-E949 collaboration, *Study of the decay* $K^+ \to \pi^+ \nu\bar{\nu}$ *in the momentum region* $140 < P_\pi < 199$ *MeV/c*, Phys. Rev. D **79** (2009) 092004 [arXiv:0903.0030] [INSPIRE].

[83] J. Heeck and H.H. Patel, *Majoron at two loops*, Phys. Rev. D **100** (2019) 095015 [arXiv:1909.02029] [INSPIRE].

Chapter 5

Limits on ALP-Neutrino Couplings from Loop-level Processes

This chapter contains the publication in Ref. [3]. In this work we present novel bounds on ALP-neutrino interactions from their loop-level impact on the ALP effective couplings to the EW gauge bosons.

The dark sector of the Universe deserves utmost attention since it heralds new laws of physics beyond the Standard Model. Neutrinos arguably constitute excellent portals to dark and weakly coupled sectors, as their interactions are not obscured by strong or electromagnetic forces. We address in this work the effective interactions between ALPs and neutrinos using the ALP EFT model-independent approach. In fact, gauge invariance forces us to consider both the couplings to charged leptons $\mathbf{c}_{ee}$ and the couplings to neutrinos $\mathbf{c}_{\nu\nu}$. These induce at one-loop ALP anomalous interactions to the EW gauge bosons, with two types of contributions according to their dependence on the lepton masses: mass-independent corrections — i.e., stemming from the chiral anomaly— and mass-dependent corrections, which are negligible for ALP couplings to at least one massive gauge boson.

We perform the first ever two-couplings-at-a-time analysis recasting bounds from the ALP-EW parameter space onto the $\{\mathbf{c}_{\nu\nu}, \mathbf{c}_{ee}\}$ couplings to neutrinos and charged leptons. We consider three particular scenarios: *(i)* assuming no ALP coupling to electrons, $\mathrm{Tr}(\mathbf{c}_{ee}) = 0$; *(ii)* assuming no ALP coupling to RH electrons, $\mathrm{Tr}(\mathbf{c}_{ee}) = \mathrm{Tr}(\mathbf{c}_{\nu\nu})$; *(iii)* considering three benchmark values of the ALP mass while constraining the entire two-dimensional $\{\mathbf{c}_{\nu\nu}, \mathbf{c}_{ee}\}$ parameter space. Bounds on ALP-electron couplings in the scenario with vanishing ALP-neutrino couplings, $\mathrm{Tr}(\mathbf{c}_{\nu\nu}) = 0$, are also presented for reference. Constraints extracted from collider data are presented here for the first time. In particular, for heavy ALP masses $m_a \gtrsim \mathcal{O}(10)$ GeV, bounds derived from high-energy searches at the LHC —nonresonant ALP searches in VBS, light-by-light scattering in Pb-Pb colllisions, diphoton production and ALP-mediated resonant tri-boson searches— populate novel territory of the ALP-neutrino parameter space for $\mathrm{Tr}(\mathbf{c}_{\nu\nu})/f_a \lesssim 0.3$ GeV^{-1} in scenario *(i)*, and $\mathrm{Tr}(\mathbf{c}_{\nu\nu})/f_a \lesssim 0.02$ GeV^{-1}, in scenario *(ii)*.

Previous works in the literature set constraints on ALP-lepton interactions based on one-coupling-at-a-time analyses and furthermore focus on ALP-charged lepton couplings, using data from rare meson decays, beam dump experiments as well as astrophysical observations and cosmology. These can be found in Ref. [149], where new bounds on the ALP couplings to the LH lepton doublet and the RH charged lepton singlet are obtained at the one-loop and two-loop levels; and Ref. [249, 271], where they set new bounds on ALP-muon and ALP-electron interactions, respectively, from their one-loop contribution to the ALP-photon coupling, while disregarding the ALP-neutrino coupling.

In this chapter we consider the ALP gauge invariant couplings to the SM LH lepton doublets and their RH counterparts. The leptonic EOM —including one-loop anomalous corrections— are discussed since they directly suggest limits on the flavor-diagonal components of ALP-neutrino couplings. In Sec. 3, we present the complete one-loop contributions stemming from ALP-lepton interactions to the effective ALP-EW couplings $\{g_{a\gamma\gamma}, g_{aWW}, g_{aZZ}, g_{a\gamma Z}\}$. These were computed with the help of the `Mathematica` packages `FeynCalc` [272] and `Package-X` [273]. Finally, the bounds on the ALP-neutrino parameter space are presented in Sec. 4. Our results evidence the need for accelerator experimental efforts targeting the heavy ALP parameter space region.

Limits on ALP-neutrino couplings from loop-level processes

J. Bonilla,* B. Gavela,† and J. Machado-Rodríguez‡

Departamento de Física Teórica and Instituto de Física Teórica UAM/CSIC, Universidad Autónoma de Madrid, Cantoblanco, 28049, Madrid, Spain and Instituto de Física Teórica IFT-UAM/CSIC, Cantoblanco, E-28049, Madrid, Spain

(Received 25 October 2023; accepted 21 February 2024; published 13 March 2024)

We obtain new bounds on effective axionlike particle (ALP)-neutrino interactions from their loop-level impact on the ALP couplings to electroweak gauge bosons γZ, ZZ and W^+W^-. Both types of interactions are connected via the chiral anomaly, which allows to overcome the fermion mass suppression of tree-level analyses. ALP couplings to charged leptons are considered simultaneously with ALP-neutrino ones, as required by gauge invariance. Complete one-loop computations are presented together with relevant kinematic limits. We leverage data obtained from rare meson decay measurements alongside observations from collider experiments, among others. The novel constraints are particularly competitive for ALP masses $\gtrsim$100 MeV, evidencing the powerful potential of future ALP searches at colliders which target its couplings to electroweak gauge bosons.

DOI: 10.1103/PhysRevD.109.055023

I. INTRODUCTION

The quest for axions that solve the strong CP-problem, and more generally axionlike particles (ALPs), is ongoing with increasing intensity. Their interest stems from their nature as pseudo-Goldstone bosons (pGBs) which are singlets of the Standard Model of particle physics (SM), and are thus the generic tell-tale of yet undiscovered symmetries in Nature, classically almost exact but hidden (aka spontaneously broken). Beyond axions, many extensions of the SM predict pGBs which are SM singlets, such as for instance the *Majoron* associated to a dynamical nature of neutrino masses [1–5], pGBs from flavor symmetries known as *flavons* [6–9], or within composite Higgs models [10], extradimensional theories [11,12], and phenomenological string models with their plethora of spontaneously broken $U(1)$ global symmetries, as well as pGBs in many inflationary theories [13].

Because ALPs are pGBs, their new physics scale f_a is much larger than their mass $m_a \ll f_a$. They are thus conveniently studied within the model-independent framework of effective field theory (EFT), i.e., in terms of a tower of operators weighted down by inverse powers of f_a. The leading operators have mass dimension five: purely derivative couplings as pertains GBs, plus shift-breaking anomalous couplings and a mass term for the ALP. In analyses of generic ALPs—to be considered below—the parameters $\{m_a, f_a\}$ are treated as free and independent (unlike in true-axion theories which solve the strong CP problem, for which their product is dynamically fixed).

For ALPs, the range of possible values of f_a and m_a is wide, leading to an incredibly rich phenomenological arena for particle and astroparticle physics. To compound their intrinsic interest, both axions and ALPs can be excellent candidates to explain the nature of dark matter (DM). An intense theoretical exploration is ongoing on ALP EFTs and their predictions for laboratory experiments, astrophysics and cosmology, together with the construction of ultraviolet (UV) complete theories. In synergy with it, a plethora of experiments, which look for ALPs in different regimes and with diversified techniques, are either already taking data or scheduled to do so in the next decade [14].

We address in this work the effective interactions between ALPs and neutrinos. At leading order in the ALP EFT these appear as combinations of ALP derivative insertions $\partial_\mu a$ and fermionic currents, that is, in the form of chirality-conserving fermion bilinears with arbitrary coefficients. Their tree-level impact on observables turns out to be proportional to the fermion masses, as it can be straightly inferred from the classical equations of motion (EOM): they show that—at the classical level—the ALP-fermionic operators are tradable by chirality-flipping ones proportional to the fermion masses [15–18]. Given the tiny masses of neutrinos, their tree-level contribution is thus extremely suppressed and negligible. In contrast, this mass

*jesus.bonilla@uam.es
†belen.gavela@uam.es
‡jonathan.machado@uam.es

suppression is overcome when the system is contemplated including one-loop effects [19]. This is obvious noting that the use of EOMs is tantamount to a chiral rotation which necessarily induces at one-loop anomalous ALP couplings, and in consequence mass-independent components. The present experimental constraints on ALP couplings to γZ, ZZ, and W^+W^- will be shown to be strong enough to suggest relevant bounds on ALP-neutrino interactions, in spite of the $\mathcal{O}(\alpha/\pi)$ weight of one-loop effects. The loop-induced impact of ALP-neutrino interactions on the coupling of ALPs to electroweak (EW) bosons will be shown to probe regions of the parameter space for ALP-lepton couplings that are otherwise unexplored.

The ALP EFT theory is constructed for scales $f_a \gg v \simeq 246$ GeV where v is the SM electroweak (EW) scale. A proper EFT formulation must then be explicitly $SU(3)\times SU(2)\times U(1)$ gauge invariant above the electroweak scale. This brings into the game the couplings of ALPs to charged leptons, as the left-handed components of the latter unavoidably accompany left-handed neutrinos. Bounds on charged ALP-lepton couplings have been previously explored [20–24] and these will be taken into account in our analysis. Furthermore, recent works [25–27] propose to study the impact of DM ALPs on neutrino propagation and oscillations, and cosmology, but they explore a much lighter range of ALP masses than that considered in this paper.

We present the complete one-loop corrections to the couplings of ALPs to on-shell EW gauge boson pairs, $\gamma\gamma$, γZ, ZZ, and WW, induced by ALP couplings to neutrinos and charged leptons. Our work expands and completes previous corrections involving ALP fermionic currents [15–17,23,28]. Neutrino masses will be disregarded, unless otherwise stated in which case the role of Pontecorvo–Maki–Nakagawa–Sakata (PMNS) mixing will be discussed. Various kinematics regions and limits are contemplated: the best—and novel—bounds on ALP-neutrino interactions will turn out to be those for relatively heavy ALPs, $m_a \gtrsim 100$ MeV up to 1 TeV, correlated with the fact that the strongest constraints on ALP couplings to heavy EW bosons stem from collider searches and from rare meson decay searches.

An additional comment is pertinent in the framework of the most general ALP EFT. The latter may include from the start dimension five anomalous ALP couplings to gauge bosons, with arbitrary coefficients. In consequence, the contribution stemming from the chiral rotation described above will confront experiment mixed with that from the putative anomalous gauge couplings of ALPs in the initial Lagrangian. In spite of this, bounds on the coefficients of ALP-neutrino flavor-diagonal couplings can be extracted from experiment, barring fine-tuned cancellations among the contributions from both sources.

The structure of this manuscript can be inferred from the Table of Contents.

II. THE ALP EFFECTIVE LAGRANGIAN

The ALP EFT Lagrangian, up to operators with mass dimension five, reads [17,18,29,30]

$$\mathcal{L}_{\rm ALP} = \frac{1}{4}\partial_\mu a \partial^\mu a - \frac{1}{2}m_a^2 a^2 + \mathcal{L}_a^{\rm gauge} + \mathcal{L}_{\partial a}^{\rm fermion}, \tag{2.1}$$

where $\mathcal{L}_a^{\rm gauge}$ stands for the anomalous ALP-gauge boson effective couplings, which at energies above EW symmetry breaking can be written as

$$\mathcal{L}_a^{\rm gauge} = -c_{\tilde{G}}\frac{a}{f_a}G^\alpha_{\mu\nu}\tilde{G}^{\mu\nu,\alpha} - c_{\tilde{W}}\frac{a}{f_a}W^i_{\mu\nu}\tilde{W}^{\mu\nu,i} - c_{\tilde{B}}\frac{a}{f_a}B_{\mu\nu}\tilde{B}^{\mu\nu}, \tag{2.2}$$

with $G^\alpha_{\mu\nu}$, $W^i_{\mu\nu}$ and $B_{\mu\nu}$ denoting the field strength of the strong and EW gauge bosons respectively ($i = 1, 2, 3$ and $\alpha = 1, \ldots, 8$), while $\mathcal{L}_{\partial a}^{\rm fermion}$ stands for the gauge-invariant ALP-fermion derivative interactions,

$$\mathcal{L}_{\partial a}^{\rm fermion} = \sum_\Psi \frac{\partial_\mu a}{f_a}\overline{\Psi}\gamma^\mu \mathbf{c}_\Psi \Psi, \tag{2.3}$$

where the sum runs over the chiral fermionic fields of the SM: $\Psi = \{Q_L, L_L, u_R, d_R, e_R\}$, each Ψ being a 3-component vector in flavor space and $\mathbf{c}_\Psi$ 3×3 being Hermitian matrices in that space.[1] Note that no coupling to putative right-handed neutrinos is considered, as neutrino masses will be neglected below. In all generality, those chiral fields in the Ψ set are not the left and right components of fermion mass eigenstates. Nevertheless, the rotation of the $\mathbf{c}_\Psi$ matrices to the mass basis [15–18] is not relevant for the main results of this paper, which focuses on purely leptonic couplings neglecting neutrino masses (i.e., all $\mathbf{c}_\Psi$ matrices will be disregarded except for $\mathbf{c}_E$ and $\mathbf{c}_L$). $\mathcal{L}_{\partial a}^{\psi}$ simplifies then to

$$\begin{aligned}\mathcal{L}_{\partial a}^{\rm fermion} &= \frac{\partial_\mu a}{f_a}\overline{L}_L\gamma^\mu \mathbf{c}_L L_L + \frac{\partial_\mu a}{f_a}\bar{e}_R\gamma^\mu \mathbf{c}_E e_R,\\ &= \frac{\partial_\mu a}{f_a}\bar{\nu}_L\gamma^\mu \mathbf{c}_L \nu_L + \frac{\partial_\mu a}{f_a}\bar{e}\gamma^\mu(\mathbf{c}_E P_R + \mathbf{c}_L P_L)e,\\ &= \frac{\partial_\mu a}{2f_a}\bar{\nu}_L\gamma^\mu(1-\gamma^5)\mathbf{c}_L\nu_L + \frac{\partial_\mu a}{2f_a}\bar{e}\gamma^\mu((\mathbf{c}_E+\mathbf{c}_L)\\ &\quad + (\mathbf{c}_E - \mathbf{c}_L)\gamma^5)e,\end{aligned} \tag{2.4}$$

where $P_{R,L}$ stands for the chirality projectors, and in the last two lines the left-handed EW lepton fields have been

[1]Note that there exists in addition a shift-invariant bosonic operator involving the Higgs doublet, $\mathcal{O}_{a\Phi} = \partial_\mu a(\Phi^\dagger i\overleftrightarrow{D}_\mu\Phi)/f_a$, which has *not* been included in Eq. (2.1), as it would be redundant given the choice made to consider all possible fermionic couplings in $\mathcal{L}_{\partial a}^{\psi}$ [17].

decomposed on their electrically charged and neutral components $L_L = (e_L, \nu_L)$, with $e = e_R + e_L$. This illustrates that the ALP-neutrino couplings are defined only in terms of $\mathbf{c}_L$, while their analysis unavoidably requires to contemplate as well the couplings of charged leptons to ALPs.

It is worth to remind that in flavor-diagonal scenarios *and at tree-level*, the "phenomenological" couplings to the physical leptons only depend on the axial component of the operators in Eq. (2.4) (see Refs. [17,18]),

$$\mathcal{L}_{\partial a}^{\text{fermion}} \supset \frac{\partial_\mu a}{f_a}\sum_\ell (\mathbf{c}_{\nu\nu})_{\ell\ell}\bar{\nu}_\ell\gamma^\mu\gamma^5\nu_\ell + \frac{\partial_\mu a}{f_a}\sum_\ell (\mathbf{c}_{ee})_{\ell\ell}\bar{\ell}\gamma^\mu\gamma^5\ell, \tag{2.5}$$

where $\mathbf{c}_{ee}$ and $\mathbf{c}_{\nu\nu}$ are defined as

$$\mathbf{c}_{ee} \equiv (\mathbf{c}_E - \mathbf{c}_L) \qquad \mathbf{c}_{\nu\nu} \equiv (-\mathbf{c}_L) \tag{2.6}$$

Indeed, the orthogonal combination, i.e., the vectorial coupling, vanishes due to the conservation of vectorial currents (lepton number) at classical level.[2] At the quantum level, though, lepton number currents are broken due to chiral anomalies and the vector components do contribute even in the flavor-diagonal case: they will induce interactions between the ALP and heavy gauge bosons, which will be taken into account. In any case, because in all generality there are only two independent set of couplings, $\{\mathbf{c}_E, \mathbf{c}_L\}$, we choose to show our results below in terms of the two phenomenological combinations defined in Eq. (2.6), as they are more transparent to confront experimental data.

At energies below EW symmetry breaking, the bosonic Lagrangian $\mathcal{L}_a^{\text{gauge}}$ in Eq. (2.2) can be rewritten in terms of the EW gauge boson mass eigenstates,

$$\begin{aligned}\mathcal{L}_a^{\text{gauge}} = &-\frac{1}{4}g_{agg}aG^\alpha_{\mu\nu}\tilde{G}^{\mu\nu,\alpha} - \frac{1}{4}g_{a\gamma\gamma}aF_{\mu\nu}\tilde{F}^{\mu\nu}\\ &-\frac{1}{4}g_{a\gamma Z}aF_{\mu\nu}\tilde{Z}^{\mu\nu} - \frac{1}{4}g_{aZZ}aZ_{\mu\nu}\tilde{Z}^{\mu\nu}\\ &-\frac{1}{2}g_{aWW}aW^+_{\mu\nu}\tilde{W}^{\mu\nu,-},\end{aligned} \tag{2.7}$$

with

$$\begin{aligned} &g_{agg} \equiv \frac{4}{f_a}c_{\tilde{G}}, \qquad g_{a\gamma\gamma} \equiv \frac{4}{f_a}(c_w^2 c_{\tilde{B}} + s_w^2 c_{\tilde{W}}),\\ &g_{aWW} \equiv \frac{4}{f_a}c_{\tilde{W}}, \qquad g_{aZZ} \equiv \frac{4}{f_a}(s_w^2 c_{\tilde{B}} + c_w^2 c_{\tilde{W}}),\\ &g_{a\gamma Z} \equiv \frac{8}{f_a}c_w s_w(c_{\tilde{W}} - c_{\tilde{B}}),\end{aligned} \tag{2.8}$$

where $c_w(s_w)$ is the cosine (sine) of the weak mixing angle.

A. Leptonic EOM

The low-energy equations of motion (EOM) for the lepton fields, taking into account one-loop anomalous corrections, can be written as

$$\begin{aligned}\frac{\partial_\mu a}{f_a}\bar{e}_R\gamma^\mu\mathbf{c}_E e_R &= -\left(i\frac{a}{f_a}\bar{e}_L\mathbf{M}_E\mathbf{c}_E e_R + \text{H.c.}\right) + \text{Tr}[\mathbf{c}_E]\frac{a}{f_a}\frac{g'^2}{16\pi^2}B_{\mu\nu}\tilde{B}^{\mu\nu},\\ \frac{\partial_\mu a}{f_a}\bar{e}_L\gamma^\mu\mathbf{c}_L e_L &= \left(i\frac{a}{f_a}\bar{e}_L\mathbf{M}_E\mathbf{c}_L e_R + \text{H.c.}\right) - \text{Tr}[\mathbf{c}_L]\frac{a}{f_a}\left[\frac{g'^2}{64\pi^2}B_{\mu\nu}\tilde{B}^{\mu\nu} + \frac{g^2}{64\pi^2}W_{\mu\nu}\tilde{W}^{\mu\nu}\right],\\ \frac{\partial_\mu a}{f_a}\bar{\nu}_L\gamma^\mu\mathbf{c}_L\nu_L &= \left(i\frac{a}{f_a}\bar{\nu}_L\mathbf{M}_\nu\mathbf{c}_L\nu_R + \text{H.c.}\right) - \text{Tr}[\mathbf{c}_L]\frac{a}{f_a}\left[\frac{g'^2}{64\pi^2}B_{\mu\nu}\tilde{B}^{\mu\nu} + \frac{g^2}{64\pi^2}W_{\mu\nu}\tilde{W}^{\mu\nu}\right],\end{aligned} \tag{2.9}$$

where $\mathbf{M}_E$ and $\mathbf{M}_\nu$ denote here the generic mass matrices for charged leptons and neutrinos, respectively, and where the anomalous contributions have been left expressed here in terms of the hypercharge and $SU(2)_L$ field strengths, $B_{\mu\nu}$ and $W_{\mu\nu}$ respectively, for notation compactness. Given the tiny values of neutrinos masses, Eq. (2.9) already shows that experimental bounds on ALP couplings to massive EW gauge bosons directly suggest limits on the flavor-diagonal components of ALP-neutrino couplings, barring fine-tuned cancellations with tree-level gauge couplings or underlying symmetries in the UV complete theory. A well-known example is the DFSZ axion [31,32], in which an extra Peccei-Quinn symmetry leads to an exact cancellation. This is then a true QCD axion, not a generic ALP.

[2]This does not hold for flavor nondiagonal couplings, which can be relevant in practice when considering ALP decays to charged leptons (e.g., ALP $\to e\mu$); these will not be considered in this work.

III. ONE-LOOP INDUCED COUPLINGS

In this section we present the complete one-loop contribution of ALP-lepton couplings in Eq. (2.4) to the strength of the ALP-EW gauge bosons $\{g_{a\gamma\gamma}, g_{aWW}, g_{aZZ}, g_{a\gamma Z}\}$

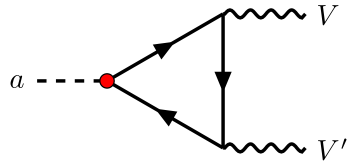

FIG. 1. One-loop diagram contributing to the ALP-gauge effective couplings originated from the ALP-fermion coupling.

defined in Eq. (2.8). These corrections correspond to the triangle diagram in Fig. 1,[3] and include all combinations of axial and vectorial insertions which stem from the SM electroweak gauge couplings. For completeness, both the anomalous and mass-dependent [35,36] one-loop corrections will be developed. For the computation of the latter, the ALP field a and the SM bosons will be taken to be on-shell, and thus the amplitudes will be written in terms of the gauge boson masses M_W and M_Z, the charged lepton masses m_ℓ and the ALP mass m_a. Nevertheless, the amplitude for any coupling with the ALP off-shell can be immediately obtained from the expressions below by simply replacing $m_a^2 \to p_a^2$, where p_a is the ALP four-momentum. All computations have been performed with the help of the *Mathematica* packages FeynCalc and PACKAGE-X [37,38].

Although neutrino masses are to be disregarded in the main text because they induce negligible corrections, their impact is nevertheless made explicit for the no flavor-mixing case in the Appendix. In turn, lepton-flavor mixing effects would be *a priori* present for final state W bosons, but the amplitudes would remain in practice equivalent to those for the no flavor-mixing scenario due to the unitarity of the PMNS matrix: we have verified that the GIM-suppressed flavor corrections are of order $\mathcal{O}(m_\nu^2 m_\ell^2/M_W^4)$ and thus totally negligible.

Without further ado, we present next the results for the amplitudes computed from the triangle diagram in Fig. 1, in the limit $m_\nu \to 0$ for all neutrino flavors.

A. Contributions to $g_{a\gamma\gamma}$

Previous computations of the ALP-photon interaction induced at one-loop by ALP-charged lepton couplings can be found in Refs. [16,17,28], whose results we verified. They stem from the diagram in Fig. 1 with charged leptons running in the loop. Being electrically neutral, neutrinos do not play a role in this two-photon channel, and the induced coupling reads

$$\begin{aligned} g_{a\gamma\gamma}^{\rm loop} &= -\frac{\alpha_{\rm em}}{\pi f_a}\left[\mathrm{Tr}(\mathbf{c}_{ee}) + 2\sum_\ell (\mathbf{c}_{ee})_{\ell\ell} m_\ell^2 \mathcal{C}_0(0,0,m_a^2,m_\ell,m_\ell,m_\ell)\right] \\ &= -\frac{\alpha_{\rm em}}{\pi f_a}\left[\mathrm{Tr}(\mathbf{c}_{ee}) - \sum_\ell (\mathbf{c}_{ee})_{\ell\ell}\tau_\ell f(\tau_\ell)^2\right], \end{aligned} \tag{3.1}$$

where $\ell = e, \mu, \tau$ here and all through the paper, $\tau_\ell \equiv 4m_\ell^2/m_a^2$, and $\mathcal{C}_0$ is the scalar 3-point Passarino-Veltman function (see Ref. [39]),

$$\mathcal{C}_0(q_1^2,q_2^2,p^2,m_1,m_2,m_3) \equiv \int_0^1 \mathrm{d}x \int_0^x \frac{\mathrm{d}y}{(x-y)yq_1^2 - (x-y)(x-1)q_2^2 - y(x-1)p^2 - ym_1^2 - (x-y)m_2^2 + (x-1)m_3^2}, \tag{3.2}$$

and

$$f(\tau) = \begin{cases} \arcsin\frac{1}{\sqrt{\tau}} & \text{for } \tau \geq 1, \\ \frac{\pi}{2} + \frac{i}{2}\log\frac{1+\sqrt{1-\tau}}{1-\sqrt{1-\tau}} & \text{for } \tau < 1. \end{cases} \tag{3.3}$$

This shows that the size of the effective ALP-photon coupling in Eq. (3.1) only depends on the ratio m_ℓ^2/m_a^2 (assuming that the ALP and both photons are on-shell particles). In particular, in the heavy ALP limit, $m_a \gg m_\ell$, the second term in Eq. (3.1), which is mass-dependent, becomes negligible, and then only the first term remains:

$$g_{a\gamma\gamma}^{\rm loop} \approx -\frac{\alpha_{\rm em}}{\pi f_a}\mathrm{Tr}(\mathbf{c}_{ee}) \quad \text{for } m_\ell \ll m_a. \tag{3.4}$$

This first term is the *anomalous* term of the triangle diagram, which is mass-independent. Basically this term corresponds to the chiral anomaly from the fermion current to which the ALP is coupled in Eq. (2.4). On the other hand, in the light ALP limit $m_a \ll m_\ell$, both terms—the anomalous and the mass-dependent one—partially cancel each other and the net coupling is suppressed as

[3] Notice that the one-loop amplitudes computed here cannot be obtained from the mixing of ALP-EFT operators via running, as the anomalous operators are only renormalized by themselves [33,34].

$$g_{a\gamma\gamma}^{\text{loop}} \approx -\frac{\alpha_{\text{em}}}{12\pi f_a}\sum_\ell (\mathbf{c}_{ee})_{\ell\ell}\frac{m_a^2}{m_\ell^2} \quad \text{for } m_\ell \gg m_a. \tag{3.5}$$

This is a well-known property of the triangle diagram for vector-like gauge interactions and massless gauge bosons such as QED [40]. This behavior will not hold in the presence of massive gauge bosons, i.e., the Z and W bosons, see below.

B. Contributions to $g_{a\gamma Z}$

Even though neutrinos—being electrically neutral—cannot run in the loop that induces $g_{a\gamma Z}$, this ALP-gauge bosons coupling can still be used to measure the physical couplings between ALPs and neutrinos as shown by its dependence on $\mathbf{c}_{\nu\nu}$. Indeed, the one-loop-induced ALP-γZ coupling reads:

$$\begin{aligned} g_{a\gamma Z}^{\text{loop}} &= \frac{\alpha_{\text{em}}}{c_w s_w \pi f_a}\left[\text{Tr}(\mathbf{c}_{\nu\nu}) - 2s_w^2\text{Tr}(\mathbf{c}_{ee}) + (1-4s_w^2)\sum_\ell (\mathbf{c}_{ee})_{\ell\ell} m_\ell^2 \mathcal{C}_0(0, M_Z^2, m_a^2, m_\ell, m_\ell, m_\ell)\right], \\ &= \frac{\alpha_{\text{em}}}{c_w s_w \pi f_a}\left[\text{Tr}(\mathbf{c}_{\nu\nu}) - 2s_w^2\text{Tr}(\mathbf{c}_{ee}) - 2(1-4s_w^2)\sum_\ell \frac{(\mathbf{c}_{ee})_{\ell\ell} m_\ell^2}{m_a^2 - M_Z^2}(f(\tau_\ell)^2 - f(\tau_\ell^Z)^2)\right], \end{aligned} \tag{3.6}$$

where $\tau_\ell^Z \equiv 4m_\ell^2/M_Z^2$ (previous computations can be found in Refs. [16,17]). The dependence on $\mathbf{c}_{\nu\nu}$ is a consequence of the chiral anomaly since the Z boson couples with different weak charges to right-handed and left-handed leptons, and thus the equation exhibits the $\mathbf{c}_L$ contribution which is shared with charged leptons, see Eq. (2.6).

Once again two distinct types of contributions appear: the first two terms in Eq. (3.6) are anomalous ones and thus mass-independent, while the mass-dependent term is proportional to m_ℓ^2 times the contribution from $f(\tau)$ functions. The latter is induced exclusively by the axial combination of couplings. Given that the Z boson is much heavier than any SM lepton, the following approximation for the $f(\tau^Z)$ function in Eq. (3.6) is pertinent:

$$f(\tau_\ell^Z)^2 \approx \frac{1}{4}\left[\pi + i\log\left(\frac{M_Z^2}{m_\ell^2}\right)\right]^2. \tag{3.7}$$

It follows that the mass-dependent term in Eq. (3.6) is always suppressed, at least, by a factor m_ℓ^2/m_Z^2, in contrast with the case for $g_{a\gamma\gamma}$ in Eq. (3.1). This means that the anomalous term in $g_{a\gamma Z}$ will not be canceled in any kinematic region of m_a. In other words, the anomalous term will always dominates $g_{a\gamma Z}$ while the mass-dependent term provides at most a correction of order $\mathcal{O}(m_\ell^2/M_Z^2)$,

$$g_{a\gamma Z}^{\text{loop}} \approx \frac{\alpha_{\text{em}}}{c_w s_w \pi f_a}\left[\text{Tr}(\mathbf{c}_{\nu\nu}) - 2s_w^2\text{Tr}(\mathbf{c}_{ee}) + \mathcal{O}\left(\frac{m_\ell^2}{M_Z^2}\right)\right]. \tag{3.8}$$

This property will also hold for all ALP couplings to heavy EW bosons considered below.

Simplified formulas of interest for different regimes of ALP mass versus m_ℓ and M_Z read:

(i) For $m_a \ll m_\ell \ll M_Z$:

$$g_{a\gamma Z}^{\text{loop}} \approx \frac{\alpha_{\text{em}}}{c_w s_w \pi f_a}\left\{\text{Tr}(\mathbf{c}_{\nu\nu}) - 2s_w^2\text{Tr}(\mathbf{c}_{ee}) - (1-4s_w^2) \times \sum_\ell \frac{(\mathbf{c}_{ee})_{\ell\ell} m_\ell^2}{2M_Z^2}\left[\pi + i\log\left(\frac{M_Z^2}{m_\ell^2}\right)\right]^2\right\}. \tag{3.9}$$

(ii) For $m_\ell \ll m_a \ll M_Z$:

$$g_{a\gamma Z}^{\text{loop}} \approx \frac{\alpha_{\text{em}}}{c_w s_w \pi f_a}\left\{\text{Tr}(\mathbf{c}_{\nu\nu}) - 2s_w^2\text{Tr}(\mathbf{c}_{ee}) - (1-4s_w^2)\sum_\ell \frac{(\mathbf{c}_{ee})_{\ell\ell} m_\ell^2}{M_Z^2}\log\left(\frac{m_a^2 M_Z^2}{m_\ell^4}\right) \times \left[\log\left(\frac{m_a}{M_Z}\right) + i\pi\right]\right\}. \tag{3.10}$$

(iii) For $m_\ell \ll M_Z \ll m_a$:

$$g_{a\gamma Z}^{\text{loop}} \approx \frac{\alpha_{\text{em}}}{c_w s_w \pi f_a}\left\{\text{Tr}(\mathbf{c}_{\nu\nu}) - 2s_w^2\text{Tr}(\mathbf{c}_{ee}) - (1-4s_w^2)\sum_\ell \frac{(\mathbf{c}_{ee})_{\ell\ell} m_\ell^2}{m_a^2}\log\left(\frac{m_a^2 M_Z^2}{m_\ell^4}\right) \times \left[\log\left(\frac{M_Z}{m_a}\right) + i\pi\right]\right\}. \tag{3.11}$$

C. Contributions to g_{aZZ}

The complete correction to the on-shell $a - ZZ$ coupling induced at one-loop by ALP-neutrino and ALP-electron couplings reads

$$g_{aZZ}^{\rm loop} = -\frac{\alpha_{\rm em}}{2c_w^2 s_w^2 \pi f_a}\Bigg\{(1-2s_w^2)\mathrm{Tr}(\mathbf{c}_{\nu\nu}) + 2s_w^4 \mathrm{Tr}(\mathbf{c}_{ee}) - \sum_\ell \frac{(\mathbf{c}_{ee})_{\ell\ell} m_\ell^2}{m_a^2 - 4M_Z^2}\Big[\mathcal{B}(m_a^2, m_\ell, m_\ell) - \mathcal{B}(M_Z^2, m_\ell, m_\ell) + [(1-4s_w^2)^2 M_Z^2 + 2s_w^2(1-2s_w^2)m_a^2]\mathcal{C}_0(m_a^2, M_Z^2, M_Z^2, m_\ell, m_\ell, m_\ell)\Big]\Bigg\}, \tag{3.12}$$

where $\mathcal{B}$ is the function `DiscB` in PACKAGE-X (see Ref. [17]), which can be written as

$$\mathcal{B}(p^2, m_1, m_2) \equiv \frac{\sqrt{\lambda(p^2, m_1^2, m_2^2)}}{p^2}\log\left(\frac{m_1^2 + m_2^2 - p^2 + \sqrt{\lambda(p^2, m_1^2, m_2^2)}}{2m_1 m_2}\right), \tag{3.13}$$

in which λ is the Källén triangle function: $\lambda(a,b,c) \equiv a^2 + b^2 + c^2 - 2ab - 2bc - 2ca$. As in the previous case, given that $m_\ell \ll M_Z$ for all SM leptons, the $\mathcal{B}$ functions in Eq. (3.12) can be approximated as

$$\mathcal{B}(M_Z^2, m_\ell, m_\ell) \approx i\pi + \log\left(\frac{m_\ell^2}{M_Z^2}\right), \tag{3.14}$$

and

$$\mathcal{C}_0(m_a^2, M_Z^2, M_Z^2, m_\ell, m_\ell, m_\ell) \approx \mathcal{C}_0(m_a^2, M_Z^2, M_Z^2, 0, 0, 0). \tag{3.15}$$

In the assumption that all particles are on-shell, the only physical process stemming from the $a - ZZ$ vertex in Fig. 1 corresponds to the decay of a heavy ALP into two Z bosons, for which the relevant kinematic regime is $m_\ell \ll m_a$, and thus

$$g_{aZZ}^{\rm loop} \approx -\frac{\alpha_{\rm em}}{2c_w^2 s_w^2 \pi f_a}\Bigg\{(1-2s_w^2)\mathrm{Tr}(\mathbf{c}_{\nu\nu}) + 2s_w^4 \mathrm{Tr}(\mathbf{c}_{ee}) - \sum_\ell \frac{(\mathbf{c}_{ee})_{\ell\ell} m_\ell^2}{m_a^2 - 4M_Z^2}\Big[\log\left(\frac{M_Z^2}{m_a^2}\right) + ((1-4s_w^2)^2 M_Z^2 + 2s_w^2(1-2s_w^2)m_a^2)\mathcal{C}_0(m_a^2, M_Z^2, M_Z^2, 0, 0, 0)\Big]\Bigg\}. \tag{3.16}$$

This expression can be simplified for ALPs much heavier than the Z boson,

$$g_{aZZ}^{\rm loop} \approx -\frac{\alpha_{\rm em}}{2c_w^2 s_w^2 \pi f_a}\Bigg\{(1-2s_w^2)\mathrm{Tr}(\mathbf{c}_{\nu\nu}) + 2s_w^4 \mathrm{Tr}(\mathbf{c}_{ee}) - 2\sum_\ell \frac{(\mathbf{c}_{ee})_{\ell\ell} m_\ell^2}{m_a^2}\Big[\log\left(\frac{M_Z}{m_a}\right) + i\pi + s_w^2(1-2s_w^2)\left(\frac{\pi^2}{3} + \log\left(\frac{M_Z^2}{m_a^2}\right)^2\right)\Big]\Bigg\}. \tag{3.17}$$

Note that this expression is also valid in the regime $m_\ell \ll M_Z \ll m_a$ for off-shell ALPs upon the replacement $m_a^2 \to p_a^2$ and as long as $M_Z^2 \ll p_a^2$.

D. Contributions to g_{aWW}

Finally, the correction to the a-WW on-shell coupling induced at one-loop by the insertion of ALP-neutrino and ALP-electron couplings reads

$$g_{aWW}^{\rm loop} = -\frac{\alpha_{\rm em}}{2s_w^2 \pi f_a}\Bigg\{\mathrm{Tr}(\mathbf{c}_{\nu\nu}) - \sum_\ell \frac{(\mathbf{c}_{ee})_{\ell\ell} m_\ell^2}{m_a^2 - 4M_W^2}\Big[\mathcal{B}(m_a^2, m_\ell, m_\ell) + \left(1 - \frac{m_\ell^2}{M_W^2}\right)\left(i\pi + \log\left(\frac{M_W^2}{m_\ell^2} - 1\right) + M_W^2 \mathcal{C}_0(m_a^2, M_W^2, M_W^2, m_\ell, m_\ell, 0)\right)\Big]\Bigg\}, \tag{3.18}$$

where the second (mass-dependent) term corresponds to the diagram in which the two fermionic legs attached to the ALP in Fig. 1 are electrons and the vertically exchanged lepton is a neutrino, and viceversa for the anomalous term. Note that all contributions are flavor diagonal at the leading order in which we work.[4]

[4]As an illustration of the (in)dependence with respects to the PMNS mixing matrix $U^{\rm PMNS}$, it is easy to see that, if leptonic mixing is considered, the $(\mathbf{c}_{ee})_{\ell\ell}$ coupling in the second term in Eq. (3.18) would be simply replaced by $\sum_i U^{\rm PMNS}_{\nu_i\ell}(\mathbf{c}_{ee})_{\ell\ell'}(U^{\rm PMNS}_{\ell'\nu_i})^* = (\mathbf{c}_{ee})_{\ell\ell'}\delta_{\ell\ell'}$, recovering the original equation for the scenario with no lepton mixing.

Taking again the limit $m_\ell \ll m_a, M_W$, the expression above simplifies to

$$g_{aWW}^{\rm loop} \approx -\frac{\alpha_{\rm em}}{2s_w^2\pi f_a}\left\{\mathrm{Tr}(\mathbf{c}_{\nu\nu}) - \sum_\ell \frac{(\mathbf{c}_{ee})_{\ell\ell} m_\ell^2}{m_a^2 - 4M_W^2}\left[\log\left(\frac{M_W^2}{m_a^2}\right) + M_W^2 \mathcal{C}_0(m_a^2, M_W^2, M_W^2, 0, 0, 0)\right]\right\}, \tag{3.19}$$

which can be further approximated for an ALP much heavier than the W boson,

$$g_{aWW}^{\rm loop} \approx -\frac{\alpha_{\rm em}}{2s_w^2\pi f_a}\left[\mathrm{Tr}(\mathbf{c}_{\nu\nu}) - \sum_\ell \frac{(\mathbf{c}_{ee})_{\ell\ell} m_\ell^2}{m_a^2}\log\left(\frac{M_W^2}{m_a^2}\right)\right]. \tag{3.20}$$

IV. BOUNDS ON ALP-NEUTRINO EFFECTIVE INTERACTIONS

We present next the bounds on ALP-neutrino coupling which follow from the experimental bounds on $\{g_{a\gamma\gamma}, g_{aWW}, g_{aZZ}, g_{a\gamma Z}\}$ couplings (barring fine-tuned cancellations with hypothetical tree-level anomalous couplings in Eq. (2.2), as explained earlier). We include bounds on the ALP-electron coupling as they impose further constraints on the ALP-neutrino sector, due to gauge invariance correlations between $\mathbf{c}_{ee}$ and $\mathbf{c}_{\nu\nu}$ that arise from the coupling to left-handed leptons $\mathbf{c}_L$, see Eq. (2.6).

In the previous section it was shown that the anomalous terms in the couplings of ALPs to massive gauge bosons suffice for the numerical analysis, given today's experimental precision,

$$g_{a\gamma Z}^{\rm loop} \approx -\frac{\alpha_{\rm em}}{s_w c_w \pi f_a}(2s_w^2 \mathrm{Tr}(\mathbf{c}_{ee}) - \mathrm{Tr}(\mathbf{c}_{\nu\nu})), \tag{4.1}$$

$$g_{aZZ}^{\rm loop} \approx -\frac{\alpha_{\rm em}}{2s_w^2 c_w^2 \pi f_a}(2s_w^4 \mathrm{Tr}(\mathbf{c}_{ee}) + (1-2s_w^2)\mathrm{Tr}(\mathbf{c}_{\nu\nu})), \tag{4.2}$$

$$g_{aWW}^{\rm loop} \approx -\frac{\alpha_{\rm em}}{2s_w^2\pi f_a}\mathrm{Tr}(\mathbf{c}_{\nu\nu}). \tag{4.3}$$

This is in contrast with the ALP-photon channel in the regime of light ALPs, $m_a \lesssim m_\ell$, in which case the mass-dependent term in Eq. (3.1) cancels the anomalous contribution, so that $g_{a\gamma\gamma}^{\rm loop} \approx 0$ is a reasonable approximation in that kinematical regime, see Eq. (3.5).

It follows from Eq. (3.1) and Eqs. (4.1)–(4.3) that the experimental bounds on the ALP-photon coupling $g_{a\gamma\gamma}$ lead to bounds on $\mathrm{Tr}(\mathbf{c}_{ee})$ only, while the experimental bounds on the ALP-WW coupling g_{aWW} can be directly translated into bounds on $\mathrm{Tr}(\mathbf{c}_{\nu\nu})$. In contrast, the data on the two ALP couplings involving the Z boson—Eqs. (4.1) and (4.2)—constrain two (different) combinations of both traces, which define flat directions of the EFT. In order to avoid such cancellations altogether, simultaneous bounds on at least two different phenomenological ALP couplings among the three in Eqs. (4.1)–(4.3) have to be considered.

The bounds on $\mathrm{Tr}(\mathbf{c}_{\nu\nu})$ and $\mathrm{Tr}(\mathbf{c}_{ee})$ relevant for the kinematical region under discussion are illustrated in Figs. 2–5. They depict the constraints derived from colliders (green and red), rare meson decays (blue and yellow), beam dump experiments (gray) and astrophysics/cosmology (purple). Figures 2 and 3 summarize the bounds obtained on $\mathrm{Tr}(\mathbf{c}_{\nu\nu})/f_a$ as a function of m_a, for two distinct values of the ALP coupling to charged leptons $\mathbf{c}_{ee}$. For reference, Fig. 4 depicts instead the constraints on $\mathrm{Tr}(\mathbf{c}_{ee})/f_a$ assuming $\mathbf{c}_{\nu\nu} = 0$. Finally, Fig. 5 sheds a different perspective: it depicts our results in the $\{\mathbf{c}_{\nu\nu}, \mathbf{c}_{ee}\}$ trace parameter space,

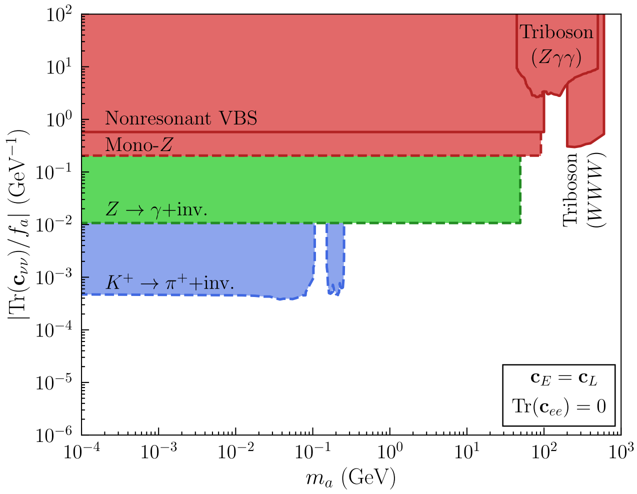

FIG. 2. Direct and loop induced bounds on $|\mathrm{Tr}(\mathbf{c}_{\nu\nu})/f_a|$ derived from several experimental searches assuming no ALP-electron couplings: $\mathbf{c}_{ee} = 0$.

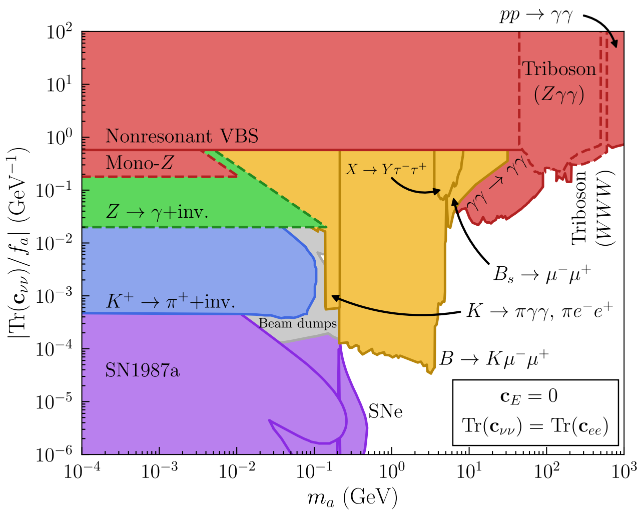

FIG. 3. Direct and loop induced bounds on $|\mathrm{Tr}(\mathbf{c}_{\nu\nu})/f_a|$ derived from several experimental searches assuming no ALP coupling to right-handed electrons ($\mathbf{c}_E = 0$) so $\mathbf{c}_{ee} = \mathbf{c}_{\nu\nu} = -\mathbf{c}_L$.

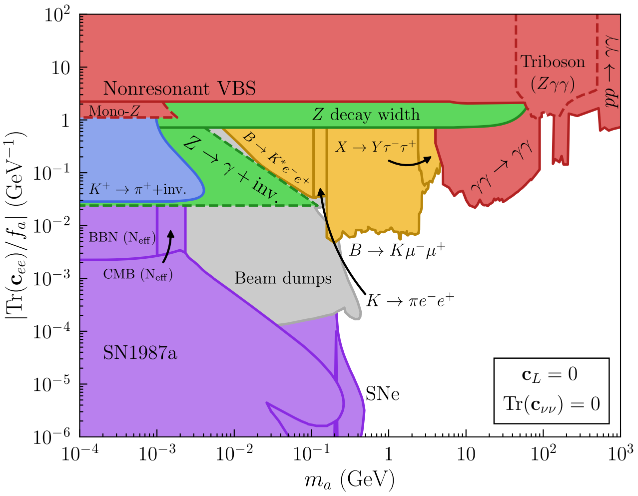

FIG. 4. Direct and loop induced bounds on $|\mathrm{Tr}(\mathbf{c}_{ee})/f_a|$ derived from several experimental searches assuming no ALP-neutrino couplings: $\mathbf{c}_{\nu\nu} = 0$.

for different values of m_a. Details on all those figures follow:

(i) The *photophobic* ALP is depicted in Fig. 2. It assumes $(\mathbf{c}_{ee})_{ii} = 0$, i.e., no tree-level flavor-diagonal ALP-charged lepton interactions. This holds for $\mathbf{c}_E = \mathbf{c}_L$, that is, if the coupling matrices for left-handed and right-handed leptons coincide. This forbids ALP decays into same-flavor charged leptons (at tree-level) and into photons (at one-loop-level), from which the popular denomination as "photophobic" follows [41]. Such a benchmark is particularly relevant for invisible searches, in which the ALP is measured as MET. Indeed, for ALPs lighter than the massive EW gauge bosons, the only possible decay is then $a \to \bar{\nu}\nu$, which is naturally suppressed by neutrino masses. It follows that the ALP can be in practice considered stable at collider distances for masses up to $m_a \leq M_Z$.

(ii) Fig. 3 illustrates another interesting—and complementary—case: an ALP which couples to charged leptons and to neutrinos with the same strength, i.e., $\mathbf{c}_{ee} = \mathbf{c}_{\nu\nu} = -\mathbf{c}_L$. In other words, it only interacts with left-handed lepton doublets, i.e., $\mathbf{c}_L \neq 0$, $\mathbf{c}_E = 0$. The limits in the photophobic case—Fig. 2—are approximately maintained, but for a reduction in the LEP and mono-Z sectors and the strengthening of the constraints from $Z\gamma\gamma$ searches, to be discussed below. More importantly, Fig. 3 exhibits strong additional constraints from rare meson decays into charged leptons and photons (in yellow), beam dump experiments (in gray) and from astrophysics and cosmology (in purple) given that the ALP-electron channel—and therefore the ALP-photon channel—is now open.

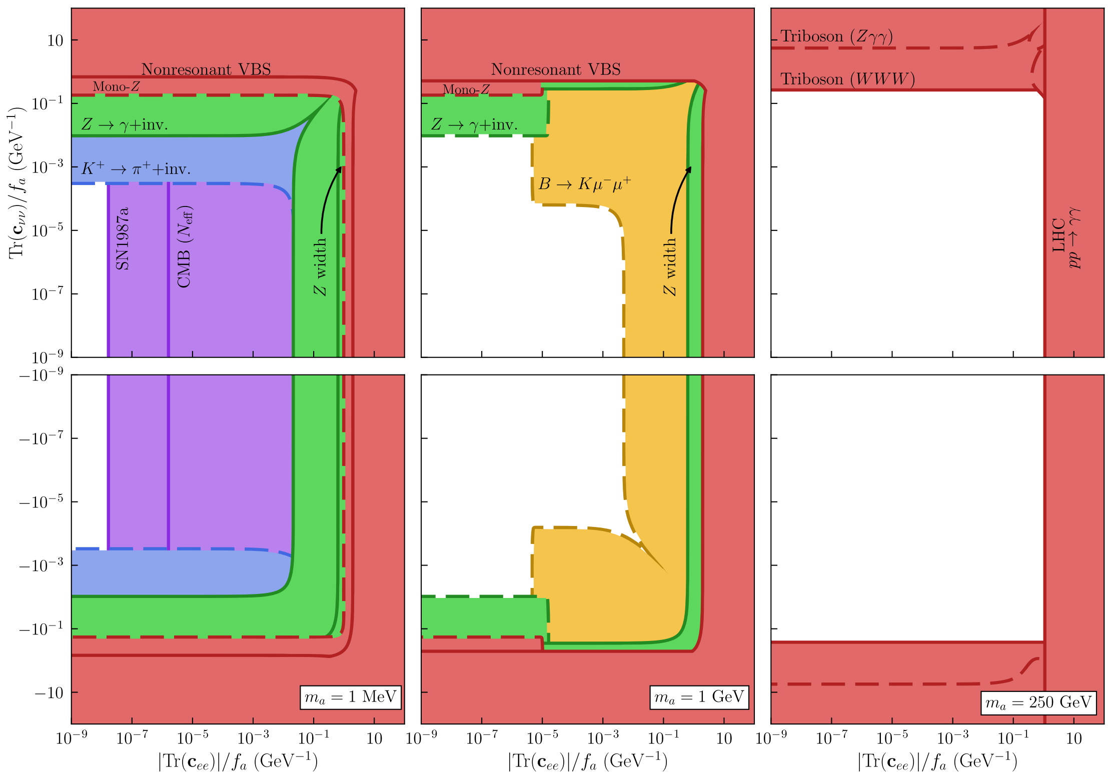

FIG. 5. Direct and loop induced bounds on the $\{|\mathrm{Tr}(\mathbf{c}_{ee})/f_a|, \mathrm{Tr}(\mathbf{c}_{\nu\nu})/f_a\}$ parameter space for different ALP masses. Rare meson decay bounds in yellow and astrophysical bounds in purple have been obtained assuming universal $\mathbf{c}_{ee}$ couplings.

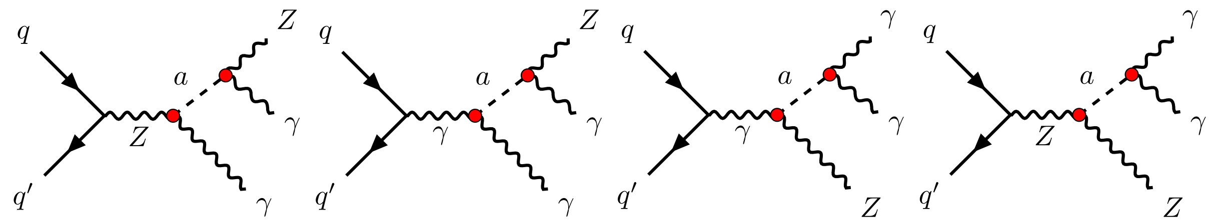

FIG. 6. Tree-level diagrams contributing to the ALP-mediated triboson process $pp \to Z\gamma\gamma$. Additional topologies (i.e., vector boson scattering) are suppressed by the kinematic cuts imposed on the original analysis.

(iii) The bounds obtained on $\mathrm{Tr}(\mathbf{c}_{ee})$ are presented in Fig. 4. These are relevant to our discussion as they further constrain the ALP-neutrino coupling in those scenarios where both $\mathbf{c}_{ee}$ and $\mathbf{c}_{\nu\nu}$ are nonzero (as in Fig. 3).

(iv) The parameter space in the $\{\mathrm{Tr}(\mathbf{c}_{\nu\nu}), \mathrm{Tr}(\mathbf{c}_{ee})\}$ plane is depicted in Fig. 5 for representative values of m_a. The white areas in this figure signal the hunting arena available for ALP-neutrino interactions.

Previous works in the literature which derived constraints on flavor-diagonal ALP-lepton couplings based on their loop-impact on ALP couplings to EW gauge bosons include:

(i) Reference [22], where new bounds on $\mathbf{c}_E$ and $\mathbf{c}_L$ were derived from rare meson decays data, at the one-loop and two-loop levels, restraining the analysis to one-coupling-at-a-time among the two ALP-lepton couplings, $\mathbf{c}_E$ or $\mathbf{c}_L$.

(ii) References [21,23] again only consider one of the two couplings. There, new bounds on the physical ALP coupling to muons and electrons, respectively, are derived from their one-loop contribution to the ALP-photon coupling, $g_{a\gamma\gamma}^{\mathrm{loop}}$, while the ALP-neutrino coupling is disregarded.

In our work we extend the analysis beyond the one-at-a-time paradigm, exploring the bidimensional ALP-lepton parameter space, and furthermore novel bounds are extracted from data sensitive to anomalous ALP couplings to Z and W bosons. Additionally, constraints represented in Figs. 2–5 as dashed contours signal limits which require extra elaboration or assumptions beyond the direct application of the original references, to be detailed below.

A. Collider searches

For heavy ALPs with masses $m_a \gtrsim \mathcal{O}(10)$ GeV, the experimental bounds on their coupling to neutrinos are dominated by the high-energy collider searches for beyond the Standard Model (BSM) physics, here depicted in red and green. These include bounds from Z observables at LEP, LHC searches on mono-Z events [42], searches for nonresonant ALPs in vector boson scattering (VBS) processes [43], light-by-light ($\gamma\gamma \to \gamma\gamma$) scattering measured in Pb-Pb collisions [44,45], diphoton production at LHC [46] and resonant triboson searches for either WWW events [47] or $Z\gamma\gamma$ events [41] mediated by heavy ALPs. Note that for the nonresonant ALP searches the theoretical expressions in the previous sections apply simply replacing m_a^2 by p_a^2, where p_a is the ALP momentum. Additional collider bounds derived in scenarios where lepton couplings are set to zero (e.g. Refs. [48,49]) are not included here, as they do not apply to our analysis.

A remarkable fact will be shown: in the heavy ALP parameter space region, sizable ALP EW interactions are still allowed at present, which evidences the need for experimental efforts targeting such couplings.

1. Triboson bounds

For the triboson data, $a \to W^+W^-$ is the dominant ALP decay mode when this channel is kinematically open, in both Figs. 2 and 3; this is consistent with the requirement assumed in data analysis [47]. Since at leading order g_{aWW}^{loop} is independent of the ALP-charged lepton coupling $\mathbf{c}_{ee}$—see Eq. (4.3)—the small differences in the WWW triboson bound between both figures are only due to mild changes in the branching ratios for ALP decay into W bosons.

The analysis of the neutral triboson channel $Z\gamma\gamma$ is more subtle. The figures show that the $Z\gamma\gamma$ triboson bound becomes stronger for $\mathbf{c}_{ee} = \mathbf{c}_{\nu\nu}$ than in the photophobic case ($\mathbf{c}_{ee} = 0$) in Ref. [41], where it was originally computed. The point is that the five diagrams in Fig. 6 contribute in the general case with both types of couplings active, while for $\mathbf{c}_{ee} = 0$ the ALP coupling to photons vanishes and only diagram 1 can contribute. The dashed $Z\gamma\gamma$ bounds in Figs. 3 and 4 are qualitative estimations obtained from the photophobic limit depicted in Fig. 2 via a scale factor computed from the MadGraph5_aMC@NLO [50,51] cross sections of the ALP-mediated process.[5] Overall, the bounds from triboson searches are shown to be superseded by those from nonresonant searches except for a narrow window in ALP masses.

[5]As the ALP-mediated $pp \to Z\gamma\gamma$ cross section presents a quadratic dependence on the ALP-couplings in the resonant scenario (see Fig. 6), we scaled the photophobic bound by a factor $(\sigma_{\mathrm{ph}}/\sigma)^{1/2}$, where σ_{ph} denotes the cross section in the photophobic case, and σ that in the alternative scenario.

2. LEP and mono- Z bbounds

The bounds from Z observables at LEP are very relevant, in particular those from the Z partial decay width to $\gamma+$ inv. [41,52] and from its total decay width[6] [41,42], here illustrated in green. They stem from experimental bounds on $g_{a\gamma Z}$ and g_{aZZ}, which are recasted via the one-loop analysis as limits on combinations of $\mathrm{Tr}(\mathbf{c}_{\nu\nu})$ and $\mathrm{Tr}(\mathbf{c}_{ee})$—Eqs. (4.1)–(4.2)—and thus the extraction of limits on $\mathrm{Tr}(\mathbf{c}_{\nu\nu})$ depends explicitly on $\mathrm{Tr}(\mathbf{c}_{ee})$.

The original mono-Z constraint is derived in Ref. [42] for a photophobic ALP, which is shown here in Fig. 2. Thus, in order to relate the former with the bound in Fig. 3, we apply a scale factor on the $pp \to Za$ cross section using again MadGraph5_aMC@NLO [50,51] as discussed above.[7] Furthermore, our bounds from $Z \to \gamma +$ inv. and mono-Z data in Fig. 2 extend to ALP masses $m_a > 3m_{\pi^0}$, as the hadronization of the ALP is 2-loop suppressed in this photophobic scenario. Finally, to ensure that the ALP remains invisible within the $\mathbf{c}_{ee} \neq 0$ scenario (see Fig. 3) we impose a decay distance larger than 1 m and 10 m [41,42] for the mono-Z and $Z \to \gamma +$ inv. bounds, respectively.

B. Rare meson decays

Rare K and B decays provide limits in certain regions of parameter space, here represented in blue and yellow. The ALP will either escape detection as *missing transverse energy* (MET) (in blue), or—in the nonphotophobic case—decay next into lighter particles such as charged leptons or photons (in yellow). All these rare processes involve flavor-changing neutral currents (FCNC), which in the SM only happen at loop level and are mediated by W bosons. Thus, they typically set strong bounds on g_{aWW}^{loop}, which can be directly translated into a bound on $\mathrm{Tr}(\mathbf{c}_{\nu\nu})/f_a$ via Eq. (4.3). Additionally, in the $\mathbf{c}_{\nu\nu} = 0$ scenario such bounds can be recasted into (weaker) bounds on $\mathrm{Tr}(\mathbf{c}_{ee})/f_a$ based on its loop-impact on $c_{\tilde{B}}$ from Eq. (2.8) (through the anomalous contribution to the $\gamma\gamma$, γZ and ZZ couplings). The bounds analyzed in this subsection can be inferred from the constraints on $\mathbf{c}_L$ and $\mathbf{c}_E$ from Figs. 26 and 27 of Ref. [22]. It follows that:

(i) For light ALPs, the best bounds stem from the search for $K^+ \to \pi^+\bar{\nu}\nu$ decays at the NA62 experiment [53], i.e., the search for $K^+ \to \pi^+ +$ invisible; this MET analysis can be directly reinterpreted in terms of ALPs which are stable within the detector. We have adapted those limits [22,53] assuming that the effect of $\mathbf{c}_E$ will be subleading with respect to that arising from $\mathbf{c}_L$.[8]

(ii) For intermediate ALP masses and the general case $\mathbf{c}_{ee} \neq 0$, Figs. 3–5 depict in yellow the limits for ALPs unstable within collider distances. These include several searches which are sensitive to: (i) the decay rate of kaons into pions plus an ALP that later decays into a e^+e^- or a $\gamma\gamma$ pair (labeled as $K \to \pi\gamma\gamma, \pi e^- e^+$) [54–57]; (ii) LHCb searches for resonant ALPs in $B \to K^{(*)}\mu^-\mu^+$ decays [58,59]; (iii) the measurement of the partial decay width of B_s into muons [60]; (iv) several decay processes which can be mediated by $a \to \tau^-\tau^+$ ($B \to K\tau^-\tau^+$ and $\Upsilon \to \gamma a(\tau\tau)$ [61]), represented here generically under the label $X \to Y\tau^-\tau^+$; and (v) LHCb measurements of the $B \to K^* e^- e^+$ branching ratio [62]. Notice that all these searches require the ALP to decay into visible particles within collider distances, and in consequence they do not apply in the scenario $\mathbf{c}_{ee} = 0$. For instance, a maximum decay length of 60 cm (see Ref. [59]) is imposed in Fig. 5 for bounds stemming from $B \to K^{(*)}\mu^-\mu^+$ searches at LHCb. For illustrative purposes, the bounds shown assume universality, this is, equal diagonal matrix elements $(\mathbf{c}_{ee})_{ii}$.

The channels with final state charged leptons require the tree-level insertion of ALP-charged lepton couplings $\mathbf{c}_{ee}$ in addition to their one-loop insertion, unlike all other data considered here.

It is worth mentioning that, in some of the rare meson processes analyzed, the ALP and/or some gauge boson(s) V are off-shell, while our expressions above for $g_{aVV'}^{\mathrm{loop}}$ were computed for on-shell external particles. Nevertheless, on one side the generalization to off-shell ALPs is straightforward as explained, and, on the other, the g_{aWW}^{loop} dependence on momenta is only present in mass-dependent terms which are subleading with respect to the anomalous—and thus momentum-independent—contributions, as discussed earlier as well, and thus the bounds depicted are solid in this respect.

C. Bounds on ALP-photon and electron couplings

Some of the bounds included in Fig. 3 arise from observables involving the ALP coupling to charged leptons, $\mathbf{c}_{ee}$, either at tree-level or at one-loop level from its impact on $g_{a\gamma\gamma}^{\mathrm{loop}}$—see Eq. (3.1)—independently of the value of the physical ALP-neutrino coupling. However, those bounds still impose limits on $\mathbf{c}_{\nu\nu}$ due to its relation with $\mathbf{c}_{ee}$ via gauge invariance [Eq. (2.6)]. These include:

[6] These are superseded in Fig. 3 by those stemming from nonresonant VBS limits.

[7] Since the ALP-mediated $pp \to Za$ cross sections depend quadratically on the ALP couplings, such scale factor is now obtained as $(\sigma_{\mathrm{ph.ph.}}/\sigma)^{1/2}$.

[8] This is justified as the bounds obtained in Fig. 27 Ref. [22] in the $\mathbf{c}_E \neq 0$ scenario are two orders of magnitude weaker than those for the $\mathbf{c}_L \neq 0$ scenario.

(i) *Astrophysics and cosmology bounds.* For a general nonphotophobic ALP, its putative decay into diphoton pairs, Primakoff emission, and ALP production via photon coalescence in a hot and dense environment would contribute as an additional cooling channel for SN1987a [23,63]—potentially shortening its neutrino burst and producing observable gamma-rays after the explosion—and would affect the luminosity evolution of low-energy supernovae [64] (labeled as SNe).[9] Similarly, it would leave a clear signature in the CMB and BBN observations through the impact on the effective number of early universe species for light enough ALPs [65,66].

(ii) *Beam dump searches* for ALP-photon and ALP-electron[10] couplings [67–72].

(iii) *High-energy collider searches* for ALP-mediated diphoton production at the LHC [46], and light-by-light ($\gamma\gamma \to \gamma\gamma$) scattering in Pb-Pb collisions [44,45].

The remaining constraints on $\mathbf{c}_{ee}$ in Fig. 4 are derived assuming $\mathrm{Tr}(\mathbf{c}_{\nu\nu}) = 0$ (i.e., $\mathbf{c}_L = 0$).

V. CONCLUSIONS

The dark sector of the Universe deserves utmost attention as it heralds new laws of physics beyond the Standard Model of particle physics. Neutrinos arguably constitute excellent portals in this search, as their interactions are not obscured by strong or electromagnetic forces. We explored here the possible effective interactions of neutrinos to axionlike particles. In addition to theoretical developments, we have derived new bounds on ALP-neutrino interactions.

The model-independent tool of the ALP EFT has been used in order to formulate the problem. Its inherent gauge invariant nature ties necessarily together the exploration of ALP couplings to neutrinos with those to charged leptons. Our analysis has thus encompassed both types of couplings, i.e., the set of $\{\mathbf{c}_{ee}, \mathbf{c}_{\nu\nu}\}$ matrices, exploring how the limits on ALP-neutrino interactions may vary depending on the assumptions about ALP interactions with charged leptons. This is in contrast with previous literature, where typically just about half of that parameter space was tackled.

Neglecting neutrino masses, the trace of ALP-neutrino couplings can be entirely traded by anomalous ALP couplings to the set of EW gauge bosons $\{g_{aWW}, g_{aZZ}, g_{a\gamma Z}\}$ as they are connected via the chiral anomaly. We have explored theoretically the one-loop impact of the former on the latter (in addition to the well known impact of ALP-charged lepton couplings on them and on $g_{a\gamma\gamma}$). The complete one-loop computations were presented for ALPs and EW gauge bosons on-shell.

We have next recasted existing bounds on anomalous couplings of EW bosons to ALPs in terms of the $\{\mathbf{c}_{ee}, \mathbf{c}_{\nu\nu}\}$ parameter space, confronting data from different type of experiments. These bounds hold barring underlying symmetries in the UV or fine-tuned cancellations between the contributions explored here and other sources of ALP-EW gauge boson anomalous couplings. While similar constraints have been set previously from rare meson decays [22], the limits on ALP-neutrino interactions extracted from collider data are presented here for the first time. These span extensive novel territory in parameter space for a wide range of ALP masses, ranging from ultralight ALPs to $\sim 10^3$ GeV ALP masses, and they sweep over several orders of magnitude in strength; data from heavy ALP searches at colliders have a particularly strong impact, see Figs. 2–5, which demonstrate the potential of high energy probes as a tool to explore ALP EW interactions and thus, indirectly, ALP-neutrino couplings.

ALP-neutrino interactions are being increasingly considered in the arena of neutrino physics, because of their intrinsic interest and for their putative impact on the cosmological history and on astrophysics issues. Hopefully this work will help to clarify the formulation of the problem and to delimitate the frontiers of this quest.

ACKNOWLEDGMENTS

We acknowledge early discussions with Carlos Argüelles, Jorge Fernández de Trocóniz, and Iván Martínez Soler. We thank Ricardo Zambujal Ferreira and Edoardo Vitagliano for comments on astrophysical bounds. The work of J. B. was supported by the Spanish Ministerio de Ciencia, Innovación y Universidades (MICIU) through the National Program FPU (Grant No. FPU18/03047). The work of J. M. R. was supported by the Spanish MICIU through the National Program FPI-Severo Ochoa (Grant No. PRE2019-089233). The authors acknowledge partial financial support by the Spanish MINECO through the Centro de excelencia Severo Ochoa Program under Grant No. SEV-2016-0597, by the Spanish "Agencia Estatal de Investigacíon" (AEI), the EU Horizon 2020 research and innovation programme under the Marie Sklodowska-Curie Grant agreement No. 860881-HIDDeN, and under the Marie Sklodowska-Curie Staff Exchange grant agreement No. 101086085-ASYMMETRY, and the EU "Fondo Europeo de Desarrollo Regional" (FEDER) through the project No. PID2019-108892RB-I00/AEI/10.13039/501100011033.

[9]The narrow gap in the SNe bound, corresponding to an ALP mass $m_a = 2m_\mu$, can be understood from Eq. (3.1) as a partial cancelation between the electron and muon contribution to $g^{\mathrm{loop}}_{a\gamma\gamma}$ at 1-loop.

[10]We assume the universality of $\mathbf{c}_{ee}$, i.e., diagonal and equally coupled to all generations, in order to extend these bounds to $\mathrm{Tr}(\mathbf{c}_{ee})$.

APPENDIX: COMPLETE EXPRESSIONS FOR ONE-LOOP COUPLINGS

1. Contributions from axial and vectorial insertions

We present the nonvanishing contributions to the one-loop induced couplings in Eqs. (3.6), (3.12) and (3.18), stemming from all combinations of axial and vectorial insertions in Fig. 1.

Contributions to $g_{a\gamma\gamma}$: Equation (3.1) is directly obtained from the Axial-Vector-Vector contribution, i.e., the combination of the axial coupling of the ALP to charged leptons and the (vectorial) couplings of the photons.

Contributions to $g_{a\gamma Z}$:

(i) Axial-vector-vector:

$$g_{a\gamma Z}^{\mathrm{AVV}} = \frac{\alpha_{\mathrm{em}}}{2c_w s_w \pi f_a}(1-4s_w^2)\sum_\ell (\mathbf{c}_{ee})_{\ell\ell}(1+2m_\ell^2)\mathcal{C}_0(0, M_Z^2, m_a^2, m_\ell, m_\ell, m_\ell). \tag{A1}$$

(ii) Vector-vector-axial:

$$g_{a\gamma Z}^{\mathrm{VVA}} = \frac{\alpha_{\mathrm{em}}}{2c_w s_w \pi f_a}[2\mathrm{Tr}(\mathbf{c}_{\nu\nu}) - \mathrm{Tr}(\mathbf{c}_{ee})]. \tag{A2}$$

Contributions to g_{aZZ}:

(i) Axial-axial-axial:

$$g_{aZZ}^{\mathrm{AAA}} = -\frac{\alpha_{\mathrm{em}}}{2c_w^2 s_w^2 \pi f_a}\left\{\frac{1}{8}[\mathrm{Tr}(\mathbf{c}_{\nu\nu}) + \mathrm{Tr}(\mathbf{c}_{ee})] - \sum_\ell \frac{(\mathbf{c}_{ee})_{\ell\ell} m_\ell^2}{m_a^2 - 4M_Z^2}\left[\mathcal{B}(m_a^2, m_\ell, m_\ell) - \mathcal{B}(M_Z^2, m_\ell, m_\ell) + \frac{m_a^2}{4}\mathcal{C}_0(m_a^2, M_Z^2, M_Z^2, m_\ell, m_\ell, m_\ell)\right]\right\}. \tag{A3}$$

(ii) Axial-vector-vector:

$$g_{aZZ}^{\mathrm{AVV}} = -\frac{\alpha_{\mathrm{em}}}{2c_w^2 s_w^2 \pi f_a}\left\{\frac{1}{8}[\mathrm{Tr}(\mathbf{c}_{\nu\nu}) + (1-4s_w^2)^2\mathrm{Tr}(\mathbf{c}_{ee})] + 2\sum_\ell (\mathbf{c}_{ee})_{\ell\ell} m_\ell^2 (1-4s_w^2)^2 \mathcal{C}_0(m_a^2, M_Z^2, M_Z^2, m_\ell, m_\ell, m_\ell)\right\}. \tag{A4}$$

(iii) Vector-axial-vector and vector-vector-axial:

$$g_{aZZ}^{\mathrm{VVA}} = \frac{\alpha_{\mathrm{em}}}{8c_w^2 s_w^2 \pi f_a}\{(-3+8s_w^2)\mathrm{Tr}(\mathbf{c}_{\nu\nu}) + (1-4s_w^2)\mathrm{Tr}(\mathbf{c}_{ee})\}. \tag{A5}$$

Contributions to g_{aWW}:

(i) Axial-axial-axial:

$$g_{aWW}^{\mathrm{AAA}} = -\frac{\alpha_{\mathrm{em}}}{16 s_w^2 \pi f_a}\left\{\mathrm{Tr}(\mathbf{c}_{\nu\nu}) + \mathrm{Tr}(\mathbf{c}_{ee}) - 4\sum_\ell \frac{(\mathbf{c}_{ee})_{\ell\ell} m_\ell^2}{m_a^2 - 4M_W^2}\left[\mathcal{B}(m_a^2, m_\ell, m_\ell) + \left(1 - \frac{m_\ell^2}{M_W^2}\right)\left(i\pi + \log\left(\frac{M_W^2}{m_\ell^2} - 1\right) + M_W^2 \mathcal{C}_0(m_a^2, M_W^2, M_W^2, m_\ell, m_\ell, 0)\right)\right]\right\}. \tag{A6}$$

(ii) Axial-vector-vector:

$$g_{aWW}^{\mathrm{AVV}} = g_{aWW}^{\mathrm{AAA}}. \tag{A7}$$

(iii) Vector-axial-vector and vector-vector-axial:

$$g_{aWW}^{\mathrm{VVA}} = \frac{\alpha_{\mathrm{em}}}{8s_w^2\pi f_a}[\mathrm{Tr}(\mathbf{c}_{ee}) - 3\mathrm{Tr}(\mathbf{c}_{\nu\nu})]. \tag{A8}$$

2. Nonvanishing neutrino masses

We present the results for the one-loop amplitudes associated to the triangle diagram in Fig. 1 for nonvanishing neutrino masses m_{ν_ℓ}. Only the g_{aZZ} and g_{aWW} anomalous couplings receive additional contributions from m_{ν_ℓ}, while $g_{a\gamma\gamma}$ and $g_{a\gamma Z}$—Eqs. (3.1) and (3.6), respectively—remain unchanged. The expressions for g_{aZZ}^{loop} and g_{aWW}^{loop} read

$$\begin{aligned} g_{aZZ}^{\mathrm{loop}} = &-\frac{\alpha_{\mathrm{em}}}{2c_w^2 s_w^2\pi f_a}\Bigg\{(1-2s_w^2)\mathrm{Tr}(\mathbf{c}_{\nu\nu}) + 2s_w^4\mathrm{Tr}(\mathbf{c}_{ee}) - \sum_\ell \frac{(\mathbf{c}_{ee})_{\ell\ell} m_\ell^2}{m_a^2 - 4M_Z^2}[\mathcal{B}(m_a^2, m_\ell, m_\ell) - \mathcal{B}(M_Z^2, m_\ell, m_\ell) \\ &+ ((1-4s_w^2)^2 M_Z^2 + 2s_w^2(1-2s_w^2)m_a^2)\mathcal{C}_0(m_a^2, M_Z^2, M_Z^2, m_\ell, m_\ell, m_\ell)] \\ &- \sum_\ell \frac{(\mathbf{c}_{\nu\nu})_{\ell\ell} m_{\nu_\ell}^2}{m_a^2 - 4M_Z^2}[\mathcal{B}(m_a^2, m_{\nu_\ell}, m_{\nu_\ell}) - \mathcal{B}(M_Z^2, m_{\nu_\ell}, m_{\nu_\ell}) + M_Z^2\mathcal{C}_0(m_a^2, M_Z^2, M_Z^2, m_{\nu_\ell}, m_{\nu_\ell}, m_{\nu_\ell})]\Bigg\}. \end{aligned} \tag{A9}$$

$$\begin{aligned} g_{aWW}^{\mathrm{loop}} = &-\frac{\alpha_{em}}{2s_w^2\pi f_a}\Bigg\{\mathrm{Tr}(\mathbf{c}_{\nu\nu}) - \sum_\ell \frac{(\mathbf{c}_{ee})_{\ell\ell} m_\ell^2}{m_a^2 - 4M_W^2}\Bigg[\mathcal{B}(m_a^2, m_\ell, m_\ell) - \mathcal{B}(M_W^2, m_\ell, m_{\nu_\ell}) \\ &- \left(1 - \frac{m_\ell^2}{M_W^2}\right)\left(\log\left(\frac{m_\ell}{m_{\nu_\ell}}\right) - M_W^2\mathcal{C}_0(m_a^2, M_W^2, M_W^2, m_\ell, m_\ell, m_{\nu_\ell})\right)\Bigg] \\ &- \sum_\ell \frac{(\mathbf{c}_{\nu\nu})_{\ell\ell} m_{\nu_\ell}^2}{m_a^2 - 4M_W^2}\Bigg[\mathcal{B}(m_a^2, m_{\nu_\ell}, m_{\nu_\ell}) - \mathcal{B}(M_W^2, m_\ell, m_{\nu_\ell}) \\ &+ \left(1 - \frac{m_{\nu_\ell}^2}{M_W^2}\right)\left(\log\left(\frac{m_\ell}{m_{\nu_\ell}}\right) + M_W^2\mathcal{C}_0(m_a^2, M_W^2, M_W^2, m_{\nu_\ell}, m_{\nu_\ell}, m_\ell)\right)\Bigg] \\ &+ \sum_\ell \frac{m_\ell^2 m_{\nu_\ell}^2}{M_W^2(m_a^2 - 4M_W^2)}\Bigg[(\mathbf{c}_{ee} - \mathbf{c}_{\nu\nu})_{\ell\ell}\log\left(\frac{m_\ell}{m_{\nu_\ell}}\right) \\ &- (\mathbf{c}_{ee})_{\ell\ell} M_W^2\mathcal{C}_0(m_a^2, M_W^2, M_W^2, m_\ell, m_\ell, m_{\nu_\ell}) - (\mathbf{c}_{\nu\nu})_{\ell\ell} M_W^2\mathcal{C}_0(m_a^2, M_W^2, M_W^2, m_{\nu_\ell}, m_{\nu_\ell}, m_\ell)\Bigg]\Bigg\}. \end{aligned} \tag{A10}$$

Note that these expression are also valid in the regime for off-shell ALPs upon the replacement $m_a^2 \to p_a^2$.

[1] G. B. Gelmini and M. Roncadelli, Left-handed neutrino mass scale and spontaneously broken lepton number, Phys. Lett. **99B**, 411 (1981).

[2] P. Langacker, R. D. Peccei, and T. Yanagida, Invisible axions and light neutrinos: Are they connected?, Mod. Phys. Lett. A **01**, 541 (1986).

[3] G. Ballesteros, J. Redondo, A. Ringwald, and C. Tamarit, Standard Model—axion—seesaw—Higgs portal inflation. Five problems of particle physics and cosmology solved in one stroke, J. Cosmol. Astropart. Phys. 08 (2017) 001.

[4] F. Arias-Aragon, E. Fernandez-Martinez, M. Gonzalez-Lopez, and L. Merlo, Neutrino masses and Hubble tension via a Majoron in MFV, Eur. Phys. J. C **81**, 28 (2021).

[5] F. Arias-Aragón, E. Fernández-Martínez, M. González-López, and L. Merlo, Dynamical minimal flavour violating inverse seesaw, J. High Energy Phys. 09 (2022) 210.

[6] A. Davidson and K. C. Wali, Minimal flavor unification via multigenerational Peccei-Quinn symmetry, Phys. Rev. Lett. **48**, 11 (1982).

[7] F. Wilczek, Axions and family symmetry breaking, Phys. Rev. Lett. **49**, 1549 (1982).

[8] L. Calibbi, F. Goertz, D. Redigolo, R. Ziegler, and J. Zupan, Minimal axion model from flavor, Phys. Rev. D **95**, 095009 (2017).

[9] Y. Ema, K. Hamaguchi, T. Moroi, and K. Nakayama, Flaxion: A minimal extension to solve puzzles in the standard model, J. High Energy Phys. 01 (2017) 096.

[10] H. Georgi and D. B. Kaplan, Composite Higgs and custodial SU(2), Phys. Lett. **145B**, 216 (1984).

[11] M. Cicoli, Axion-like particles from string compactifications, in *Proceedings of the 9th Patras Workshop on Axions, WIMPs and WISPs* (2013), pp. 235–242, arXiv:1309.6988.

[12] B. Bellazzini, A. Mariotti, D. Redigolo, F. Sala, and J. Serra, *R*-axion at colliders, Phys. Rev. Lett. **119**, 141804 (2017).

[13] T. Damour and A. M. Polyakov, The string dilaton and a least coupling principle, Nucl. Phys. **B423**, 532 (1994).

[14] K. Choi, S. H. Im, and C. Sub Shin, Recent progress in the physics of axions and axion-like particles, Annu. Rev. Nucl. Part. Sci. **71**, 225 (2021).

[15] M. Chala, G. Guedes, M. Ramos, and J. Santiago, Running in the ALPs, Eur. Phys. J. C **81**, 181 (2021).

[16] M. Bauer, M. Neubert, S. Renner, M. Schnubel, and A. Thamm, The low-energy effective theory of axions and ALPs, J. High Energy Phys. 04 (2021) 063.

[17] J. Bonilla, I. Brivio, M. B. Gavela, and V. Sanz, One-loop corrections to ALP couplings, J. High Energy Phys. 11 (2021) 168.

[18] J. Bonilla, A. de Giorgi, B. Gavela, L. Merlo, and M. Ramos, The cost of an ALP solution to the neutral B-anomalies, J. High Energy Phys. 02 (2023) 138.

[19] S. Bansal, G. Paz, A. Petrov, M. Tammaro, and J. Zupan, Enhanced neutrino polarizability, J. High Energy Phys. 05 (2023) 142.

[20] C. O'HARE, cajohare/axionlimits: Axionlimits, 10.5281/zenodo.3932430 (2020).

[21] A. Caputo, G. Raffelt, and E. Vitagliano, Muonic boson limits: Supernova redux, Phys. Rev. D **105**, 035022 (2022).

[22] M. Bauer, M. Neubert, S. Renner, M. Schnubel, and A. Thamm, Flavor probes of axion-like particles, J. High Energy Phys. 09 (2022) 056.

[23] R. Z. Ferreira, M. C. D. Marsh, and E. Müller, Strong supernovae bounds on ALPs from quantum loops, J. Cosmol. Astropart. Phys. 11 (**2022**) 057.

[24] V. K. Oikonomou, Axion-neutrino couplings, late-time phase transitions and the far infrared physics, Phys. Dark Universe **42**, 101335 (2023).

[25] G.-Y. Huang and N. Nath, Neutrinophilic axion-like dark matter, Eur. Phys. J. C **78**, 922 (2018).

[26] M. M. Reynoso, O. A. Sampayo, and A. M. Carulli, Neutrino interactions with ultralight axion-like dark matter, Eur. Phys. J. C **82**, 274 (2022).

[27] A. Lichkunov and A. Studenikin, Neutrino mixing angle and neutrino oscillation in ALPs matter, in *Proceedings of the 41st International Conference on High Energy Physics* (2023), arXiv:2302.06390.

[28] M. Bauer, M. Neubert, and A. Thamm, Collider probes of axion-like particles, J. High Energy Phys. 12 (2017) 044.

[29] H. Georgi, D. B. Kaplan, and L. Randall, Manifesting the invisible axion at low-energies, Phys. Lett. **169B**, 73 (1986).

[30] K. Choi, K. Kang, and J. E. Kim, Effects of η' in low-energy axion physics, Phys. Lett. B **181**, 145 (1986).

[31] A. R. Zhitnitsky, On possible suppression of the axion hadron interactions. (In Russian), Sov. J. Nucl. Phys. **31**, 260 (1980), https://www.osti.gov/biblio/7063072.

[32] M. Dine, W. Fischler, and M. Srednicki, A simple solution to the strong *CP* problem with a harmless axion, Phys. Lett. **104B**, 199 (1981).

[33] C. Cheung and C.-H. Shen, Nonrenormalization theorems without supersymmetry, Phys. Rev. Lett. **115**, 071601 (2015).

[34] Z. Bern, J. Parra-Martinez, and E. Sawyer, Nonrenormalization and operator mixing via on-shell methods, Phys. Rev. Lett. **124**, 051601 (2020).

[35] J. F. Gunion, H. E. Haber, and C. Kao, Searching for the *CP*-odd higgs boson of the minimal supersymmetric model at hadron supercolliders, Phys. Rev. D **46**, 2907 (1992).

[36] J. L. Diaz-Cruz, C. G. Honorato, J. A. Orduz-Ducuara, and M. A. Perez, One-loop decays $A^0 \to ZZ, Z\gamma, \gamma\gamma$ within the 2HDM and its search at the LHC, Phys. Rev. D **90**, 095019 (2014).

[37] H. H. Patel, Package-X 2.0: A Mathematica package for the analytic calculation of one-loop integrals, Comput. Phys. Commun. **218**, 66 (2017).

[38] V. Shtabovenko, R. Mertig, and F. Orellana, FeynCalc 9.3: New features and improvements, Comput. Phys. Commun. **256**, 107478 (2020).

[39] G. Passarino and M. J. G. Veltman, One loop corrections for e^+e^- annihilation into $\mu^+\mu^-$ in the Weinberg model, Nucl. Phys. **B160**, 151 (1979).

[40] J. Quevillon and C. Smith, Axions are blind to anomalies, Eur. Phys. J. C **79**, 822 (2019).

[41] N. Craig, A. Hook, and S. Kasko, The photophobic ALP, J. High Energy Phys. 09 (2018) 028.

[42] I. Brivio, M. B. Gavela, L. Merlo, K. Mimasu, J. M. No, R. del Rey, and V. Sanz, ALPs effective field theory and collider signatures, Eur. Phys. J. C **77**, 572 (2017).

[43] J. Bonilla, I. Brivio, J. Machado-Rodríguez, and J. F. de Trocóniz, Nonresonant searches for axion-like particles in vector boson scattering processes at the LHC, J. High Energy Phys. 06 (2022) 113.

[44] A. M. Sirunyan *et al.* (CMS Collaboration), Evidence for light-by-light scattering and searches for axion-like particles in ultraperipheral PbPb collisions at $\sqrt{s_{\rm NN}} = 5.02$ TeV, Phys. Lett. B **797**, 134826 (2019).

[45] G. Aad *et al.* (ATLAS Collaboration), Measurement of light-by-light scattering and search for axion-like particles with 2.2 nb^{-1} of Pb + Pb data with the ATLAS detector, J. High Energy Phys. 03 (2021) 243; 11 (2021) 50.

[46] A. Mariotti, D. Redigolo, F. Sala, and K. Tobioka, New LHC bound on low-mass diphoton resonances, Phys. Lett. B **783**, 13 (2018).

[47] A. M. Sirunyan *et al.* (CMS Collaboration), Search for the production of $W^\pm W^\pm W^\mp$ events at $\sqrt{s} = 13$ TeV, Phys. Rev. D **100**, 012004 (2019).

[48] M. Aiko and M. Endo, Electroweak precision test of axion-like particles, J. High Energy Phys. 05 (2023) 147.

[49] M. Aiko and M. Endo, Higgs probes of axion-like particles, J. High Energy Phys. 11 (2023) 046.

[50] J. Alwall, R. Frederix, S. Frixione, V. Hirschi, F. Maltoni, O. Mattelaer, H. S. Shao, T. Stelzer, P. Torrielli, and M. Zaro, The automated computation of tree-level and

next-to-leading order differential cross sections, and their matching to parton shower simulations, J. High Energy Phys. 07 (2014) 079.
[51] R. Frederix, S. Frixione, V. Hirschi, D. Pagani, H. S. Shao, and M. Zaro, The automation of next-to-leading order electroweak calculations, J. High Energy Phys. 07 (2018) 185; 11 (2021) 85.
[52] M. Acciarri *et al.* (L3 Collaboration), Search for new physics in energetic single photon production in e^+e^- annihilation at the Z resonance, Phys. Lett. B **412**, 201 (1997).
[53] E. Cortina Gil *et al.* (NA62 Collaboration), Measurement of the very rare $K^+ \to \pi^+\nu\bar{\nu}$ decay, J. High Energy Phys. 06 (2021) 093.
[54] A. V. Artamonov *et al.* (E949 Collaboration), Search for the decay $K^+ \to \pi^+\gamma\gamma$ in the π^+ momentum region $P > 213$ MeV/c, Phys. Lett. B **623**, 192 (2005).
[55] C. Lazzeroni *et al.* (NA62 Collaboration), Study of the $K^\pm \to \pi^\pm\gamma\gamma$ decay by the NA62 experiment, Phys. Lett. B **732**, 65 (2014).
[56] A. Lai *et al.* (NA48 Collaboration), Precise measurement of the decay $K_L \to \pi^0\gamma\gamma$, Phys. Lett. B **536**, 229 (2002).
[57] E. Abouzaid *et al.* (KTeV Collaboration), Final results from the KTeV experiment on the decay $K_L \to \pi^0\gamma\gamma$, Phys. Rev. D **77**, 112004 (2008).
[58] R. Aaij *et al.* (LHCb Collaboration), Search for hidden-sector bosons in $B^0 \to K^{*0}\mu^+\mu^-$ decays, Phys. Rev. Lett. **115**, 161802 (2015).
[59] R. Aaij *et al.* (LHCb Collaboration), Search for long-lived scalar particles in $B^+ \to K^+\chi(\mu^+\mu^-)$ decays, Phys. Rev. D **95**, 071101 (2017).
[60] J. Albrecht, E. Stamou, R. Ziegler, and R. Zwicky, Flavoured axions in the tail of $B_q \to \mu^+\mu^-$ and $B \to \gamma^*$ form factors, J. High Energy Phys. 09 (2021) 139.
[61] J. P. Lees *et al.* (*BABAR* Collaboration), Search for a low-mass scalar Higgs boson decaying to a tau pair in single-photon decays of $\Upsilon(1S)$, Phys. Rev. D **88**, 071102 (2013).
[62] R. Aaij *et al.* (LHCb Collaboration), Angular analysis of the $B^0 \to K^{*0}e^+e^-$ decay in the low $-$ q^2 region, J. High Energy Phys. 04 (2015) 064.
[63] M. Diamond, D. F. G. Fiorillo, G. Marques-Tavares, and E. Vitagliano, Axion-sourced fireballs from supernovae, Phys. Rev. D **107**, 103029 (2023); **108**, 049902(E) (2023).
[64] A. Caputo, H.-T. Janka, G. Raffelt, and E. Vitagliano, Low-energy supernovae severely constrain radiative particle decays, Phys. Rev. Lett. **128**, 221103 (2022).
[65] D. Ghosh and D. Sachdeva, Constraints on axion-lepton coupling from big bang nucleosynthesis, J. Cosmol. Astropart. Phys. 10 (2020) 060.
[66] P. F. Depta, M. Hufnagel, and K. Schmidt-Hoberg, Updated BBN constraints on electromagnetic decays of MeV-scale particles, J. Cosmol. Astropart. Phys. 04 (2021) 011.
[67] F. Bergsma *et al.* (CHARM Collaboration), Search for axion like particle production in 400-GeV proton—copper interactions, Phys. Lett. **157B**, 458 (1985).
[68] E. M. Riordan *et al.*, A search for short lived axions in an electron beam dump experiment, Phys. Rev. Lett. **59**, 755 (1987).
[69] J. Blumlein *et al.*, Limits on neutral light scalar and pseudoscalar particles in a proton beam dump experiment, Z. Phys. C **51**, 341 (1991).
[70] M. J. Dolan, T. Ferber, C. Hearty, F. Kahlhoefer, and K. Schmidt-Hoberg, Revised constraints and Belle II sensitivity for visible and invisible axion-like particles, J. High Energy Phys. 12 (2017) 094; 03 (2021) 190(E).
[71] D. Banerjee *et al.* (NA64 Collaboration), Search for axion-like and scalar particles with the NA64 experiment, Phys. Rev. Lett. **125**, 081801 (2020).
[72] L. Waites, A. Thompson, A. Bungau, J. M. Conrad, B. Dutta, W.-C. Huang, D. Kim, M. Shaevitz, and J. Spitz, Axion-like particle production at beam dump experiments with distinct nuclear excitation lines, Phys. Rev. D **107**, 095010 (2023).

Chapter 6

Running beyond ALPs: Shift-breaking and CP-violating Effects

This chapter contains the publication in Ref. [2]. In this work we present the full renormalization group equations (RGEs) of the SMEFT extended with a real scalar singlet up to dimension-five with one-loop accuracy. We include CP-odd as well as shift-breaking interactions and keep track of all mixing effects across energies.

If a new scalar particle is ever discovered at experiments, there are two fundamental questions to address: *(i)* Does it interact with the Higgs, the only scalar in the SM? *(ii)* How close is it to an axion-like particle? In order to answer these questions, effective field theories offer a model-independent approach to describe the low-energy effects —beyond the renormalizable level— of an hypothetical UV complete theory. Previous studies allow us to connect the complete SM+scalar singlet EFT —"singlet EFT" from now on— to that of the "shift-symmetric limit" [36, 134, 135], i.e. the ALP EFT. We also make use of the flavor invariants built in Ref. [153], which quantify the amount of shift symmetry breaking. In addition, there is a growing interest on ALP CP-odd interactions [274–279], since CP is at the heart of the flavor problem and constitutes an excellent window to new physics (e.g. the neutron EDM). Since RGEs characterize the evolution with energy of the fundamental parameters of a theory, which can affect the stability of these answers, an in-depth study of the RGEs of the complete singlet EFT is key in the quest for BSM signals in the precision era of particle physics.

The RGEs of the singlet EFT were previously obtained in the literature in two particular scenarios: ignoring CP violating new physics [134]; or under the assumption that the singlet is an ALP, i.e., including only shift-preserving and anomalous interactions [36, 135]. Our work is therefore the most complete study on the singlet EFT so far. We obtain the running of the Wilson coefficients both in the high-energy and the low-energy EFTs —resulting from integrating the top quark, the Higgs, the Z and the W—, and perform the matching between them at tree level. These results are implemented in our new `Mathematica` package —`ALPRunner` [280]— which can be used to study in detail the phenomenology of the singlet EFT. Among its main functionalities, it can be used to solve the RGEs for a given UV scenario or to translate low-energy experimental bounds into constraints on the high-energy parameters of the theory.

This chapter is structured as follows. The complete singlet EFT, including CP-violating and shift-breaking interactions up to dimension-five, is first reviewed. We work in the basis of independent Green's functions in Ref. [134]. The connection to the ALP EFT, which is an important case limit of our study, is also discussed. Next, the RGEs of the high-energy EFT are presented, followed by the discussion of the matching to the low-energy EFT. We also review in detail the causes and interesting implications of mixing in the scalar sector —often disregarded in the literature—, such as new correlations among the triple and quartic Higgs couplings. Analytical expressions for the mixing angle between the Higgs and the singlet are provided. The RGEs of the low-energy EFT are presented as well. Finally, we illustrate the non-trivial impact of running in the phenomenology of the scalar singlet by computing the strongest EDM constraints on particular high-energy EFT scenarios with only two non-vanishing BSM couplings: *(i)* We first consider two gauge scenarios with either couplings to the hypercharge gauge bosons B or gluons, setting boounds on the singlet couplings to the anomalous and kinetic terms, $X_{\mu\nu}\widetilde{X}^{\mu\nu}$ and $X_{\mu\nu}X^{\mu\nu}$, respectively; *(ii)* Finally, we consider the 3×3 singlet coupling to the down quark sector and the Higgs, with only two real non-vanishing components. These results have been obtained making use of dedicated routines implemented in the `ALPRunner` package. All its features and some basic guidelines are presented in this section.

The results presented in this work improve significantly our understanding of the phenomenology of scalar extensions of the SM and the impact of running and mixing in the most general singlet EFT studied so far in the literature. The full set of RGEs, implemented in our package `ALPRunner` —with functions to solve them numerically and perform the matching—, will contribute to future phenomenological analyses looking for BSM physics signals in the scalar sector.

The computations are based on dedicated routines that rely on `FeynRules` [281], `FeynArts` [282] and `FormCalc` [283], and have been cross-checked with `matchmakereft` [284].

Published for SISSA by Springer

Received: *September 28, 2023*
Accepted: *November 1, 2023*
Published: *November 21, 2023*

Running beyond ALPs: shift-breaking and CP-violating effects

Supratim Das Bakshi,[a] **Jonathan Machado-Rodríguez**[b] **and Maria Ramos**[b]

[a] *CAFPE and Departamento de Física Teórica y del Cosmos, Universidad de Granada, Campus de Fuentenueva, E-18071 Granada, Spain*
[b] *Departamento de Física Teórica and Instituto de Física Teórica IFT-UAM/CSIC, Universidad Autónoma de Madrid, Cantoblanco, E-28049, Madrid, Spain*

E-mail: sdb@ugr.es, jonathan.machado@uam.es, maria.pestanadaluz@uam.es

Abstract: We compute the renormalization group equations (RGEs) of the Standard Model effective field theory (EFT) extended with a real scalar singlet, up to dimension-five and one-loop accuracy. We compare our renormalization results with those found in the shift-symmetry preserving limit, which characterizes axion-like particles (ALPs). The matching and running equations below the electroweak scale are also obtained, including the mixing effects in the scalar sector. Such mixing leads to interesting phenomenological consequences that are absent in the EFT at the renormalizable level, namely new correlations among the triplet and quartic Higgs couplings are predicted. All RGEs obtained in this work are implemented in a new Mathematica package — `ALPRunner`, together with functions to solve the running numerically for an arbitrary set of UV parameters. As an application, we obtain electric dipole moment constraints on particular regions of the singlet parameter space, and quantify the level of shift-breaking in these regions.

Keywords: Axions and ALPs, Effective Field Theories, New Light Particles, Renormalization and Regularization

ArXiv ePrint: 2306.08036

https://doi.org/10.1007/JHEP11(2023)133

Contents

1 Introduction

Singlet scalars are one of the most promising candidates of beyond the Standard Model (BSM) physics. Not only can they provide solutions to long-standing puzzles of the SM, but their elusive nature can also explain their challenging detection, in spite of the increasing experimental efforts which span a wide range of energies and sophisticated techniques [1].

If a new scalar particle is ever discovered, compelling questions will be addressed which could impact significantly our knowledge of Nature. One of these questions is how much the exotic scalar can interact with the only other we know, the Higgs boson. If the Higgs is afterall a composite particle, a plausible solution to the electroweak (EW) hierarchy problem [2, 3], it should be accompanied by several other scalar "siblings", most predicted to transform as singlets under the SM gauge group [4–8]. The size of the scalar interactions, being UV dependent, could therefore provide valuable information about the underlying dynamics responsible for EW symmetry breaking (EWSB) [4]. Moreover, the Higgs-singlet portal is one of the simplest avenues to generate the dark matter relic density we observe [9–11], or even a first order phase transition, in turn connected with the possibility of explaining baryogenesis [12–15]. The amount of CP violation the singlet carries would be then a key property to determine the viability of this scenario.

Another prominent question to face will be how much the new singlet looks like an axion-like particle (ALP). The existence of ALPs is a common prediction of more fundamental constructions, like string theory [16, 17]. They are furthermore motivated by another fine-tuning problem in the SM, the strong CP problem, which is the fine adjustment one is required to make (of more than ten orders of magnitude) to explain the absence of CP-violation in the QCD vacuum. To successfully solve this problem, the singlet interactions would have to preserve a shift-symmetry of very high quality [18–21].

At the renormalizable level, the answers to these questions lie on measuring the strength of only a few singlet interactions with the SM particles. For instance, in the absence of mixing, the communication between a scalar singlet and the SM is entirely dictated by triplet and quartic interactions which are in turn related by the Higgs vacuum expectation value (VEV). Instead, if the two scalars mix, the singlet can also develop universal couplings to the SM fermions which are Yukawa suppressed, and moreover incompatible with a shift-symmetry.

Effective corrections can however change the answer to these questions, while renormalization group (RG) running can affect their stability. Therefore, in this work, we present the one-loop renormalization group equations (RGEs) characterizing the evolution across energy scales of all singlet interactions with the SM, up to mass dimension five. The RGEs of the singlet effective field theory (EFT) were previously obtained in two particular limits: ignoring CP-odd couplings (under the assumption that the singlet is a pseudoscalar) [22]; or including only shift-preserving interactions, that is assuming the singlet is an ALP [23, 24]. Our work is therefore the most complete study of the singlet EFT presented in the literature so far, not only at the level of RGEs, but also in what concerns all effective contributions to the scalar mass mixing. We obtain the running of the Wilson coefficients both in the high-energy (HE) and in the low-energy (LE) EFTs, the latter resulting from integrating out the heavy top quark, the Higgs and the Z and W gauge bosons. The matching between the two theories is also obtained at tree level, including the effects which arise from scalar mixing. The shift-symmetric limit of our results is commented throughout the work.

As an application, we obtain the electric dipole moment (EDM) constraints on particular UV scenarios taking the full running of couplings into account. In particular, we set constraints on the CP violation arising from a CP-even BSM scenario, due to the mixing with the Yukawa couplings of the SM. We also exemplify how the experimental constraints of a generic singlet can be directly compared with those of an ALP. This comparison is based on the analysis presented in ref. [25], where the shift-symmetry flavour invariants induced by the singlet-fermionic couplings were constructed.

All the results obtained in this work are provided in a new Mathematica package, `ALPRunner` [26], that can be used to study in detail the phenomenology of the singlet EFT. The main functionalities are described in appendix A. Using this tool, it is straightforward for the user to find the whole set of EFT parameters generated at an IR scale given the inputs defined in the UV. A procedure is also implemented such that, given low-energy bounds, constraints can be placed on the UV parameters of the theory.

The structure of this work can be easily understood from the table of contents.

JHEP11(2023)133

2 The complete singlet EFT

The renormalisable Lagrangian of the SM extended with a real scalar singlet (s) reads [27–29]:

$$\begin{aligned}\mathcal{L}_{\mathrm{SM}+s} =& \frac{1}{2}(\partial_\mu s)(\partial^\mu s) - \frac{1}{2}m_s^2 s^2 - \frac{\kappa_s}{3!}s^3 - \frac{\lambda_s}{4!}s^4 - \kappa_{s\phi}s\phi^\dagger\phi - \frac{\lambda_{s\phi}}{2}s^2\phi^\dagger\phi \\ & - \frac{1}{4}G^A_{\mu\nu}G^{A\mu\nu} - \frac{1}{4}W^a_{\mu\nu}W^{a\mu\nu} - \frac{1}{4}B_{\mu\nu}B^{\mu\nu} + \theta_{\mathrm{QCD}}\frac{g_s^2}{32\pi^2}G^A_{\mu\nu}\widetilde{G}^{A\mu\nu} \\ & + \sum_{\psi=q,l,u,d,e}\overline{\psi}^\alpha i\not{D}\psi^\alpha - \left(y^u_{\alpha\beta}\overline{q_L}^\alpha\tilde{\phi}u^\beta_R + y^d_{\alpha\beta}\overline{q_L}^\alpha\phi d^\beta_R + y^e_{\alpha\beta}\overline{l_L}^\alpha\phi e^\beta_R + \mathrm{h.c.}\right) \\ & + (D_\mu\phi)^\dagger(D^\mu\phi) + \mu^2\phi^\dagger\phi - \lambda(\phi^\dagger\phi)^2\,, \end{aligned} \tag{2.1}$$

where we have used e_R, u_R and d_R to denote the right-handed (RH) leptons and quarks; while l_L and q_L are the left-handed (LH) counterparts. In turn, y^u, y^d, and y^e are the SM Yukawa matrices. We represent the Higgs doublet by $\phi = (\phi^+, \phi^0)^T$ and its charge conjugate by $\widetilde{\phi} = i\,\sigma_2\phi^*$. $G^A_{\mu\nu}$, $W^a_{\mu\nu}$, and $B_{\mu\nu}$ are the field strength tensors of the SM gauge groups $\mathrm{SU}(3)_C$, $\mathrm{SU}(2)_L$, and $\mathrm{U}(1)_Y$, respectively. The corresponding gauge couplings are denoted by g_i, with $i = 1, 2, 3$. The dual strength tensor of the gluon field is defined as $\widetilde{G}^{A,\mu\nu} \equiv \frac{1}{2}\epsilon_{\mu\nu\rho\sigma}G^{A,\rho\sigma}$ and similarly for the other gauge fields. We use the minus sign convention for the covariant derivative.

At dimension-five and assuming lepton number conservation, a minimal basis for the SM+s EFT is given by the following operators [22]:

$$\begin{aligned}\mathcal{L}^{\mathrm{eff}}_{\mathrm{SM}+s} =& \mathcal{L}_{\mathrm{SM}+s} + s\Big[i\,\overline{q_L}a_{su\phi}\widetilde{\phi}u_R + i\,\overline{q_L}a_{sd\phi}\phi d_R + i\,\overline{l_L}a_{se\phi}\phi e_R + \mathrm{h.c.}\Big] + a_{s^5}s^5 \\ & + a_{s^3}s^3(\phi^\dagger\phi) + a_s s(\phi^\dagger\phi)^2 + a_{s\widetilde{G}}sG^A_{\mu\nu}\widetilde{G}^{A\mu\nu} + a_{s\widetilde{W}}sW^a_{\mu\nu}\widetilde{W}^{a\mu\nu} \\ & + a_{s\widetilde{B}}sB_{\mu\nu}\widetilde{B}^{\mu\nu} + a_{sG}sG^A_{\mu\nu}G^{A\mu\nu} + a_{sW}sW^a_{\mu\nu}W^{a\mu\nu} + a_{sB}sB_{\mu\nu}B^{\mu\nu}\,, \end{aligned} \tag{2.2}$$

where $a_{s\psi\phi}$ are complex matrices in flavour space to account for both CP-conserving and CP-violating interactions. In our notation, all $a_i \equiv a_i^0/\Lambda$ are dimension-full couplings, with Λ denoting the cutoff scale up until which the EFT is a valid expansion. In what follows, we assume s is a pseudoscalar. The previous EFT and the results to obtain next are however valid beyond this assumption.

To order v/Λ, the dimension-five Wilson coefficients are only renormalized by other dimension-five couplings:

$$16\pi^2\mu\frac{\mathrm{d}a_i}{\mathrm{d}\mu} = \gamma^{(1)}_{ij}a_j\,. \tag{2.3}$$

The anomalous dimensions $\gamma^{(1)}$ were computed in ref. [22] for the CP-even sector in isolation. We generalize eq. (2.3) by including the contributions from CP-odd couplings. In this more general scenario, dimension-five terms renormalize lower dimensional interactions as well, due to the presence of light mass scales in the theory. This effect is absent assuming only CP-even interactions as, in this case, there is a $\mathcal{Z}_2$ symmetry acting on $s \to -s$, under which the (non-) renormalizable sector of the EFT is (odd) even.

JHEP11(2023)133

Considering renormalizable couplings, we therefore expect, schematically, the following structure:

$$16\pi^2\mu\frac{\mathrm{d}\kappa_i}{\mathrm{d}\mu} = \gamma^{(2)}_{ij}\kappa_j + \gamma^{(3)}_{ij}m^2 a_j\,, \tag{2.4}$$

$$16\pi^2\mu\frac{\mathrm{d}\lambda_i}{\mathrm{d}\mu} = \gamma^{(4)}_{ij}\lambda_j + \gamma^{(5)}_{ijk}\kappa_j a_k\,. \tag{2.5}$$

where $m = m_s,\ \mu$. The RGEs of the CP-odd couplings in eq. (2.4) are presented for the first time in this work, as well as the contributions stemming from $\gamma^{(5)}$.

2.1 A comparison with the ALP basis

In order to account for the most generic interactions, we did not impose shift-symmetry in the EFT defined in eq. (2.2), as commonly done in studies of axions and ALPs, which arise as the Goldstone bosons of a spontaneously broken global symmetry. In particular, the axion is a prediction of the Peccei-Quinn mechanism [18–21] to solve the strong CP problem, which requires an exact shift symmetry in the axion Lagrangian, broken at the quantum level by the anomalous interaction with gluons. Upon QCD confinement, such interaction generates a periodic potential for the axion, $V(s) = V(s + 2\pi f_s)$, with f_s denoting the field decay constant. Such potential also predicts a strict relation between the mass and decay constant for the axion field, that ALPs are not required to abide.

Up to a bare mass term, the minimal set of ALP interactions can be described by the following EFT [30]:

$$\mathcal{L}_{\mathrm{ALP}} = \frac{1}{2}(\partial_\mu s)^2 + \sum_\psi \frac{\partial_\mu s}{f_s}\overline{\psi}c_\psi\gamma^\mu\psi + \sum_X c_X\frac{g_X^2}{16\pi^2}\frac{s}{f_s}X_{\mu\nu}\widetilde{X}^{\mu\nu}\,, \tag{2.6}$$

where ψ runs over q_L, l_L, u_R, d_R, e_R, c_ψ are hermitian matrices in flavour space and $X = G, W, B$. When the gauge boson sector of this theory is considered in isolation, the 2π periodicity imposes that $c_X \in \mathbb{Z}$ [31]. While the shift $s \to s + 2\pi f_s$ modifies the interaction Lagrangian, the action is left invariant whenever this quantization condition is fulfilled. It is well known that a chiral rotation produces, however, additional interactions which modify this condition [32]. In other words, the requirement $c_X \in \mathbb{Z}$ follows from the ALP periodicity only in the basis of eq. (2.6).

Consequently, in this basis, the running of c_X couplings is expected to vanish,[1] as found in previous works [22–24] (up to two-loop accuracy in the gauge couplings). On the other hand, there is no constraint on the running of the derivative couplings.

In the interaction basis considered in this work (eq. (2.2)), the singlet periodicity is explicitly broken. Therefore, no quantization constraint applies.[2] The previous discussion still connects to our work in two main ways:

[1] This argument is valid up to the inclusion of a potential, whose truncation can break explicitly the ALP periodicity.

[2] There can be other reasons preventing the one-loop running of the couplings of a general scalar singlet.

JHEP11(2023)133

- The more restrictive running in the SM+s EFT invariant under discrete ALP shifts constitutes an important case limit of our study, which should be recovered from the complete RGEs to be derived next.

- Using the freedom to write the derivative interactions between the ALP and fermions in terms of chirality-flipping operators, it is straightforward to find the conditions to preserve shift-symmetry in the basis of eq. (2.2). Hence, the ALP phenomenology can be studied using the EFT basis of this work, even though it is not possible in general to map the couplings back to the chirality-preserving basis in eq. (2.6).

Indeed, by integrating by parts the second term in eq. (2.6) and using the SM equations of motion (EOMs), we obtain the fermionic operators in eq. (2.2) with the following coefficients [22]:

$$a_{su\phi} = \frac{i}{f_s}\left(y^u c_u - c_q y^u\right), \quad a_{sd\phi} = \frac{i}{f_s}\left(y^d c_d - c_q y^d\right), \quad a_{se\phi} = \frac{i}{f_s}\left(y^e c_e - c_l y^e\right). \qquad (2.7)$$

These three conditions are sufficient to preserve a continuous shift-symmetry at the perturbative level in our EFT, up to terms in the scalar potential. However these conditions are implicit and do not, in general, allow to identify the c-matrices given a set of $a_{s\psi\phi}$ couplings.

Only under specific assumptions, such as Minimal Flavour Violation or in the presence of just one fermion generation coupled to the ALP, it is possible to trade completely c_l, c_q by their RH counterparts and find one-to-one correspondence between the chirality-preserving and chirality-flipping couplings [22–24]. In those cases, to match the results derived using the basis in eq. (2.6) and ours, shifts on the anomalous couplings also need to be taken into account, that arise from the axial anomaly equation [33]:

$$a_{s\tilde{G}} = \frac{g_3^2}{16\pi^2 f_s}\left[c_G - \frac{1}{2}\mathrm{Tr}\left(c_u + c_d - 2c_q\right)\right], \qquad (2.8)$$

$$a_{s\tilde{W}} = \frac{g_2^2}{16\pi^2 f_s}\left[c_W + \frac{1}{2}\mathrm{Tr}\left(3c_q + c_l\right)\right], \qquad (2.9)$$

$$a_{s\tilde{B}} = \frac{g_1^2}{16\pi^2 f_s}\left[c_B - \mathrm{Tr}\left(\frac{4}{3}c_u + \frac{1}{3}c_d - \frac{1}{6}c_q + c_e - \frac{1}{2}c_l\right)\right]. \qquad (2.10)$$

Assuming this set of boundary conditions (eqs. (2.7)–(2.10)), the results obtained with any of the two bases must agree within an accuracy of $\mathcal{O}(\alpha/\Lambda)$. Finally, we remark that the general basis adopted in this work can be used to study the fate of shift-symmetric scenarios under running, without having to refer implicitly to the matrices c_ψ. This has become possible with the work presented in ref. [25], where the complete set of flavour invariants associated to the singlet shift-symmetry was constructed, and shown to form a closed set under RG evolution.

3 High-energy anomalous dimensions

We renormalize the SM+s EFT by computing the divergences in the basis of independent Green's functions of ref. [22]; see appendix B. We use the background field method (BFM)

JHEP11(2023)133

and work in the Feynman gauge with $\mathrm{d} = 4 - 2\epsilon$ spacetime dimensions. The computations are based on dedicated routines that rely on `FeynRules` [34], `FeynArts` [35], and `FormCalc` [36]. All of our results have been cross-checked with `matchmakereft` [37], from which we have obtained the μ^2 contributions.

The one-loop divergences of the renormalizable couplings read:

$$
\begin{aligned}
m_s'^2 &= -\frac{1}{32\pi^2\epsilon}\left(\lambda_s m_s^2 + \kappa_s^2 + 4\kappa_{s\phi}^2 - 4\lambda_{s\phi}\mu^2\right), && (3.1)\\
\mu'^2 &= \frac{1}{32\pi^2\epsilon}\left(2\kappa_{s\phi}^2 + \lambda_{s\phi}m_s^2 + \frac{1}{2}\left(g_1^2 + 3g_2^2 - 12\lambda\right)\mu^2\right), && (3.2)\\
\kappa_s' &= -\frac{3}{4\pi^2\epsilon}\left(\frac{1}{8}\kappa_s\lambda_s + \frac{1}{2}\kappa_{s\phi}\lambda_{s\phi} - 5a_{s^5}m_s^2 + a_{s^3}\mu^2\right), && (3.3)\\
\kappa_{s\phi}' &= -\frac{1}{32\pi^2\epsilon}\left(\kappa_s\lambda_{s\phi} - \frac{1}{2}\kappa_{s\phi}\left[g_1^2 + 3g_2^2 - 8(3\lambda + \lambda_{s\phi})\right] - 6a_{s^3}m_s^2 + 12a_s\mu^2\right), && (3.4)\\
\lambda_s' &= -\frac{1}{4\pi^2\epsilon}\left(\frac{3}{8}\lambda_s^2 + \frac{3}{2}\lambda_{s\phi}^2 - 12\left(\kappa_{s\phi}a_{s^3} + 5\kappa_s a_{s^5}\right)\right), && (3.5)\\
\lambda_{s\phi}' &= -\frac{1}{8\pi^2\epsilon}\left\{\lambda_{s\phi}\left[\lambda_{s\phi} + \frac{1}{4}\lambda_s + 3\lambda - \frac{1}{8}\left(g_1^2 + 3g_2^2\right)\right]\right.\\
&\qquad\left. -\left[3\kappa_s a_{s^3} + 6\left(a_s + a_{s^3}\right)\kappa_{s\phi}\right]\right\}, && (3.6)\\
\lambda' &= -\frac{1}{32\pi^2\epsilon}\left\{\frac{3}{8}\left(g_1^4 + 3g_2^4 + 2g_1^2g_2^2\right) - \left(g_1^2 + 3g_2^2\right)\lambda + 24\lambda^2 + \frac{\lambda_{s\phi}^2}{2}\right.\\
&\qquad\left. - 8\kappa_{s\phi}a_s - 2\mathrm{Tr}\left[3\left(y_u^\dagger y_u y_u^\dagger y_u + y_d^\dagger y_d y_d^\dagger y_d\right) + y_e^\dagger y_e y_e^\dagger y_e\right]\right\}, && (3.7)\\
y_u' &= \frac{1}{16\pi^2\epsilon}\left[y_d y_d^\dagger y_u + \frac{1}{36}\left(25g_1^2 + 27g_2^2 + 192g_3^2\right)y_u + i\kappa_{s\phi}a_{su\phi}\right], && (3.8)\\
y_d' &= \frac{1}{16\pi^2\epsilon}\left[y_u y_u^\dagger y_d + \frac{1}{36}\left(g_1^2 + 27g_2^2 + 192g_3^2\right)y_d + i\kappa_{s\phi}a_{sd\phi}\right], && (3.9)\\
y_e' &= \frac{3}{64\pi^2\epsilon}\left[\left(3g_1^2 + g_2^2\right)y_e + \frac{4i}{3}\kappa_{s\phi}a_{se\phi}\right]. && (3.10)
\end{aligned}
$$

As we work in BFM approach, the divergences of the gauge couplings are automatically fixed by the wave function renormalization (WFR) factors of the gauge bosons [38]. The latter are not modified by the presence of CP-odd terms and can therefore be read from ref. [22].

We obtain the following divergences for the effective couplings:[3]

$$
\begin{aligned}
a_{s^5}' &= -\frac{1}{16\pi^2\epsilon}\left(5\lambda_s a_{s^5} + \lambda_{s\phi}a_{s^3}\right), && (3.11)\\
a_{s^3}' &= -\frac{1}{32\pi^2\epsilon}\left[\left(12\lambda + 3\lambda_s + 12\lambda_{s\phi} - \frac{g_1^2}{2} - \frac{3g_2^2}{2}\right)a_{s^3} + 6\lambda_{s\phi}a_s + 20\lambda_{s\phi}a_{s^5}\right], && (3.12)
\end{aligned}
$$

[3] In several of the following terms, the unit matrix in flavour space is left implicit.

$$a'_s = -\frac{1}{32\pi^2\epsilon}\Bigg\{ \left(48\lambda + 8\lambda_{s\phi} - g_1^2 - 3g_2^2\right) a_s - 3\left(g_1^4 + g_1^2 g_2^2\right) a_{sB} - 3\left(3g_2^4 + g_1^2 g_2^2\right) a_{sW}$$

$$+ 6\lambda_{s\phi} a_{s^3} + 8\text{Im}\left\{\text{Tr}\left[3\left(y_d^\dagger y_d y_d^\dagger a_{sd\phi} + y_u^\dagger y_u y_u^\dagger a_{su\phi}\right) + y_e^\dagger y_e y_e^\dagger a_{se\phi}\right]\right\}\Bigg\}, \quad (3.13)$$

$$a'_{su\phi} = -\frac{1}{16\pi^2\epsilon}\left\{a_{su\phi}\left[\lambda_{s\phi} - \left(\frac{25g_1^2}{36} + \frac{3g_2^2}{4} + \frac{16g_3^2}{3}\right)\right] - y_d y_d^\dagger a_{su\phi} - a_{sd\phi} y_d^\dagger y_u \right.$$

$$\left. + y_d a_{sd\phi}^\dagger y_u - i\left(\frac{4g_1^2}{3} a_{sB} + 16 g_3^2 a_{sG}\right) y_u\right\}, \quad (3.14)$$

$$a'_{sd\phi} = -\frac{1}{16\pi^2\epsilon}\left\{a_{sd\phi}\left[\lambda_{s\phi} - \left(\frac{g_1^2}{36} + \frac{3g_2^2}{4} + \frac{16g_3^2}{3}\right)\right] - y_u y_u^\dagger a_{sd\phi} - a_{su\phi} y_u^\dagger y_d + \right.$$

$$\left. + y_u a_{su\phi}^\dagger y_d + i\left(\frac{2}{3} g_1^2 a_{sB} - 16 g_3^2 a_{sG}\right) y_d\right\}, \quad (3.15)$$

$$a'_{se\phi} = -\frac{1}{16\pi^2\epsilon}\left\{a_{se\phi}\left[\lambda_{s\phi} - \left(\frac{9g_1^2}{4} + \frac{3g_2^2}{4}\right)\right] - 6 i g_1^2 a_{sB} y_e\right\}, \quad (3.16)$$

$$r'_{sq} = \frac{1}{32\pi^2\epsilon}\left[a_{sd\phi} y_d^\dagger + a_{su\phi} y_u^\dagger - \left(\frac{g_1^2}{3} a_{s\widetilde{B}} + 9 g_2^2 a_{s\widetilde{W}} + 16 g_3^2 a_{s\widetilde{G}}\right)\right], \quad (3.17)$$

$$r'_{sl} = \frac{1}{32\pi^2\epsilon}\left(a_{se\phi} y_e^\dagger - 3 g_1^2 a_{s\widetilde{B}} - 9 g_2^2 a_{s\widetilde{W}}\right), \quad (3.18)$$

$$r'_{su} = -\frac{1}{16\pi^2\epsilon}\left(a_{su\phi}^\dagger y_u - \frac{8g_1^2}{3} a_{s\widetilde{B}} - 8 g_3^2 a_{s\widetilde{G}}\right), \quad (3.19)$$

$$r'_{sd} = -\frac{1}{16\pi^2\epsilon}\left(a_{sd\phi}^\dagger y_d - \frac{2}{3} g_1^2 a_{s\widetilde{B}} - 8 g_3^2 a_{s\widetilde{G}}\right), \quad (3.20)$$

$$r'_{se} = -\frac{1}{16\pi^2\epsilon}\left(a_{se\phi}^\dagger y_e - 6 g_1^2 a_{s\widetilde{B}}\right), \quad (3.21)$$

$$r'_{s\phi\Box} = -\frac{1}{16\pi^2\epsilon}\left\{\text{Tr}\left[3 y_d a_{sd\phi}^\dagger - 3 y_u^\dagger a_{su\phi} + y_e a_{se\phi}^\dagger\right] + \frac{3}{2} i\left[g_1^2 a_{sB} + 3 g_2^2 a_{sW}\right]\right\}, \quad (3.22)$$

where the r-couplings are associated to redundant operators which will be redefined away; see appendix B. All other counterterms vanish up to the EFT and loop order we are interested in.

The divergences obtained above can be projected onto the minimal basis of eq. (2.2) using suitable field redefinitions, which can be implemented via the EFT EOMs within $\mathcal{O}(1/\Lambda)$ accuracy. In this procedure, we neglect $\mathcal{O}(\alpha/4\pi)$ corrections that arise from the anomaly equations which relate chirality-preserving operators with the chirality-flipping ones in our basis; see eqs. (2.8)–(2.10). This would lead to $\mathcal{O}(\alpha/4\pi)^2$ corrections which are beyond the scope of our analysis. The on-shell results are obtained after the following replacements:[4]

$$\begin{aligned}\kappa'_s &\to \kappa'_s + 6 m_s^2 r'_{s\Box} \\ &= -\frac{3}{4\pi^2\epsilon}\left[\frac{1}{8}\kappa_s\lambda_s + \frac{1}{2}\kappa_{s\phi}\lambda_{s\phi} - 5 a_{s^5} m_s^2 + \mu^2 a_{s^3}\right],\end{aligned} \quad (3.23)$$

[4]These replacements differ from those in ref. [22], where only the CP-even components of the flavour couplings were considered.

$$\begin{aligned}\kappa'_{s\phi}\to&\,\kappa'_{s\phi}-2\mathrm{Im}\left[r'_{s\phi\Box}\right]\mu^2+r'_{\phi s\Box}m_s^2\\&=-\frac{1}{32\pi^2\epsilon}\Bigg\{\kappa_s\lambda_{s\phi}-\frac{1}{2}\kappa_{s\phi}\left[g_1^2+3g_2^2-8(3\lambda+\lambda_{s\phi})\right]-6a_{s^3}m_s^2+12\mu^2a_s\\&\quad-6\mu^2\left(g_1^2a_{sB}+3g_2^2a_{sW}\right)+4\mu^2\mathrm{Im}\left[\mathrm{Tr}\left[3\left(y_u^\dagger a_{su\phi}-y_d a_{sd\phi}^\dagger\right)-y_e a_{se\phi}^\dagger\right]\right]\Bigg\},\end{aligned}\tag{3.24}$$

$$\begin{aligned}\lambda'_s\to&\,\lambda'_s+12\kappa_s r'_{s\Box}\\&=-\frac{1}{4\pi^2\epsilon}\left[\frac{3}{8}\lambda_s^2+\frac{3}{2}\lambda_{s\phi}^2-12\left(\kappa_{s\phi}a_{s^3}+5\kappa_s a_{s^5}\right)\right],\end{aligned}\tag{3.25}$$

$$\begin{aligned}\lambda'_{s\phi}\to&\,\lambda'_{s\phi}+2\kappa_{s\phi}r'_{s\Box}-4\kappa_{s\phi}\mathrm{Im}\left[r'_{s\phi\Box}\right]+\kappa_s r'_{\phi s\Box}\\&=-\frac{1}{8\pi^2\epsilon}\Bigg\{\lambda_{s\phi}\left[\lambda_{s\phi}+\frac{1}{4}\lambda_s+3\lambda-\frac{1}{8}\left(g_1^2+3g_2^2\right)\right]-\left[3\kappa_s a_{s^3}+2\left(3a_s+3a_{s^3}\right)\kappa_{s\phi}\right]\\&\quad-3\kappa_{s\phi}\left(g_1^2a_{sB}+3g_2^2a_{sW}\right)+2\kappa_{s\phi}\mathrm{Im}\left[\mathrm{Tr}\left[3\left(y_u^\dagger a_{su\phi}-y_d a_{sd\phi}^\dagger\right)-y_e a_{se\phi}^\dagger\right]\right]\Bigg\},\end{aligned}\tag{3.26}$$

$$\begin{aligned}\lambda'\to&\,\lambda'+\kappa_{s\phi}r'_{\phi s\Box}\\&=-\frac{1}{32\pi^2\epsilon}\Bigg\{\frac{3}{8}\left(g_1^4+3g_2^4+2g_1^2g_2^2\right)-\left(g_1^2+3g_2^2\right)\lambda+24\lambda^2+\frac{\lambda_{s\phi}^2}{2}-8\kappa_{s\phi}a_s\\&\quad-2\mathrm{Tr}\left[3\left(y_u^\dagger y_u y_u^\dagger y_u+y_d^\dagger y_d y_d^\dagger y_d\right)+y_e^\dagger y_e y_e^\dagger y_e\right]\Bigg\},\end{aligned}\tag{3.27}$$

$$\begin{aligned}a'_{su\phi}\to&\,a'_{su\phi}-r'_{s\phi\Box}y_u-r'_{sq}y_u+y_u(r'_{su})^\dagger\\&=-\frac{1}{(4\pi)^2\epsilon}\Bigg\{\left[\lambda_{s\phi}-\frac{25}{36}g_1^2-\frac{3}{4}g_2^2-\frac{16}{3}g_3^2\right]a_{su\phi}+\mathrm{Tr}\left[3\left(y_u^\dagger a_{su\phi}-y_d a_{sd\phi}^\dagger\right)-y_e a_{se\phi}^\dagger\right]y_u\\&\quad-\frac{1}{2}a_{sd\phi}y_d^\dagger y_u+\frac{1}{2}a_{su\phi}y_u^\dagger y_u+y_d a_{sd\phi}^\dagger y_u-y_d y_d^\dagger a_{su\phi}+y_u y_u^\dagger a_{su\phi}\\&\quad-\left[\frac{17}{6}\left(ia_{sB}+a_{s\widetilde{B}}\right)g_1^2+\frac{9}{2}\left(ia_{sW}+a_{s\widetilde{W}}\right)g_2^2+16\left(ia_{sG}+a_{s\tilde{G}}\right)\right]y_u\Bigg\},\end{aligned}\tag{3.28}$$

$$\begin{aligned}a'_{sd\phi}\to&\,a'_{sd\phi}+r'^{*}_{s\phi\Box}y_d-r'_{sq}y_d+y_d r^\dagger_{sd}\\&=-\frac{1}{(4\pi)^2\epsilon}\Bigg\{\left[\lambda_{s\phi}-\frac{1}{36}g_1^2-\frac{3}{4}g_2^2-\frac{16}{3}g_3^2\right]a_{sd\phi}+\mathrm{Tr}\left[3\left(y_d^\dagger a_{sd\phi}-y_u a_{su\phi}^\dagger\right)+y_e^\dagger a_{se\phi}\right]y_d\\&\quad-\frac{1}{2}a_{su\phi}y_u^\dagger y_d+\frac{1}{2}a_{sd\phi}y_d^\dagger y_d+y_u a_{su\phi}^\dagger y_d-y_u y_u^\dagger a_{sd\phi}+y_d y_d^\dagger a_{sd\phi}\\&\quad-\left[\frac{5}{6}\left(ia_{sB}+a_{s\widetilde{B}}\right)g_1^2+\frac{9}{2}\left(ia_{sW}+a_{s\widetilde{W}}\right)g_2^2+16\left(ia_{sG}+a_{s\tilde{G}}\right)\right]y_d\Bigg\},\end{aligned}\tag{3.29}$$

JHEP11(2023)133

$$
\begin{aligned}
a'_{se\phi} &\to a'_{se\phi} + r'^{*}_{s\phi\Box} y_e - r'_{sl} y_e + y_e r^{\dagger}_{se} \\
&= -\frac{1}{(4\pi)^2 \epsilon} \Bigg\{ \left[\lambda_{s\phi} - \frac{9}{4} g_1^2 - \frac{3}{4} g_2^2 \right] a_{se\phi} + \mathrm{Tr}\left[3 \left(y_d^{\dagger} a_{sd\phi} - y_u a^{\dagger}_{su\phi} \right) + y_e^{\dagger} a_{se\phi} \right] y_e \\
&\quad + \frac{1}{2} a_{se\phi} y_e^{\dagger} y_e + y_e y_e^{\dagger} a_{se\phi} - \frac{3}{2} \left[5 \left(i a_{sB} + a_{s\widetilde{B}} \right) g_1^2 + 3 \left(i a_{sW} + a_{s\widetilde{W}} \right) g_2^2 \right] y_e \Bigg\},
\end{aligned} \tag{3.30}
$$

$$
\begin{aligned}
a'_{s^5} &\to a'_{s^5} - \frac{\lambda_s}{3!} r'_{s\Box} \\
&= -\frac{1}{16\pi^2 \epsilon} \left(5 \lambda_s a_{s^5} + \lambda_{s\phi} a_{s^3} \right),
\end{aligned} \tag{3.31}
$$

$$
\begin{aligned}
a'_{s^3} &\to a'_{s^3} + \left[\mathrm{Im}\left(r'_{s\phi\Box} \right) - r'_{s\Box} \right] \lambda_{s\phi} - \frac{\lambda_s}{3!} r'_{\phi s\Box} \\
&= -\frac{1}{32\pi^2 \epsilon} \Bigg\{ \left(12\lambda + 3\lambda_s + 12\lambda_{s\phi} - \frac{g_1^2}{2} - \frac{3g_2^2}{2} \right) a_{s^3} + 4\lambda_{s\phi} \left(\frac{3}{2} a_s + 5 a_{s^5} \right) \\
&\quad + 3\lambda_{s\phi} \left(g_1^2 a_{sB} + 3 g_2^2 a_{sW} \right) + 2\lambda_{s\phi} \mathrm{Im} \left[\mathrm{Tr}\left[3 \left(y_d a^{\dagger}_{sd\phi} - a_{su\phi} y_u^{\dagger} \right) + y_e a^{\dagger}_{se\phi} \right] \right] \Bigg\},
\end{aligned} \tag{3.32}
$$

$$
\begin{aligned}
a'_s &\to a'_s + 4\lambda \mathrm{Im}\left(r'_{s\phi\Box} \right) - \lambda_{s\phi} r'_{\phi s\Box} \\
&= -\frac{1}{32\pi^2 \epsilon} \Bigg\{ \left(48\lambda + 8\lambda_{s\phi} - g_1^2 - 3g_2^2 \right) a_s + 6\lambda_{s\phi} a_{s^3} - 3 \left(g_1^4 + g_1^2 g_2^2 - 4\lambda g_1^2 \right) a_{sB} \\
&\quad - 3 \left(3 g_2^4 + g_1^2 g_2^2 - 12\lambda g_2^2 \right) a_{sW} + 8 \mathrm{Im} \Bigg[\mathrm{Tr}\Big[3 \left(y_d^{\dagger} y_d y_d^{\dagger} a_{sd\phi} + y_u^{\dagger} y_u y_u^{\dagger} a_{su\phi} \right) \\
&\quad + y_e^{\dagger} y_e y_e^{\dagger} a_{se\phi} + \lambda \left(3 y_d a^{\dagger}_{sd\phi} - 3 y_u^{\dagger} a_{su\phi} + y_e a^{\dagger}_{se\phi} \right) \Big] \Bigg] \Bigg\}.
\end{aligned} \tag{3.33}
$$

We can now obtain the anomalous dimensions of all couplings in the singlet EFT. Taking the CP-even limit of our results, we find exact agreement with those presented in ref. [22].

The complete expressions for the RGEs are provided in the `ALPRunner` package [26] published along this work. Instead, a more graphic picture is presented in tables 1 and 2, where we show the structure of the anomalous dimension matrices, resulting from one-loop insertions of the SM and new physics (NP) couplings up to $\mathcal{O}(1/\Lambda)$. Each Wilson coefficient in the rows is renormalized by the non-zero coefficients in the columns. We have highlighted in blue the contributions which deviate from naive dimensional analysis [39] by at least one order of magnitude, and which are therefore expected to play an important role in the singlet phenomenology.

Most of the zeros in these tables are trivial. For example, it is not possible to insert an s^5 operator in a one-loop diagram without leaving at least 3 external singlet legs, which explains the non-renormalization results in the first column of table 1. On the other hand, operators with n singlet fields can renormalize others with $m > n$ singlet fields via the insertion of renormalizable NP interactions. Interestingly, both sXX and $sX\widetilde{X}$ operators renormalize the fermionic interactions of the singlet, while sXX renormalizes also the mixed interactions in the scalar sector.

	s^5	$s^3\phi^\dagger\phi$	$s(\phi^\dagger\phi)^2$	$s\overline{\Psi}_L\phi\psi_R$	sXX	$sX\widetilde{X}$
s^5	λ_s	$\lambda_{s\phi}$	0	0	0	0
$s^3\phi^\dagger\phi$	$\lambda_{s\phi}$	$\lambda_s + \lambda_{s\phi} + \lambda + y_t^2$	$\lambda_{s\phi}$	$\lambda_{s\phi} y_t$	$\lambda_{s\phi} g_2^2$	0
$s(\phi^\dagger\phi)^2$	0	$\lambda_{s\phi}$	$\lambda_{s\phi} + \lambda + y_t^2$	$y_t^3 + \lambda y_t$	λg_2^2	0
$s\overline{\Psi}_L\phi\psi_R$	0	0	0	$\lambda_{s\phi} + y_t^2$	$g_3^2 y_t$	$g_3^2 y_t$
sXX	0	0	0	0	g_3^2	0
$sX\widetilde{X}$	0	0	0	0	0	g_3^2

Table 1. Structure of the dimension-five anomalous dimension matrix. Only BSM and the leading SM contributions are kept. For instance, y_t (the top-quark Yukawa coupling) and $g_{2,3}$ are the largest contributions in their respective sub-classes. Terms in blue show the contributions that deviate significantly from naive dimensional analysis; see the text for details.

	s^5	$s^3(\phi^\dagger\phi)$	$s(\phi^\dagger\phi)^2$	$s\overline{\Psi}_L\phi\psi_R$	sXX	$sX\widetilde{X}$
s^3	m_s^2	μ^2	0	0	0	0
$s(\phi^\dagger\phi)$	0	m_s^2	μ^2	$y_t\mu^2$	$g_2^2\mu^2$	0
s^4	κ_s	$\kappa_{s\phi}$	0	0	0	0
$s^2(\phi^\dagger\phi)$	0	$\kappa_s + \kappa_{s\phi}$	$\kappa_{s\phi}$	$y_t\kappa_{s\phi}$	$g_2^2\kappa_{s\phi}$	0
$(\phi^\dagger\phi)^2$	0	0	$\kappa_{s\phi}$	0	0	0

Table 2. Structure of the renormalizable anomalous dimension matrix induced by effective interactions. Terms in blue show the contributions that deviate significantly from naive dimensional analysis; see the text for details.

At one-loop, in the most generic basis, we find that the pseudoscalar interactions with gauge bosons run proportionally to the gauge coupling,

$$\beta_{a_{s\widetilde{B},sB}} = \frac{41}{3} g_1^2 a_{s\widetilde{B}}(a_{sB})\,, \tag{3.34}$$

$$\beta_{a_{s\widetilde{W},sW}} = -\frac{19}{3} g_2^2 a_{s\widetilde{W}}(a_{sW})\,, \tag{3.35}$$

$$\beta_{a_{s\widetilde{G},sG}} = -14 g_3^2 a_{s\widetilde{G}}(a_{sG})\,. \tag{3.36}$$

In fact, if we redefine $a_{sX,\,s\widetilde{X}} \equiv g_X^2 c_{X,\,\widetilde{X}}$, we find that the $c_{X,\,\widetilde{X}}$ couplings do not run at

JHEP11(2023)133

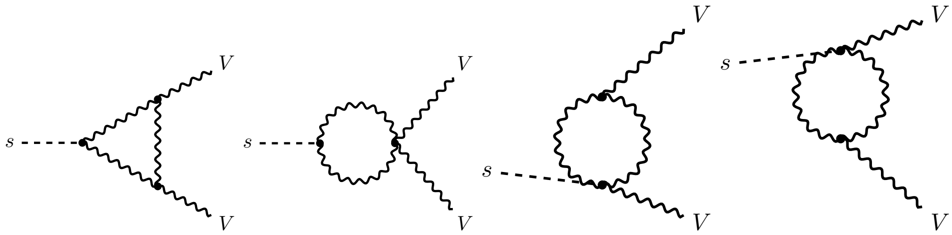

Figure 1. One-loop diagrams that contribute to the $s \to VV$ divergent amplitude, V denoting any SM vector, at order $\mathcal{O}\,(1/\Lambda)$.

all [22–24]. This follows from a non-trivial cancellation of the diagrams shown in figure 1 and agrees with the considerations presented in the previous section. Indeed, considering the gauge sector in isolation, the CP-even couplings $c_{\widetilde{X}}$ cannot be multiplicatively renormalized since they are multiplied by an effective angle that is 2π periodic. The additional pseudoscalar interactions in the EFT could in principle break the scale invariance of these couplings, as they explicitly break this periodicity. However, no one-loop diagram can be constructed with a single insertion of $s\overline{\psi}\psi\phi$ (or other) terms. On the other hand, the CP-odd couplings c_X are not renormalized because X^2 is the trace of the conserved energy momentum tensor [40].

Regarding the singlet-fermion interactions, our results show that they produce at low energies interactions between the pseudoscalar and the Higgs, both at the renormalizable and non-renormalizable levels. These effects are absent in shift-symmetric scenarios, that is for an ALP, as in this case the fermionic interactions grow with momentum and hence can only renormalize themselves [23]. Furthermore, the presence of the SM Yukawas in the RGEs of the singlet fermionic couplings implies that CP-even UV setups are not, in general, stable upon running.

4 Matching at the electroweak scale

After the Higgs field develops a VEV, at energies $v \sim 246\,\text{GeV}$, the SM particles develop masses. Given the large hierarchy between the masses of the EW bosons and the top quark, in comparison to that of the remaining particles in the SM, the former can be integrated out rendering a simpler low-energy EFT (LEFT). While this theory can be fully general and matched to different models above the EW scale, we present in section 4.2 the tree-level matching results assuming that the singlet s is the only BSM *d.o.f.* in the UV. With this aim, we start by diagonalizing the mass matrix of the scalar sector.

4.1 Scalar mixing

The scalar mass matrix induced by the interactions in our EFT reads

$$\mathbf{M}^2_{\text{eff}} = \mathbf{M}^2_0 + \mathbf{M}^2_1\,, \tag{4.1}$$

where

$$\mathbf{M}^2_0 = \begin{pmatrix} m_s^2 + \frac{\lambda_{s\phi}}{2}v^2 + v_s\left(\kappa_s + \frac{\lambda_s}{2}v_s\right) & v\left(\kappa_{s\phi} + \lambda_{s\phi}v_s\right) \\ v\left(\kappa_{s\phi} + \lambda_{s\phi}v_s\right) & -\mu^2 + 3\lambda v^2 + \kappa_{s\phi}v_s + \frac{\lambda_{s\phi}}{2}v_s^2 \end{pmatrix}, \tag{4.2}$$

and

$$\mathbf{M}_1^2 = \begin{pmatrix} -3a_{s^3}v^2v_s - 20a_{s^5}v_s^3 & -v\left(a_sv^2 + 3a_{s^3}v_s^2\right) \\ -v\left(a_sv^2 + 3a_{s^3}v_s^2\right) & -v_s\left(3a_sv^2 + a_{s^3}v_s^2\right) \end{pmatrix}. \tag{4.3}$$

In the expressions above, v is the observed Higgs VEV, determined from muon decay measurements, while v_s denotes the singlet VEV which solves the tadpole equations

$$\mu^2 = \lambda v^2 + \frac{1}{2}v_s\left(2\kappa_{s\phi} + \lambda_{s\phi}v_s\right) - a_sv^2v_s - a_{s^3}v_s^3\,, \tag{4.4}$$

$$2m_s^2v_s + \kappa_{s\phi}v^2 = -\lambda_{s\phi}v^2v_s - \kappa_sv_s^2 - \frac{\lambda_s}{3}v_s^3 + \frac{a_s}{2}v^4 + 3a_{s^3}v^2v_s^2 + 10a_{s^5}v_s^4\,. \tag{4.5}$$

Moreover, $(v,\, v_s)$ is guaranteed to be a minimum of the scalar potential if it satisfies the following conditions:

$$\mathrm{Det}(\mathbf{M}_{\text{eff}}^2) > 0 \quad \text{and} \quad \mathrm{Tr}(\mathbf{M}_{\text{eff}}^2) > 0\,. \tag{4.6}$$

The mass matrix in eq. (4.2) can be diagonalized by the rotation

$$\begin{pmatrix} s \\ h \end{pmatrix} = \begin{pmatrix} \cos\theta & -\sin\theta \\ \sin\theta & \cos\theta \end{pmatrix}\begin{pmatrix} \hat{s} \\ \hat{h} \end{pmatrix}, \tag{4.7}$$

with

$$\tan 2\theta = \frac{-2a_sv^3 + 40a_{s^5}v_s^4/v - \frac{4}{3}v_s/v\left(6m_s^2 + 3\kappa_sv_s + \lambda_sv_s^2\right)}{\left(4a_s - 6a_{s^3}\right)v^2v_s - 40a_{s^5}v_s^3 + 2m_s^2 + \left(-4\lambda + \lambda_{s\phi}\right)v^2 + v_s\left(2\kappa_s + \lambda_sv_s\right)}\,. \tag{4.8}$$

To obtain this expression, we have used eqs. (4.4) and (4.5) to rewrite $(\mu^2,\, \kappa_{s\phi})$ in terms of the remaining parameters in the EFT. In the absence of CP-odd interactions, $v_s = 0$ is a solution of the tadpole equations consistent with the SM assignment of the Higgs parameters, i.e. $\mu^2 = \lambda v^2$. In this limit, the weak and the physical bases of the scalar sector automatically coincide. From the expression above, it is also clear that at the renormalizable level, if the UV parameters are chosen so that v_s vanishes, no mixing with the Higgs boson can arise. Neglecting the effective interactions, our expressions agree exactly with the results obtained in previous works [12, 15, 41]. Nonetheless and in spite of the popularity of the singlet framework, there are several studies in the literature exploring the consequences of scalar mixing that neglect the implications of $v_s \neq 0$.

The correlation between the singlet VEV and the scalar mixing is broken by the dimension-five interactions. Indeed, if the coupling a_s is generated by the UV model, $h - s$ mixing can arise even for $v_s = 0$. This scenario is very particular as it implies an alignment between renormalizable and effective interactions, $\kappa_{s\phi} \sim a_sv^2$, leading to

$$\tan 2\theta \to \frac{2a_sv^3}{\left(4\lambda + \lambda_{s\phi}\right)v^2 - m_s^2}\,. \tag{4.9}$$

Therefore, in full generality, we keep track of the v_s dependence in the physical couplings arising from this framework:

$$\begin{aligned}\mathcal{L}_{s,h} \supset & -\frac{1}{2}\hat{m}_s^2s^2 - \frac{1}{2}\hat{m}_h^2h^2 - \frac{\hat{\kappa}_s}{3!}s^3 - \frac{\hat{\kappa}_{s^2h}}{2}s^2h - \frac{\hat{\kappa}_{sh^2}}{2}sh^2 - \frac{\hat{\kappa}_h}{3!}h^3 \\ & - \frac{\hat{\lambda}_s}{4!}s^4 - \frac{\hat{\lambda}_{s^3h}}{3!}s^3h - \frac{\hat{\lambda}_{s^2h^2}}{4}s^2h^2 - \frac{\hat{\lambda}_{sh^3}}{3!}sh^3 - \frac{\hat{\lambda}_h}{4!}h^4 \\ & + \hat{a}_{s^5}s^5 + \hat{a}_{s^4h}s^4h + \hat{a}_{s^3h^2}s^3h^2 + \hat{a}_{s^2h^3}s^2h^3 + \hat{a}_{sh^4}sh^4 + \hat{a}_{h^5}h^5\,,\end{aligned} \tag{4.10}$$

JHEP11(2023)133

where for instance the quartic couplings read as

$$\hat{\lambda}_h = 6\,(\lambda - a_s v_s + 4\theta v a_s)\ , \tag{4.11}$$

$$\hat{\lambda}_s = \lambda_s - 24\,(\theta v a_{s^3} + 5 v_s a_{s^5})\ , \tag{4.12}$$

in the small mixing limit. They are related to the physical scalar masses via the relations:

$$\hat{m}_h^2 = 2\lambda v^2 - 2a_s v^2 v_s + \theta \frac{2}{v}\left[2m_s^2 v_s + \kappa_s v_s^2 + \frac{\lambda_s}{3} v_s^3 + a_s \frac{v^4}{2} - 10 a_{s^5} v_s^4\right], \tag{4.13}$$

$$\hat{m}_s^2 = m_s^2 - \hat{m}_h^2 + 2\lambda v^2 + \frac{\lambda_{s\phi}}{2} v^2 + \frac{\lambda_s}{2} v_s^2 + \kappa_s v_s - v_s\left[2a_s v^2 + 3a_{s^3} v^2 + 20 a_s^5 v_s^2\right]. \tag{4.14}$$

It is also interesting to point out the relation between the triple and quartic Higgs couplings in the presence of the singlet, taking into account all effective contributions up to $\mathcal{O}(1/\Lambda)$:

$$\hat{\lambda}_h v - \hat{\kappa}_h = \theta\left[\frac{33}{2} v^2 a_s + 30 \frac{v_s^4}{v^2} a_{s^5} - \frac{v_s}{v^2}\left(6m_s^2 + 3\kappa_s v_s + \lambda_s v_s^2\right)\right]; \tag{4.15}$$

or, in terms of physical parameters,

$$\frac{1}{2}\hat{\lambda}_h v - \hat{\kappa}_h = -\frac{3}{2}\frac{\hat{m}_h^2}{v} + 24\theta \hat{a}_{sh^4} v^2\,. \tag{4.16}$$

From this expression, it follows that the SM relation between the two physical Higgs couplings can only be broken by non-renormalizable singlet interactions.

A similar effect occurs in the singlet-Higgs portal couplings. To give an example, in the particular case of $v_s \to 0$, we find that:

$$\hat{\lambda}_{s^2h^2} - \hat{\kappa}_{s^2h} = \theta\left[\kappa_s + v^2\,(9a_{s^3} - 7a_s)\right], \tag{4.17}$$

where θ is now determined from eq. (4.9). The parameters on the right-hand-side of this equation can be further traded by the physical ones, using the results in appendix C:

$$\hat{\lambda}_{s^2h^2} v - \hat{\kappa}_{s^2h} = \theta\left[\hat{\kappa}_s + 4v^2\,(6\hat{a}_{s^3h^2} - 7\hat{a}_{sh^4})\right]. \tag{4.18}$$

The gauge sector receives also corrections from a non-vanishing v_s. After redefining the gauge couplings,

$$g_i \to \hat{g}_i\,(1 - 2v_s a_{sV_i})\ ,\ \text{with}\ \vec{a}_{sV} = (a_{sB},\, a_{sW},\, a_{sG})\ , \tag{4.19}$$

as well as the gauge bosons

$$V_i \to \hat{V}_i\,(1 + 2v_s a_{sV_i})\ , \tag{4.20}$$

such that the product $g_i V_i$ remains invariant, the physical vector masses read the same as in the SM.[5]

[5]Loop effects can however modify these relations; see for example ref. [42].

Furthermore, the singlet develops renormalizable interactions with the EW gauge bosons due to the mixing with the Higgs particle:

$$\mathcal{L}_{\Phi,V} \supset \sum_{\Phi=s,\,h}\left[\left(c_{\phi Z}+c_{\Phi^2 Z}\Phi\right)\Phi Z^2+\left(c_{\Phi W}+c_{\Phi^2 W}\Phi\right)\Phi W^2\right], \tag{4.21}$$

where

$$c_{hZ}=\frac{\hat{g}_2}{2c_w}m_Z\,,\qquad c_{hW}=\hat{g}_2 m_W\,,\qquad c_{h^2Z}=\frac{\hat{g}_2^2}{8c_w^2}\,,\qquad c_{h^2W}=\frac{\hat{g}_2^2}{4}\,, \tag{4.22}$$

$$c_{sZ}=\frac{\hat{g}_2}{2c_w}\theta m_Z\,,\qquad c_{sW}=\hat{g}_2\theta m_W\,,\qquad c_{s^2Z}=0\,,\qquad c_{s^2W}=0\,. \tag{4.23}$$

In turn, by mixing with the singlet, the Higgs particle can also couple to *all* gauge bosons at the non-renormalizable level:

$$\begin{aligned}\mathcal{L}_{\Phi,V} \supset \sum_{\Phi=s,\,h}\Big[&\hat{a}_{\Phi AA}\Phi A_{\mu\nu}A^{\mu\nu}+\hat{a}_{\Phi ZZ}\Phi Z_{\mu\nu}Z^{\mu\nu}+\hat{a}_{\Phi AZ}\Phi A_{\mu\nu}Z^{\mu\nu}+\hat{a}_{\Phi WW}\Phi W^+_{\mu\nu}W^{-\mu\nu}\\ &+\hat{a}_{\Phi GG}\Phi G^A_{\mu\nu}G^{A\mu\nu}+\hat{a}_{\Phi A\tilde{A}}\Phi A_{\mu\nu}\widetilde{A}^{\mu\nu}+\hat{a}_{\Phi Z\widetilde{Z}}\Phi Z_{\mu\nu}\widetilde{Z}^{\mu\nu}+\hat{a}_{\Phi A\tilde{Z}}\Phi A_{\mu\nu}\widetilde{Z}^{\mu\nu}\\ &+\hat{a}_{\Phi W\widetilde{W}}\Phi W^+_{\mu\nu}\widetilde{W}^{-\mu\nu}+\hat{a}_{\Phi G\tilde{G}}\Phi G^A_{\mu\nu}\widetilde{G}^{A\mu\nu}+\dots\Big],\end{aligned} \tag{4.24}$$

where the ellipsis represent additional 4-body interactions, with at least 2 heavy fields, which will not be important in the discussion that follows. The CP-even couplings above are given by:

$$\begin{aligned}\hat{a}_{sAA}&=c_w^2 a_{sB}+s_w^2 a_{sW}\,, & \hat{a}_{sZZ}&=s_w^2 a_{sB}+c_w^2 a_{sW}\,,\\ \hat{a}_{sAZ}&=2s_w c_w(a_{sW}-a_{sB})\,, & \hat{a}_{sWW}&=2a_{sW}\,,\\ \hat{a}_{sGG}&=a_{sG}\,, & \hat{a}_{hVV}&=-\theta\hat{a}_{sVV}\,,\end{aligned} \tag{4.25}$$

while the CP-odd ones are obtained upon the replacement $V\to\widetilde{V}$ and are in agreement with the expressions in the literature [43]. Note that, in the limit $a_{sW}=a_{sB}$, the singlet coupling to a mixed state of gauge bosons vanishes.

The QCD vacuum also receives contributions from the singlet VEV, as expected from the axion mechanism,

$$\hat{\theta}_{\rm QCD}=\theta_{\rm QCD}+32\frac{\pi^2}{g_3^2}a_{s\tilde{G}}v_s\,. \tag{4.26}$$

Turning to the fermionic sector, we perform the usual unitary rotations into the mass basis [44]:

$$\begin{aligned}\psi_L&\to V_{\psi_L}\psi_L\,,\\ \psi_R&\to V_{\psi_R}\psi_R\,,\end{aligned} \tag{4.27}$$

with $\psi = u, d, e$ and $V_{u_L}^\dagger V_{d_L} \equiv V_{\rm CKM}$, $V_{\rm CKM}$ denoting the CKM matrix. The physical Yukawa couplings are then

$$\hat{y}_u = V_{u_L}^\dagger \left(y_u - i\, a_{su\phi} v_s\right) V_{u_R}\,, \tag{4.28}$$
$$\hat{y}_d = V_{d_L}^\dagger \left(y_d - i\, a_{sd\phi} v_s\right) V_{d_R}\,, \tag{4.29}$$
$$\hat{y}_e = V_{e_L}^\dagger \left(y_e - i\, a_{se\phi} v_s\right) V_{e_R}\,, \tag{4.30}$$

with the usual relation to the fermion masses:

$$\hat{m}_\psi = \frac{v}{\sqrt{2}} \hat{y}_\psi\,. \tag{4.31}$$

The corresponding Lagrangian, including the interactions with the scalar sector, reads:

$$\mathcal{L}_{\Phi,\psi} \supset \sum_{\psi=u,d,e} \Bigg\{ \overline{\psi} i \not{D} \psi - \Big[\overline{\psi_L} \hat{m}_\psi \psi_R + h \bar{\psi}_L \hat{c}_{h\psi} \psi_R - i\, s \bar{\psi}_L \hat{c}_{s\psi} \psi_R \tag{4.32}$$
$$- s^2 \bar{\psi}_L \hat{a}_{s^2\psi} \psi_R - i\, sh \bar{\psi}_L \hat{a}_{sh\psi} \psi_R - h^2 \bar{\psi}_L \hat{a}_{h^2\psi} \psi_R + \text{h.c.} \Big] \Bigg\}\,,$$

where

$$\hat{c}_{s\psi} = \frac{1}{\sqrt{2}} V_{\psi_L}^\dagger \Big[i\,\theta y_\psi + a_{s\psi\phi} \left(v + \theta v_s\right) \Big] V_{\psi_R}\,, \tag{4.33}$$
$$\hat{c}_{h\psi} = \frac{1}{\sqrt{2}} V_{\psi_L}^\dagger \Big[y_\psi - i\, a_{s\psi\phi} \left(v_s - \theta v\right) \Big] V_{\psi_R}\,, \tag{4.34}$$
$$\hat{a}_{s^2\psi} = V_{\psi_L}^\dagger \frac{i\,\theta a_{s\psi\phi}}{\sqrt{2}} V_{\psi_R}\,, \tag{4.35}$$
$$\hat{a}_{h^2\psi} = -\hat{a}_{s^2\psi}\,, \tag{4.36}$$
$$\hat{a}_{sh\psi} = V_{\psi_L}^\dagger \frac{a_{s\psi\phi}}{\sqrt{2}} V_{\psi_R}\,. \tag{4.37}$$

4.2 The low-energy singlet EFT

We can now integrate out the heavy *d.o.f.* to obtain the LEFT description of the interactions among light particles (including the singlet). To dimension-five, the most general and minimal LEFT Lagrangian can be written as

$$\begin{aligned}\mathcal{L}_{\rm LEFT} = {} & \frac{1}{2}(\partial_\mu s)(\partial^\mu s) - \frac{1}{2}\tilde{m}_s^2 s^2 - \frac{\tilde{\kappa}_s}{3!} s^3 - \frac{\tilde{\lambda}_s}{4!} s^4 - \frac{1}{4} G_{\mu\nu}^A G^{A\mu\nu} - \frac{1}{4} A_{\mu\nu} A^{\mu\nu} + \tilde{\theta}_{\rm QCD} G_{\mu\nu}^A \widetilde{G}^{A\mu\nu} \\ & + \sum_{\psi=u,d,e} \Big[\overline{\psi} i \not{D} \psi - \overline{\psi_L} \tilde{m}_\psi \psi_R + i\, s \overline{\psi_L} \tilde{c}_\psi \psi_R + s^2 \overline{\psi_L} \tilde{a}_\psi \psi_R + \text{h.c.} \Big] + \tilde{a}_{s^5} s^5 \\ & + \tilde{a}_{sA} s A_{\mu\nu} A^{\mu\nu} + \tilde{a}_{sG} s G_{\mu\nu}^A G^{A\mu\nu} + \tilde{a}_{s\tilde{A}} s A_{\mu\nu} \widetilde{A}^{\mu\nu} + \tilde{a}_{s\tilde{G}} s G_{\mu\nu}^A \widetilde{G}^{A\mu\nu} \\ & + \sum_{\psi=u,d,e} \Big[\overline{\psi_L} \tilde{a}_{\psi A} \sigma^{\mu\nu} \psi_R A_{\mu\nu} + \overline{\psi_L} \tilde{a}_{\psi G} \sigma^{\mu\nu} T_A \psi_R G_{\mu\nu}^A + \text{h.c.} \Big]\,,\end{aligned} \tag{4.38}$$

where the non-renormalizable couplings are dimensionfull, $\tilde{a} \equiv \tilde{a}^0/v$.

The parameters in this tilde basis can be fully fixed at the scale $\mu = v$ by requiring that both theories, before and after EWSB, describe the same physics. While the RGEs we will derive next include all the couplings in eq. (4.38), below we present the matching equations assuming that the UV model is well described by the SM+s EFT, presented in section 2. At tree level, we obtain:

$$\tilde{\theta}_{\rm QCD} = \hat{\theta}_{\rm QCD}\,, \tag{4.39}$$

$$\tilde{\kappa}_s = \hat{\kappa}_s\,, \qquad \tilde{m}_s = \hat{m}_s\,, \tag{4.40}$$

$$\tilde{\lambda}_s = \hat{\lambda}_s - 3\left(\frac{\hat{\kappa}_{s^2h}}{\hat{m}_h}\right)^2\,, \tag{4.41}$$

$$\tilde{m}_\psi = \hat{m}_\psi\,, \qquad \tilde{c}_\psi = \hat{c}_{s\psi}\,, \tag{4.42}$$

$$\tilde{a}_\psi = \hat{a}_{s^2\psi} + \frac{\hat{\kappa}_{s^2h}\hat{c}_{h\psi}}{\hat{m}_h^2}\,, \tag{4.43}$$

$$\tilde{a}_{s^5} = \hat{a}_{s^5} + \frac{7}{5!}\frac{\hat{\kappa}_{s^2h}\hat{\lambda}_{s^3h}}{\hat{m}_h^2}\,, \tag{4.44}$$

$$\tilde{a}_{sV} = \hat{a}_{sV}, \qquad \text{and} \quad \tilde{a}_{s\widetilde{V}} = \hat{a}_{s\widetilde{V}}\,, \tag{4.45}$$

with all other Wilson coefficients vanishing. Special care needs to be taken with respect to contributions of $\mathcal{O}(\hat{\kappa}_{s^2h}/\hat{m}_h^2)$. While naively they seem to be of the same order as that of operators we are neglecting in the LEFT, in fact $\hat{\kappa}_{s^2h}/\hat{m}_h^2 \sim \mathcal{O}(1/v)$ in the small mixing limit. On the contrary, since $\hat{c}_{h\psi} \sim \mathcal{O}(\tilde{m}_\psi/v)$, the second term in eq. (4.43) should be neglected in our study. Large mixing angles can however spoil this power counting; see eq. (4.13) and appendix C.

Finally, we remark that with the results of the previous section, where we have obtained the full matching to the physical basis including operators with more than one heavy particle, the accuracy of the previous relations could be easily improved beyond tree level.

5 Low-energy anomalous dimensions

The steps to perform renormalization in the LEFT are the same as described in the HE regime. An important difference is however the set of redundant operators that can be induced, at one loop level, by those in eq. (4.38); see appendix B. We have fixed the one-loop divergences of operators in the Green's basis using `matchmakereft` [37]. The subsequent projection onto the minimal basis was performed analytically using the LEFT EOMs [22]. Up to CP-odd terms, the RGEs resulting from this procedure agree exactly with those presented in ref. [22], which were obtained with distinct methods. The full set of equations is written in the `ALPRunner` package published along this work. Here, we discuss only some contributions that we find particularly interesting.

Contrarily to the results in the HE EFT, in the LEFT the singlet-gauge boson couplings can run; for instance:

$$\begin{aligned}\beta_{\tilde{a}_{s\widetilde{G}}} &= \left(-\frac{46}{3}\tilde{g}_3^2 + 2\mathrm{Tr}\left[\tilde{c}_e\tilde{c}_e^\dagger + 3\tilde{c}_d\tilde{c}_d^\dagger + 3\tilde{c}_u\tilde{c}_u^\dagger\right]\right)\tilde{a}_{s\widetilde{G}} \\ &\quad - 2g_3\mathrm{Tr}\left[\tilde{a}_{dG}\tilde{c}_d^\dagger + \tilde{a}_{uG}\tilde{c}_u^\dagger + \mathrm{h.c.}\right]\,,\end{aligned} \tag{5.1}$$

and similarly for $\beta_{\tilde{a}_{sG}}$ upon the replacement $\tilde{a}_{\psi G} \to \mathrm{i}\tilde{a}_{\psi G}$. The first contribution in eq. (5.1) stems entirely from the running of the gauge coupling, such that if all other contributions vanish, $\tilde{c}_{\widetilde{G}} \equiv \tilde{a}_{s\widetilde{G}}/\tilde{g}_3^2$ remains scale invariant. This occurs if the UV physics above EWSB can be described by the SM+s EFT with $\theta \ll 1$, as in this case $\tilde{c}_\psi$ couplings are $\mathcal{O}(1/\Lambda)$. We might still wonder about the additive contributions to this RGE due to the presence of dipole operators, in view of the arguments presented in section 2.1, as these operators could be generated by additional field content in the UV without spoiling shift-symmetry. Nonetheless, if this symmetry is assumed, that is in the ALP scenario, $\tilde{a}_{\psi G}\tilde{c}_\psi$ terms are at most $\mathcal{O}(\Lambda^{-2})$.

Therefore, up to the EFT expansion order considered in this work, the running of $\tilde{a}_{s\widetilde{X}}$ couplings is consistent with the expectations discussed in section 2.1. To test their robustness at one-loop level, the inclusion of dimension-six operators in the ALP EFT is required.

Moreover, we find that no contributions to the mass are generated by the LEFT running assuming the singlet is an ALP. For a generic pseudoscalar however, apart from multiplicative contributions, the mass can be renormalized by the trilinear coupling $\tilde{\kappa}_s^2$ as well as by $\tilde{m}_\psi^2\tilde{c}_\psi^2$ and $\tilde{m}_\psi^3\tilde{a}_\psi$ terms.

In turn, the singlet mass renormalizes the mass of fermions in the LEFT. This contribution is again absent once matching this theory to the ALP EFT in the UV, up to the expansion order we are considering.

Regarding the running of fermionic couplings, we obtain:

$$\begin{aligned}\beta_{\tilde{c}_e} = &-6\tilde{e}^2\tilde{c}_e - 24\tilde{e}^2\tilde{m}_e\tilde{a}_{s\widetilde{A}} - 24i\tilde{e}^2\tilde{m}_e\tilde{a}_{sA} + 2\mathrm{Tr}\left[\tilde{c}_e\tilde{c}_e^\dagger + 3\left(\tilde{c}_u\tilde{c}_u^\dagger + \tilde{c}_d\tilde{c}_d^\dagger\right)\right]\tilde{c}_e \\ &+ 3\tilde{c}_e\tilde{c}_e^\dagger\tilde{c}_e + 2\mathrm{Tr}\left[\tilde{m}_e\tilde{c}_e^\dagger\tilde{a}_e - 2\tilde{a}_e\tilde{m}_e^\dagger\tilde{c}_e + \tilde{a}_e\tilde{c}_e^\dagger\tilde{m}_e - 2\tilde{c}_e\tilde{m}_e^\dagger\tilde{a}_e\right] \\ &- 2i\tilde{\kappa}_s\tilde{a}_e - 12\tilde{e}^2\left(\tilde{m}_e\tilde{c}_e^\dagger\tilde{a}_{eA} - \tilde{a}_{eA}\tilde{m}_e^\dagger\tilde{c}_e + \tilde{a}_{eA}\tilde{c}_e^\dagger\tilde{m}_e - \tilde{c}_e\tilde{m}_e^\dagger\tilde{a}_{eA}\right),\end{aligned} \tag{5.2}$$

simplifying into the first three terms upon the use of eqs. (4.39)–(4.45) in the absence of scalar mixing. Similarly to this case, $\tilde{a}_{sV}\tilde{c}_\psi$ are the only new terms in the RGEs of both $\tilde{a}_\psi$ and $\tilde{a}_{\psi V}$ couplings relatively to the CP-even scenario explored in ref. [22].

The RGE of the singlet self-coupling is also modified in the presence of CP-odd interactions:

$$\beta_{\tilde{\lambda}_s} \supset -480\tilde{\kappa}_s\tilde{a}_{s^5} + 60i\,\tilde{\kappa}_s\mathrm{Tr}\left[\tilde{a}_e^\dagger\tilde{c}_e + 3\left(\tilde{a}_u^\dagger\tilde{c}_u + \tilde{a}_d^\dagger\tilde{c}_d\right) + \text{h.c.}\right], \tag{5.3}$$

where the large deviations from naive dimensional analysis are apparent.

Besides, the running of the pure CP-odd couplings in the theory is given by:

$$\begin{aligned}
\beta_{\tilde{\kappa}_s} &= 3\tilde{\kappa}_s\tilde{\lambda}_s + 6\tilde{\kappa}_s \mathrm{Tr}\left[\tilde{c}_e\tilde{c}_e^\dagger + 3\left(\tilde{c}_u\tilde{c}_u^\dagger + \tilde{c}_d\tilde{c}_d^\dagger\right)\right] + 24i\,\mathrm{Tr}\Big[\tilde{m}_e^\dagger\tilde{c}_e\tilde{c}_e^\dagger\tilde{c}_e + 3\tilde{m}_u^\dagger\tilde{c}_u\tilde{c}_u^\dagger\tilde{c}_u \\
&\quad + 3\tilde{m}_d^\dagger\tilde{c}_d\tilde{c}_d^\dagger\tilde{c}_d + \text{h.c.}\Big] - 120\tilde{m}_s^2\tilde{a}_{s^5} + 60i\,\tilde{m}_s^2\mathrm{Tr}\Big[\tilde{c}_e\tilde{a}_e^\dagger + 3\left(\tilde{c}_u\tilde{a}_u^\dagger + \tilde{c}_d\tilde{c}_a^\dagger\right) + \text{h.c.}\Big] \\
&\quad + 24i\,\mathrm{Tr}\Big[\tilde{m}_e\tilde{m}_e^\dagger\tilde{a}_e\tilde{c}_e^\dagger + \tilde{m}_e\tilde{c}_e^\dagger\tilde{m}_e\tilde{a}_e^\dagger + \tilde{m}_e\tilde{c}_e^\dagger\tilde{a}_e\tilde{m}_e^\dagger + 3\left(\tilde{m}_u\tilde{m}_u^\dagger\tilde{a}_u\tilde{c}_u^\dagger + \tilde{m}_u\tilde{c}_u^\dagger\tilde{m}_u\tilde{a}_u^\dagger\right) \\
&\quad + 3\left(\tilde{m}_u\tilde{c}_u^\dagger\tilde{a}_u\tilde{m}_u^\dagger + \tilde{m}_d\tilde{m}_d^\dagger\tilde{a}_d\tilde{c}_d^\dagger + \tilde{m}_d\tilde{c}_d^\dagger\tilde{m}_d\tilde{a}_d^\dagger + \tilde{m}_d\tilde{c}_d^\dagger\tilde{a}_d\tilde{m}_d^\dagger\right) + \text{h.c.}\Big]\,; \qquad (5.4) \\
\beta_{\tilde{a}_{s^5}} &= 10\tilde{a}_{s^5}\mathrm{Tr}\left[\tilde{c}_e\tilde{c}_e^\dagger + 3\left(\tilde{c}_u\tilde{c}_u^\dagger + \tilde{c}_d\tilde{c}_d^\dagger\right)\right] + \frac{i}{3}\,\tilde{\lambda}_s\mathrm{Tr}\left[\tilde{a}_e\tilde{c}_e^\dagger + 3\left(\tilde{a}_u\tilde{c}_u^\dagger + \tilde{a}_d\tilde{c}_d^\dagger\right) + \text{h.c.}\right] \\
&\quad + 10\tilde{\lambda}_s\tilde{a}_{s^5} + 4i\,\mathrm{Tr}\left[\tilde{a}_e^\dagger\tilde{c}_e\tilde{c}_e^\dagger\tilde{c}_e + 3\left(\tilde{a}_u^\dagger\tilde{c}_u\tilde{c}_u^\dagger\tilde{c}_u + \tilde{a}_d^\dagger\tilde{c}_d\tilde{c}_d^\dagger\tilde{c}_d\right) + \text{h.c.}\right]. \qquad (5.5)
\end{aligned}$$

6 ALPRunner usage: phenomenological application

In this section, we show the non-trivial impact of running in phenomenological studies of the singlet by computing the strongest EDM constraints on particular UV scenarios (where only two BSM couplings are assumed non-zero). We use the EDM expressions obtained in ref. [45].[6] To include all the running effects computed in this work, namely contributions from scalar mixing, we take into account the energy evolution of the couplings involved in such expressions.[7]

Before presenting the results, we illustrate below the main features of the new ALPRunner package. Our EDM analyses are based on dedicated routines which can be generalized to scan the HE parameter space and impose bounds on more general UV scenarios than those considered in this section. The functions available are enumerated in table 3.

Users can download the package from the link in ref. [26] and initialize it in the following way:

```
In[1]:= Needs["ALPRunner'"]

Out[1]=

        SDB, JMR, MR.
        arXiv:2306.08036
```

[6]We found a mismatch by a factor of 4 in the expression for the fermionic contribution to the $G\widetilde{G}G$ Weinberg operator, with respect to the results in ref. [46], the latter leading to stronger bounds.

[7]To avoid double counting, the $\log^2$ contributions obtained in [45], that arise from the (partial) renormalization of the singlet couplings, are not considered.

The complete RGE of a given Wilson coefficient can be obtained via the function '`rge$variable_name`' (e.g. `rge$asB`). Additional functions have been included to solve numerically the running equations for user-given boundary conditions (BCs). In the code line below, the SM BCs (defined at the scale $\Lambda' = 172\,\text{GeV}$) are stored in the list '`smLOWBC`'. The following function finds then the values of the SM couplings at a user-set UV scale ($\Lambda = 10^3\,\text{GeV}$ in the example below), which are compatible with the given low-scale BCs.

```
In[2]:= rgeSMtoΛreset[smLOWBC,10^3,172];
```

The BSM BCs are stored in a different list, '`bsmBC`', defined at the Λ scale. The nomenclature used for the Wilson coefficients in the package is the same as in eq. (2.2). Moreover, we have included a function '`basisChange`' to translate operators from the derivative basis in eq. (2.6) to the EFT basis used in this work. After defining the BCs, the function '`rgePSEFTparamsolvereset`' solves the HE RGEs parametrically.[8] For instance, in the example below, two UV parameters remain free, $a_{s\widetilde{B}} \equiv$ `asBt` and $a_{sB} \equiv$ `asB`:

```
In[3]:= rgePSEFTparamsolvereset[bsmBC,10^3,172,
                                 {{asBt,asBtparam},{asB,asBparam}}];
```

In the next step, we show how to match automatically the HE and the LE EFT couplings, as described in section 4. In this procedure, the UV values of the Higgs coupling and scale, μ and λ, are fixed in order to comply with the experimental constraints[9] $v = 246\,\text{GeV}$ and $\hat{m}_h(v) = 125\,\text{GeV}$ [47]. The singlet VEV is then directly obtained from eqs. (4.4) and (4.5), as well as the mixing angle defined in eq. (4.8). Points $(v,\, v_s)$ which are not minima of the scalar potential are discarded.

Under these conditions and with fixed v_s, the LE BCs are set by the function '`bcLE`', as written below.

```
In[4]:= boundaryConditionLE = bcLE[PSLEFTmatching[172],
                                   rgePSEFTparamsolve,{2*10^-6,3*10^-6}];
```

The first argument in this function requires the matching conditions (defined internally), which are defined in terms of the UV couplings that result from solving parametrically the HE RGEs, given in the second argument. The latter have been evaluated for specific values of $(a_{s\widetilde{B}},\, a_{sB}) = (2 \times 10^{-6},\, 3 \times 10^{-6})$.

Given the LE BCs, the following function solves numerically the LE RGEs, outputing the EFT parameters at a given IR scale (chosen below to be 5 GeV):

```
In[5]:= rgeLEreset[boundaryConditionLE,172,5];
```

[8]If the user wishes to fix numerically the BCs for *all* BSM parameters, the function '`rgePSEFTreset[bsmBC,1000,172]`' should be called instead.

[9]This module is discussed in detail in the notebook file '`ALPRunner_Guide.nb`' [26].

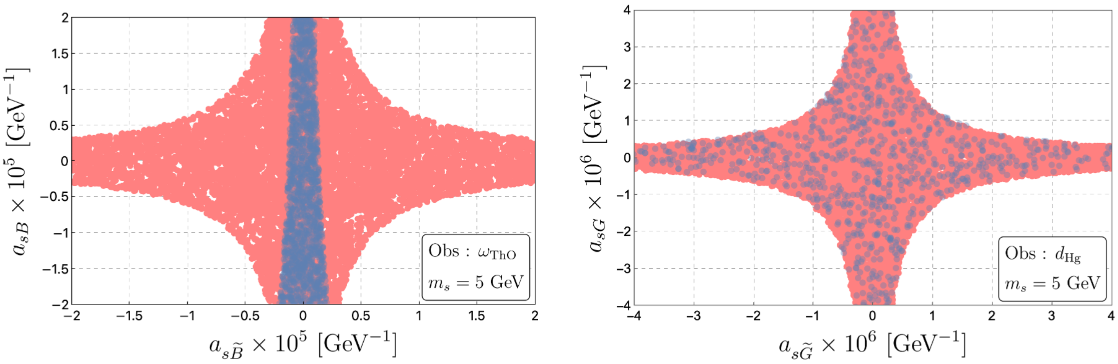

Figure 2. EDM constraints on the UV gauge scenarios discussed in the text for $\Lambda = 1$ TeV and $m_s = 5\,\text{GeV}$. The red points are allowed in the scenarios with vanishing $\kappa_{s\phi}$, but are further constrained to the blue region for $\kappa_{s\phi} = -0.1$. The running of all couplings in the EFT is considered, from the scale Λ down to $\mu = 5\,\text{GeV}$. The leading observable setting the bounds is identified in the plot legend.

After these steps, any LE Wilson coefficients can be determined at a scale $< v$, e.g.

```
In[6]:= WCOsAt[5.2]/.rgeLE

Out[6]= 1.47055*10^-6
```

If the user is interested in generating several UV points, to understand namely which of those are bounded by IR constraints, the following scan function can be used:

```
In[100]:= scanHEspace[bsmBC,1000,172,5,
                {{asBt,asBtparam},{asB,asBparam}},
                {10000,{-5*10^-6,+5*10^-6},{-5*10^-6,+5*10^-6}},
                Observable, "File.m"];
```

where the first argument is the list of HE BCs; the second, third and fourth arguments are, respectively, the UV, matching and IR scales; the fifth is the list of UV parameters that the user chooses to let free (and which are not defined in `bsmBC`); whereas the sixth entry corresponds to the number and interval of random points to be generated. Finally, the two last arguments encode the expression — defined by the user — that will be evaluated at the IR scale, for each point that was generated, and the file where the information will be stored. In the analyses presented below, '`Observable`' is a list of expressions of the different contributions to EDMs induced by the singlet interactions — defined in eq. 9 of ref. [45] — that we have subsequently compared with the relevant experimental bounds, in order to constrain a given UV scenario. Some results are shown in figures 2 and 3.

UV gauge scenarios. Assuming that only $(a_{s\widetilde{B}}, a_{sB})$ are generated by the UV, the constraints presented in the left panel of figure 2 imply that

$$|a_{s\widetilde{B}}\, a_{sB}| \lesssim 6 \times 10^{-11}\ \text{GeV}^{-2}\,, \tag{6.1}$$

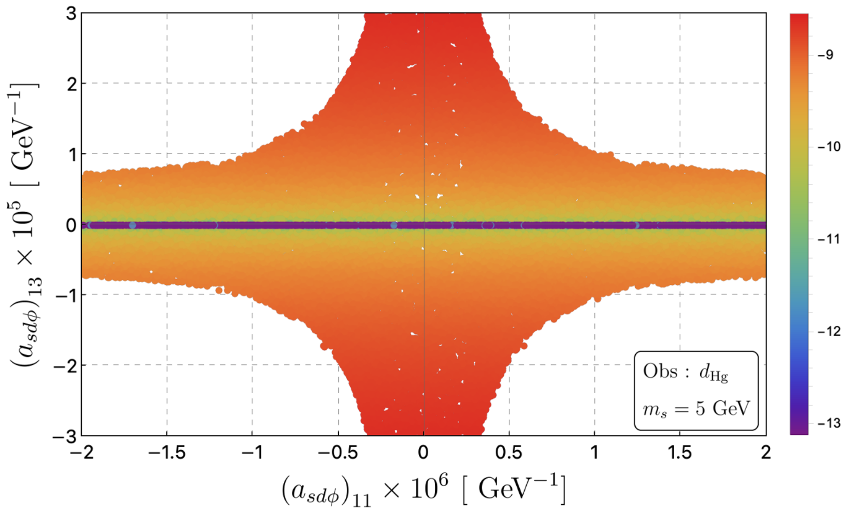

Figure 3. EDM constraints on the fermionic UV scenario discussed in the text for $\Lambda = 1$ TeV and $m_s = 5$ GeV. The leading observable setting the bounds is identified in the plot legend. The colour bar identifies the size (in log scale) of the shift-breaking invariants; see eq. (6.3).

for $m_s = 5$ GeV. This bound is set by measurements of the electron EDM using the molecule ThO [48] and agrees with the results reported in ref. [45]. The results are largely insensitive to m_s. Tree level mixing effects can have a non-negligible contribution to the fermion coupling and therefore modify the bound obtained above. For instance, assuming $\kappa_{s\phi} \sim -0.1$, which leads to $\theta \sim \mathcal{O}(10^{-3})$, we find a stronger constraint on the gauge couplings as represented by the blue points in figure 2, which turns out to be largely independent of a_{sB}. This is because, for a (red) point in the positive quadrant that was allowed by the previous analysis, the θ contribution in eq. (4.33) dominates over the others induced by running. As such, the EDM contribution, which essentially goes as $\mathrm{Re}[\tilde{c}_e]a_{sB} + \mathrm{Im}[\tilde{c}_e]a_{s\widetilde{B}}$ becomes a function of $a_{s\widetilde{B}}$ only. However, the width of the new allowed region is not exactly constant and more points are allowed in the $a_{sB} < 0$ area. This is due to a possible cancellation between the imaginary terms in eq. (4.33), that is, those induced by running vs. those induced by scalar mixing.

In the right panel of figure 2, we have explored another UV scenario where only the singlet-gluon couplings are assumed non-zero. The leading observable setting the bounds in this case is the neutron EDM of the ^{199}Hg atom [49], which requires

$$|a_{s\widetilde{G}}\, a_{sG}| \lesssim 1.3 \times 10^{-12}\ \mathrm{GeV}^{-2}\,, \tag{6.2}$$

for $m_s = 5$ GeV. This bound is within the same order of magnitude than the one obtained in ref. [45][10] and is insensitive to the value of $\kappa_{s\phi}$.

UV fermionic scenarios. In figure 3, we instead explored a UV fermionic scenario where the only non-vanishing couplings are $(a_{sd\phi})_{11}$ and $(a_{sd\phi})_{13}$, assumed to take real

[10] We however do not consider the running of the EDM Lagrangian, eq. (9) in ref. [45], from 5 GeV down to 1 GeV.

values.[11] This setup aims to illustrate an important point: strong EDM bounds can be applied to some CP-even BSM scenarios. The CP violation induced in this case stems from the mixing of the CP-even physics with the SM Yukawa couplings,[12] induced by the fermion mass diagonalization and the RGEs (see table 1). As in the previous case, the leading observable setting the bounds is the neutron EDM.

In figure 3, we have also represented the size of the shift-breaking invariants,[13] i.e.

$$I_\Sigma \equiv \frac{1}{\Lambda}\sqrt{(I_d^1)^2 + (I_d^2)^2 + (I_d^3)^2}\,, \tag{6.3}$$

for each point represented in the plot. We see that the most shift-symmetric points lie close to the horizontal axis. In particular, ALPs lie exactly in the blind direction of the plot, since the UV texture

$$a_{sd\phi}(\Lambda) = \begin{pmatrix} \times & 0 & \times \\ 0 & 0 & 0 \\ 0 & 0 & 0 \end{pmatrix} \tag{6.4}$$

is not compatible with an exact shift-symmetry. Using `ALPRunner`, it is straightforward to generalize this flavour matrix and obtain meaningful bounds in the ALP parameter space.

7 Conclusions

In this work, we have computed the energy evolution of all couplings in the most general EFT obtained by extending the SM with a real (pseudo) scalar singlet. Our results are valid up to one-loop accuracy and order $1/\Lambda$ in the EFT expansion. The renormalization group equations have been furthermore included in a new Mathematica package — `ALPRunner` — with functions to solve the running numerically, as well as to match directly the high-energy with the low-energy EFT couplings, assuming that the singlet is the only BSM *d.o.f.* at energies above the EW scale.

We have found that CP-odd couplings in the singlet EFT are, in general, renormalized by CP-even ones due to the mixing with the Yukawa couplings of the SM. Namely, CP-even fermiophilic scenarios can generate, at low energies, CP-odd couplings between the singlet and the Higgs boson, both at the renormalizable and effective levels. This is possible due to the RGE mixing of operators of different mass dimensions, which is a common feature of both the high-energy and low-energy EFTs. Moreover, BSM operators can renormalize pure SM ones, such as the Higgs quartic coupling. At the matching level, we have computed all effective contributions to scalar mixing, which modify important relations among the physical couplings. In particular, we found that via this mixing and only at dimension-five, the SM relation between the triplet and quartic Higgs couplings can be distorted. Furthermore, it is possible for the singlet to have a vanishing VEV and still mix with the Higgs boson, an effect that is absent in the renormalizable framework, and which could

[11] We work in a UV basis where $V_{d_L} = V_{\rm CKM}$ and $V_{u_L} = 1$.

[12] A general study on the generation of this "opportunistic" CP violation was presented in ref. [50], in the framework of the SM EFT.

[13] These invariants are defined in eq. (5) of ref. [25].

be of phenomenological relevance. (While mixing effects are expected to be small from experimental searches [51], the current interpretations assume correlations that do not necessarily hold at the effective level. A re-interpretation of the experimental analyses is therefore necessary to quantify the actual size of these effects.[14])

Throughout this work, we have also discussed the shift-symmetric limit of our results and showed that they are in perfect agreement with the quantization rules imposed by the ALP periodicity. Conversely, for a generic singlet, the couplings to gauge bosons can in general run and the interpretation of the experimental bounds must take this running effect into account.

Finally, as an application of our results, we obtained EDM bounds on particular UV scenarios. We have shown that the constraints on the singlet couplings to the abelian gauge boson can be significantly impacted by the presence of scalar mixing. Generic constraints on the singlet parameter space can be obtained for more general UV setups using the package presented along this work, as we have explained in section 6. The diagonalization of the scalar and fermion systems has been implemented in the package, as well as the full dependence of the EFT coefficients on the scalar VEVs. An algorithm was included to make sure the UV inputs comply with EW constraints. Finally, the shift-breaking invariants [25] of the singlet EFT have also been defined in the package, such that the phenomenology of a more shift-symmetric singlet, or that of an ALP, can be studied in full detail with `ALPRunner`.

Acknowledgments

We are grateful to Quentin Bonnefoy, Mikael Chala, Víctor Enguita, Renato Fonseca, Belén Gavela, Jonathan Kley, Javier Fuentes-Martín, Luca Merlo and Jorge Fernández de Trocóniz for illuminating discussions, and José Santiago and Pablo Olgoso for helping with `matchmakereft` [37]. We thank Luca Di Luzio and Paride Paradisi for pointing out a misunderstanding in the computation of the EDM contributions. We thank Anisha and Guilherme Guedes for comments on the manuscript, and Sunando Patra for suggestions on Mathematica utilities, and functions imported (and modified) from `CoDEx` [52]. The work of M. R. is supported by the Marie Sklodowska-Curie grant agreement No 860881-HIDDeN. The work of J.M.R. is supported by the Spanish MICIU through the National Program FPI-Severo Ochoa (grant number PRE2019-089233). S.D.B. acknowledges financial support from the Spanish Research Agency (Agencia Estatal de Investigación) under the grants No. PID2019-106087GB-C21/ 10.13039/501100011033 and PID2021-128396NB-100/AEI/10.13039/501100011-033; by the Junta de Andalucía (Spain) under the grants No FQM- 101, A-FQM-467-UGR18 and P18-FR-4314 (FEDER). J.M.R. acknowledges partial financial support from the Spanish Research Agency through the grants IFT Centro de excelencia Severo Ochoa Program No CEX2020-001007-S and PID2019-108892RB-I00, funded by MCIN/AEI/ 10.13039/50110001103. The logo of `ALPRunner` was inspired by output from DALL.E 2 of OpenAI.

[14]For example, new contributions to the coupling s^2h (see eq. (C.3)) could potentially lead to new regions of the parameter space compatible with larger values of θ.

A `ALPRunner` toolbox

Function	Details
`rg$variablename`	Prints the RGE of `variablename`. `Names["rg$*"]` returns the list of all RGE variables.
`rgePSEFTreset`	Solves numerically the RGEs in the unbroken-phase. The output is saved in `rgePSEFT`.
`rgePSEFTparamsolvereset`	Solves parametrically the RGEs in the unbroken-phase. The output is saved in `rgePSEFTparamsolve`.
`PSLEFTmatching`	Matches the unbroken and broken phase EFT couplings.
`bcLE`	Creates the boundary conditions for the `rgeLEreset` function.
`rgeLEreset`	Solves numerically the RGEs in the broken-phase. The output is saved in `rgeLE`.
`scanHEspace`	Scans a multi-dimensional parameter space and accepts/ rejects the points given (user-defined) observables.
`basisChange`	Translates couplings defined in the derivate basis to the one used in this work.
`Iu1`	Evaluates the shift invariant structure 'I_u^1'. All 14 invariants are defined, and are called by 'Iu1', 'Id1', 'Ie1', 'Iud1', etc.

Table 3. Main functions provided by `ALPRunner`. For more details, see '`ALPRunner_Guide.nb`' in [26].

JHEP11(2023)133

B Green's bases

Scalar	Yukawa	Gauge	Derivative
$\mathcal{O}_{s^5} = s^5$	$\mathcal{O}_{su\phi} = is\overline{q_L}\tilde{\phi}u_R$	$\mathcal{O}_{s\widetilde{B}} = sB_{\mu\nu}\widetilde{B}^{\mu\nu}$	$\mathcal{R}_{s\phi\Box} = is\phi^\dagger D^2\phi$
$\mathcal{O}_{s^3} = s^3(\phi^\dagger\phi)$	$\mathcal{O}_{sd\phi} = is\overline{q_L}\phi d_R$	$\mathcal{O}_{s\widetilde{W}} = sW_{\mu\nu}\widetilde{W}^{\mu\nu}$	$\mathcal{R}_{s\Box} = s^2\partial^2 s$
$\mathcal{O}_{s} = s(\phi^\dagger\phi)^2$	$\mathcal{O}_{se\phi} = is\overline{l_L}\phi e_R$	$\mathcal{O}_{s\widetilde{G}} = sG_{\mu\nu}\widetilde{G}^{\mu\nu}$	$\mathcal{R}_{\phi s\Box} = \phi^\dagger\phi\partial^2 s$
		$\mathcal{O}_{sB} = sB_{\mu\nu}B^{\mu\nu}$	$\mathcal{R}_{sq} = is\overline{q_L}\not{D}q_L$
		$\mathcal{O}_{sW} = sW_{\mu\nu}W^{\mu\nu}$	$\mathcal{R}_{sl} = is\overline{l_L}\not{D}l_L$
		$\mathcal{O}_{sG} = sG_{\mu\nu}G^{\mu\nu}$	$\mathcal{R}_{su} = is\overline{u_R}\not{D}u_R$
			$\mathcal{R}_{sd} = is\overline{d_R}\not{D}d_R$
			$\mathcal{R}_{se} = is\overline{e_R}\not{D}e_R$

Table 4. Green's basis of the SM+s EFT at dimension-five [22]. The operators labelled with $\mathcal{R}$ are redundant when evaluating an amplitude on-shell.

Scalar	Yukawa	Gauge	Dipole	Derivative
$\tilde{\mathcal{O}}_{s^5} = s^5$	$\tilde{\mathcal{O}}_{u} = s^2\overline{u_L}u_R$	$\tilde{\mathcal{O}}_{s\widetilde{A}} = sA_{\mu\nu}\widetilde{A}^{\mu\nu}$	$\tilde{\mathcal{O}}_{uA} = \overline{u_L}\sigma^{\mu\nu}u_R A_{\mu\nu}$	$\tilde{\mathcal{R}}_{s\Box} = s^2\partial^2 s$
	$\tilde{\mathcal{O}}_{d} = s^2\overline{d_L}d_R$	$\tilde{\mathcal{O}}_{s\widetilde{G}} = sG_{\mu\nu}\widetilde{G}^{\mu\nu}$	$\tilde{\mathcal{O}}_{dA} = \overline{d_L}\sigma^{\mu\nu}d_R A_{\mu\nu}$	$\tilde{\mathcal{R}}_{u\Box} = \overline{u_L}D^2 u_R$
	$\tilde{\mathcal{O}}_{e} = s^2\overline{e_L}e_R$	$\tilde{\mathcal{O}}_{sA} = sA_{\mu\nu}A^{\mu\nu}$	$\tilde{\mathcal{O}}_{eA} = \overline{e_L}\sigma^{\mu\nu}e_R A_{\mu\nu}$	$\tilde{\mathcal{R}}_{d\Box} = \overline{d_L}D^2 d_R$
		$\tilde{\mathcal{O}}_{sG} = sG_{\mu\nu}G^{\mu\nu}$	$\tilde{\mathcal{O}}_{uG} = \overline{u_L}\sigma^{\mu\nu}T_A u_R G^A_{\mu\nu}$	$\tilde{\mathcal{R}}_{e\Box} = \overline{e_L}D^2 e_R$
			$\tilde{\mathcal{O}}_{dG} = \overline{d_L}\sigma^{\mu\nu}T_A d_R G^A_{\mu\nu}$	$\tilde{\mathcal{R}}_{su_L} = is\overline{u_L}\not{D}u_L$
			$\tilde{\mathcal{O}}_{eG} = \overline{e_L}\sigma^{\mu\nu}T_A e_R G^A_{\mu\nu}$	$\tilde{\mathcal{R}}_{sd_L} = is\overline{d_L}\not{D}d_L$
				$\tilde{\mathcal{R}}_{se_L} = is\overline{e_L}\not{D}e_L$
				$\tilde{\mathcal{R}}_{su_R} = is\overline{u_R}\not{D}u_R$
				$\tilde{\mathcal{R}}_{sd_R} = is\overline{d_R}\not{D}d_R$
				$\tilde{\mathcal{R}}_{se_R} = is\overline{e_R}\not{D}e_R$

Table 5. Green's basis of the SM+s LEFT at dimension-five [22]. The operators labeled with $\mathcal{R}$ are redundant when evaluating an amplitude on-shell.

JHEP11(2023)133

C Scalar couplings in the physical basis

The scalar interactions defined in the physical basis of eq. (4.10) read as follows, in the small mixing angle limit:

$$\hat{\kappa}_s = \kappa_s + v_s\lambda_s + 3\theta v\lambda_{s\phi} - 3\Big[v\,(v + 6\theta v_s)\,a_{s^3} + 20v_s^2 a_{s^5}\Big]\,, \tag{C.1}$$

$$\begin{aligned}\hat{\kappa}_{s^2h} &= -\theta\kappa_s + 2\theta\kappa_{s\phi} - \theta v_s\lambda_s + (v + 2\theta v_s)\,\lambda_{s\phi}\\ &\quad + 3\Big\{\Big[\theta\left(v^2 - 2v_s^2\right) - 2v_s v\Big]a_{s^3} - 2\theta v^2 a_s + 20\theta v_s^2 a_{s^5}\Big\}\,,\end{aligned} \tag{C.2}$$

$$\hat{\kappa}_{sh^2} = \kappa_{s\phi} + 6\theta v\lambda + (v_s - 2\theta v)\,\lambda_{s\phi} - 3\Big[v\,(2\theta v_s + v)\,a_s + v_s\,(v_s - 4\theta v)\,a_{s^3}\Big]\,, \tag{C.3}$$

$$\hat{\kappa}_h = 3\Big\{2v\lambda - \theta\kappa_{s\phi} - \theta v_s\lambda_{s\phi} + \Big[v\,(3\theta v - 2v_s)\,a_s + 3\theta v_s^2 a_{s^3}\Big]\Big\}\,, \tag{C.4}$$

$$\hat{\lambda}_s = \lambda_s - 24\,(\theta v a_{s^3} + 5v_s a_{s^5})\;, \tag{C.5}$$

$$\hat{\lambda}_{s^3h} = -\theta\lambda_s + 3\theta\lambda_{s\phi} + 6\Big[-(3\theta v_s + v)\,a_{s^3} + 20\theta v_s a_{s^5}\Big]\,, \tag{C.6}$$

$$\hat{\lambda}_{s^2h^2} = \lambda_{s\phi} - 6\Big[2\theta v a_s + (v_s - 2\theta v)\,a_{s^3}\Big]\,, \tag{C.7}$$

$$\hat{\lambda}_{sh^3} = 3\Big\{2\theta\lambda - \theta\lambda_{s\phi} + 2\Big[-(\theta v_s + v)\,a_s + 3\theta v_s a_{s^3}\Big]\Big\}\,, \tag{C.8}$$

$$\hat{\lambda}_h = 6\Big[\lambda - a_s\,(v_s - 4\theta v)\Big]\,, \tag{C.9}$$

$$\hat{a}_{s^5} = a_{s^5}\;, \tag{C.10}$$

$$\hat{a}_{s^4h} = \theta\,(a_{s^3} - 5a_{s^5})\;, \tag{C.11}$$

$$\hat{a}_{s^3h^2} = \frac{a_{s^3}}{2}\,, \tag{C.12}$$

$$\hat{a}_{s^2h^3} = \theta\left(a_s - \frac{3}{2}a_{s^3}\right)\;, \tag{C.13}$$

$$\hat{a}_{sh^4} = \frac{a_s}{4}\,, \tag{C.14}$$

$$\hat{a}_{h^5} = -\frac{\theta}{4}a_s\,. \tag{C.15}$$

References

[1] M. Bauer, M. Neubert and A. Thamm, *Collider probes of axion-like particles*, *JHEP* **12** (2017) 044 [arXiv:1708.00443] [INSPIRE].

[2] D.B. Kaplan and H. Georgi, SU(2) × U(1) *breaking by vacuum misalignment*, *Phys. Lett. B* **136** (1984) 183 [INSPIRE].

[3] D.B. Kaplan, H. Georgi and S. Dimopoulos, *Composite Higgs scalars*, *Phys. Lett. B* **136** (1984) 187 [INSPIRE].

JHEP11(2023)133

[4] B. Gripaios, A. Pomarol, F. Riva and J. Serra, *Beyond the minimal composite Higgs model*, *JHEP* **04** (2009) 070 [arXiv:0902.1483] [INSPIRE].

[5] M. Chala, $h \to \gamma\gamma$ *excess and dark matter from composite Higgs models*, *JHEP* **01** (2013) 122 [arXiv:1210.6208] [INSPIRE].

[6] L. Vecchi, *The natural composite Higgs*, arXiv:1304.4579 [INSPIRE].

[7] B. Bellazzini, C. Csáki and J. Serra, *Composite Higgses*, *Eur. Phys. J. C* **74** (2014) 2766 [arXiv:1401.2457] [INSPIRE].

[8] G. Cacciapaglia, G. Ferretti, T. Flacke and H. Serôdio, *Light scalars in composite Higgs models*, *Front. in Phys.* **7** (2019) 22 [arXiv:1902.06890] [INSPIRE].

[9] J. McDonald, *Gauge singlet scalars as cold dark matter*, *Phys. Rev. D* **50** (1994) 3637 [hep-ph/0702143] [INSPIRE].

[10] C.P. Burgess, M. Pospelov and T. ter Veldhuis, *The minimal model of nonbaryonic dark matter: a singlet scalar*, *Nucl. Phys. B* **619** (2001) 709 [hep-ph/0011335] [INSPIRE].

[11] G. Arcadi, A. Djouadi and M. Raidal, *Dark matter through the Higgs portal*, *Phys. Rept.* **842** (2020) 1 [arXiv:1903.03616] [INSPIRE].

[12] S. Profumo, M.J. Ramsey-Musolf and G. Shaughnessy, *Singlet Higgs phenomenology and the electroweak phase transition*, *JHEP* **08** (2007) 010 [arXiv:0705.2425] [INSPIRE].

[13] J.R. Espinosa, B. Gripaios, T. Konstandin and F. Riva, *Electroweak baryogenesis in non-minimal composite Higgs models*, *JCAP* **01** (2012) 012 [arXiv:1110.2876] [INSPIRE].

[14] M. Chala, G. Nardini and I. Sobolev, *Unified explanation for dark matter and electroweak baryogenesis with direct detection and gravitational wave signatures*, *Phys. Rev. D* **94** (2016) 055006 [arXiv:1605.08663] [INSPIRE].

[15] J. Ellis et al., *The scalar singlet extension of the standard model: gravitational waves versus baryogenesis*, *JHEP* **01** (2023) 093 [arXiv:2210.16305] [INSPIRE].

[16] E. Witten, *Some properties of* $O(32)$ *superstrings*, *Phys. Lett. B* **149** (1984) 351 [INSPIRE].

[17] T. Banks and M. Dine, *Couplings and scales in strongly coupled heterotic string theory*, *Nucl. Phys. B* **479** (1996) 173 [hep-th/9605136] [INSPIRE].

[18] R.D. Peccei and H.R. Quinn, *Constraints imposed by CP conservation in the presence of instantons*, *Phys. Rev. D* **16** (1977) 1791 [INSPIRE].

[19] R.D. Peccei and H.R. Quinn, *CP conservation in the presence of instantons*, *Phys. Rev. Lett.* **38** (1977) 1440 [INSPIRE].

[20] S. Weinberg, *A new light boson?*, *Phys. Rev. Lett.* **40** (1978) 223 [INSPIRE].

[21] F. Wilczek, *Problem of strong* P *and* T *invariance in the presence of instantons*, *Phys. Rev. Lett.* **40** (1978) 279 [INSPIRE].

[22] M. Chala, G. Guedes, M. Ramos and J. Santiago, *Running in the ALPs*, *Eur. Phys. J. C* **81** (2021) 181 [arXiv:2012.09017] [INSPIRE].

[23] M. Bauer et al., *The low-energy effective theory of axions and ALPs*, *JHEP* **04** (2021) 063 [arXiv:2012.12272] [INSPIRE].

[24] J. Bonilla, I. Brivio, M.B. Gavela and V. Sanz, *One-loop corrections to ALP couplings*, *JHEP* **11** (2021) 168 [arXiv:2107.11392] [INSPIRE].

JHEP11(2023)133

[25] Q. Bonnefoy, C. Grojean and J. Kley, *Shift-invariant orders of an axionlike particle*, *Phys. Rev. Lett.* **130** (2023) 111803 [arXiv:2206.04182] [INSPIRE].

[26] S. Das Bakshi, J. Machado and M. Ramos., *ALPRunner GitHub repository*, https://github.com/sdbakshi13/ALPRunner.

[27] D. O'Connell, M.J. Ramsey-Musolf and M.B. Wise, *Minimal extension of the standard model scalar sector*, *Phys. Rev. D* **75** (2007) 037701 [hep-ph/0611014] [INSPIRE].

[28] V. Barger et al., *LHC phenomenology of an extended standard model with a real scalar singlet*, *Phys. Rev. D* **77** (2008) 035005 [arXiv:0706.4311] [INSPIRE].

[29] B. Gripaios and D. Sutherland, *An operator basis for the standard model with an added scalar singlet*, *JHEP* **08** (2016) 103 [arXiv:1604.07365] [INSPIRE].

[30] H. Georgi, D.B. Kaplan and L. Randall, *Manifesting the invisible axion at low-energies*, *Phys. Lett. B* **169** (1986) 73 [INSPIRE].

[31] P. Agrawal et al., *Some open questions in axion theory*, in the proceedings of the *Snowmass* 2021, (2022) [arXiv:2203.08026] [INSPIRE].

[32] K. Fraser and M. Reece, *Axion periodicity and coupling quantization in the presence of mixing*, *JHEP* **05** (2020) 066 [arXiv:1910.11349] [INSPIRE].

[33] I. Brivio et al., *ALPs effective field theory and collider signatures*, *Eur. Phys. J. C* **77** (2017) 572 [arXiv:1701.05379] [INSPIRE].

[34] A. Alloul et al., *FeynRules* 2.0 *— a complete toolbox for tree-level phenomenology*, *Comput. Phys. Commun.* **185** (2014) 2250 [arXiv:1310.1921] [INSPIRE].

[35] T. Hahn, *Generating Feynman diagrams and amplitudes with FeynArts* 3, *Comput. Phys. Commun.* **140** (2001) 418 [hep-ph/0012260] [INSPIRE].

[36] T. Hahn, S. Paßehr and C. Schappacher, *FormCalc* 9 *and extensions*, *PoS* **LL2016** (2016) 068 [arXiv:1604.04611] [INSPIRE].

[37] A. Carmona, A. Lazopoulos, P. Olgoso and J. Santiago, *Matchmakereft: automated tree-level and one-loop matching*, *SciPost Phys.* **12** (2022) 198 [arXiv:2112.10787] [INSPIRE].

[38] L.F. Abbott, *Introduction to the background field method*, *Acta Phys. Polon. B* **13** (1982) 33 [INSPIRE].

[39] B.M. Gavela, E.E. Jenkins, A.V. Manohar and L. Merlo, *Analysis of general power counting rules in effective field theory*, *Eur. Phys. J. C* **76** (2016) 485 [arXiv:1601.07551] [INSPIRE].

[40] C. Grojean, E.E. Jenkins, A.V. Manohar and M. Trott, *Renormalization group scaling of Higgs operators and* $\Gamma(h \to \gamma\gamma)$, *JHEP* **04** (2013) 016 [arXiv:1301.2588] [INSPIRE].

[41] A. Beniwal, M. Lewicki, M. White and A.G. Williams, *Gravitational waves and electroweak baryogenesis in a global study of the extended scalar singlet model*, *JHEP* **02** (2019) 183 [arXiv:1810.02380] [INSPIRE].

[42] M. Aiko and M. Endo, *Electroweak precision test of axion-like particles*, *JHEP* **05** (2023) 147 [arXiv:2302.11377] [INSPIRE].

[43] J. Bonilla et al., *The cost of an ALP solution to the neutral B-anomalies*, *JHEP* **02** (2023) 138 [arXiv:2209.11247] [INSPIRE].

[44] P. Langacker, *Grand unified theories and proton decay*, *Phys. Rept.* **72** (1981) 185 [INSPIRE].

[45] L. Di Luzio, R. Gröber and P. Paradisi, *Hunting for CP-violating axionlike particle interactions*, *Phys. Rev. D* **104** (2021) 095027 [arXiv:2010.13760] [INSPIRE].

[46] W. Dekens et al., *Unraveling models of CP violation through electric dipole moments of light nuclei*, *JHEP* **07** (2014) 069 [arXiv:1404.6082] [INSPIRE].

[47] Particle Data Group collaboration, *Review of particle physics*, *PTEP* **2022** (2022) 083C01 [INSPIRE].

[48] ACME collaboration, *Improved limit on the electric dipole moment of the electron*, *Nature* **562** (2018) 355 [INSPIRE].

[49] B. Graner, Y. Chen, E.G. Lindahl and B.R. Heckel, *Reduced limit on the permanent electric dipole moment of* ^{199}*Hg*, *Phys. Rev. Lett.* **116** (2016) 161601 [*Erratum ibid.* **119** (2017) 119901] [arXiv:1601.04339] [INSPIRE].

[50] Q. Bonnefoy, E. Gendy, C. Grojean and J.T. Ruderman, *Opportunistic CP violation*, *JHEP* **06** (2023) 141 [arXiv:2302.07288] [INSPIRE].

[51] R.K. Ellis et al., *Physics briefing book: input for the European strategy for particle physics update* 2020, arXiv:1910.11775 [INSPIRE].

[52] S. Das Bakshi, J. Chakrabortty and S.K. Patra, *CoDEx: Wilson coefficient calculator connecting SMEFT to UV theory*, *Eur. Phys. J. C* **79** (2019) 21 [arXiv:1808.04403] [INSPIRE].

Part III

Conclusions

Conclusions

This thesis is devoted to explore and expand our current knowledge of the *phenomenology of axion-like particles*, which are the telltale signs of hidden global symmetries. ALPs are neutral pseudoscalar pseudo-Goldstone bosons arising from any BSM spontaneously broken global symmetry. Therefore, their motivation extends beyond *axions* and the strong-CP problem. Due to their pGB nature, ALPs are more conveniently studied in the (model-idependent) EFT framework. We use the linear ALP EFT throughout this work, plus computational tools, including new ones developed within.

ALPs at colliders

In Chapter 4 [1] we have proposed a new search window for ALPs at colliders: EW vector boson scattering proccesses at the LHC, mediated by a very off-shell or *nonresonant* ALP, i.e. too light to be produced resonantly. We have reinterpreted four Run 2 public CMS VBS analyses targetting the production of ZZ, $Z\gamma$, $W^{\pm}\gamma$, $W^{\pm}Z$ and same-sign $W^{\pm}W^{\pm}$ pairs in association with two jets [234–237].

Nonresonant ALP searches were proposed for the first time in Ref. [146] in the context of ALP-mediated diboson production. The authors illustrate the power of this kind of searches by deriving new limits on the product of the ALP coupling to gluons and the ALP couplings to the EW gauge bosons, from gluon-initiated diboson production data [264, 265]. In our work we have studied for the first time nonresonant ALP signals in EW VBS processes at the LHC, making use of the first Run 2 measurements of VBS processes reported by the CMS Collaboration [234–237]. The main advantages of combining nonresonant ALP searches and VBS are three:

- Signals and limits are independent of the ALP mass and decay width for masses up to 100 GeV.
- The derivative nature of ALP interactions cause a harder scaling with energy than usual SM-mediated channels, causing deviations in the tails of the invariant/transverse mass spectra.
- VBS provides access to the ALP couplings to the EW gauge bosons independently of the coupling to gluons.

New upper limits in the gauge-invariant ALP-EW parameter space $(c_{\widetilde{W}}/f_a, c_{\widetilde{B}}/f_a)$ have been obtained and projected onto the phenomenological ALP couplings to EW gauge bosons $\{g_{a\gamma\gamma}, g_{a\gamma Z}, g_{aZZ}, g_{aWW}\}$ to facilitate the comparison with other results. Among the five VBS channels considered, the most constraining bounds are currently set by $Z\gamma$ and $W^{\pm}W^{\pm}$. Our results are very competitive with other collider limits, and also probe previously unexplored regions of the ALP parameter space for masses up to 100 GeV.

We have obtained conservative projected limits for higher integrated luminosities up to 3000 fb^{-1}. The key observation is that —using this novel technique— a discovery window for ALPs is still open at the LHC when operating at its full luminosity. Already at Run 3, limits can be improved with respect to those derived from the four Run 2 CMS analyses [234–237], and even more so if dedicated experimental searches at ATLAS and CMS with optimized strategies for nonresonant ALP-mediated VBS processes take place. Furthermore, promising preliminary results of ongoing research indicate that our limits can be further improved at Run 3 if the resonant region is included in the analysis.

In Chapter 5 [3], we have explored the one-loop impact of ALP-neutrino couplings on ALP interactions with EW gauge bosons. We have explicitly respected the gauge invariance of the ALP EFT, which implies to consider simultaneously ALP couplings to neutrinos and charged leptons. Thus, in contrast with previous literature, our analysis goes beyond the one-coupling-at-a-time paradigm, exploring how the limits on ALP-neutrino interactions change dependending on ALP interactions with charged leptons.

Up to the negligible effect of neutrino masses, the trace of ALP-neutrino couplings can be traded fully by ALP interactions with EW gauge bosons with couplings $\{g_{a\gamma\gamma}, g_{a\gamma Z}, g_{aZZ}, g_{aWW}\}$, via the chiral anomaly. This allows to recast constraints on ALP-EW anomalous couplings into bounds on ALP-neutrino couplings. We have recasted bounds from different type of experiments, which hold barring underlying symmetries in the UV or fine-tuned cancellations between the loop-induced effects studied here and other contributions.

While related loop-induced bounds have been previously obtained from low-energy data in one-coupling-at-a-time analyses of data from rare meson decays as well as astrophysical/cosmological observations [149, 249, 271], limits extracted from collider data are presented here for the first time. These probe novel territory in the ALP-neutrino parameter space, and span over a wide range of ALP masses up to $\sim 10^3$ GeV. Particularly, constraints from heavy ALP searches at colliders have a strong impact. Sizable ALP-EW interactions are still allowed at present. This work evidences the potential of future high-energy searches targeting ALP-EW couplings to indirectly probe the ALP-neutrino parameter space.

ALP effective field theory

We have presented the full renormalization group equations of the SMEFT extended with a real scalar singlet up to dimension-five with one-loop accuracy and compared it with the RGEs for the ALP. All CP-violating and shift-breaking interactions, as well as mixing effects in the scalar sector, are taken into account. The ALP EFT corresponds to the "shift-symmetric limit" of the singlet EFT. In fact, the general basis adopted in our work can be used to study ALP phenomenology, making use of the complete set of flavor invariants built in Ref. [153], which quantify the amount of shift-symmetry breaking in the EFT.

We have found that CP-odd interactions in the singlet EFT are in general renormalized by CP-even ones due to the mixing with the Yukawa couplings of the SM. For instance, a CP-even fermiophilic singlet scenario in the UV can lead to CP-violating portal interactions with the Higgs boson at low energies, both at the renormalizable and effective level. Moreover, new physics couplings can renormalize SM operators, such as the Higgs quartic coupling. Concerning mixing effects in the scalar sector we find: *(i)* a mixing-induced distortion of the SM relation between the triple and quartic Higgs couplings; *(ii)* that a vanishing singlet *vev* and a non-zero mixing with the Higgs are compatible. This mixing phenomenology arises only at dimension five and goes beyond correlations commonly assumed in the literature.

The singlet EFT RGEs are furthermore included in our new `Mathematica` package —`ALPRunner` [280]—, which provides functions that solve the running numerically and match the high-energy couplings with those in the low-energy EFT. Additional functionalities include:

- Algorithm to ensure EW constraints given a set of UV parameters.
- Diagonalization of the scalar and fermion masses.
- Tool to translate low-energy bounds into constraints on a multi-dimensional UV parameter space.
- Evaluation of the shift-breaking flavor invariants [153], which allows to study in detail the phenomenology of a "true" ALP.

Finally, as an application of our study, we have obtained bounds on ALP parameters from EDM constraints for three particular cases: *(i)* ALP couplings to the anomalous and kinetic terms of the weak hypercharge gauge boson B; *(ii)* analogous couplings to gluons; and *(iii)* CP-even ALP couplings to quarks[1]. We have proved that constraints on ALP-gauge couplings are notably affected by ALP-Higgs mixing in the first scenario, while unchanged in the second. Finally, the third case illustrates that strong EDM bounds can be applied to CP-even BSM scenarios.

This last work is the most complete study of the singlet EFT presented in the literature so far. It improves significantly our understanding of the phenomenology of scalar extensions of the SM, the impact of running and mixing, as well as that of CP-violating and shift-breaking interactions. The full set of RGEs as well as the `ALPRunner` package consitute useful tools for future phenomenological analyses looking for BSM physics signals in the scalar sector.

[1]In this scenario the only source of CP violation is the SM CKM matrix.

Conclusiones

Esta tesis está dedicada a explorar y expandir nuestro conocimiento actual de la *fenomenología de partículas tipo axión* (o *ALPs* por sus siglas en inglés), que son señales distintivas de simetrías globales ocultas. Las ALPs son partículas pseudoscalares neutras, pseudo-bosones de Goldstone (pBG), que surgen de cualquier nueva simetría global —es decir, más allá del modelo estándar,— rota espontáneamente. Por lo tanto, su motivación va más allá de los *axiones* y del problema de CP fuerte. Debido a su naturaleza de pBG, los ALPs se estudian de manera más conveniente, independientemente del modelo de ALPs, en el marco de las teorías efectivas de campos (TEC). Utilizamos la TEC lineal del ALP a lo largo en este trabajo, además de herramientas computacionales de simulación y cálculo especializadas, incluidas algunas nuevas desarrolladas a lo largo de esta tésis..

ALPs en colisionadores

En el Capítulo 4 [1] hemos propuesto una nueva ventana de búsqueda para ALPs en colisionadores: procesos de *scattering* de bosones vectoriales electrodébiles (o *VBS* por sus siglas en inglés) en el LHC, mediados por un ALP no resonante, es decir, demasiado ligero para ser producido resonantemente. Hemos reinterpretado cuatro análisis públicos de VBS del Run 2 de CMS que apuntan a la producción de pares ZZ, $Z\gamma$, $W^{\pm}\gamma$, $W^{\pm}Z$ y $W^{\pm}W^{\pm}$ en asociación con dos jets [234–237].

Las búsquedas de ALP no resonantes fueron propuestas por primera vez en la Ref. [146] en el contexto de la producción de dibosones mediada por ALPs. Los autores ilustran el poder de este tipo de búsquedas obteniendo nuevos límites sobre el producto del acoplo del ALP a gluones y los acoplos del ALP a los bosones electrodébiles, a partir de medidas de producción de dibosones iniciada por gluones [264, 265]. En nuestro trabajo, hemos estudiado por primera vez señales de ALP no resonantes en procesos VBS en el LHC utilizando las primeras medidas del *Run 2* de procesos VBS reportadas por la Colaboración CMS [234–237]. Las principales ventajas de combinar búsquedas de ALP no resonantes y VBS son tres:

- Las señales y los límites son independientes de la masa y la anchur de desintegración del ALP para masas de hasta 100 GeV.
- La naturaleza derivativa de las interacciones del ALP causa un aumento más pronunciado con la energía que en los canales habituales mediados por el SM, provocando desviaciones en las colas de los espectros de masa invariante/transversa.
- Los procesos de VBS permiten acceder a los acoplos del ALP con los bosones de electrodébiles, independientemente del acoplo a gluones.

Se han obtenido nuevos límites superiores en el espacio de parámetros de los acoplos electrodébiles del ALP ($c_{\widetilde{W}}/f_a, c_{\widetilde{B}}/f_a$) y se han proyectado sobre los acoplos fenomenológicos del ALP a los bosones de *gauge* electrodébiles $\{g_{a\gamma\gamma}, g_{a\gamma Z}, g_{aZZ}, g_{aWW}\}$ para facilitar la comparación con otros resultados. Entre los cinco canales de VBS considerados, los límites más restrictivos proceden de los canales $Z\gamma$ y $W^{\pm}W^{\pm}$. Los resultados obtenidos son muy competitivos con otros límites de colisionadores, y también exploran regiones nuevas del espacio de parámetros del ALP para masas de hasta 100 GeV.

Hemos obtenido límites conservadores proyectados a luminosidades integradas más altas de hasta 3000 fb^{-1}. La clave es que —usando esta nueva técnica— hay una ventana de descubrimiento de ALPs abierta en el LHC, cuando éste opere a su máxima luminosidad. Ya en el *Run 3*, los límites pueden mejorarse con respecto a los derivados de los cuatro análisis públicos del *Run 2* de CMS [234–237], y aún más si se llevan a cabo búsquedas experimentales dedicadas en ATLAS y CMS con estrategias optimizadas para procesos de VBS mediados por ALPs no resonantes. Además, resultados preliminares prometedores de una investigación en curso indican que nuestros límites pueden mejorarse aún más en el *Run 3* si se incluye la región resonante en el análisis.

En el Capítulo 5 [3], hemos explorado el impacto a un *loop* de los acoplos ALP-neutrino en las interacciones de ALP con bosones *gauge* electrodébiles. Hemos respetado explícitamente la *gauge* de la TEC del ALP, lo que implica considerar simultáneamente los acoplos del ALP a neutrinos y leptones cargados. Por lo tanto, a diferencia de la literatura anterior, nuestro análisis va más allá del paradigma de un acoplo a la vez, explorando cómo los límites sobre las interacciones ALP-neutrino cambian dependiendo de las interacciones del ALP con leptones cargados.

Ignorando efectos despreciables debidos a las masas de los neutrinos, la traza de los acoplos ALP-neutrino puede intercambiarse por completo por interacciones del ALP con los bosones *gauge* electrodébiles, con acoplos $\{g_{a\gamma\gamma}, g_{a\gamma Z}, g_{aZZ}, g_{aWW}\}$, a través de la anomalía quiral. Esto permite "traducir" los límites que afectan al espacio de parámetros de los acoplos anómalos ALP-EW en límites sobre los acoplos ALP-neutrino. Hemos reformulado los límites de diferentes tipos de experimentos, que se mantienen a menos que haya simetrías subyacentes en el UV o cancelaciones finas entre los efectos a un*loop* estudiados aquí y otras contribuciones.

Aunque en la literatura hay límites similares inducidos a un *loop* considerando un acoplo a la vez en análisis de datos de experimentos a baja energía, como decaimientos raros de mesones, u observaciones astrofísicas/cosmológicas [149, 249, 271], los límites obtenidos a partir de datos de colisionadores se presentan aquí por primera vez. Exploran un territorio novedoso en el espacio de parámetros ALP-neutrino y abarcan un amplio rango de masas de ALPs de hasta $\sim 10^3$ GeV. Concretamente, los límites derivados de búsquedas de ALPs pesados en colisionadores tienen un notorio impacto. Las interacciones del ALP con los bosones *gauge* electrodébiles siguen estando considerablemente permitidas en la actualidad. Este trabajo evidencia el potencial de futuras búsquedas de alta energía enfocadas en las interacciones ALP-bosones electrodébiles y, por lo tanto, indirectamente, en los acoplos ALP-neutrino.

Teoría efectiva de campos de ALP

Hemos presentado las ecuaciones completas del grupo de renormalización de la TEC del Modelo Estándar (ME) —conocida como *SMEFT*, por sus siglas en inglés— extendida con un singlete escalar real hasta dimensión cinco y con precisión de un *loop*, y las hemos comparado con las ecuaciones del grupo de renormalización (EGR) del ALP. Todas las interacciones que violan la simetría CP y *shift*, así como los efectos de mezcla en el sector escalar, se han tenido en cuenta. La TEC del ALP corresponde al límite en que se preserva la simetría *shift* en la TEC del singlete escalar. De hecho, la base de operadores adoptada en nuestro trabajo puede emplearse para estudiar la fenomenología del ALP, haciendo uso del conjunto completo de invariantes de sabor construidos en la Ref. [153], que cuantifican la cantidad de ruptura de simetría *shift* en la TEC.

Hemos concluído que las interacciones antisimétricas bajo CP en la TEC del singlete escalar son renormalizadas en general por las interacciones que preservan CP debido a la mezcla con los acoplos Yukawa del ME. Por ejemplo, un escenario con un singlete escalar "fermiofílico" que preserve la simetría CP en la TEC a altas energías puede originar interacciones "portal" entre el Higgs y el singlete que violen CP a bajas energías, tanto a nivel renormalizable como efectivo. Además, los acoplos de nueva física pueden renormalizar los operadores del ME, como el acoplo cuártico del Higgs. En cuanto a los efectos de mezcla en el sector escalar, encontramos: *(i)* una distorsión respecto al ME de la relación entre los acoplos triples y cuárticos del Higgs; *(ii)* que un valor esperado del vacío o *vev* nulo para el singlete escalar es compatible con efectos de mezcla con el Higgs. Esta fenomenología de mezcla surge sólo a dimensión cinco y va más allá de las correlaciones comúnmente asumidas en la literatura.

Las EGR de la TEC del singlete escalar están además incluidas en nuestro nuevo paquete de `Mathematica` —`ALPRunner` [280]—, que proporciona funciones que resuelven el *running* numéricamente y realizan el *matching* de los acoplos de alta energía con los de la TEC a baja energía. Las funcionalidades adicionales incluyen:

- Algoritmo para asegurar las restricciones electrodébiles dado un conjunto de parámetros en el UV.
- Diagonalización de las masas escalares y fermiónicas.
- Herramienta para traducir límites de baja energía en restricciones sobre un espacio multidimensional de parámetros de la TEC a altas energías.
- Evaluación de los invariantes de sabor que rompen la simetría *shift* [153], que permite estudiar en detalle la fenomenología de un "verdadero" ALP.

Finalmente, como una aplicación de nuestro estudio, hemos obtenido límites sobre los parámetros del ALP a partir de restricciones al momento dipolar eléctrico (MDE) para tres casos particulares: *(i)* acoplos del ALP a los términos anómalos y cinéticos del bosón de hypercarga débil B; *(ii)* acoplos análogos al caso anterior, pero a gluones; y *(iii)* acoplos del ALP a quarks simétricos bajo transformaciones de CP[2]. Hemos demostrado que los límites sobre los acoplos ALP-*gauge* se ven notablemente afectados por los efectos de mezcla ALP-Higgs en el primer escenario, mientras que permanecen inalterados en el segundo. Finalmente, el tercer caso ilustra que fuertes límites derivados del MDE pueden aplicarse a escenarios más allá del ME que son simétricos bajo CP.

Este último trabajo es el estudio más completo de la TEC de un singlete escalar real presentado en la literatura hasta la fecha. Mejora significativamente nuestra comprensión de la fenomenología de las extensiones escalares del ME, el impacto del *running* y la mezcla ALP-Higgs, así como de las interacciones que violan CP y rompen la simetría *shift*. El conjunto completo de EGR, así como el paquete `ALPRunner`, constituyen her-

[2]En este escenario, la única fuente de violación de CP es la matriz CKM del ME.

ramientas útiles para futuros análisis fenomenológicos que busquen señales de física más allá del ME en el sector escalar.

Bibliography

[1] J. Bonilla, I. Brivio, J. Machado-Rodríguez, and J. F. de Trocóniz, "Nonresonant searches for axion-like particles in vector boson scattering processes at the LHC," *JHEP*, vol. 06, p. 113, 2022. DOI: 10.1007/JHEP06(2022)113. arXiv: 2202.03450 [hep-ph].

[2] S. Das Bakshi, J. Machado-Rodríguez, and M. Ramos, "Running beyond ALPs: shift-breaking and CP-violating effects," *JHEP*, vol. 11, p. 133, 2023. DOI: 10.1007/JHEP11(2023)133. arXiv: 2306.08036 [hep-ph].

[3] J. Bonilla, B. Gavela, and J. Machado-Rodríguez, "Limits on ALP-neutrino couplings from loop-level processes," *Phys. Rev. D*, vol. 109, no. 5, p. 055 023, 2024. DOI: 10.1103/PhysRevD.109.055023. arXiv: 2309.15910 [hep-ph].

[4] J. Bonilla, I. Brivio, J. Machado, and J. F. de Trocóniz, "Nonresonant Searches for Axion-Like Particles at the LHC: Implications for Vector Boson Scattering," *PoS*, vol. EPS-HEP2021, p. 692, 2022. DOI: 10.22323/1.398.0692.

[5] A. Crivellin and B. Mellado, "Anomalies in Particle Physics," Sep. 2023. DOI: 10.1038/s42254-024-00703-6. arXiv: 2309.03870 [hep-ph].

[6] F. Englert and R. Brout, "Broken Symmetry and the Mass of Gauge Vector Mesons," *Phys. Rev. Lett.*, vol. 13, J. C. Taylor, Ed., pp. 321–323, 1964. DOI: 10.1103/PhysRevLett.13.321.

[7] P. W. Higgs, "Broken Symmetries and the Masses of Gauge Bosons," *Phys. Rev. Lett.*, vol. 13, J. C. Taylor, Ed., pp. 508–509, 1964. DOI: 10.1103/PhysRevLett.13.508.

[8] G. S. Guralnik, C. R. Hagen, and T. W. B. Kibble, "Global Conservation Laws and Massless Particles," *Phys. Rev. Lett.*, vol. 13, J. C. Taylor, Ed., pp. 585–587, 1964. DOI: 10.1103/PhysRevLett.13.585.

[9] Y. Nambu and G. Jona-Lasinio, "Dynamical Model of Elementary Particles Based on an Analogy with Superconductivity. 1.," *Phys. Rev.*, vol. 122, T. Eguchi, Ed., pp. 345–358, 1961. DOI: 10.1103/PhysRev.122.345.

[10] J. Goldstone, "Field Theories with Superconductor Solutions," *Nuovo Cim.*, vol. 19, pp. 154–164, 1961. DOI: 10.1007/BF02812722.

[11] S. Chatrchyan *et al.*, "Observation of a New Boson at a Mass of 125 GeV with the CMS Experiment at the LHC," *Phys. Lett. B*, vol. 716, pp. 30–61, 2012. DOI: 10.1016/j.physletb.2012.08.021. arXiv: 1207.7235 [hep-ex].

[12] G. Aad *et al.*, "Observation of a new particle in the search for the Standard Model Higgs boson with the ATLAS detector at the LHC," *Phys. Lett. B*, vol. 716, pp. 1–29, 2012. DOI: 10.1016/j.physletb.2012.08.020. arXiv: 1207.7214 [hep-ex].

[13] R. L. Workman *et al.*, "Review of Particle Physics," *PTEP*, vol. 2022, p. 083C01, 2022. DOI: 10.1093/ptep/ptac097.

[14] N. Cabibbo, "Unitary Symmetry and Leptonic Decays," *Phys. Rev. Lett.*, vol. 10, pp. 531–533, 1963. DOI: 10.1103/PhysRevLett.10.531.

[15] M. Kobayashi and T. Maskawa, "CP Violation in the Renormalizable Theory of Weak Interaction," *Prog. Theor. Phys.*, vol. 49, pp. 652–657, 1973. DOI: 10.1143/PTP.49.652.

[16] B. Pontecorvo, "Mesonium and anti-mesonium," *Sov. Phys. JETP*, vol. 6, p. 429, 1957.

[17] Z. Maki, M. Nakagawa, and S. Sakata, "Remarks on the unified model of elementary particles," *Prog. Theor. Phys.*, vol. 28, pp. 870–880, 1962. DOI: 10.1143/PTP.28.870.

[18] I. Esteban, M. C. Gonzalez-Garcia, M. Maltoni, T. Schwetz, and A. Zhou, "The fate of hints: updated global analysis of three-flavor neutrino oscillations," *JHEP*, vol. 09, p. 178, 2020. DOI: 10.1007/JHEP09(2020)178. arXiv: 2007.14792 [hep-ph].

[19] S. Weinberg, "Baryon and Lepton Nonconserving Processes," *Phys. Rev. Lett.*, vol. 43, pp. 1566–1570, 1979. DOI: 10.1103/PhysRevLett.43.1566.

[20] T. Yanagida, "Horizontal Symmetry and Masses of Neutrinos," *Prog. Theor. Phys.*, vol. 64, p. 1103, 1980. DOI: 10.1143/PTP.64.1103.

[21] P. Minkowski, "$\mu \to e\gamma$ at a Rate of One Out of 10^9 Muon Decays?" *Phys. Lett. B*, vol. 67, pp. 421–428, 1977. DOI: 10.1016/0370-2693(77)90435-X.

[22] R. N. Mohapatra and G. Senjanovic, "Neutrino Mass and Spontaneous Parity Nonconservation," *Phys. Rev. Lett.*, vol. 44, p. 912, 1980. DOI: 10.1103/PhysRevLett.44.912.

[23] M. Gell-Mann, P. Ramond, and R. Slansky, "Complex Spinors and Unified Theories," *Conf. Proc. C*, vol. 790927, pp. 315–321, 1979. arXiv: 1306.4669 [hep-th].

[24] M. Magg and C. Wetterich, "Neutrino Mass Problem and Gauge Hierarchy," *Phys. Lett. B*, vol. 94, pp. 61–64, 1980. DOI: 10.1016/0370-2693(80)90825-4.

[25] J. Schechter and J. W. F. Valle, "Neutrino Masses in SU(2) x U(1) Theories," *Phys. Rev. D*, vol. 22, p. 2227, 1980. DOI: 10.1103/PhysRevD.22.2227.

[26] C. Wetterich, "Neutrino Masses and the Scale of B-L Violation," *Nucl. Phys. B*, vol. 187, pp. 343–375, 1981. DOI: 10.1016/0550-3213(81)90279-0.

[27] G. Lazarides, Q. Shafi, and C. Wetterich, "Proton Lifetime and Fermion Masses in an SO(10) Model," *Nucl. Phys. B*, vol. 181, pp. 287–300, 1981. DOI: 10.1016/0550-3213(81)90354-0.

[28] R. N. Mohapatra and G. Senjanovic, "Neutrino Masses and Mixings in Gauge Models with Spontaneous Parity Violation," *Phys. Rev. D*, vol. 23, p. 165, 1981. DOI: 10.1103/PhysRevD.23.165.

[29] R. Foot, H. Lew, X. G. He, and G. C. Joshi, "Seesaw Neutrino Masses Induced by a Triplet of Leptons," *Z. Phys. C*, vol. 44, p. 441, 1989. DOI: 10.1007/BF01415558.

[30] E. Ma, "Pathways to naturally small neutrino masses," *Phys. Rev. Lett.*, vol. 81, pp. 1171–1174, 1998. DOI: 10.1103/PhysRevLett.81.1171. arXiv: hep-ph/9805219.

[31] E. Ma and D. P. Roy, "Heavy triplet leptons and new gauge boson," *Nucl. Phys. B*, vol. 644, pp. 290–302, 2002. DOI: 10.1016/S0550-3213(02)00815-5. arXiv: hep-ph/0206150.

[32] T. Hambye, Y. Lin, A. Notari, M. Papucci, and A. Strumia, "Constraints on neutrino masses from leptogenesis models," *Nucl. Phys. B*, vol. 695, pp. 169–191, 2004. DOI: 10.1016/j.nuclphysb.2004.06.027. arXiv: hep-ph/0312203.

[33] B. Bajc, M. Nemevsek, and G. Senjanovic, "Probing seesaw at LHC," *Phys. Rev. D*, vol. 76, p. 055 011, 2007. DOI: 10.1103/PhysRevD.76.055011. arXiv: hep-ph/0703080.

[34] I. Dorsner and P. Fileviez Perez, "Upper Bound on the Mass of the Type III Seesaw Triplet in an SU(5) Model," *JHEP*, vol. 06, p. 029, 2007. DOI: 10.1088/1126-6708/2007/06/029. arXiv: hep-ph/0612216.

[35] P. Fileviez Perez, "Supersymmetric Adjoint SU(5)," *Phys. Rev. D*, vol. 76, p. 071 701, 2007. DOI: 10.1103/PhysRevD.76.071701. arXiv: 0705.3589 [hep-ph].

[36] J. Bonilla, I. Brivio, M. B. Gavela, and V. Sanz, "One-loop corrections to ALP couplings," *JHEP*, vol. 11, p. 168, 2021. DOI: 10.1007/JHEP11(2021)168. arXiv: 2107.11392 [hep-ph].

[37] A. A. Belavin, A. M. Polyakov, A. S. Schwartz, and Y. S. Tyupkin, "Pseudoparticle Solutions of the Yang-Mills Equations," *Phys. Lett. B*, vol. 59, J. C. Taylor, Ed., pp. 85–87, 1975. DOI: 10.1016/0370-2693(75)90163-X.

[38] G. 't Hooft, "Computation of the Quantum Effects Due to a Four-Dimensional Pseudoparticle," *Phys. Rev. D*, vol. 14, M. A. Shifman, Ed., pp. 3432–3450, 1976, [Erratum: Phys.Rev.D 18, 2199 (1978)]. DOI: 10.1103/PhysRevD.14.3432.

[39] C. G. Callan Jr., R. F. Dashen, and D. J. Gross, "Toward a Theory of the Strong Interactions," *Phys. Rev. D*, vol. 17, M. A. Shifman, Ed., p. 2717, 1978. DOI: 10.1103/PhysRevD.17.2717.

[40] S. Weinberg, "The U(1) Problem," *Phys. Rev. D*, vol. 11, pp. 3583–3593, 1975. DOI: 10.1103/PhysRevD.11.3583.

[41] G. 't Hooft, "How Instantons Solve the U(1) Problem," *Phys. Rept.*, vol. 142, pp. 357–387, 1986. DOI: 10.1016/0370-1573(86)90117-1.

[42] G. 't Hooft, "Symmetry Breaking Through Bell-Jackiw Anomalies," *Phys. Rev. Lett.*, vol. 37, M. A. Shifman, Ed., pp. 8–11, 1976. DOI: 10.1103/PhysRevLett.37.8.

[43] S. L. Adler, "Axial vector vertex in spinor electrodynamics," *Phys. Rev.*, vol. 177, pp. 2426–2438, 1969. DOI: 10.1103/PhysRev.177.2426.

[44] J. S. Bell and R. Jackiw, "A PCAC puzzle: $\pi^0 \to \gamma\gamma$ in the σ model," *Nuovo Cim. A*, vol. 60, pp. 47–61, 1969. DOI: 10.1007/BF02823296.

[45] A. Hook, "TASI Lectures on the Strong CP Problem and Axions," *PoS*, vol. TASI2018, p. 004, 2019. arXiv: 1812.02669 [hep-ph].

[46] J. Redondo, *Course on axions at the GGI lectures on the theory of fundamental interactions*, https://www.ggi.infn.it/ggilectures/ggilectures2019/img/axion-lectures.pdf, Jan. 2019.

[47] K. Fujikawa, "Path Integral Measure for Gauge Invariant Fermion Theories," *Phys. Rev. Lett.*, vol. 42, pp. 1195–1198, 1979. DOI: 10.1103/PhysRevLett.42.1195.

[48] O. W. Greenberg, "CPT violation implies violation of Lorentz invariance," *Phys. Rev. Lett.*, vol. 89, p. 231 602, 2002. DOI: 10.1103/PhysRevLett.89.231602. arXiv: hep-ph/0201258.

[49] E. P. Shabalin, "Electric Dipole Moment of Quark in a Gauge Theory with Left-Handed Currents," *Sov. J. Nucl. Phys.*, vol. 28, p. 75, 1978.

[50] M. B. Gavela, A. Le Yaouanc, L. Oliver, O. Pene, J. C. Raynal, and T. N. Pham, "CP Violation Induced by Penguin Diagrams and the Neutron Electric Dipole Moment," *Phys. Lett. B*, vol. 109, pp. 215–220, 1982. DOI: 10.1016/0370-2693(82)90756-0.

[51] M. B. Gavela, A. Le Yaouanc, L. Oliver, O. Pene, J. C. Raynal, and T. N. Pham, "Contribution of the Triangle Graphs to the Neutron Electric Dipole Moment," *Z. Phys. C*, vol. 23, p. 251, 1984. DOI: 10.1007/BF01546193.

[52] A. Czarnecki and B. Krause, "Neutron electric dipole moment in the standard model: Valence quark contributions," *Phys. Rev. Lett.*, vol. 78, pp. 4339–4342, 1997. DOI: 10.1103/PhysRevLett.78.4339. arXiv: hep-ph/9704355.

[53] S. Dar, "The Neutron EDM in the SM: A Review," Aug. 2000. arXiv: hep-ph/0008248.

[54] V. Baluni, "CP Violating Effects in QCD," *Phys. Rev. D*, vol. 19, pp. 2227–2230, 1979. DOI: 10.1103/PhysRevD.19.2227.

[55] R. J. Crewther, P. Di Vecchia, G. Veneziano, and E. Witten, "Chiral Estimate of the Electric Dipole Moment of the Neutron in Quantum Chromodynamics," *Phys. Lett. B*, vol. 88, p. 123, 1979, [Erratum: Phys.Lett.B 91, 487 (1980)]. DOI: 10.1016/0370-2693(79)90128-X.

[56] K. Kanaya and M. Kobayashi, "Strong CP Violation in the Chiral σ Model," *Prog. Theor. Phys.*, vol. 66, p. 2173, 1981. DOI: 10.1143/PTP.66.2173.

[57] H. J. Schnitzer, "The Soft Pion Skyrmion Lagrangian and Strong CP Violation," *Phys. Lett. B*, vol. 139, pp. 217–222, 1984. DOI: 10.1016/0370-2693(84)91248-6.

[58] P. Cea and G. Nardulli, "A Realistic Calculation of the Electric Dipole Moment of the Neutron Induced by Strong CP Violation," *Phys. Lett. B*, vol. 144, pp. 115–118, 1984. DOI: 10.1016/0370-2693(84)90187-4.

[59] M. M. Musakhanov and Z. Z. Israilov, "THE ELECTRIC DIPOLE MOMENT OF THE NEUTRON IN THE CHIRAL BAG MODEL," *Phys. Lett. B*, vol. 137, pp. 419–421, 1984. DOI: 10.1016/0370-2693(84)91747-7.

[60] M. A. Morgan and G. A. Miller, "The Neutron Electric Dipole Moment in the Cloudy Bag Model," *Phys. Lett. B*, vol. 179, pp. 379–384, 1986. DOI: 10.1016/0370-2693(86)90497-1.

[61] R. K. Ellis *et al.*, "Physics Briefing Book: Input for the European Strategy for Particle Physics Update 2020," Oct. 2019. arXiv: 1910.11775 [hep-ex].

[62] J. Beringer *et al.*, "Review of Particle Physics (RPP)," *Phys. Rev. D*, vol. 86, p. 010 001, 2012. DOI: 10.1103/PhysRevD.86.010001.

[63] M. Dine, P. Draper, and G. Festuccia, "Instanton Effects in Three Flavor QCD," *Phys. Rev. D*, vol. 92, no. 5, p. 054 004, 2015. DOI: 10.1103/PhysRevD.92.054004. arXiv: 1410.8505 [hep-ph].

[64] S. Aoki *et al.*, "Review of lattice results concerning low-energy particle physics," *Eur. Phys. J. C*, vol. 77, no. 2, p. 112, 2017. DOI: 10.1140/epjc/s10052-016-4509-7. arXiv: 1607.00299 [hep-lat].

[65] J. E. Kim, "A COMPOSITE INVISIBLE AXION," *Phys. Rev. D*, vol. 31, p. 1733, 1985. DOI: 10.1103/PhysRevD.31.1733.

[66] K. Choi and J. E. Kim, "DYNAMICAL AXION," *Phys. Rev. D*, vol. 32, p. 1828, 1985. DOI: 10.1103/PhysRevD.32.1828.

[67] A. Hook, "Anomalous solutions to the strong CP problem," *Phys. Rev. Lett.*, vol. 114, no. 14, p. 141 801, 2015. DOI: 10.1103/PhysRevLett.114.141801. arXiv: 1411.3325 [hep-ph].

[68] P. Agrawal and K. Howe, "A Flavorful Factoring of the Strong CP Problem," *JHEP*, vol. 12, p. 035, 2018. DOI: 10.1007/JHEP12(2018)035. arXiv: 1712.05803 [hep-ph].

[69] K. S. Babu and R. N. Mohapatra, "A Solution to the Strong CP Problem Without an Axion," *Phys. Rev. D*, vol. 41, p. 1286, 1990. DOI: 10.1103/PhysRevD.41.1286.

[70] S. M. Barr, D. Chang, and G. Senjanovic, "Strong CP problem and parity," *Phys. Rev. Lett.*, vol. 67, pp. 2765–2768, 1991. DOI: 10.1103/PhysRevLett.67.2765.

[71] R. N. Mohapatra and A. Rasin, "Simple supersymmetric solution to the strong CP problem," *Phys. Rev. Lett.*, vol. 76, pp. 3490–3493, 1996. DOI: 10.1103/PhysRevLett.76.3490. arXiv: hep-ph/9511391.

[72] R. Kuchimanchi, "Solution to the strong CP problem: Supersymmetry with parity," *Phys. Rev. Lett.*, vol. 76, pp. 3486–3489, 1996. DOI: 10.1103/PhysRevLett.76.3486. arXiv: hep-ph/9511376.

[73] R. N. Mohapatra and A. Rasin, "A Supersymmetric solution to CP problems," *Phys. Rev. D*, vol. 54, pp. 5835–5844, 1996. DOI: 10.1103/PhysRevD.54.5835. arXiv: hep-ph/9604445.

[74] R. T. D'Agnolo and A. Hook, "Finding the Strong CP problem at the LHC," *Phys. Lett. B*, vol. 762, pp. 421–425, 2016. DOI: 10.1016/j.physletb.2016.09.061. arXiv: 1507.00336 [hep-ph].

[75] A. E. Nelson, "Naturally Weak CP Violation," *Phys. Lett. B*, vol. 136, pp. 387–391, 1984. DOI: 10.1016/0370-2693(84)92025-2.

[76] S. M. Barr, "Solving the Strong CP Problem Without the Peccei-Quinn Symmetry," *Phys. Rev. Lett.*, vol. 53, p. 329, 1984. DOI: 10.1103/PhysRevLett.53.329.

[77] L. Bento, G. C. Branco, and P. A. Parada, "A Minimal model with natural suppression of strong CP violation," *Phys. Lett. B*, vol. 267, pp. 95–99, 1991. DOI: 10.1016/0370-2693(91)90530-4.

[78] M. Dine and P. Draper, "Challenges for the Nelson-Barr Mechanism," *JHEP*, vol. 08, p. 132, 2015. DOI: 10.1007/JHEP08(2015)132. arXiv: 1506.05433 [hep-ph].

[79] R. D. Peccei and H. R. Quinn, "CP Conservation in the Presence of Instantons," *Phys. Rev. Lett.*, vol. 38, pp. 1440–1443, 1977. DOI: 10.1103/PhysRevLett.38.1440.

[80] R. D. Peccei and H. R. Quinn, "Constraints Imposed by CP Conservation in the Presence of Instantons," *Phys. Rev. D*, vol. 16, pp. 1791–1797, 1977. DOI: 10.1103/PhysRevD.16.1791.

[81] S. Weinberg, "A New Light Boson?" *Phys. Rev. Lett.*, vol. 40, pp. 223–226, 1978. DOI: 10.1103/PhysRevLett.40.223.

[82] F. Wilczek, "Problem of Strong P and T Invariance in the Presence of Instantons," *Phys. Rev. Lett.*, vol. 40, pp. 279–282, 1978. DOI: 10.1103/PhysRevLett.40.279.

[83] K. Choi, K. Kang, and J. E. Kim, "Effects of η' in Low-energy Axion Physics," *Phys. Lett. B*, vol. 181, pp. 145–149, 1986. DOI: 10.1016/0370-2693(86)91273-6.

[84] H. Georgi, D. B. Kaplan, and L. Randall, "Manifesting the Invisible Axion at Low-energies," *Phys. Lett. B*, vol. 169, pp. 73–78, 1986. DOI: 10.1016/0370-2693(86)90688-X.

[85] P. Di Vecchia, G. Rossi, G. Veneziano, and S. Yankielowicz, "Spontaneous CP breaking in QCD and the axion potential: an effective Lagrangian approach," *JHEP*, vol. 12, p. 104, 2017. DOI: 10.1007/JHEP12(2017)104. arXiv: 1709.00731 [hep-th].

[86] D. S. M. Alves and N. Weiner, "A viable QCD axion in the MeV mass range," *JHEP*, vol. 07, p. 092, 2018. DOI: 10.1007/JHEP07(2018)092. arXiv: 1710.03764 [hep-ph].

[87] S. R. Coleman, "The Uses of Instantons," *Subnucl. Ser.*, vol. 15, M. A. Shifman, Ed., p. 805, 1979.

[88] D. B. Kaplan, "Opening the Axion Window," *Nucl. Phys. B*, vol. 260, pp. 215–226, 1985. DOI: 10.1016/0550-3213(85)90319-0.

[89] G. Grilli di Cortona, E. Hardy, J. Pardo Vega, and G. Villadoro, "The QCD axion, precisely," *JHEP*, vol. 01, p. 034, 2016. DOI: 10.1007/JHEP01(2016)034. arXiv: 1511.02867 [hep-ph].

[90] G. Alonso-Álvarez, M. B. Gavela, and P. Quilez, "Axion couplings to electroweak gauge bosons," *Eur. Phys. J. C*, vol. 79, no. 3, p. 223, 2019. DOI: 10.1140/epjc/s10052-019-6732-5. arXiv: 1811.05466 [hep-ph].

[91] J. E. Kim, "Weak Interaction Singlet and Strong CP Invariance," *Phys. Rev. Lett.*, vol. 43, p. 103, 1979. DOI: 10.1103/PhysRevLett.43.103.

[92] M. A. Shifman, A. I. Vainshtein, and V. I. Zakharov, "Can Confinement Ensure Natural CP Invariance of Strong Interactions?" *Nucl. Phys. B*, vol. 166, pp. 493–506, 1980. DOI: 10.1016/0550-3213(80)90209-6.

[93] A. R. Zhitnitsky, "On Possible Suppression of the Axion Hadron Interactions. (In Russian)," *Sov. J. Nucl. Phys.*, vol. 31, p. 260, 1980.

[94] M. Dine, W. Fischler, and M. Srednicki, "A Simple Solution to the Strong CP Problem with a Harmless Axion," *Phys. Lett. B*, vol. 104, pp. 199–202, 1981. DOI: 10.1016/0370-2693(81)90590-6.

[95] A. Hook, "Solving the Hierarchy Problem Discretely," *Phys. Rev. Lett.*, vol. 120, no. 26, p. 261 802, 2018. DOI: 10.1103/PhysRevLett.120.261802. arXiv: 1802.10093 [hep-ph].

[96] L. Di Luzio, B. Gavela, P. Quilez, and A. Ringwald, "An even lighter QCD axion," *JHEP*, vol. 05, p. 184, 2021. DOI: 10.1007/JHEP05(2021)184. arXiv: 2102.00012 [hep-ph].

[97] B. Gavela, P. Quílez, and M. Ramos, "The QCD axion sum rule," *JHEP*, vol. 04, p. 056, 2024. DOI: 10.1007/JHEP04(2024)056. arXiv: 2305.15465 [hep-ph].

[98] J. F. Donoghue and L. F. Li, "Properties of Charged Higgs Bosons," *Phys. Rev. D*, vol. 19, p. 945, 1979. DOI: 10.1103/PhysRevD.19.945.

[99] H. E. Haber, G. L. Kane, and T. Sterling, "The Fermion Mass Scale and Possible Effects of Higgs Bosons on Experimental Observables," *Nucl. Phys. B*, vol. 161, pp. 493–532, 1979. DOI: 10.1016/0550-3213(79)90225-6.

[100] V. D. Barger, J. L. Hewett, and R. J. N. Phillips, "New Constraints on the Charged Higgs Sector in Two Higgs Doublet Models," *Phys. Rev. D*, vol. 41, pp. 3421–3441, 1990. DOI: 10.1103/PhysRevD.41.3421.

[101] V. A. Rubakov, "Grand unification and heavy axion," *JETP Lett.*, vol. 65, pp. 621–624, 1997. DOI: 10.1134/1.567390. arXiv: hep-ph/9703409.

[102] Z. Berezhiani, L. Gianfagna, and M. Giannotti, "Strong CP problem and mirror world: The Weinberg-Wilczek axion revisited," *Phys. Lett. B*, vol. 500, pp. 286–296, 2001. DOI: 10.1016/S0370-2693(00)01392-7. arXiv: hep-ph/0009290.

[103] L. Gianfagna, M. Giannotti, and F. Nesti, "Mirror world, supersymmetric axion and gamma ray bursts," *JHEP*, vol. 10, p. 044, 2004. DOI: 10.1088/1126-6708/2004/10/044. arXiv: hep-ph/0409185.

[104] S. D. H. Hsu and F. Sannino, "New solutions to the strong CP problem," *Phys. Lett. B*, vol. 605, pp. 369–375, 2005. DOI: 10.1016/j.physletb.2004.11.040. arXiv: hep-ph/0408319.

[105] H. Fukuda, K. Harigaya, M. Ibe, and T. T. Yanagida, "Model of visible QCD axion," *Phys. Rev. D*, vol. 92, no. 1, p. 015 021, 2015. DOI: 10.1103/PhysRevD.92.015021. arXiv: 1504.06084 [hep-ph].

[106] C.-W. Chiang, H. Fukuda, M. Ibe, and T. T. Yanagida, "750 GeV diphoton resonance in a visible heavy QCD axion model," *Phys. Rev. D*, vol. 93, no. 9, p. 095 016, 2016. DOI: 10.1103/PhysRevD.93.095016. arXiv: 1602.07909 [hep-ph].

[107] S. Dimopoulos, A. Hook, J. Huang, and G. Marques-Tavares, "A collider observable QCD axion," *JHEP*, vol. 11, p. 052, 2016. DOI: 10.1007/JHEP11(2016)052. arXiv: 1606.03097 [hep-ph].

[108] T. Gherghetta, N. Nagata, and M. Shifman, "A Visible QCD Axion from an Enlarged Color Group," *Phys. Rev. D*, vol. 93, no. 11, p. 115 010, 2016. DOI: 10.1103/PhysRevD.93.115010. arXiv: 1604.01127 [hep-ph].

[109] A. Kobakhidze, "Heavy axion in asymptotically safe QCD," Jul. 2016. arXiv: 1607.06552 [hep-ph].

[110] P. Agrawal and K. Howe, "Factoring the Strong CP Problem," *JHEP*, vol. 12, p. 029, 2018. DOI: 10.1007/JHEP12(2018)029. arXiv: 1710.04213 [hep-ph].

[111] M. K. Gaillard, M. B. Gavela, R. Houtz, P. Quilez, and R. Del Rey, "Color unified dynamical axion," *Eur. Phys. J. C*, vol. 78, no. 11, p. 972, 2018. DOI: 10.1140/epjc/s10052-018-6396-6. arXiv: 1805.06465 [hep-ph].

[112] M. A. Buen-Abad and J. Fan, "Dynamical axion misalignment with small instantons," *JHEP*, vol. 12, p. 161, 2019. DOI: 10.1007/JHEP12(2019)161. arXiv: 1911.05737 [hep-ph].

[113] A. Hook, S. Kumar, Z. Liu, and R. Sundrum, "High Quality QCD Axion and the LHC," *Phys. Rev. Lett.*, vol. 124, no. 22, p. 221 801, 2020. DOI: 10.1103/PhysRevLett.124.221801. arXiv: 1911.12364 [hep-ph].

[114] C. Csáki, M. Ruhdorfer, and Y. Shirman, "UV Sensitivity of the Axion Mass from Instantons in Partially Broken Gauge Groups," *JHEP*, vol. 04, p. 031, 2020. DOI: 10.1007/JHEP04(2020)031. arXiv: 1912.02197 [hep-ph].

[115] T. Gherghetta and M. D. Nguyen, "A Composite Higgs with a Heavy Composite Axion," *JHEP*, vol. 12, p. 094, 2020. DOI: 10.1007/JHEP12(2020)094. arXiv: 2007.10875 [hep-ph].

[116] Y. Chikashige, R. N. Mohapatra, and R. D. Peccei, "Are There Real Goldstone Bosons Associated with Broken Lepton Number?" *Phys. Lett. B*, vol. 98, pp. 265–268, 1981. DOI: 10.1016/0370-2693(81)90011-3.

[117] G. B. Gelmini and M. Roncadelli, "Left-Handed Neutrino Mass Scale and Spontaneously Broken Lepton Number," *Phys. Lett. B*, vol. 99, pp. 411–415, 1981. DOI: 10.1016/0370-2693(81)90559-1.

[118] G. Ballesteros, J. Redondo, A. Ringwald, and C. Tamarit, "Standard ModelaxionseesawHiggs portal inflation. Five problems of particle physics and cosmology solved in one stroke," *JCAP*, vol. 08, p. 001, 2017. DOI: 10.1088/1475-7516/2017/08/001. arXiv: 1610.01639 [hep-ph].

[119] F. Wilczek, "Axions and Family Symmetry Breaking," *Phys. Rev. Lett.*, vol. 49, pp. 1549–1552, 1982. DOI: 10.1103/PhysRevLett.49.1549.

[120] L. Calibbi, F. Goertz, D. Redigolo, R. Ziegler, and J. Zupan, "Minimal axion model from flavor," *Phys. Rev. D*, vol. 95, no. 9, p. 095 009, 2017. DOI: 10.1103/PhysRevD.95.095009. arXiv: 1612.08040 [hep-ph].

[121] Y. Ema, K. Hamaguchi, T. Moroi, and K. Nakayama, "Flaxion: a minimal extension to solve puzzles in the standard model," *JHEP*, vol. 01, p. 096, 2017. DOI: 10.1007/JHEP01(2017)096. arXiv: 1612.05492 [hep-ph].

[122] P. W. Graham, D. E. Kaplan, and S. Rajendran, "Cosmological Relaxation of the Electroweak Scale," *Phys. Rev. Lett.*, vol. 115, no. 22, p. 221 801, 2015. DOI: 10.1103/PhysRevLett.115.221801. arXiv: 1504.07551 [hep-ph].

[123] Z. G. Berezhiani and M. Y. Khlopov, "The Theory of broken gauge symmetry of families. (In Russian)," *Sov. J. Nucl. Phys.*, vol. 51, pp. 739–746, 1990.

[124] J. Jaeckel, "A Family of WISPy Dark Matter Candidates," *Phys. Lett. B*, vol. 732, pp. 1–7, 2014. DOI: 10.1016/j.physletb.2014.03.005. arXiv: 1311.0880 [hep-ph].

[125] E. Witten, "Some Properties of O(32) Superstrings," *Phys. Lett. B*, vol. 149, pp. 351–356, 1984. DOI: 10.1016/0370-2693(84)90422-2.

[126] J. P. Conlon, "The QCD axion and moduli stabilisation," *JHEP*, vol. 05, p. 078, 2006. DOI: 10.1088/1126-6708/2006/05/078. arXiv: hep-th/0602233.

[127] M. Cicoli, M. Goodsell, and A. Ringwald, "The type IIB string axiverse and its low-energy phenomenology," *JHEP*, vol. 10, p. 146, 2012. DOI: 10.1007/JHEP10(2012)146. arXiv: 1206.0819 [hep-th].

[128] H. M. Georgi, L. J. Hall, and M. B. Wise, "Grand Unified Models With an Automatic Peccei-Quinn Symmetry," *Nucl. Phys. B*, vol. 192, pp. 409–416, 1981. DOI: 10.1016/0550-3213(81)90433-8.

[129] K.-S. Choi, H. P. Nilles, S. Ramos-Sanchez, and P. K. S. Vaudrevange, "Accions," *Phys. Lett. B*, vol. 675, pp. 381–386, 2009. DOI: 10.1016/j.physletb.2009.04.028. arXiv: 0902.3070 [hep-th].

[130] M. Cicoli, "Axion-like Particles from String Compactifications," in *9th Patras Workshop on Axions, WIMPs and WISPs*, 2013, pp. 235–242. DOI: 10.3204/DESY-PROC-2013-04/cicoli_michele. arXiv: 1309.6988 [hep-th].

[131] A. G. Dias, A. C. B. Machado, C. C. Nishi, A. Ringwald, and P. Vaudrevange, "The Quest for an Intermediate-Scale Accidental Axion and Further ALPs," *JHEP*, vol. 06, p. 037, 2014. DOI: 10.1007/JHEP06(2014)037. arXiv: 1403.5760 [hep-ph].

[132] H. Georgi and D. B. Kaplan, "Composite Higgs and Custodial SU(2)," *Phys. Lett. B*, vol. 145, pp. 216–220, 1984. DOI: 10.1016/0370-2693(84)90341-1.

[133] I. Brivio *et al.*, "ALPs Effective Field Theory and Collider Signatures," *Eur. Phys. J. C*, vol. 77, no. 8, p. 572, 2017. DOI: 10.1140/epjc/s10052-017-5111-3. arXiv: 1701.05379 [hep-ph].

[134] M. Chala, G. Guedes, M. Ramos, and J. Santiago, "Running in the ALPs," *Eur. Phys. J. C*, vol. 81, no. 2, p. 181, 2021. DOI: 10.1140/epjc/s10052-021-08968-2. arXiv: 2012.09017 [hep-ph].

[135] M. Bauer, M. Neubert, S. Renner, M. Schnubel, and A. Thamm, "The Low-Energy Effective Theory of Axions and ALPs," *JHEP*, vol. 04, p. 063, 2021. DOI: 10.1007/JHEP04(2021)063. arXiv: 2012.12272 [hep-ph].

[136] M. Freytsis, Z. Ligeti, and J. Thaler, "Constraining the Axion Portal with $B \to K l^+ l^-$," *Phys. Rev. D*, vol. 81, p. 034 001, 2010. DOI: 10.1103/PhysRevD.81.034001. arXiv: 0911.5355 [hep-ph].

[137] K. Mimasu and V. Sanz, "ALPs at Colliders," *JHEP*, vol. 06, p. 173, 2015. DOI: 10.1007/JHEP06(2015)173. arXiv: 1409.4792 [hep-ph].

[138] J. Jaeckel and M. Spannowsky, "Probing MeV to 90 GeV axion-like particles with LEP and LHC," *Phys. Lett. B*, vol. 753, pp. 482–487, 2016. DOI: 10.1016/j.physletb.2015.12.037. arXiv: 1509.00476 [hep-ph].

[139] E. Izaguirre, T. Lin, and B. Shuve, "Searching for Axionlike Particles in Flavor-Changing Neutral Current Processes," *Phys. Rev. Lett.*, vol. 118, no. 11, p. 111 802, 2017. DOI: 10.1103/PhysRevLett.118.111802. arXiv: 1611.09355 [hep-ph].

[140] M. Bauer, M. Neubert, and A. Thamm, "Collider Probes of Axion-Like Particles," *JHEP*, vol. 12, p. 044, 2017. DOI: 10.1007/JHEP12(2017)044. arXiv: 1708.00443 [hep-ph].

[141] N. Craig, A. Hook, and S. Kasko, "The Photophobic ALP," *JHEP*, vol. 09, p. 028, 2018. DOI: 10.1007/JHEP09(2018)028. arXiv: 1805.06538 [hep-ph].

[142] C. Frugiuele, E. Fuchs, G. Perez, and M. Schlaffer, "Relaxion and light (pseudo)scalars at the HL-LHC and lepton colliders," *JHEP*, vol. 10, p. 151, 2018. DOI: 10.1007/JHEP10(2018)151. arXiv: 1807.10842 [hep-ph].

[143] M. Bauer, M. Heiles, M. Neubert, and A. Thamm, "Axion-Like Particles at Future Colliders," *Eur. Phys. J. C*, vol. 79, no. 1, p. 74, 2019. DOI: 10.1140/epjc/s10052-019-6587-9. arXiv: 1808.10323 [hep-ph].

[144] J. Ebadi, S. Khatibi, and M. Mohammadi Najafabadi, "New probes for axionlike particles at hadron colliders," *Phys. Rev. D*, vol. 100, no. 1, p. 015 016, 2019. DOI: 10.1103/PhysRevD.100.015016. arXiv: 1901.03061 [hep-ph].

[145] L. Merlo, F. Pobbe, S. Rigolin, and O. Sumensari, "Revisiting the production of ALPs at B-factories," *JHEP*, vol. 06, p. 091, 2019. DOI: 10.1007/JHEP06(2019)091. arXiv: 1905.03259 [hep-ph].

[146] M. B. Gavela, J. M. No, V. Sanz, and J. F. de Trocóniz, "Nonresonant Searches for Axionlike Particles at the LHC," *Phys. Rev. Lett.*, vol. 124, no. 5, p. 051 802, 2020. DOI: 10.1103/PhysRevLett.124.051802. arXiv: 1905.12953 [hep-ph].

[147] M. Bauer, M. Neubert, S. Renner, M. Schnubel, and A. Thamm, "Axionlike Particles, Lepton-Flavor Violation, and a New Explanation of a_μ and a_e," *Phys. Rev. Lett.*, vol. 124, no. 21, p. 211 803, 2020. DOI: 10.1103/PhysRevLett.124.211803. arXiv: 1908.00008 [hep-ph].

[148] M. Bauer, M. Neubert, S. Renner, M. Schnubel, and A. Thamm, "Consistent Treatment of Axions in the Weak Chiral Lagrangian," *Phys. Rev. Lett.*, vol. 127, no. 8, p. 081 803, 2021. DOI: 10.1103/PhysRevLett.127.081803. arXiv: 2102.13112 [hep-ph].

[149] M. Bauer, M. Neubert, S. Renner, M. Schnubel, and A. Thamm, "Flavor probes of axion-like particles," *JHEP*, vol. 09, p. 056, 2022. DOI: 10.1007/JHEP09(2022)056. arXiv: 2110.10698 [hep-ph].

[150] J. Beacham *et al.*, "Physics Beyond Colliders at CERN: Beyond the Standard Model Working Group Report," *J. Phys. G*, vol. 47, no. 1, p. 010 501, 2020. DOI: 10.1088/1361-6471/ab4cd2. arXiv: 1901.09966 [hep-ex].

[151] P. Agrawal *et al.*, "Feebly-interacting particles: FIPs 2020 workshop report," *Eur. Phys. J. C*, vol. 81, no. 11, p. 1015, 2021. DOI: 10.1140/epjc/s10052-021-09703-7. arXiv: 2102.12143 [hep-ph].

[152] L. Di Luzio, B. Gavela, P. Quilez, and A. Ringwald, "Dark matter from an even lighter QCD axion: trapped misalignment," *JCAP*, vol. 10, p. 001, 2021. DOI: 10.1088/1475-7516/2021/10/001. arXiv: 2102.01082 [hep-ph].

[153] Q. Bonnefoy, C. Grojean, and J. Kley, "Shift-Invariant Orders of an Axionlike Particle," *Phys. Rev. Lett.*, vol. 130, no. 11, p. 111 803, 2023. DOI: 10.1103/PhysRevLett.130.111803. arXiv: 2206.04182 [hep-ph].

[154] M. B. Gavela, J. Gonzalez-Fraile, M. C. Gonzalez-Garcia, L. Merlo, S. Rigolin, and J. Yepes, "CP violation with a dynamical Higgs," *JHEP*, vol. 10, p. 044, 2014. DOI: 10.1007/JHEP10(2014)044. arXiv: 1406.6367 [hep-ph].

[155] J. S. R. Chisholm, "Change of variables in quantum field theories," *Nucl. Phys.*, vol. 26, no. 3, pp. 469–479, 1961. DOI: 10.1016/0029-5582(61)90106-7.

[156] S. Kamefuchi, L. O'Raifeartaigh, and A. Salam, "Change of variables and equivalence theorems in quantum field theories," *Nucl. Phys.*, vol. 28, pp. 529–549, 1961. DOI: 10.1016/0029-5582(61)90056-6.

[157] C. O'Hare, `Cajohare/axionlimits:axionlimits` *(version v1.0)*, "https://doi.org/10.5281/zenodo.3932430", Jul. 2020.

[158] M. B. Gavela, R. Houtz, P. Quilez, R. Del Rey, and O. Sumensari, "Flavor constraints on electroweak ALP couplings," *Eur. Phys. J. C*, vol. 79, no. 5, p. 369, 2019. DOI: 10.1140/epjc/s10052-019-6889-y. arXiv: 1901.02031 [hep-ph].

[159] F. Ertas and F. Kahlhoefer, "On the interplay between astrophysical and laboratory probes of MeV-scale axion-like particles," *JHEP*, vol. 07, p. 050, 2020. DOI: 10.1007/JHEP07(2020)050. arXiv: 2004.01193 [hep-ph].

[160] S. Gori, G. Perez, and K. Tobioka, "KOTO vs. NA62 Dark Scalar Searches," *JHEP*, vol. 08, p. 110, 2020. DOI: 10.1007/JHEP08(2020)110. arXiv: 2005.05170 [hep-ph].

[161] K. J. Kelly, S. Kumar, and Z. Liu, "Heavy axion opportunities at the DUNE near detector," *Phys. Rev. D*, vol. 103, no. 9, p. 095 002, 2021. DOI: 10.1103/PhysRevD.103.095002. arXiv: 2011.05995 [hep-ph].

[162] A. M. Galda, M. Neubert, and S. Renner, "ALP SMEFT interference," *JHEP*, vol. 06, p. 135, 2021. DOI: 10.1007/JHEP06(2021)135. arXiv: 2105.01078 [hep-ph].

[163] D. Wang, L. Wu, J. M. Yang, and M. Zhang, "Photon-jet events as a probe of axionlike particles at the LHC," *Phys. Rev. D*, vol. 104, no. 9, p. 095 016, 2021. DOI: 10.1103/PhysRevD.104.095016. arXiv: 2102.01532 [hep-ph].

[164] J. Ren, D. Wang, L. Wu, J. M. Yang, and M. Zhang, "Detecting an axion-like particle with machine learning at the LHC," *JHEP*, vol. 11, p. 138, 2021. DOI: 10.1007/JHEP11(2021)138. arXiv: 2106.07018 [hep-ph].

[165] D. A. Dicus, E. W. Kolb, V. L. Teplitz, and R. V. Wagoner, "Astrophysical Bounds on the Masses of Axions and Higgs Particles," *Phys. Rev. D*, vol. 18, p. 1829, 1978. DOI: 10.1103/PhysRevD.18.1829.

[166] G. Raffelt and L. Stodolsky, "Mixing of the Photon with Low Mass Particles," *Phys. Rev. D*, vol. 37, p. 1237, 1988. DOI: 10.1103/PhysRevD.37.1237.

[167] S. Andriamonje *et al.*, "An Improved limit on the axion-photon coupling from the CAST experiment," *JCAP*, vol. 04, p. 010, 2007. DOI: 10.1088/1475-7516/2007/04/010. arXiv: hep-ex/0702006.

[168] V. Anastassopoulos *et al.*, "New CAST Limit on the Axion-Photon Interaction," *Nature Phys.*, vol. 13, pp. 584–590, 2017. DOI: 10.1038/nphys4109. arXiv: 1705.02290 [hep-ex].

[169] S. J. Asztalos *et al.*, "A SQUID-based microwave cavity search for dark-matter axions," *Phys. Rev. Lett.*, vol. 104, p. 041 301, 2010. DOI: 10.1103/PhysRevLett.104.041301. arXiv: 0910.5914 [astro-ph.CO].

[170] N. Du *et al.*, "A Search for Invisible Axion Dark Matter with the Axion Dark Matter Experiment," *Phys. Rev. Lett.*, vol. 120, no. 15, p. 151 301, 2018. DOI: 10.1103/PhysRevLett.120.151301. arXiv: 1804.05750 [hep-ex].

[171] T. Braine *et al.*, "Extended Search for the Invisible Axion with the Axion Dark Matter Experiment," *Phys. Rev. Lett.*, vol. 124, no. 10, p. 101 303, 2020. DOI: 10.1103/PhysRevLett.124.101303. arXiv: 1910.08638 [hep-ex].

[172] C. Bartram *et al.*, "Search for Invisible Axion Dark Matter in the 3.34.2 μeV Mass Range," *Phys. Rev. Lett.*, vol. 127, no. 26, p. 261 803, 2021. DOI: 10.1103/PhysRevLett.127.261803. arXiv: 2110.06096 [hep-ex].

[173] N. Crisosto, P. Sikivie, N. S. Sullivan, D. B. Tanner, J. Yang, and G. Rybka, "ADMX SLIC: Results from a Superconducting *LC* Circuit Investigating Cold Axions," *Phys. Rev. Lett.*, vol. 124, no. 24, p. 241 101, 2020. DOI: 10.1103/PhysRevLett.124.241101. arXiv: 1911.05772 [astro-ph.CO].

[174] S. Lee, S. Ahn, J. Choi, B. R. Ko, and Y. K. Semertzidis, "Axion Dark Matter Search around 6.7 μeV," *Phys. Rev. Lett.*, vol. 124, no. 10, p. 101 802, 2020. DOI: 10.1103/PhysRevLett.124.101802. arXiv: 2001.05102 [hep-ex].

[175] J. Jeong *et al.*, “Search for Invisible Axion Dark Matter with a Multiple-Cell Haloscope,” *Phys. Rev. Lett.*, vol. 125, no. 22, p. 221 302, 2020. DOI: 10.1103/PhysRevLett.125.221302. arXiv: 2008.10141 [hep-ex].

[176] O. Kwon *et al.*, “First Results from an Axion Haloscope at CAPP around 10.7 μeV,” *Phys. Rev. Lett.*, vol. 126, no. 19, p. 191 802, 2021. DOI: 10.1103/PhysRevLett.126.191802. arXiv: 2012.10764 [hep-ex].

[177] Y. Lee *et al.*, “Searching for Invisible Axion Dark Matter with an 18 T Magnet Haloscope,” *Phys. Rev. Lett.*, vol. 128, no. 24, p. 241 805, 2022. DOI: 10.1103/PhysRevLett.128.241805. arXiv: 2206.08845 [hep-ex].

[178] J. Kim *et al.*, “Near-Quantum-Noise Axion Dark Matter Search at CAPP around 9.5 μeV,” *Phys. Rev. Lett.*, vol. 130, no. 9, p. 091 602, 2023. DOI: 10.1103/PhysRevLett.130.091602. arXiv: 2207.13597 [hep-ex].

[179] A. K. Yi *et al.*, “Axion Dark Matter Search around 4.55 μeV with Dine-Fischler-Srednicki-Zhitnitskii Sensitivity,” *Phys. Rev. Lett.*, vol. 130, no. 7, p. 071 002, 2023. DOI: 10.1103/PhysRevLett.130.071002. arXiv: 2210.10961 [hep-ex].

[180] S. De Panfilis *et al.*, “Limits on the Abundance and Coupling of Cosmic Axions at 4.5-Microev < m(a) < 5.0-Microev,” *Phys. Rev. Lett.*, vol. 59, p. 839, 1987. DOI: 10.1103/PhysRevLett.59.839.

[181] L. Zhong *et al.*, “Results from phase 1 of the HAYSTAC microwave cavity axion experiment,” *Phys. Rev. D*, vol. 97, no. 9, p. 092 001, 2018. DOI: 10.1103/PhysRevD.97.092001. arXiv: 1803.03690 [hep-ex].

[182] K. M. Backes *et al.*, “A quantum-enhanced search for dark matter axions,” *Nature*, vol. 590, no. 7845, pp. 238–242, 2021. DOI: 10.1038/s41586-021-03226-7. arXiv: 2008.01853 [quant-ph].

[183] M. J. Jewell *et al.*, “New results from HAYSTACs phase II operation with a squeezed state receiver,” *Phys. Rev. D*, vol. 107, no. 7, p. 072 007, 2023. DOI: 10.1103/PhysRevD.107.072007. arXiv: 2301.09721 [hep-ex].

[184] D. Alesini *et al.*, “Galactic axions search with a superconducting resonant cavity,” *Phys. Rev. D*, vol. 99, no. 10, p. 101 101, 2019. DOI: 10.1103/PhysRevD.99.101101. arXiv: 1903.06547 [physics.ins-det].

[185] D. Alesini *et al.*, “Search for invisible axion dark matter of mass $m_a = 43$ μeV with the QUAX–$a\gamma$ experiment,” *Phys. Rev. D*, vol. 103, no. 10, p. 102 004, 2021. DOI: 10.1103/PhysRevD.103.102004. arXiv: 2012.09498 [hep-ex].

[186] D. Alesini *et al.*, “Search for Galactic axions with a high-Q dielectric cavity,” *Phys. Rev. D*, vol. 106, no. 5, p. 052 007, 2022. DOI: 10.1103/PhysRevD.106.052007. arXiv: 2208.12670 [hep-ex].

[187] B. T. McAllister *et al.*, “The ORGAN Experiment: An axion haloscope above 15 GHz,” *Phys. Dark Univ.*, vol. 18, pp. 67–72, 2017. DOI: 10.1016/j.dark.2017.09.010. arXiv: 1706.00209 [physics.ins-det].

[188] A. P. Quiskamp, B. T. McAllister, P. Altin, E. N. Ivanov, M. Goryachev, and M. E. Tobar, “Direct search for dark matter axions excluding ALP cogenesis in the 63- to 67-μeV range with the ORGAN experiment,” *Sci. Adv.*, vol. 8, no. 27, abq3765, 2022. DOI: 10.1126/sciadv.abq3765. arXiv: 2203.12152 [hep-ex].

[189] J. L. Ouellet *et al.*, “First Results from ABRACADABRA-10 cm: A Search for Sub-μeV Axion Dark Matter,” *Phys. Rev. Lett.*, vol. 122, no. 12, p. 121 802, 2019. DOI: 10.1103/PhysRevLett.122.121802. arXiv: 1810.12257 [hep-ex].

[190] C. P. Salemi *et al.*, "Search for Low-Mass Axion Dark Matter with ABRACADABRA-10 cm," *Phys. Rev. Lett.*, vol. 127, no. 8, p. 081 801, 2021. DOI: 10.1103/PhysRevLett.127.081801. arXiv: 2102.06722 [hep-ex].

[191] A. V. Gramolin, D. Aybas, D. Johnson, J. Adam, and A. O. Sushkov, "Search for axion-like dark matter with ferromagnets," *Nature Phys.*, vol. 17, no. 1, pp. 79–84, 2021. DOI: 10.1038/s41567-020-1006-6. arXiv: 2003.03348 [hep-ex].

[192] M. Betz, F. Caspers, M. Gasior, M. Thumm, and S. W. Rieger, "First results of the CERN Resonant Weakly Interacting sub-eV Particle Search (CROWS)," *Phys. Rev. D*, vol. 88, no. 7, p. 075 014, 2013. DOI: 10.1103/PhysRevD.88.075014. arXiv: 1310.8098 [physics.ins-det].

[193] K. Ehret *et al.*, "New ALPS Results on Hidden-Sector Lightweights," *Phys. Lett. B*, vol. 689, pp. 149–155, 2010. DOI: 10.1016/j.physletb.2010.04.066. arXiv: 1004.1313 [hep-ex].

[194] R. Ballou *et al.*, "New exclusion limits on scalar and pseudoscalar axionlike particles from light shining through a wall," *Phys. Rev. D*, vol. 92, no. 9, p. 092 002, 2015. DOI: 10.1103/PhysRevD.92.092002. arXiv: 1506.08082 [hep-ex].

[195] M. Ajello *et al.*, "Search for Spectral Irregularities due to PhotonAxionlike-Particle Oscillations with the Fermi Large Area Telescope," *Phys. Rev. Lett.*, vol. 116, no. 16, p. 161 101, 2016. DOI: 10.1103/PhysRevLett.116.161101. arXiv: 1603.06978 [astro-ph.HE].

[196] D. Noordhuis, A. Prabhu, S. J. Witte, A. Y. Chen, F. Cruz, and C. Weniger, "Novel Constraints on Axions Produced in Pulsar Polar-Cap Cascades," *Phys. Rev. Lett.*, vol. 131, no. 11, p. 111 004, 2023. DOI: 10.1103/PhysRevLett.131.111004. arXiv: 2209.09917 [hep-ph].

[197] M. Diamond, D. F. G. Fiorillo, G. Marques-Tavares, I. Tamborra, and E. Vitagliano, "Multimessenger Constraints on Radiatively Decaying Axions from GW170817," *Phys. Rev. Lett.*, vol. 132, no. 10, p. 101 004, 2024. DOI: 10.1103/PhysRevLett.132.101004. arXiv: 2305.10327 [hep-ph].

[198] A. Ayala, I. Domínguez, M. Giannotti, A. Mirizzi, and O. Straniero, "Revisiting the bound on axion-photon coupling from Globular Clusters," *Phys. Rev. Lett.*, vol. 113, no. 19, p. 191 302, 2014. DOI: 10.1103/PhysRevLett.113.191302. arXiv: 1406.6053 [astro-ph.SR].

[199] M. J. Dolan, F. J. Hiskens, and R. R. Volkas, "Advancing globular cluster constraints on the axion-photon coupling," *JCAP*, vol. 10, p. 096, 2022. DOI: 10.1088/1475-7516/2022/10/096. arXiv: 2207.03102 [hep-ph].

[200] N. Vinyoles, A. Serenelli, F. L. Villante, S. Basu, J. Redondo, and J. Isern, "New axion and hidden photon constraints from a solar data global fit," *JCAP*, vol. 10, p. 015, 2015. DOI: 10.1088/1475-7516/2015/10/015. arXiv: 1501.01639 [astro-ph.SR].

[201] A. Caputo, H.-T. Janka, G. Raffelt, and E. Vitagliano, "Low-Energy Supernovae Severely Constrain Radiative Particle Decays," *Phys. Rev. Lett.*, vol. 128, no. 22, p. 221 103, 2022. DOI: 10.1103/PhysRevLett.128.221103. arXiv: 2201.09890 [astro-ph.HE].

[202] E. Müller, F. Calore, P. Carenza, C. Eckner, and M. C. D. Marsh, "Investigating the gamma-ray burst from decaying MeV-scale axion-like particles produced in supernova explosions," *JCAP*, vol. 07, p. 056, 2023. DOI: 10.1088/1475-7516/2023/07/056. arXiv: 2304.01060 [astro-ph.HE].

[203] D. Wadekar and Z. Wang, "Strong constraints on decay and annihilation of dark matter from heating of gas-rich dwarf galaxies," *Phys. Rev. D*, vol. 106, no. 7, p. 075 007, 2022. DOI: 10.1103/PhysRevD.106.075007. arXiv: 2111.08025 [hep-ph].

[204] R. Janish and E. Pinetti, "Hunting Dark Matter Lines in the Infrared Background with the James Webb Space Telescope," Oct. 2023. arXiv: 2310.15395 [hep-ph].

[205] W. Yin *et al.*, "First Result for Dark Matter Search by WINERED," Feb. 2024. arXiv: 2402.07976 [astro-ph.CO].

[206] M. Regis *et al.*, "Searching for light in the darkness: Bounds on ALP dark matter with the optical MUSE-faint survey," *Phys. Lett. B*, vol. 814, p. 136 075, 2021. DOI: 10.1016/j.physletb.2021.136075. arXiv: 2009.01310 [astro-ph.CO].

[207] D. Grin, G. Covone, J.-P. Kneib, M. Kamionkowski, A. Blain, and E. Jullo, "A Telescope Search for Decaying Relic Axions," *Phys. Rev. D*, vol. 75, p. 105 018, 2007. DOI: 10.1103/PhysRevD.75.105018. arXiv: astro-ph/0611502.

[208] K. Nakayama and W. Yin, "Anisotropic cosmic optical background bound for decaying dark matter in light of the LORRI anomaly," *Phys. Rev. D*, vol. 106, no. 10, p. 103 505, 2022. DOI: 10.1103/PhysRevD.106.103505. arXiv: 2205.01079 [hep-ph].

[209] P. Carenza, G. Lucente, and E. Vitagliano, "Probing the blue axion with cosmic optical background anisotropies," *Phys. Rev. D*, vol. 107, no. 8, p. 083 032, 2023. DOI: 10.1103/PhysRevD.107.083032. arXiv: 2301.06560 [hep-ph].

[210] J. W. Foster *et al.*, "Deep Search for Decaying Dark Matter with XMM-Newton Blank-Sky Observations," *Phys. Rev. Lett.*, vol. 127, no. 5, p. 051 101, 2021. DOI: 10.1103/PhysRevLett.127.051101. arXiv: 2102.02207 [astro-ph.CO].

[211] K. Perez, K. C. Y. Ng, J. F. Beacom, C. Hersh, S. Horiuchi, and R. Krivonos, "Almost closing the νMSM sterile neutrino dark matter window with NuSTAR," *Phys. Rev. D*, vol. 95, no. 12, p. 123 002, 2017. DOI: 10.1103/PhysRevD.95.123002. arXiv: 1609.00667 [astro-ph.HE].

[212] K. C. Y. Ng *et al.*, "New Constraints on Sterile Neutrino Dark Matter from $NuSTAR$ M31 Observations," *Phys. Rev. D*, vol. 99, p. 083 005, 2019. DOI: 10.1103/PhysRevD.99.083005. arXiv: 1901.01262 [astro-ph.HE].

[213] B. M. Roach *et al.*, "Long-exposure NuSTAR constraints on decaying dark matter in the Galactic halo," *Phys. Rev. D*, vol. 107, no. 2, p. 023 009, 2023. DOI: 10.1103/PhysRevD.107.023009. arXiv: 2207.04572 [astro-ph.HE].

[214] F. Calore, A. Dekker, P. D. Serpico, and T. Siegert, "Constraints on light decaying dark matter candidates from 16 yr of INTEGRAL/SPI observations," *Mon. Not. Roy. Astron. Soc.*, vol. 520, no. 3, pp. 4167–4172, 2023. DOI: 10.1093/mnras/stad457. arXiv: 2209.06299 [hep-ph].

[215] F. Capozzi, R. Z. Ferreira, L. Lopez-Honorez, and O. Mena, "CMB and Lyman-α constraints on dark matter decays to photons," *JCAP*, vol. 06, p. 060, 2023. DOI: 10.1088/1475-7516/2023/06/060. arXiv: 2303.07426 [astro-ph.CO].

[216] H. Liu, W. Qin, G. W. Ridgway, and T. R. Slatyer, "Exotic energy injection in the early Universe. II. CMB spectral distortions and constraints on light dark matter," *Phys. Rev. D*, vol. 108, no. 4, p. 043 531, 2023. DOI: 10.1103/PhysRevD.108.043531. arXiv: 2303.07370 [astro-ph.CO].

[217] D. Cadamuro, "Cosmological limits on axions and axion-like particles," Ph.D. dissertation, Munich U., 2012. arXiv: 1210.3196 [hep-ph].

[218] P. F. Depta, M. Hufnagel, and K. Schmidt-Hoberg, "Robust cosmological constraints on axion-like particles," *JCAP*, vol. 05, p. 009, 2020. DOI: 10.1088/1475-7516/2020/05/009. arXiv: 2002.08370 [hep-ph].

[219] K. Langhoff, N. J. Outmezguine, and N. L. Rodd, "Irreducible Axion Background," *Phys. Rev. Lett.*, vol. 129, no. 24, p. 241 101, 2022. DOI: 10.1103/PhysRevLett.129.241101. arXiv: 2209.06216 [hep-ph].

[220] F. Bergsma *et al.*, "Search for Axion Like Particle Production in 400-GeV Proton - Copper Interactions," *Phys. Lett. B*, vol. 157, pp. 458–462, 1985. DOI: 10.1016/0370-2693(85)90400-9.

[221] E. M. Riordan *et al.*, "A Search for Short Lived Axions in an Electron Beam Dump Experiment," *Phys. Rev. Lett.*, vol. 59, p. 755, 1987. DOI: 10.1103/PhysRevLett.59.755.

[222] M. J. Dolan, T. Ferber, C. Hearty, F. Kahlhoefer, and K. Schmidt-Hoberg, "Revised constraints and Belle II sensitivity for visible and invisible axion-like particles," *JHEP*, vol. 12, p. 094, 2017, [Erratum: JHEP 03, 190 (2021)]. DOI: 10.1007/JHEP12(2017)094. arXiv: 1709.00009 [hep-ph].

[223] J. Blumlein *et al.*, "Limits on neutral light scalar and pseudoscalar particles in a proton beam dump experiment," *Z. Phys. C*, vol. 51, pp. 341–350, 1991. DOI: 10.1007/BF01548556.

[224] D. Banerjee *et al.*, "Search for Axionlike and Scalar Particles with the NA64 Experiment," *Phys. Rev. Lett.*, vol. 125, no. 8, p. 081 801, 2020. DOI: 10.1103/PhysRevLett.125.081801. arXiv: 2005.02710 [hep-ex].

[225] A. M. Sirunyan *et al.*, "Evidence for light-by-light scattering and searches for axion-like particles in ultraperipheral PbPb collisions at $\sqrt{s_{\rm NN}} = 5.02$ TeV," *Phys. Lett. B*, vol. 797, p. 134 826, 2019. DOI: 10.1016/j.physletb.2019.134826. arXiv: 1810.04602 [hep-ex].

[226] G. Aad *et al.*, "Measurement of light-by-light scattering and search for axion-like particles with 2.2 nb^{-1} of Pb+Pb data with the ATLAS detector," *JHEP*, vol. 03, p. 243, 2021, [Erratum: JHEP 11, 050 (2021)]. DOI: 10.1007/JHEP03(2021)243. arXiv: 2008.05355 [hep-ex].

[227] S. Knapen, T. Lin, H. K. Lou, and T. Melia, "Searching for Axionlike Particles with Ultraperipheral Heavy-Ion Collisions," *Phys. Rev. Lett.*, vol. 118, no. 17, p. 171 801, 2017. DOI: 10.1103/PhysRevLett.118.171801. arXiv: 1607.06083 [hep-ph].

[228] F. Abudinén *et al.*, "Search for Axion-Like Particles produced in e^+e^- collisions at Belle II," *Phys. Rev. Lett.*, vol. 125, no. 16, p. 161 806, 2020. DOI: 10.1103/PhysRevLett.125.161806. arXiv: 2007.13071 [hep-ex].

[229] M. Ablikim *et al.*, "Search for an axion-like particle in radiative J/ψ decays," *Phys. Lett. B*, vol. 838, p. 137 698, 2023. DOI: 10.1016/j.physletb.2023.137698. arXiv: 2211.12699 [hep-ex].

[230] D. Aloni, C. Fanelli, Y. Soreq, and M. Williams, "Photoproduction of Axionlike Particles," *Phys. Rev. Lett.*, vol. 123, no. 7, p. 071 801, 2019. DOI: 10.1103/PhysRevLett.123.071801. arXiv: 1903.03586 [hep-ph].

[231] P. Astier *et al.*, “Search for eV (pseudo)scalar penetrating particles in the SPS neutrino beam,” *Phys. Lett. B*, vol. 479, pp. 371–380, 2000. DOI: 10.1016/S0370-2693(00)00375-0.

[232] F. Capozzi *et al.*, “New constraints on ALP couplings to electrons and photons from ArgoNeuT and the MiniBooNE beam dump,” *Phys. Rev. D*, vol. 108, no. 7, p. 075 019, 2023. DOI: 10.1103/PhysRevD.108.075019. arXiv: 2307.03878 [hep-ph].

[233] J. W. D. Halliday *et al.*, “New bounds on heavy axions with an X-ray free electron laser,” Apr. 2024. arXiv: 2404.17333 [hep-ph].

[234] A. M. Sirunyan *et al.*, “Evidence for electroweak production of four charged leptons and two jets in proton-proton collisions at $\sqrt{s} = 13$ TeV,” *Phys. Lett. B*, vol. 812, p. 135 992, 2021. DOI: 10.1016/j.physletb.2020.135992. arXiv: 2008.07013 [hep-ex].

[235] A. Tumasyan *et al.*, “Measurement of the electroweak production of Zγ and two jets in proton-proton collisions at $\sqrt{s} = 13$ TeV and constraints on anomalous quartic gauge couplings,” *Phys. Rev. D*, vol. 104, p. 072 001, 2021. DOI: 10.1103/PhysRevD.104.072001. arXiv: 2106.11082 [hep-ex].

[236] A. M. Sirunyan *et al.*, “Observation of electroweak production of Wγ with two jets in proton-proton collisions at $\sqrt{s} = 13$ TeV,” *Phys. Lett. B*, vol. 811, p. 135 988, 2020. DOI: 10.1016/j.physletb.2020.135988. arXiv: 2008.10521 [hep-ex].

[237] A. M. Sirunyan *et al.*, “Measurements of production cross sections of WZ and same-sign WW boson pairs in association with two jets in proton-proton collisions at $\sqrt{s} = 13$ TeV,” *Phys. Lett. B*, vol. 809, p. 135 710, 2020. DOI: 10.1016/j.physletb.2020.135710. arXiv: 2005.01173 [hep-ex].

[238] A. M. Sirunyan *et al.*, “Search for the production of $W^{\pm}W^{\pm}W^{\mp}$ events at $\sqrt{s} =$ 13 TeV,” *Phys. Rev. D*, vol. 100, no. 1, p. 012 004, 2019. DOI: 10.1103/PhysRevD.100.012004. arXiv: 1905.04246 [hep-ex].

[239] E. Cortina Gil *et al.*, “Measurement of the very rare $K^{+}\to\pi^{+}\nu\overline{\nu}$ decay,” *JHEP*, vol. 06, p. 093, 2021. DOI: 10.1007/JHEP06(2021)093. arXiv: 2103.15389 [hep-ex].

[240] “Search for new physics in monojet events in pp collisions at sqrt(s)= 8 TeV,” Mar. 2013.

[241] “Search for New Phenomena in Monojet plus Missing Transverse Momentum Final States using 10fb-1 of pp Collisions at sqrts=8 TeV with the ATLAS detector at the LHC,” Nov. 2012.

[242] G. Haghighat, D. Haji Raissi, and M. Mohammadi Najafabadi, “New collider searches for axionlike particles coupling to gluons,” *Phys. Rev. D*, vol. 102, no. 11, p. 115 010, 2020. DOI: 10.1103/PhysRevD.102.115010. arXiv: 2006.05302 [hep-ph].

[243] F. Esser, M. Madigan, V. Sanz, and M. Ubiali, “On the coupling of axion-like particles to the top quark,” *JHEP*, vol. 09, p. 063, 2023. DOI: 10.1007/JHEP09(2023)063. arXiv: 2303.17634 [hep-ph].

[244] A. Tumasyan *et al.*, “Search for heavy resonances decaying to ZZ or ZW and axion-like particles mediating nonresonant ZZ or ZH production at $\sqrt{s} = 13$ TeV,” *JHEP*, vol. 04, p. 087, 2022. DOI: 10.1007/JHEP04(2022)087. arXiv: 2111.13669 [hep-ex].

[245] G. Aad *et al.*, "Search for new phenomena in events with two opposite-charge leptons, jets and missing transverse momentum in pp collisions at $\sqrt{\mathrm{s}} = 13$ TeV with the ATLAS detector," *JHEP*, vol. 04, p. 165, 2021. DOI: 10.1007/JHEP04(2021)165. arXiv: 2102.01444 [hep-ex].

[246] A. Tumasyan *et al.*, "Measurement of differential $t\bar{t}$ production cross sections in the full kinematic range using lepton+jets events from proton-proton collisions at $\sqrt{s} = 13$ TeV," *Phys. Rev. D*, vol. 104, no. 9, p. 092 013, 2021. DOI: 10.1103/PhysRevD.104.092013. arXiv: 2108.02803 [hep-ex].

[247] G. Aad *et al.*, "Measurements of differential cross-sections in top-quark pair events with a high transverse momentum top quark and limits on beyond the Standard Model contributions to top-quark pair production with the ATLAS detector at $\sqrt{s} = 13$ TeV," *JHEP*, vol. 06, p. 063, 2022. DOI: 10.1007/JHEP06(2022)063. arXiv: 2202.12134 [hep-ex].

[248] J. P. Lees *et al.*, "Search for $B \to K^{(*)}\nu\overline{\nu}$ and invisible quarkonium decays," *Phys. Rev. D*, vol. 87, no. 11, p. 112 005, 2013. DOI: 10.1103/PhysRevD.87.112005. arXiv: 1303.7465 [hep-ex].

[249] R. Z. Ferreira, M. C. D. Marsh, and E. Müller, "Strong supernovae bounds on ALPs from quantum loops," *JCAP*, vol. 11, p. 057, 2022. DOI: 10.1088/1475-7516/2022/11/057. arXiv: 2205.07896 [hep-ph].

[250] E. Aprile *et al.*, "Light Dark Matter Search with Ionization Signals in XENON1T," *Phys. Rev. Lett.*, vol. 123, no. 25, p. 251 801, 2019. DOI: 10.1103/PhysRevLett.123.251801. arXiv: 1907.11485 [hep-ex].

[251] E. Aprile *et al.*, "Excess electronic recoil events in XENON1T," *Phys. Rev. D*, vol. 102, no. 7, p. 072 004, 2020. DOI: 10.1103/PhysRevD.102.072004. arXiv: 2006.09721 [hep-ex].

[252] E. Aprile *et al.*, "Emission of single and few electrons in XENON1T and limits on light dark matter," *Phys. Rev. D*, vol. 106, no. 2, p. 022 001, 2022. DOI: 10.1103/PhysRevD.106.022001. arXiv: 2112.12116 [hep-ex].

[253] E. Aprile *et al.*, "Search for New Physics in Electronic Recoil Data from XENONnT," *Phys. Rev. Lett.*, vol. 129, no. 16, p. 161 805, 2022. DOI: 10.1103/PhysRevLett.129.161805. arXiv: 2207.11330 [hep-ex].

[254] F. Capozzi and G. Raffelt, "Axion and neutrino bounds improved with new calibrations of the tip of the red-giant branch using geometric distance determinations," *Phys. Rev. D*, vol. 102, no. 8, p. 083 007, 2020. DOI: 10.1103/PhysRevD.102.083007. arXiv: 2007.03694 [astro-ph.SR].

[255] G. Aad *et al.*, "Search for new phenomena in events with an energetic jet and missing transverse momentum in pp collisions at $\sqrt{s}$ =13 TeV with the ATLAS detector," *Phys. Rev. D*, vol. 103, no. 11, p. 112 006, 2021. DOI: 10.1103/PhysRevD.103.112006. arXiv: 2102.10874 [hep-ex].

[256] A. Mariotti, D. Redigolo, F. Sala, and K. Tobioka, "New LHC bound on low-mass diphoton resonances," *Phys. Lett. B*, vol. 783, pp. 13–18, 2018. DOI: 10.1016/j.physletb.2018.06.039. arXiv: 1710.01743 [hep-ph].

[257] H. Georgi, *Weak Interactions and Modern Particle Theory*. 1984, ISBN: 978-0-8053-3163-9.

[258] J. Gasser, M. E. Sainio, and A. Svarc, "Nucleons with chiral loops," *Nucl. Phys. B*, vol. 307, pp. 779–853, 1988. DOI: 10.1016/0550-3213(88)90108-3.

[259] S. Scherer, "Introduction to chiral perturbation theory," *Adv. Nucl. Phys.*, vol. 27, J. W. Negele and E. W. Vogt, Eds., p. 277, 2003. arXiv: hep-ph/0210398.

[260] M. Buschmann, C. Dessert, J. W. Foster, A. J. Long, and B. R. Safdi, "Upper Limit on the QCD Axion Mass from Isolated Neutron Star Cooling," *Phys. Rev. Lett.*, vol. 128, no. 9, p. 091 102, 2022. DOI: 10.1103/PhysRevLett.128.091102. arXiv: 2111.09892 [hep-ph].

[261] K. Hirata *et al.*, "Observation of a Neutrino Burst from the Supernova SN 1987a," *Phys. Rev. Lett.*, vol. 58, K. C. Wali, Ed., pp. 1490–1493, 1987. DOI: 10.1103/PhysRevLett.58.1490.

[262] K. S. Hirata *et al.*, "Observation in the Kamiokande-II Detector of the Neutrino Burst from Supernova SN 1987a," *Phys. Rev. D*, vol. 38, pp. 448–458, 1988. DOI: 10.1103/PhysRevD.38.448.

[263] A. Lella *et al.*, "Getting the most on supernova axions," *Phys. Rev. D*, vol. 109, no. 2, p. 023 001, 2024. DOI: 10.1103/PhysRevD.109.023001. arXiv: 2306.01048 [hep-ph].

[264] A. M. Sirunyan *et al.*, "Search for a heavy resonance decaying into a Z boson and a Z or W boson in $2\ell 2$q final states at $\sqrt{s} = 13$ TeV," *JHEP*, vol. 09, p. 101, 2018. DOI: 10.1007/JHEP09(2018)101. arXiv: 1803.10093 [hep-ex].

[265] A. M. Sirunyan *et al.*, "Search for physics beyond the standard model in high-mass diphoton events from proton-proton collisions at $\sqrt{s} = 13$ TeV," *Phys. Rev. D*, vol. 98, no. 9, p. 092 001, 2018. DOI: 10.1103/PhysRevD.98.092001. arXiv: 1809.00327 [hep-ex].

[266] S. Carra *et al.*, "Constraining off-shell production of axionlike particles with Zγ and WW differential cross-section measurements," *Phys. Rev. D*, vol. 104, no. 9, p. 092 005, 2021. DOI: 10.1103/PhysRevD.104.092005. arXiv: 2106.10085 [hep-ex].

[267] J. Alwall *et al.*, "The automated computation of tree-level and next-to-leading order differential cross sections, and their matching to parton shower simulations," *JHEP*, vol. 07, p. 079, 2014. DOI: 10.1007/JHEP07(2014)079. arXiv: 1405.0301 [hep-ph].

[268] feynrules.irmp.ucl.ac.be/wiki/ALPsEFT.

[269] T. Sjöstrand *et al.*, "An introduction to PYTHIA 8.2," *Comput. Phys. Commun.*, vol. 191, pp. 159–177, 2015. DOI: 10.1016/j.cpc.2015.01.024. arXiv: 1410.3012 [hep-ph].

[270] J. de Favereau *et al.*, "DELPHES 3, A modular framework for fast simulation of a generic collider experiment," *JHEP*, vol. 02, p. 057, 2014. DOI: 10.1007/JHEP02(2014)057. arXiv: 1307.6346 [hep-ex].

[271] A. Caputo, G. Raffelt, and E. Vitagliano, "Muonic boson limits: Supernova redux," *Phys. Rev. D*, vol. 105, no. 3, p. 035 022, 2022. DOI: 10.1103/PhysRevD.105.035022. arXiv: 2109.03244 [hep-ph].

[272] V. Shtabovenko, R. Mertig, and F. Orellana, "FeynCalc 9.3: New features and improvements," *Comput. Phys. Commun.*, vol. 256, p. 107 478, 2020. DOI: 10.1016/j.cpc.2020.107478. arXiv: 2001.04407 [hep-ph].

[273] H. H. Patel, "Package-X 2.0: A Mathematica package for the analytic calculation of one-loop integrals," *Comput. Phys. Commun.*, vol. 218, pp. 66–70, 2017. DOI: 10.1016/j.cpc.2017.04.015. arXiv: 1612.00009 [hep-ph].

[274] D. V. Kirpichnikov, V. E. Lyubovitskij, and A. S. Zhevlakov, "Constraints on CP-odd ALP couplings from EDM limits of fermions," *Particles*, vol. 3, no. 4, pp. 719–728, 2020. DOI: 10.3390/particles3040047. arXiv: 2004.13656 [hep-ph].

[275] L. Di Luzio, R. Gröber, and P. Paradisi, "Hunting for CP-violating axionlike particle interactions," *Phys. Rev. D*, vol. 104, no. 9, p. 095 027, 2021. DOI: 10.1103/PhysRevD.104.095027. arXiv: 2010.13760 [hep-ph].

[276] C. Grojean, J. Kley, and C.-Y. Yao, "Hilbert series for ALP EFTs," *JHEP*, vol. 11, p. 196, 2023. DOI: 10.1007/JHEP11(2023)196. arXiv: 2307.08563 [hep-ph].

[277] L. Di Luzio, G. Levati, and P. Paradisi, "The chiral Lagrangian of CP-violating axion-like particles," *JHEP*, vol. 2024, no. 02, p. 020, 2024. DOI: 10.1007/JHEP02(2024)020. arXiv: 2311.12158 [hep-ph].

[278] F. Anzuini, A. Gomez-Banon, J. A. Pons, A. Melatos, and P. D. Lasky, "Axion sourcing in dense stellar matter via CP-violating couplings," *Phys. Rev. D*, vol. 109, no. 8, p. 083 030, 2024. DOI: 10.1103/PhysRevD.109.083030. arXiv: 2311.13776 [hep-ph].

[279] L. Di Luzio, H. Gisbert, G. Levati, P. Paradisi, and P. Sørensen, "CP-Violating Axions: A Theory Review," Dec. 2023. arXiv: 2312.17310 [hep-ph].

[280] github.com/sdbakshi13/ALPRunner.

[281] A. Alloul, N. D. Christensen, C. Degrande, C. Duhr, and B. Fuks, "FeynRules 2.0 - A complete toolbox for tree-level phenomenology," *Comput. Phys. Commun.*, vol. 185, pp. 2250–2300, 2014. DOI: 10.1016/j.cpc.2014.04.012. arXiv: 1310.1921 [hep-ph].

[282] T. Hahn, "Generating Feynman diagrams and amplitudes with FeynArts 3," *Comput. Phys. Commun.*, vol. 140, pp. 418–431, 2001. DOI: 10.1016/S0010-4655(01)00290-9. arXiv: hep-ph/0012260.

[283] T. Hahn, S. PaSSehr, and C. Schappacher, "FormCalc 9 and Extensions," *PoS*, vol. LL2016, L. Salinas and C. Torres, Eds., p. 068, 2016. DOI: 10.1088/1742-6596/762/1/012065. arXiv: 1604.04611 [hep-ph].

[284] A. Carmona, A. Lazopoulos, P. Olgoso, and J. Santiago, "Matchmakereft: automated tree-level and one-loop matching," *SciPost Phys.*, vol. 12, no. 6, p. 198, 2022. DOI: 10.21468/SciPostPhys.12.6.198. arXiv: 2112.10787 [hep-ph].